Uncertainty quantification of fatigue design loads when compared with in-service measurements on ship-shaped

Hageman, R.B.

DOI
10.4233/uuid:60b5d240-221c-4d91-8d87-3b24c59acd50

Publication date
2022

Document Version
Final published version

Citation (APA)
Hageman, R. B. (2022). *Uncertainty quantification of fatigue design loads when compared with in-service measurements on ship-shaped*. [Dissertation (TU Delft), Delft University of Technology]. https://doi.org/10.4233/uuid:60b5d240-221c-4d91-8d87-3b24c59acd50

Important note
To cite this publication, please use the final published version (if applicable).
Please check the document version above.

UNCERTAINTY QUANTIFICATION OF FATIGUE DESIGN LOADS WHEN COMPARED WITH IN-SERVICE MEASUREMENTS ON SHIP-SHAPED OFFSHORE STRUCTURES

UNCERTAINTY QUANTIFICATION OF FATIGUE DESIGN LOADS WHEN COMPARED WITH IN-SERVICE MEASUREMENTS ON SHIP-SHAPED OFFSHORE STRUCTURES

Dissertation

for the purpose of obtaining the degree of doctor
at Delft University of Technology,
by the authority of the Rector Magnificus prof. dr. ir. T.H.J.J. van der Hagen,
chair of the Board of Doctorates,
to be publicly defended on
Wednesday 22 June 2022 at 12:30 o'clock

by

Remco Bastiaan HAGEMAN

Master of Science in Marine Technology,
Delft University of Technology, The Netherlands
born in Terneuzen, The Netherlands.

This dissertation has been approved by the promotors.

Composition of the doctoral committee:

Rector Magnificus,	chairperson
Prof. dr. ir. M.L. Kaminski,	Delft University of Technology, promotor
Dr. L. Pahlavan,	Delft University of Technology, copromotor
Independent members:	
Prof. dr. ir. R.H.M. Huijsmans,	Delft University of Technology
Prof. dr. K.T. Ma,	National Taiwan University, Taiwan
Prof. dr. B.J. Leira,	Norwegian University of Science and Technology, Norway
Prof. dr. ir. W. De Waele,	Ghent University, Belgium
Dr. D. Zarouchas,	Delft University of Technology
Prof. ir. J.J. Hopman,	Delft University of Technology, reserve member

Keywords: Hydrodynamic loads, uncertainty quantification, offshore production units, in-service measurements
Printed by: proefschriften.nl
Cover design: Marina de Jonghe

ISBN 978-94-6421-756-8

An electronic version of this dissertation is available at
http://repository.tudelft.nl/.

CONTENTS

SUMMARY

Floating offshore structures are continuously subjected to wave loads and loading originating from operational activities. These loads lead to cracks growing in the structure, a process known as fatigue accumulation. The analysis of fatigue accumulation is subject to large uncertainties. This is related to the high sensitivity of fatigue accumulation with respect to the local stresses in the structure. Structural designs are analysed in advance to ensure they can fulfil the intended service life. To account for the uncertainties in the analysis, safety factors are applied. These safety factors on fatigue life can be as large as 10 for certain structural details.

The spectral fatigue assessment procedure is most commonly used for the design of new structures. At several stages, models or assumptions are used which introduce uncertainty in the analysis process. In this research, the uncertainties in stresses which lead to fatigue accumulation have been examined. A number of parameters have been introduced to allow quantification of these effects on the fatigue accumulation process. The factors defined in this study relate to the contribution of the long-term wave environment, the sea state definition, the hydrodynamic and structural numerical models, weak and strong non-linear responses, the fatigue assessment method and loading-induced effects.

The analyses are conducted using measurements from production units during operation in an offshore environment. Measurements from seven different units with a similar instrumentation setup have been used. These units are equipped with a variety of sensors including wave buoys or radar, motion sensors, loading computer and strain gauges. To ensure durability, strain sensors are installed on several non-critical elements at some distance from stress concentrations. At such locations, a uniform stress field governs which results in more accurate measurements. The sensors are positioned such that the local stresses are governed, as much as possible, by a single load effect. The variety of data sources available allows for the subdivision of the total uncertainty into multiple components as described above. This aids in understanding the importance of the separate assumptions made in the design process. Observations for individual units were conducted. By comparing the results obtained on multiple units, some generalized observations about the uncertainties were made.

Uncertainties related to the long-term wave environment and short-term wave definition, were examined first. Dedicated wave buoys were used as sources of wave data. As alternative data source, information from hindcast models was used. These data sources were compared to obtain a general estimate of the uncertainty in long-term wave environments. The difference in fatigue accumulation when using these sources can be up to a factor of two. In cyclone-prone environments, the statistical uncertainty introduced by the presence of cyclone events is quite large and was assessed at 50%. Accurate sea state definitions are also quite important. Uncertainty arising from spectral definitions and wave spreading was quantified to be a factor of two on fatigue life. The importance of

correctly modelling a confused sea state by using multiple wave systems varied strongly depending on the location. In the West-Africa region, the sea states are characterized by a strongly dominant swell. In other locations, a strongly confused sea state with multiple components was found and correct modelling of these components proved essential for an accurate fatigue assessment.

The mismatch between the measured stress and those obtained using the numerical model is typically around 20% on stress for structural details subjected to global bending loads. However, on the structural details with wave pressure loads, deviations of the stress were found to be a factor of three. These deviations varied strongly between units and were mainly related to the linearisation of the intermittent wetting. The fatigue assessment method showed a higher accumulation rate than the directly assessed fatigue rate using strain gauges. A typical difference between them is 10%. However, the method becomes more conservative at higher fatigue accumulation rates. Therefore, the difference on the total accumulated fatigue life is larger, and typically a factor of two.

Weak and strong non-linear effects have been quantified. Only minor weak non-linear effects were found on the global loading effects. However, significant weak non-linear effects in the side shell were found as a result of intermittent wetting. This is considered an important feature which requires more attention, especially for systems operating at constant draft. Strong non-linear effects, whipping and springing, were examined. Over the entire lifetime, the contribution of these effects did not exceed 15% at the analysed structural details. However, in unfavourable sea states, the contribution of whipping can be up to 20%. On large units, non-linear springing was found in sea states with low wave periods. In these sea states, the contribution of springing to the overall fatigue accumulation can exceed 100%.

The main fatigue accumulation on cargo supporting structures, such as stringers, is related to loading cycles. The stress cycles at these details consist of contributions from cargo level variations in adjacent tanks, temperature-induced variations, wave-induced loads and secondary ballast and cargo loads. The variation of filling levels in adjacent tanks provides the largest contribution to the stress variation. However, the small additional stresses from the other sources result in a fatigue accumulation which is 50% larger than that based on cargo level variations alone. These effects are not fully accounted for in numerical analyses.

Fatigue assessment procedures involve a large number of assumptions and modelling choices. In most cases, these assumptions introduce an additional safety margin on the fatigue life. However, a number of features in the applied loads were identified that can lead to higher stresses. Due to the high sensitivity of fatigue accumulation with respect to the stress level, the applied safety margins can be consumed quickly under disadvantageous conditions. Monitoring of an asset in service can help to quantify these uncertainties in the load prediction and can provide insight in the true safety margins of an offshore structure.

SAMENVATTING

Drijvende offshore constructies worden continue blootgesteld aan belastingen door golven en operationele activiteiten. Deze belastingen leiden tot scheurgroei in de constructie, wat bekend staat als vermoeiing. De analyse van vermoeiingsopbouw gaat gepaard met grote onzekerheden. Deze zijn het resultaat van de grote gevoeligheid van vermoeiing ten gevolge van de lokale spanningen in de constructie. Het ontwerp van een offshore constructie wordt voor de bouw doorgerekend zodat de gewenste levensduur veilig bereikt kan worden. Door grote veiligheidsfactoren te gebruiken wordt rekening gehouden met de eerder genoemde onzekerheden in de analyse. Deze veiligheidsfactoren kunnen zo groot zijn als een factor 10 op levensduur voor bepaalde constructie-details.

In een ontwerpstadium wordt vermoeiing meestal bepaald met een spectrale vermoeiingsberekening. In diverse stadia van dit proces worden modellen gebruikt of aannames gedaan. Deze introduceren onzekerheden in de procedure. In dit onderzoek, worden de onzekerheden in de spanningen, welke leiden tot vermoeiing, onderzocht. Enkele parameters zijn geïntroduceerd om deze onzekerheden te kunnen kwantificeren. De factoren die in deze studie gedefinieerd zijn, hebben betrekking op de lange termijn omgevingscondities, de gebruikte golfmodellen, hydromechanische en constructieve numerieke modellen, zwakke en sterke niet-lineariteiten in de belastingen, de vermoeiingsberekening methode en belastingen ten gevolge van beladingscondities.

De analyses zijn uitgevoerd met behulp van metingen aan diverse constructies gedurende operaties op hun productie locatie. Metingen van zeven verschillende eenheden met een soortgelijk instrumentatie plan zijn gebruikt. Verschillende sensor types, bijvoorbeeld golfboeien en -radars, bewegingssensoren, beladingscomputers en rekstroken, zijn gebruikt. Voor de robuustheid van het meetsysteem, zijn de rekstroken geplaatst op niet-kritieke locaties op enige afstand van de spanningsconcentraties. Op dergelijke locaties heerst er een uniform spanningsveld wat resulteert in betrouwbaardere metingen. De reksensoren zijn, zoveel als mogelijk, aangebracht op locaties waar een enkel belastingsfenomeen domineert. De verschillende types sensoren maken het mogelijk om de onzekerheden op te splitsen in meerdere componenten zoals hierboven beschreven. Dit helpt om het belang van de verschillende aannames in het ontwerpproces te begrijpen. Resultaten zijn bepaald voor de verschillende constructies, maar door onderlinge resultaten te vergelijken zijn ook enkele algemene opmerkingen over de onzekerheden geplaatst.

Onzekerheden met betrekking tot de lange termijn omgevingscondities en korte termijn golfbescrhijving zijn als eerste behandeld. Golfboeien zijn gebruikt als primaire bron voor golfdata. Als alternatieve data bron zijn oceanografische golfmodellen gebruikt. Deze data bronnen zijn vergeleken om een globale inschatting van de onzekerheid ten gevolge van lange termijn condities te maken. De verschillen in vermoeiingsopbouw tussen deze verschillende bronnen kan een factor twee zijn. In omgevingen waar cyclonen voorkomen, is de statistische onzekerheid door het al dan niet aanwezig zijn

van dergelijke stormen aanzienlijk. Een onzekerheid van 50% op levensduur is hiervoor afgeleid. Nauwkeurige beschrijving van de omgevingscondities is ook van belang. Onzekerheden ten gevolge van de spectrale vorm en golfspreiding zijn bepaald als een facor twee op levensduur. Het belang van het correct modelleren van condities met meerdere golfsystemen, is sterk locatie afhankelijk. In West-Afrika worden de golfcondities sterk bepaald door een enkel systeem van deining. Op andere locaties kunnen duidelijk te onderscheiden golfsystemen worden gezien. Het correct modelleren van zulke condities is essentieel.

Het verschil tussen de gemeten spanningen en die welke met het numerieke model worden bepaald kan oplopen tot waardes van 20% voor details welke belast worden door globale vervormingen van de romp. Op details waar lokale golfdrukken de dominante belasting zijn, zijn verschillen van een factor drie gevonden. Deze verschillen varieerden sterk tussen de verschillende offshore eenheden. De methode van linearisatie van discontinue golfdrukken is hier vooral verantwoordelijk voor geacht. De berekeningsmethodiek voor vermoeiing gaf over het algemeen hogere waardes dan de vermoeiing welke direct vanuit de rekstroken werd bepaald. Gemiddeld is het verschil ongeveer 10%. Echter, de berekeningsmethodiek wordt behoudender naarmate de belasting toeneemt. Daarom is het verschil op de totale levensduur veel groter, typisch een factor twee.

Zwakke en sterke niet-lineariteiten zijn gekwantificeerd. De bijdrage van zwakke niet-lineariteiten was zeer beperkt voor globale belastingen. Een grotere bijdrage is gevonden in de huid constructie. Dit wordt beschouwd als een uitkomst welke meer aandacht verdient voor systemen met constante diepgang. Sterke niet-lineaire effecten zoals whipping en springing, zijn ook onderzocht. De bijdrage van deze effecten op de gehele levensduur van de constructies bleef beperkt tot maximaal 15%. In zware condities zijn instantane bijdrages van whipping tot 20% gezien. Op grote eenheden is niet-lineaire springing gevonden in condities met een lage golfperiode. De bijdrage van springing in deze condities kan oplopen tot 100%.

De belangrijkste bijdrage aan vermoeiing op lading ondersteunende constructie elementen is gerelateerd aan beladingscycli. De spanningswisselingen op dergelijke details zijn opgebouwd uit bijdrages gerelateerd aan variaties van belading in aanliggende ruimtes, temperatuur gerelateerde globale vervormingen, golf geïnduceerde belastingen en beladingsvariaties elders in de constructie. De variatie van belastingen in aanliggende ruimtes geeft de grootste bijdrage aan de spanningsvariaties. Echter, de kleine spanningscomponenten van de andere effecten resulteren in een vermoeiingsbijdrage die 50% groter is dan op basis van enkel de niveau variaties in aanliggende ruimtes. Deze effecten worden niet volledig in numerieke analyses meegenomen.

Een groot aantal aannames en modellen worden gebruikt in het beoordelen van vermoeiing in offshore constructies. In de meeste gevallen introduceren deze aannames een extra veiligheidsmarge in het ontwerp. Een aantal aspecten in de belastingen zijn gevonden die kunnen leiden tot hogere vermoeiingsconsumptie. Gegeven de grote gevoeligheid ten opzichte van de opgelegde spanningen kan dit in onvoordelige condities leiden tot het opsouperen van de gebruikte veiligheidsmarges. Door constructies tijdens hun operationele leven te bemeten, kunnen de onzekerheden in de voorspelling van belastingen gekwantificeerd worden en kan inzicht in de werkelijke veiligheidsmarges van de constructie verkregen worden.

ACRONYMS

AIC	Akaike Information Criterion
BIC	Bayesian Information Criterion
Bret	Bretschneider
BT	Ballast Tank
c2	cos^2
c8	cos^8
CT	Cargo Tank
DFF	Design Fatigue Factor
(I)FEM	(Inverse) Finite Element Method
FPSO	Floating Production Storage Offloading unit
Gaus	Gaussian
HF	High Frequent
JW	Jonswap
LBSG	Long Base Strain Gauge
LC	Load Case
LCr	Longcrested
LF	Low Frequent
MBWM	Motion-based wave measurement
MLE	Maximum Likelihood Estimation
N/A	Not Applicable
OH	Ochi-Hubble
PoE	Probability of Exceedance
PS	Port side
RAO	Response Amplitude Operator
RBI	Risk-Based Inspection
SB	Starboard side
SCF	Stress Concentration Factor
std	Standard deviation
TAF	Tool Accuracy Factor
TL	Tank Level
WF	Wave Frequent
WN	Wrapped-Normal

List of Symbols

a	Fatigue resistance intersect parameter
D	Fatigue Damage
D_c	Cosine spreading function
D_{WN}	Wrapped-Normal spreading function
D_{LC}	Long-Crested spreading function
D_ζ	Wave spreading function
g	Gravitational acceleration
$G(\mu,\beta)$	Gumbel distribution with parameters (μ,β)
h	Height (of water column)
H_s	Significant wave height
$\mathscr{L}$	Loglikelihood function
$L(\mu,\sigma)$	Lognormal distribution with parameters (μ,σ)
m	Fatigue resistance slope parameter
m_i	i-th order spectral moment
$N(\mu,\sigma)$	Normal distribution with parameters (μ,σ)
N	Number of cycles
p	Probability density function
S_ζ	Wave spectrum
S_σ	Stress spectrum
T_p	Peak period
T_z	Zero-crossing period
$WB(\lambda,\kappa)$	Weibull distribution with parameters (λ,κ)
α	Fatigue load uncertainty parameter
Γ	Gamma function
γ	Peakedness factor of Jonswap spectrum
Δp	Pressure range
$\Delta\sigma$	Stress range
δ	Kronecker delta
θ	Direction
θ_R	Relative direction
λ	Ochi-Hubble spectrum parameter
σ	Stress

σ_G	Spectral width parameter of Gaussian spectrum
ω	Angular frequency
ω_p	Peak frequency

1

INTRODUCTION

A journey of a thousand miles begins with a single step

Lao Tzu

1

1.1. MOTIVATION

Floating offshore structures are continuously exposed to varying loads. Under these repetitive load cycles, cracks can initiate and grow in highly stressed areas of the structure. This process is known as fatigue accumulation. During the design of offshore structures, calculations to predict fatigue accumulation are executed.

Crack growth and fatigue accumulation are very sensitive to the local stresses in the structure. The fatigue accumulation increases with the stress level to the power three or higher [1]. In the fatigue design, many assumptions and modelling choices are made. An early study supported by multiple classification societies [2] shows the large variation in fatigue calculations which can be expected. While numerical methods have been further developed since then, the study is exemplary of the high uncertainties that are typically associated with fatigue assessments.

When using models and methods, the procedures aim to err on the side of caution due to this large sensitivity. In addition to the safety margins introduced through the calculation procedure, an additional safety margin, the Design Fatigue Factor (DFF), is introduced. For a given structural detail, this factor depends on its criticality and accessibility and can be as high as 10. This means that structural details of an offshore unit that is supposed to remain on station for 25 years have to be designed for a lifetime of 250 years. Lotsberg [3] presents a list of criteria that can be used to select the appropriate DFF for a given structural detail.

These large safety factors are required because fatigue accumulation is highly non-linear with respect to the loads and structural stress. These safety margins are included to prevent structural failures due to adverse conditions. A large variety of sources of these adverse conditions can be identified. Examples include the material and building defects, corrosion, adverse environmental loads and accidents. When one or multiple load effects are not properly included, a quick deterioration of the fatigue life can be expected. However, when no or limited adverse conditions occur, the structure has a large reserve capacity. Therefore, the operating life of these high-value offshore units, can often be extended (far) beyond the original service life.

Beginning fatigue cracks may occur in a large number of locations and are often hard to identify in an offshore environment. Any underestimation of the fatigue loads may therefore go unnoticed for a prolonged period of time. This raises the question which sources of uncertainties in fatigue design become important over time and if they consume the applied safety margins. Also, if the mode of operation of the unit is of importance, changing the mode of operation could lead to a rapid structural degradation in the extended life.

Generally, frequent inspection and if necessary, maintenance and repair, help to maintain the desired safety level, in shipping and traditional offshore industry. This is achieved by performing limited inspections at regular time intervals. The procedure does not typically provide explicit information on the actual safety levels. An explicit assessment of the safety level and maintaining this level through regular inspections is the basis of an alternative inspection planning methodology known as Risk-Based Inspection (RBI) [4]. It should be noted that RBI encompasses not only fatigue criteria, but also include other degradation effects such as corrosion.

Rather than using deterministic approaches, RBI uses statistical methods, known as

reliability methods, which use explicit formulations of the uncertainties in the design procedure in the form of statistical parameters, marginal probability functions or joint probability functions. First applications of such methods date back to the 1980s and 1990s. An overview of the basic approaches are provided by Mansour [5] and Ditlevsen and Madsen [6]. These methodologies remain the basis of most modern-day analyses. An early example of the application of reliability methods in shipbuilding is given by White and Ayyub [7].

RBI procedures have originally been developed in other industries, such as the process industry [8]. Applications of this methodology in offshore include the work by Lee *et al.* [9] which shows the development of inspection planning during the initial stages of the FPSO field development or the work by Shabakhty *et al.* [10] which includes a similar analysis for a jackup structure with the aim of maintaining a predefined safety level through planned inspections.

By executing monitoring of the hull structure, additional information of the structure is obtained which should help its operator to improve the maintenance actions. This is widely recognised by classification societies, but the procedures to do so are relatively new and still in development, see e.g. the codes by ABS, BV and DNV [11–13]. This is the result of a large variety of ships and offshore structures and a similarly large variety of monitoring procedures. This thesis provides an example application of how monitoring data can be used to quantify uncertainties in support of further development of these methodologies.

Both for the improvement of design methodologies as well as the execution of inspection planning according to RBI, it is important to understand where the uncertainties in the fatigue design originate from. By assessing the relative contribution of each of these sources, the most important contributions can be examined further and, where possible, monitored for specific applications. This scheme ensures an efficient reduction of the overall uncertainty encountered in the fatigue design.

The uncertainties used in reliability assessments or to quantify design procedures often date back to original sources in the 1980s, such as the work by Wirsching [14]. Since then, design procedures have been modified and the applicability of information from that era to modern design approaches can be questioned. Studies which compare calculation procedures to assess fatigue accumulation on ship-like structures have been executed more recently. Examples of such studies include the work performed by Francois *et al.* [2] on an FPSO cross section and Rörup [15] on a cross section of a bulk carrier. These studies typically show a variation in the results which is a factor of two or larger on lifetime for specific details. Moreover, the different calculations do provide a different ordering of critical elements. Proper identification of critical areas is important as it will provide guidance to inspectors when conducting offshore integrity inspection. Hence, the need for assessment of uncertainties in such calculations remains relevant. This work aims to provide insight in the uncertainty of the prediction of the hydrodynamic and operational loads acting on floating offshore structures.

Sources of uncertainty can be qualified through theoretical reasoning. However, quantifying these parameters for a full size structure is not always possible through numerical simulations or scale experiments as the physics involved cannot be modelled efficiently or obeys a scaling law other than Froude scaling. Moreover, not all sources

of uncertainty are known a-priori or may be unfairly dismissed. The benefit of using in-service measurements is that a more complete overview of the relevant uncertainties is achieved, though at the cost of a more challenging interpretation of these measurements. It should be noted that some unknown unknowns will always remain as a result of the limited number of monitoring locations. The use of data from multiple units creates some perspective in the overall performance of industry practice. When given proper maintenance, dedicated monitoring systems can be sustained for a long period of time and may provide detailed information over the operational life of a unit.

Efforts of integrating monitoring data with structural models are now leading to the development of true digital twins [16]. For such models, it is important to develop dedicated procedures to deal with missing data and ensure a fair comparison of all data sources. Results from in-service measurements can be supplemented with numerical simulations where necessary to be able to cover a wide variety of uncertainties.

1.2. RESEARCH OBJECTIVES

The goal of this study is to provide insights in the accuracy of assessing fatigue loads on floating offshore units. Understanding the limitations of design procedures and their accuracy will help to improve in the development of new designs and aid in the proper through-life assessment of units already in operation. This work presents some details obtained from various monitoring schemes to investigate how the information can be collected and used.

The research objectives of this study are:

1. to define a framework in which the relevant uncertainties in the fatigue loads can be assessed and compared
2. to assess the uncertainty on fatigue life expectations introduced through design assumptions, methods and models using measurements from multiple units

The objectives will be reached by comparing performance of fatigue life assessment methods on different units in various operating environments. The goal is to develop qualitative indications of the different uncertainties of the various types of units. These indications can be used as a reference for analysts when addressing the relative importance of each decision when conducting fatigue assessments.

1.3. BRIEF DESCRIPTION OF UNITS

For this research use has been made of measurements conducted onboard seven floating production units with a very similar instrumentation setup [17], see two examples in Figure 1.1. The first set of monitoring data used in this research dates from 2007 [18]. Subsequent measurement campaigns on the different units have been initiated over the period from 2011 to 2019. An overview of the location of the monitored units is provided in Figure 1.2.

Four units, all of them barge shaped structures, are spread-moored in the West-Africa region. These are denoted *WA*1 to *WA*4. The environmental conditions are dominated by benign or moderate swells from the South to South West direction. The units are moored with a heading aligned with the main wave direction. The conditions near unit

Figure 1.1: Typical FPSOs as instrumented with Structural Hull Monitoring System, both spread-moored (left) and turret-moored (right) units.

*WA*2 are somewhat deviating. At this location, the swell conditions consist of smaller waves and the windsea condition with smaller period is of higher importance relative to the swell condition. Three of these units have a length in excess of 300 metres. The last unit, *WA*3, is somewhat smaller and is a production unit without storage capacity. The total amount of data from these units which has been used in this research is 1, 5, 6 and 7 years, respectively.

The other units are turret-moored units and are more ship shaped structures. Unit *NS* is located west of Shetland which is a very harsh environment with frequent storms and generally tough weather conditions. Unit *SA-AUS* has been operated in South-Africa and redeployed in Australia. These units are of similar shape with a length of around 250 metre. The environment in South-Africa is quite harsh because in this area two swell components, one from the Atlantic Ocean and one from the Indian Ocean, coexist. The environment in Australia is very mild with two wave systems, one from the east and one from South-West. However, this area can also experience cyclones. Unit *AUS* is another large unit operating in Australia. The total amount of data from these units which has been used in this research is 1, 2 and 4 years, respectively.

1.4. LIMITATIONS OF RESEARCH

The goal of this thesis is to provide insight in the uncertainties in loading mechanisms which contribute to fatigue accumulation on offshore structures. Fatigue accumulation is a broad research subject with a large number of related topics that require attention and which are examined by other academic and industry researchers. In this study, fatigue resistance and the validity of fatigue accumulation, as expressed through the Palmgren-Miner summation [19], are not discussed. An evaluation and perspective on these closely related research topics will be provided in Chapter 2. An extensive quantification of uncertainties in the fatigue loads in the design process is provided. However, the question as to how these uncertainties should be incorporated in future designs, inspection schemes or lifetime extensions, is not addressed.

From the seven units, a total of 26 years of measurement data has been used. The instrumentation setup on these units is comparable, although individual differences be-

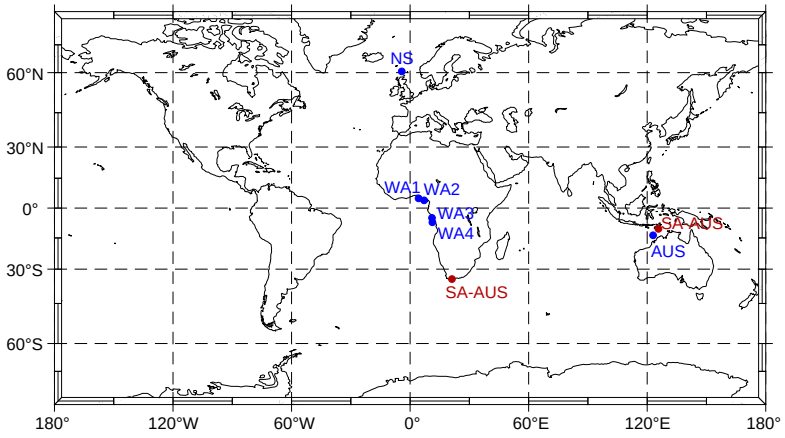

Figure 1.2: Approximate location of the instrumented units. The blue markers indicate locations where active monitoring is going on, while the red markers indicate fields where production has been ceased. The units are denoted by an indicator representing their operating area.

tween the units do exist. Availability of several spread-moored units in the West-Africa region allows for some generalization of the results for this region. For other regions, only data from one or two units is available which does not allow for generalization. However, trends and characteristics can be identified. The procedures presented in this document can be applied to other floaters and their results can be compared against those of the units presented herein.

1.5. OUTLINE OF THIS DOCUMENT

Chapter 2 presents the methodology used in this research. This chapter provides a review of the fatigue assessment procedure and indicates the models and assumptions used in this process. An overview of the loading mechanism considered in this study is presented. Finally, a framework in which various sources of uncertainty in the fatigue loads are introduced is provided as well as the procedures used to quantify them.

Chapter 3 discusses the data collection procedure. It presents a typical instrumentation setup used onboard the various offshore units. Properties of the sensors and other data sources are discussed.

The results of this study are presented in Chapter 4. The individual uncertainties as identified in the framework from Chapter 2 are quantified from the measurements of the individual units. When possible, generalized results are presented. This chapter concludes with an overview on the importance of the individual uncertainties on fatigue accumulation.

Chapter 5 presents further discussion of the observed results. Some general remarks on the interpretation of the results from this study are presented and findings of similar efforts in other industries, particularly shipping, are examined and compared.

Conclusions and recommendations are provided in Chapter 6.

2

METHODOLOGY

Dans les champs de l'observation le hasard ne favorise que les esprits préparés
In the fields of observation chance favours only the prepared mind

Louis Pasteur

2.1. OUTLINE

This chapter describes the methodology used in the assessment of uncertainties of fatigue loads. Section 2.2 describes how a typical fatigue assessment is conducted. The nature of the various loading phenomena acting on the hull of floating offshore structures is described in further detail in section 2.3. Section 2.4 shows how the different sources of uncertainty can be incorporated in the calculation process. Finally, section 2.5 discusses how these uncertainties are evaluated in this research and section 2.6 addresses the definition of associated statistical concepts.

2.2. FATIGUE ASSESSMENT

The growth of fatigue cracks in the structure depends on both the stresses acting on the local details as well as the resistance of these details to withstand the stresses. Section 2.2.1 briefly reviews the fatigue resistance models. Section 2.2.2 reviews the typical calculations used when evaluating fatigue life in a single sea state and section 2.2.3 discusses how the fatigue over the entire lifetime is assessed.

2.2.1. FATIGUE RESISTANCE

The fundamental models which describe crack growth in structures originated in the 1960s [1]. The Paris law describes the crack growth rate as function of the stress level and local crack geometry. Cracks often occur in welded structural details which feature both initial defects and high local stresses. The size of initial defects in the weld is related to weld quality, while the stress level is influenced by the local weld geometry and can be modelled using a Stress Concentration Factor (SCF). The Paris law is still considered the most accurate model of capturing crack growth, but has some practical drawbacks when conducting analyses at the design stage for a large number of structural details in a vessel.

First of all, the dimensions of initial defects in the welds have an important contribution to the crack growth rate in the initial phases of crack development. However, the dimensions of such flaws cannot be determined in advance and can only be obtained using high-end equipment such as X-Ray scanning. This is not practical for the large number of welded details in a regular ship-shaped structure. Secondly, the time-dependent loading history needs to be incorporated. The model incorporates load sequences which are also not known in advance. This lack of knowledge will result in uncertainties in the input of the crack growth simulations which will result in more significant uncertainties in its output.

A more simplified method to assess fatigue life on floating structures is based on the Palmgren-Miner linear fatigue hypothesis [19]. This hypothesis assumes time-invariance meaning it neglects load sequence effects. The uncertainties in the fatigue assessment can be captured through a statistical description of fatigue resistance. The curves describing fatigue resistance are known as Wohler curves or S-N curves and have been developed from systematic test sequences with constant amplitude stress cycles. The curves relate stress level to number of cycles until failure. Design curves are defined at two standard deviation below the mean curves. Consequently, a fatigue damage equal to unity corresponds to the situation where there is a 2.3% chance of a through-thickness

crack being present [20].

Equation 2.1 provides the algebraic expression of a single-slope S-N curve, that is the number of cycles until failure, N, as function of stress range $\Delta\sigma$. In this research, all results will be based on single-slope S-N curves with an inverse slope, m, of 3, although different intersect parameters a are used. The calculation uses closed stress cycles, i.e. an upward and downward change in stress of the same magnitude. As a consequence of the choices above all relative numbers in this thesis can be fairly compared and provide meaningful statements on fatigue loads.

$$N(\Delta\sigma) = \frac{a}{\Delta\sigma^m} \tag{2.1}$$

An example of an S-N curve is shown in Figure 2.1. A multitude of S-N curves is available in order to describe different detail geometries in different surrounding environments, including air, seawater and in the presence of cathodic protection.

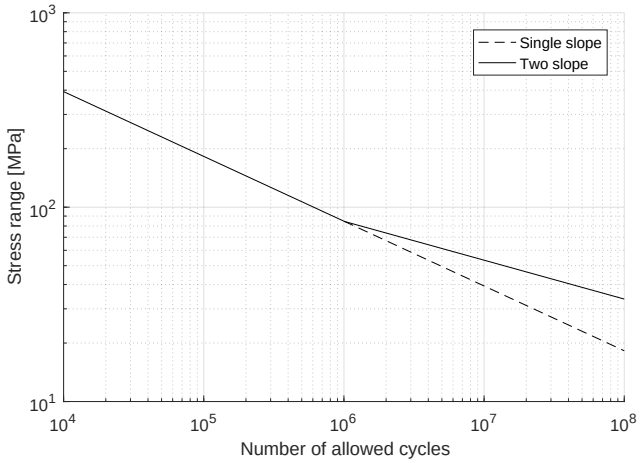

Figure 2.1: Example of S-N curves used in fatigue design. The depicted curve is the D-class curve for structural details exposed to seawater with cathodic protection [21].

Kerdabadi *et al.* [22] have replaced the S-N curve approach in a reliability analysis with a fracture mechanics based solution. The implementation used in that study, ensured that the crack growth model yielded more conservative results compared to the S-N curve approach. However, the crack growth models are computationally expensive as one has to perform a simulation over time. Moreover, the crack growth models feature significant uncertainties in input variables which are not explicitly included in the S-N curve calculations.

CONSIDERATIONS WHEN USING S-N CURVES

The S-N curves have been developed for thin plated elements. Correction models can be used to adjust the expected lifetime for thicker plates. To account for this thickness effect, different design codes use different reference thicknesses, which range between

25 and 32 mm. Offshore structures and sometimes deck plating of ships use larger plate thicknesses. The stress concentrations in thick-plated structures can have a small negative influence on fatigue life [20].

Below a specific stress level, the fatigue crack barely grows. However, there can still be build-up of energy through plastic deformation at the crack tip which facilitates further crack growth. To distinguish between direct crack growth and the energy build-up, S-N curves can distinguish a high-stress and low-stress zone with different parameters. This type of S-N curve is referred to as a two-slope curve, whereas single-slope curves assume the crack growth mechanism to be valid for all stress levels, which is a more conservative assumption.

The fatigue accumulation is based on a variation of stress levels. However, under the influence of a static mean stress, this stress cycle can be either fully in tensile, fully in compression or a combination of tensile and compressive stress. When a compressive stress persists, the crack remains closed during the load cycle and the crack growth will be diminished. Correction models to account for this effect may be applied, see e.g. [23]. This mean stress effect is often quantified using the stress ratio which is defined as the ratio of the minimum and maximum stress of a cycle.

Welded structures contain residual stresses. Such stresses can be alleviated when large deformation occur in the structure for the first time. This situation, known as a shakedown [24], leads to local plastic deformations in the welds which reduces the residual stresses. The residual stresses can also be reduced, but not fully eliminated, by adopting improved welding procedures. Application of such procedures will allow for prolonged lifetime estimates.

The uncertainty in the fatigue assessment based on S-N curves is significant and is represented by the scatter found in the fatigue resistance curves. However, by defining the curves at the 2.3% exceedance level, a safety margin is already introduced. These features make the fatigue assessment using S-N curves a much more practical method for industry. For specific simplifications, such as details in compressive loads and stresses in thick plates, correction models are available and can be used to achieve better lifetime [20]. To allow for a fair comparison between fatigue loads, such correction methods are not adopted throughout this thesis.

DEVELOPMENTS ON FATIGUE RESISTANCE MODELS

Several efforts are ongoing which aim to reduce the scatter which is typically observed in an S-N curve based fatigue resistance model.

A more detailed description of the stress state in the weld can help to reduce the uncertainty in these models. For example, the Total Stress Concept by Den Besten [25] shows a reduction in the uncertainty of the fatigue resistance curves after a reformulation of the stress state parameters. The fatigue resistance model itself can still be described by a S N type formulation.

The Palmgren-Miner fatigue accumulation hypothesis itself also introduces some uncertainty in the fatigue assessment procedure. Most notably, the hypothesis neglects any influence from different sequencing of the loads. Load sequences can be incorporated when using a fracture mechanics based analysis model.

An extensive survey on the uncertainty resulting from the adoption of the Palmgren-Miner hypothesis was performed for the Ship Structure Committee [26]. A more recent

survey, albeit more limited in scope, was conducted by Tammer and Kaminski [4]. A number of different stochastic models to capture the performance of the fatigue criterion have been evaluated. However, the work by Wirsching [14], in which the results of several fatigue experiments on representative structures has been analysed jointly, is considered the most representative. The proposed model represents the fatigue criterion using a lognormal distribution with a mean value of 1 and standard deviation of 0.3. This shows that significant uncertainty in the fatigue evaluation method exists.

The work by Leonetti *et al.* [27] provides a modification of the fatigue criterion by providing a formulation of the fatigue rate which depends on the current fatigue accumulation or equivalently, the loading history. The development of this model was based on the Paris Law and thereby more accurately represents the crack growth characteristics. The model can be described by a single additional parameter which depends on the weld notch geometry.

In a case study by Deul [28], a comparison between several fatigue criteria was made for application on a naval vessel. The author concluded that for this application, in which the actual fatigue life often exceed the predicted lifetime, the nonlinear damage accumulation yielded better results.

In fatigue critical areas, multiple loading mechanisms may coexist. In such cases, the uni-axial stress state may change to a condition in which multiple stress component with their respective frequencies and magnitudes, occur. In a recent study, van Lieshout [29] has shown the large changes in fatigue life that can be expected under these circumstances. In this study, fatigue analyses will be executed for locations with a well-defined uni-axial stress loading.

2.2.2. FATIGUE EVALUATION

A consequence of the time invariant property of the Palmgren-Miner hypothesis is that the fatigue accumulation of a number of stress cycles is equal to the summation of the fatigue contribution of each individual cycle. Combined with the fatigue resistance described in equation 2.1, the fatigue accumulation over M closed stress cycles with arbitrary magnitude can be assessed using equation 2.2.

$$D(M) = \sum_{i=1}^{M} D_i = \sum_{i=1}^{M} \frac{1}{N(\Delta\sigma_i)} = \sum_{i=1}^{M} \frac{\Delta\sigma_i^m}{a} \tag{2.2}$$

Each structural detail will experience a large number and variety of stress cycles $\Delta\sigma_i$ during its lifetime. Fatigue failure is defined as the condition where $D(M)$ equals or exceed 1. However, for design assessments an additional safety margin, the Design Fatigue Factor, DFF, see e.g. Lotsberg [3], is introduced in which case the maximum allowable value of $D(M)$ becomes $\frac{1}{DFF}$. This factor is introduced to account for the uncertainties in the calculation process and typically ranges from 2 to 10 depending on the importance of the structural detail and its accessibility for inspections and repair. The large values used for the DFF underline the influence of uncertainties in the fatigue design process.

TIME DOMAIN

Time traces of the stresses provide the most direct way of obtaining stress ranges for a fatigue assessment through the Miner summation. Once a list of stress cycles has been

obtained, this can be inserted directly into the Miner summation in equation 2.2.

When dealing with an irregular time trace, obtaining the stress cycles is not straightforward. A mixture of small and large amplitude cycles needs to be distinguished. The method to do so is called Rainflow counting with the procedure by Rychlik accepted as standard [30]. The implementation from WAFO is used to conduct Rainflow counting [31]. Other procedures, such as the ASTM standard [32], are mostly equivalent and the main differences between the procedures relate to the way in which residual cycles or non-closed hysteresis loops are being processed.

When using time traces all relevant loading mechanisms can be included. This is a benefit when measured stresses are available, for example from in-service measurements. During the design stage, these time traces need to be explicitly calculated. A calculation tool which incorporates all loading mechanisms is required. Calculations including nonlinear wave loads are however seldom executed as these are very computationally expensive. These are more commonly executed for research purposes or to establish correction factors for nonlinear loads for a limited number of cases. The spectral calculation method is much more computationally efficient in design.

SPECTRAL DOMAIN

When applying spectral calculations, one subdivides the operational life of the structure in time windows of short duration. During these windows the operational and environmental conditions are considered ergodic. Typical time windows range from 30-minutes to 6-hours with 3-hours being the most often applied time window in calculations. The fatigue accumulation in such a condition can be assessed using the reasoning in this section. The procedure is presented in many earlier research contributions, e.g. by Nolte and Hansford [33].

In a typical spectral calculation, one assumes that all structural stresses are linearly related to the waves. To assess the structural response at time t, a convolution of the wave time history with the Response Amplitude Operator (RAO) is required. In frequency domain, an equivalent operation is to perform a multiplication of the wave energy spectrum S_ζ and the square of the response operator to obtain the response energy spectrum S_σ.

$$S_\sigma(\omega) = RAO^2_\sigma(\omega|LC)S_\zeta(\omega) \tag{2.3}$$

The RAO is determined for a given loading condition LC. A consequence of the assumption on linearity between waves and structural stress is that statistical properties of the waves also apply to the structural stress. In particular, the surface elevation is assumed to be normally distributed which leads to a distribution of peak and through wave heights that complies with a Rayleigh distribution, see Journee [34] for this derivation. Therefore, the distribution of stress ranges $p(\Delta\sigma)$ also follows a Rayleigh distribution.

The response from wave loads also depends on relative wave direction. In case of wave spreading or multiple wave systems from different directions, equation 2.3 can be extended with direction dependency and the total response can be evaluated by integrating over all directions:

$$S_\sigma(\omega) = \oint_0^{360} RAO^2_\sigma(\omega,\theta|LC)S_\zeta(\omega,\theta)d\theta \tag{2.4}$$

The number of stress cycles in a sea state of duration T is given by the division of T and the zero-crossing period of the stress T_z. The period can be calculated using the zero- and second-order integration of the stress response spectrum as follows:

$$\begin{aligned} m_0 &= \int_0^\infty S_\sigma(\omega)\, d\omega \\ m_2 &= \int_0^\infty \omega^2 S_\sigma(\omega)\, d\omega \\ T_z &= 2\pi\sqrt{\frac{m_0}{m_2}} \end{aligned} \tag{2.5}$$

Using the probability distribution of stress ranges, the number of cycles around magnitude $\Delta\sigma$, denoted as $n(\Delta\sigma)$, can be expressed as:

$$n(\Delta\sigma) = \frac{T}{T_z}\int_{\Delta\sigma-\frac{d\Delta\sigma}{2}}^{\Delta\sigma+\frac{d\Delta\sigma}{2}} p(\Delta\sigma)\, d\Delta\sigma \tag{2.6}$$

Following the Miner summation, the fatigue contribution of these cycles can be expressed as:

$$D(\Delta\sigma) = n_T(\Delta\sigma)\frac{\Delta\sigma^m}{a} = \frac{T}{T_z}\frac{1}{a}\int_{\Delta\sigma-\frac{d\Delta\sigma}{2}}^{\Delta\sigma+\frac{d\Delta\sigma}{2}} p(\Delta\sigma)\Delta\sigma^m\, d\Delta\sigma \tag{2.7}$$

which can be integrated over the entire range of stress ranges to obtain the total fatigue accumulation in period T:

$$D = \int_0^\infty D(\Delta\sigma) = \frac{T}{T_z}\frac{1}{a}\int_0^\infty p(\Delta\sigma)\Delta\sigma^m\, d\Delta\sigma \tag{2.8}$$

It was argued before that the stress ranges follow a Rayleigh distribution whose probability density function is given by:

$$p(x) = \frac{x}{B^2}e^{-\frac{x^2}{2B^2}} \tag{2.9}$$

The parameter B is a scale parameter and is related to the magnitude of the response. In case the Rayleigh distribution is used to describe the distribution of amplitudes, B equals the standard deviation of the stress which equals the square root of the integral of the stress response spectrum, $\sqrt{m_0}$, see Lee and Kang [35]. When assessing stress ranges instead of amplitudes, the value equals twice this parameters. The analytical formula of the Rayleigh distribution can be inserted in the fatigue calculation to obtain the following:

$$D = \frac{T}{T_z}\frac{1}{a}\int_0^\infty \frac{\Delta\sigma}{B^2}e^{-\frac{\Delta\sigma^2}{2B^2}}\Delta\sigma^m\, d\Delta\sigma = \frac{T}{T_z}\int_0^\infty \frac{\Delta\sigma^{m+1}}{B^2}e^{-\frac{\Delta\sigma^2}{2B^2}}\, d\Delta\sigma \tag{2.10}$$

This integral can be simplified using the definition of the gamma function, which is defined as:

$$\Gamma(x) = \int_0^\infty y^{x-1} e^{-y} dy \tag{2.11}$$

With the following values substituted for x and y, the following derivation can be made:

$$\begin{aligned} x &= 1 + \frac{m}{2} \\ y &= \frac{1}{2}(\frac{\Delta\sigma}{B})^2 \\ dy &= \frac{\Delta\sigma}{B^2} d\Delta\sigma \\ \Gamma(1 + \frac{m}{2}) &= \frac{1}{\sqrt{2}^m B^{m+2}} \int_0^\infty \Delta\sigma^m e^{-\frac{\Delta\sigma^2}{2B^2}} d\Delta\sigma \end{aligned} \tag{2.12}$$

This final expression can be inserted in equation 2.10, after which an elegant closed-form expression for the fatigue accumulation is obtained:

$$D = \frac{T}{T_z} \frac{1}{a} (\sqrt{2}B)^m \Gamma(1 + \frac{m}{2}) \tag{2.13}$$

The equation above is valid only when using a single-slope S-N curve. The integral provided in the gamma function can be subdivided in two parts by using incomplete gamma functions. This will allow for an integration with respect to stress ranges over the two different sections of the S-N curve.

The spectral calculation requires both stationarity of operating conditions and statistical convergence of the loads in each considered condition. These requirements are contradictory when selecting appropriate time windows. In order to ensure statistical convergence longer time frames are more appropriate. However, performing calculations for an operational vessel, longer time series will result in more variation in operational and environmental conditions. For the analysis of permanently moored offshore structures in a mild environment, longer time windows can be used. However, for ships which change speed and heading and sail through different areas, the use of shorter time windows may be more appropriate to accurately capture the operational behaviour of the vessel.

The spectral fatigue assessment assumes that all stresses are proportional to wave loads acting on the hull. However, this is not true for all loading mechanisms as will be described in more detail in section 2.3. Such load effects can be included in a spectral calculation by piecewise linearisation.

When comparing the time domain and spectral domain methods, the time domain method is better able to account for nonlinear responses. However, it is very computationally expensive and requires simulations for every operational and loading condition. Preferably, multiple simulations of the same conditions are conducted to account for variability in the wave environment, known as seed effects. The spectral assessement is a very efficient calculation procedure which allows for the assessment of many conditions in short time. Because nonlinear loading effects are either small or the linearisation

procedures are considered adequate, this method has become the preferred method for fatigue analysis in hulls of offshore structures.

2.2.3. FATIGUE ASSESSMENT OVER LIFETIME

Following the reasoning of the Miner summation, the wave-induced fatigue accumulation over the structure's life can be assessed through a summation over all relevant conditions while respecting the exposure time of each condition. This can be summarized using the following summation:

$$D_{WF} = \sum_{LC} \sum_{\theta} \sum_{H_S} \sum_{T_P} p(LC, \theta, H_S, T_P) D(LC, \theta, H_S, T_P) \tag{2.14}$$

The parameter LC indicates a summation over all loading conditions and θ indicates the summation over all directions. The inclusion of all environmental conditions denoted in the scatter diagram is given by the double summation over wave height H_S and period T_P. $p(LC, \theta, H_S, T_P)$ denotes the probability of the combined environmental and operational conditions. It should be noticed that the parameters are not independent. The different environmental parameters will have a strong correlation, but the loading conditions can be independent of the environment. Therefore, this probability can be evaluated using:

$$p(LC, \theta, H_S, T_P) = p(LC)\, p(\theta, H_S, T_P) \tag{2.15}$$

On some units, operations will aim to avoid full loading conditions during heavy weather to reduce the loads on the structure. For such cases, the probability $p(LC, \theta, H_S, T_P)$ cannot be subdivided per equation 2.15. However, when doing so, the fatigue assessment will become more conservative as rare full load conditions in heavy weather are introduced in the calculation.

In the design stage, the method used to calculate the fatigue accumulation per condition $D(LC, \theta, H_S, T_P)$ can be based on multiple methods such as simplified analytical formulas, spectral assessment, time-domain assessment using simulations or model test data. For a consistent assessment, the calculation method for each condition has to be the same. In practice, a full coverage of all conditions is only feasible using a simplified or spectral calculation method. However, correction factors can be derived from time-domain simulations or model tests for a limited number of cases. These correction factors can be extrapolated to cover the entire range of operating and environmental conditions and be used to improve the fatigue assessment over all conditions.

When evaluating wave-induced fatigue accumulation over a longer period of time, the accumulated fatigue following equation 2.14 is used. This is in the end the design parameter of interest and can be compared against design values and class requirements. However, when assessing the performance of design methods, the fatigue accumulation in a single condition, as given by equation 2.13, is used. This will be referred to as fatigue rate and expressed as fatigue accumulation per hour, i.e. T is set to one hour for all cases, which allows for cross-comparison of the different results.

Offshore production units have specific and quite predictable loading-offloading cycles which depend strongly on their production capacities and field performance. The

stresses resulting from these loading-offloading cycles can be very high and lead to local plastic deformations. The contribution of such low-frequent large amplitude stress cycles can be incorporated through dedicated calculations.

The fatigue resulting from variations in the loading conditions can be calculated independently. The static stress range between different loading conditions is calculated by Finite Element Analysis. A wave-induced stress component is added to account for an increase in the overall stress cycle due to wave action, see also figure 2.2. If necessary, correction factors are included to account for stress redistribution and strain hardening of the material resulting from local plasticity. A single predefined S-N curve is to be used for the assessment independent of local detail geometry. Most classification societies provide similar approaches on how to assess the loading-induced fatigue. However, there are different approaches used for combining wave- and low-frequency fatigue components, see the design codes by ABS, BV, DNV and LR [21, 36–38] for more details.

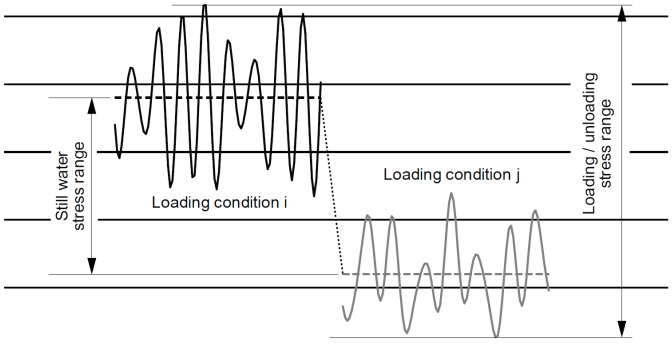

Figure 2.2: Stress range used in loading-induced fatigue assessment, obtained from BV code [36].

Permanently moored offshore structures are designed according to location specific weather expectations. However, the unit needs to move from the construction location, usually the far east, to its field. Depending on the location of the field, transportation time can be as long as 3 month. For units operating in mild weather conditions, the fatigue accumulation during the transportation can be significant and the fatigue accumulation during this period is considered separately using equation 2.14. For this assessment, a dedicated set of wave statistics are used to describe the expected weather conditions. Moreover, a single dedicated loading condition is used.

2.3. LOADING PHENOMENA

Figure 2.3 shows an example of a stress time series obtained from a strain sensor at the deck of an offshore unit in several representations. Numerous physical phenomena contribute to the stresses as observed in this figure. These phenomena can be conveniently organized by means of their frequency content. The bottom graph of figure 2.3 shows the frequency spectrum of the signal in the upper graph. The spectrum shows a number of distinct frequency responses.

The leftmost part of the energy spectrum contains the low-frequency (LF) response.

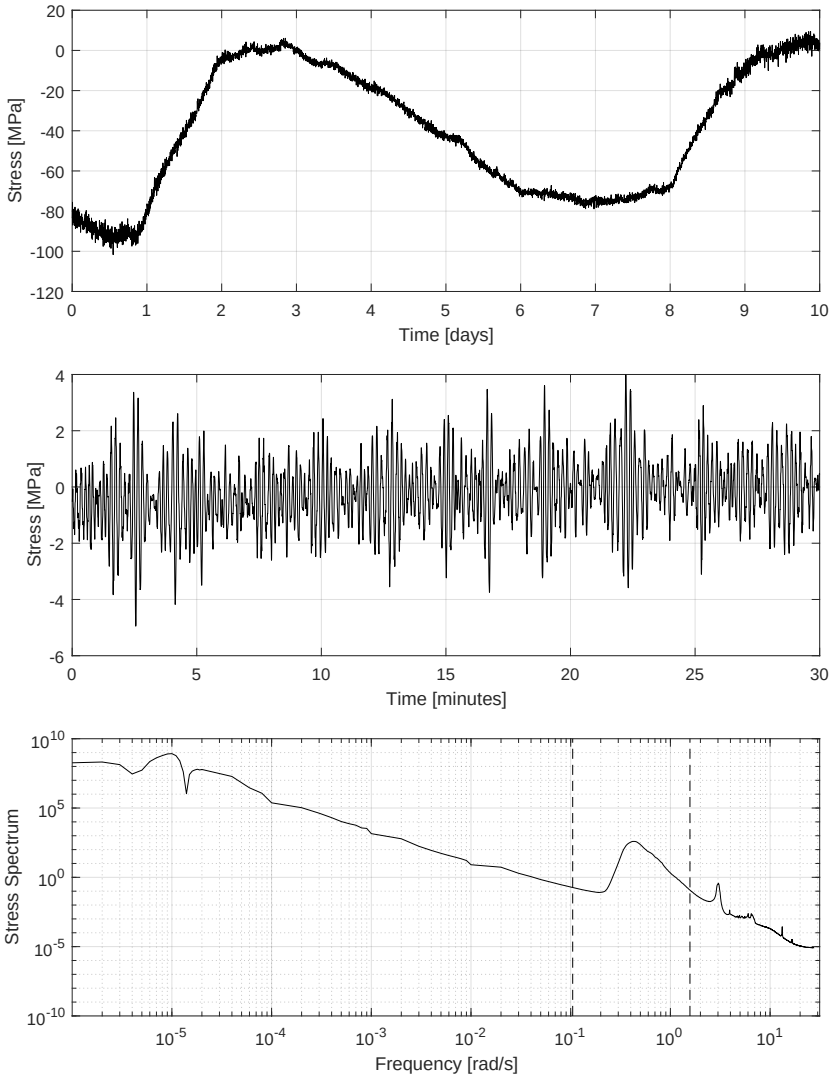

Figure 2.3: Example of measured stress time series over several days (top), half an hour (middle) and the corresponding energy spectrum (bottom) from an offshore unit. Note that the data of the energy spectrum is plotted on a double log-scale which clearly shows the different frequency contents, but obscures the relative importance of the different peaks. The vertical dashed lines indicate the frequencies associated with 60 and 4 seconds respectively. The figure shows peak responses around $10^{-5} rad/s$ (equivalent to 7 day period), around $0.5 rad/s$ (equivalent to a period of 12 seconds) and $3 rad/s$ (equivalent to 2 second period).

The typical frequencies associated with these responses correlate with periods of hours or even longer. Typical loading phenomena that lead to this type of responses are thermal induced loads resulting from day and night rhythm or loads related to cargo carrying. The wave-frequency (WF) responses are generally the most dominant response in offshore structures. This response is the direct result of wave action on the hull. This leads to global hull girder deformations, but also to local pressure variations acting on the side shell and bottom plating. However, ship motions are also the result of wave action and cargo onboard the ship will experience accelerations which in turn result in additional forces acting on the internal structure. Any response with frequencies exceeding those of the wave-frequency are referred to as high-frequency (HF) response. This component is the result of dynamic response of the primary or secondary hull structure. The HF response in the hull structure can be the result of an impulse load, in which case it is referred to as whipping, or continuous excitation, in which case it is referred to as springing. These HF responses are generally not considered explicitly during design, but safety factors are used instead.

For a number of considered details, the relative importance of the different frequency contributions is determined. In order to assess the importance of the high-frequency component with respect to the wave-frequency component, the stress time series per sea state can be examined. The fatigue accumulation of such a time series can be determined using Rainflow counting and includes both the wave and high-frequency components. By applying a low pass filter, the high-frequency component is removed from the time series. By performing another Rainflow counting analysis on this filtered time series, the fatigue accumulation comprising only the wave-frequency component is obtained. By comparing the fatigue accumulation from the unfiltered and filtered time series, the relative importance of the high-frequency component can be obtained.

The same procedure cannot be applied to assess the relative contribution of the low-frequency component. The reason is that the ratio of frequencies between the low and wave-frequency components is much larger. Figure 2.3 shows that this ratio is in the order of 10^4 to 10^5, whereas in case of the wave and high-frequency components, this ratio is in the order of 10. Instead, the low-frequency fatigue is determined independently of the other components. The high and wave-frequency fatigue is determined for each time window of limited duration, for example 30 minutes. At the same time, minima and maxima of every 30-minute period are obtained. To assess the low-frequency fatigue, a new time series is generated using these utmost values. The low-frequency fatigue contribution is obtained from this time series by rainflow counting. This method will be referred to as an interval analysis in this thesis. Validation of the interval method for usage in this thesis will be executed first.

Rainflow counting can be applied to the full continuous stress history to obtain the fatigue accumulation as a result of all load effects. This procedure is considered to be the most accurate method of capturing fatigue accumulation on a longer time series. However, it is unfeasible to perform this analysis due to the length of such time series, which can span multiple years. A limited duration example was used to test the validity of the interval procedure described above. The four time histories as presented in Figure 2.4 show high-, wave- and low-frequency loading effects on four measurement locations on stringers where significant loading-induced stress variations can be seen.

Table 2.1 shows the associated fatigue results. This shows that the fatigue accumulation obtained using the interval procedure is within one percent of the direct fatigue assessment and it can be concluded that the interval procedure provides a sufficiently accurate total fatigue accumulation. The separation between the different loading components is only provided here as reference. A more detailed and complete discussion is provided in section 4.7.

In the following subsections, the basic load components will be discussed starting with the wave-frequency components, followed by the high-frequency components and concluding with the low-frequency components.

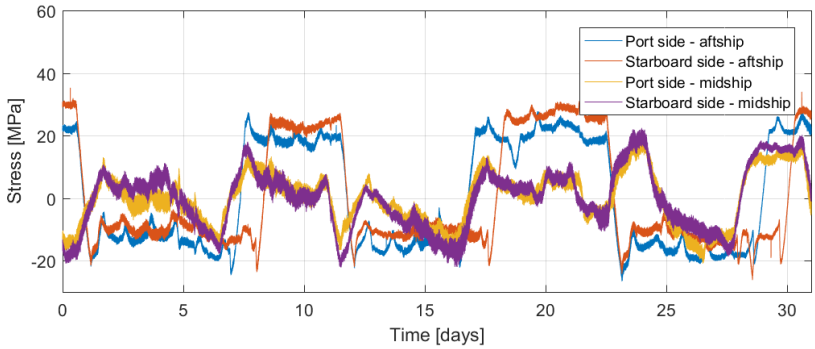

Figure 2.4: Example of stresses sustained during one month on four stringer locations.

Fatigue accumulation [$*10^{-6}$]	PS aftship	SB aftship	PS midship	SB midship
Total Fatigue - continuous analysis	0.522	0.654	2.264	2.228
Total Fatigue - interval analysis	0.520	0.652	2.265	2.230
Wave- and high-frequency part	*0.215*	*0.289*	*2.119*	*2.045*
Low-frequency part	*0.305*	*0.363*	*0.146*	*0.186*

Table 2.1: Results of fatigue assessment using separated wave-frequency and low-frequency components as shown in Figure 2.4.

2.3.1. HULL GIRDER BENDING

Normally the largest loads on hull structures arise from global hull girder bending. The wave induced pressure on the bottom plating are continuously fluctuating while waves travel along the hull. This results in primary, secondary and tertiary deformations of the hull structure. The deformations can take place as a result of vertical and horizontal bending or torsion and shear or axial forces. In order to facilitate the operations onboard, a minimization of roll motions is aimed for. Therefore, spread-moored offshore units will generally be oriented such that the bow or stern is aligned with the dominant wave direction. On turret-moored units, neglecting any potential active heading control, the heading is achieved as an equilibrium between yaw forces exerted from wind, wave and

current forces. These configurations will often result in bow, astern or slightly quartering sea conditions. These will result in high vertical bending loads and smaller horizontal bending and torsion. Moreover, the hull of an offshore unit typically has a closed cross-section, which is very stiff when loaded in torsion and hence torsion-induced stresses are typically very small.

Hull girder bending moments have long been identified as one of the primary concerns in the structural design of offshore units. To facilitate design studies, approximation formulas are available to estimate the hull girder bending moment using only main particulars. These formulas are typically defined for a specific type of ship or offshore unit. Such methods have long been used in the shipping industry where a more complex shape of the hull results in a less intuitive calculation of the bending moment. Early examples include the method of Sikora [39] for naval vessels.

An example of how direct calculations of hull girder bending moments have been used to obtain new design criteria is given by Hautecloque *et al.* [40]. This formulation is developed for application in the assessment of container ships by BV [41]. However, the underlying data set comprises a larger variety of ship types, including tankers. This has been done to "avoid inconsistency between load formulations", see Derbanne *et al.* [42]. A similar accuracy has been obtained for the blunt ships which would potentially also allow the application to ship-shaped offshore units.

Such formulas provide simple but powerful tools in early design stage, but are not accepted as a method to assess the final design. For that aim, numerical tools are needed. Hydrodynamic design tools can be subdivided in three types. First of all, the strip theory programs which reduce the three dimensional hull to two dimensional sections. Secondly, the three dimensional potential-based boundary element methods which use either Green functions or Rankine sources, also known as panel methods. Viscous effects in these methods can be introduced using elements based on Morrison equations. Lastly, RANS type application are increasingly being investigated, but the high computational costs for these methods result in only few applications for dedicated purposes.

Compared to stationary offshore structures, hydrodynamic analyses for ships are much more complicated due to the increased complexity of the hull shape and incorporation of forward speed. This has lead to a wide variety of analysis procedures which is discussed by the ISSC [43]. The methods vary in the way in which, among other effects, weak nonlinearities, forward speed, wave modelling and slamming are incorporated. Therefore, similar analysis for ship structures may show an even larger uncertainty in the point by point evaluation of fatigue accumulation. However, the overall safety margin on the accumulated fatigue consumption may not be so different. In shipping, traditional empirical methods are more commonly used for designs. However, direct computations are nowadays increasingly applied to replace or strengthen the empirical procedures, see e.g. the joint effort by Derbanne *et al.* [42] or Hautecloque *et al.* [40]. Liao *et al.* [44] showed that direct calculation of the loads on tanker and bulk carriers can result in significant higher response than predicted by the governing rules, though and this difference is yet to be fully understood.

Developments in the strip theory methods are oriented towards the inclusion of nonlinearity in the response. The work by Vásque *et al.* [45] shows that the assessment of the sagging bending moment works well in moderate conditions, but is still off in extreme

conditions. The inclusion of nonlinearity in the calculation of radiation and diffraction forces is another valuable improvement, see e.g. Rajendran *et al.* [46].

The inclusion of nonlinearities in the assessment of the response is the main area for improvement in the panel based methods as well, see e.g. Kukkanen [47]. Nonlinearities in the diffraction forces are being developed for application in Green function based panel methods. Examples showing the improvement obtained with such procedures are given by Sengupta *et al.* [48] for a container ship and Kukkanen and Matusiak [49] for a ro-ro vessel. Even more advanced methods using transient Green functions to account for free surface and forward speed effects exist. These methods are very computationally expensive, but perform well in challenging cases, such as the seakeeping performance of small high-speed crafts as presented in the study by van Walree and Struijk [50].

Normally, the input waves are considered to be linear. However, the work performed by Shivaji and Sen [51] shows that Rankine panel methods are able to deal with steep nonlinear wave conditions as well. Wave nonlinearity is an important aspect when operating in steep, high waves.

RANS type calculations to address seakeeping are rare. Oberhagemann *et al.* [52] discusses various methods that ensure that the critical conditions are identified using more efficient calculation methods. In the near future, such methods may be used to properly calibrate properties of more efficient calculation tools or as improved input for parameters in design methods [53].

The direct response to wave loads contain a nonlinear component. Bow flare in container ships is responsible for a considerable difference hogging and sagging in this type of ship. An early investigation into this effect comparing the performance of a strip theory and diffraction program was conducted by Adegeest [54]. New-build offshore units have limited bow flare and experience much smaller nonlinearities from such effects.

Rörup *et al.* [15] presents a comparison of a fatigue assessment using a variety of approaches to assess the fatigue accumulation from global hull girder bending. Seven different hydrodynamic analyses including strip theory, diffraction using Green functions and Rankine sources have been tested using a structural model of a bulk carrier. The peak values of the RAOs of vertical bending moment calculated using Green function methods are within 5% of each other. However, the Rankine source method and especially strip theory methods provide higher peak value with differences up to 15%. The comparison becomes worse in oblique seas. At 30 degree off-head direction, the methods using Green functions show an RAO with similar peak frequency and reduced amplitude of around 15%. The other methods show a peak value which is similar to the head waves condition with a reduced peak frequency.

Hageman *et al.* [55] shows a comparison of different hydrodynamic calculation methods for a naval vessel, including a semi-empirical formulation by Sikora [56], a strip theory method and two diffraction programs using Green functions. The calculated bending moments are compared against a set of around 2-year of in-service measurements. The strip theory method shows higher bending moments compared to the measurements and other methods. Remarkably, the empirical model provides a decent average result, although with some more variation in between the individual conditions. This highlights the power of such models as an early design method.

Clauss *et al.* [57] compares the performance of two strip theory methods and one

panel method with a model test in an extreme condition. The midship vertical bending moment is overestimated by all methods in comparison with the model tests which is attributed by the authors to viscous effects omitted in the calculations. Mohammadi *et al.* [58] shows another comparison between strip theory and panel method, although this time a more complicated trimaran shape is considered. A comparison between sectional loads obtained from panel methods using Green functions and Rankine sources is provided by von Graefe *et al.* [59]. This comparison shows an improved performance of the Rankine source method, although the difference becomes more pronounced at higher speed.

It can be concluded that a wide variety of methods exist which can be used to address wave-frequent hull girder loads. The different methods accommodate different situations for which the loads are to be determined. When using an appropriate procedure for the conditions at hand, the global loads can be predicted quite well on average. However, on a case by case analysis significant uncertainties may persist. Understanding and insight in these uncertainties are important for further development of hydrodynamic tools. However, they are also important when assessing the influence of these tools on fatigue life predictions.

2.3.2. WHIPPING

While operating in a seaway, wave impacts which lead to an impulsive load acting on the hull, known as slamming, can occur. The response of the hull structure is dominated by the lower flexural modes of the hull. This type of response is known as whipping. The study of slamming impacts is often related to extreme loads acting on the structure. The whipping response can lead to a maximum response which is significantly larger than the response resulting from linear excitation. The effect of whipping on fatigue accumulation has received less attention in literature.

The study of slamming and whipping is focused on ship structures. Ships are more susceptible to slamming loads because slamming is more likely to occur at higher speeds and steeper waves. Moreover, ship structures have more surfaces at lower angles with respect to the waterline, such as bow flare, but also flat shaped aftbodies as often seen on cruise vessels which can lead to aftship slamming, see Kapsenberg *et al.* [60]. Whipping is often examined for slender, flexible structures, such as container ships, and depends on the mass distribution at the time of impact, see Senjanović [61]. However, the extensive study by Storhaug showed that whipping response can be equally important for blunt ships. A case study considered by this author included the analysis of an ore carrier for which the fatigue accumulation was increased with 44% as a result of whipping response [62].

The occurrence of slamming impacts is a highly stochastic process depending on both ship geometry, operation and wave conditions. Wave height, direction and steepness as well as vessel speed and loading conditions all contribute to the likelihood of slamming, making slamming impacts challenging to predict and model. Early work by Ochi [63] has resulted in simple, but powerful criteria to assess the risk of whipping based on keel clearance and re-entry speed. Bereznitski [64] indicated that the duration of the impact in relation to the natural period of the structure is of importance. The importance of a nonlinear wave description when assessing wave impacts is highlighted by

Guedes Soares *et al.* [65].

A quick first estimate of whipping moments can be achieved through empirical methods. These methods can provide only a coarse approximation of the whipping induced response for a limited range of applications, such as the method by Sikora *et al.* [56] for fast displacement ships or the method by de Lauzon *et al.* [66] for container ships, and should not be used in final design stages.

Methods used for calculating the slamming impact loads are still evolving. The foundations of the well known Generalized Wagner Model have been published nearly a century ago by Wagner [67]. An overview of the critical developments in the field of slamming impact assessment since then is provided in the research by Kapsenberg [68].

Model tests remain the most proven method to assess slamming influences. To obtain proper statistical data on slamming, long model test sequences are needed. It will not be possible to execute tests for all conditions. Rather, interpolation methods which are calibrated using model test data can be used to provide an estimate for all conditions, see e.g. Drummen *et al.* [69]. Traditional seakeeping methods used to assess the wave-induced response, as discussed in section 2.3.1, can be extended to account for the whipping response. Particularly, the integrated solution of the hydroelastic problem by coupling the hydrodynamic and structural response is being investigated, see e.g. Tuitman [70] for an implementation of such a procedure.

Strip theory methods incorporating structural flexibility of the hull are well established. These methods are applied in dedicated studies, such as the work by Zhu and Moan [71] to assess the influence of heading angles on the response of a 13,000 TEU container ship. However, Drummen [72] already indicated that such methods can produce over conservative results by neglecting the 3D effects.

Panel methods based on Green's functions incorporating hydroelasticity have been used. A validation study of such a method is provided by de Lauzon *et al.* [73]. Kim *et al.* [74] introduces hydroelasticity into a panel method based on Rankine sources. Kim and Kim [75] used this method to carry out sensitivity studies on a 10,000 TEU container ship.

RANS-based methods linking the structural response and the hydrodynamic flow problem are under development, see e.g. el Moctar *et al.* [76], and it is believed that such methods will find further application in the future, see the discussion by Kapsenberg [77].

In this study, flexural modes other than vertical bending are not expected to provide significant response and are not explicitly examined. Container ships, which feature a very open cross-section and are therefore susceptible to torsion, have shown an insignificant contribution from the torsion flexural response to the overall fatigue accumulation due to the high damping of this mode. This effect is demonstrated using in-service measurements by e.g. Ki *et al.*, Storhaug *et al.* and Hageman *et al.* [78–80].

2.3.3. SPRINGING

Dynamic vibrations of the primary hull structure are the result of continuous excitation at frequencies which are close to or higher order multiples of the natural frequency of the vessel. Vibrations in a ship structure due to wave loading is referred to as springing. While whipping response shows a strong decaying behaviour in time, springing shows a

more constant response with an amplitude which is very lowly damped, see the work by Gunseteren [81].

Normally the natural frequencies of ship structures are an order of magnitude higher than dominant wave frequencies. Therefore, springing has historically occurred primarily when a ship is sailing in bow quartering or head seas. In these conditions the wave encounter frequency increases which can result in frequencies close to the hull frequencies. To avoid springing in these conditions, the captain can reduce speed or change heading. Therefore, springing has not been perceived as a major contributor to overall response. However, with the presence of larger and more flexible vessels the natural periods of the hull reduce. Especially nonlinear springing, where the wave period is an integer multiple of the natural period of the hull, is more commonly seen.

Although the excitation forces are different, the development of calculation tools to assess whipping and springing often goes hand in hand because the physical modelling of the hydroelastic response is the same. A general discussion on hydroelasticity in calculation tools is provided in the previous section. Examples where strip theory methods have been applied to specifically assess springing responses are provided by Heo *et al.* and Lin *et al.* [82, 83]. RANS methods can include the higher order springing excitation, as is shown by Hänininen *et al.* [84] for a large cruise vessel.

Some springing response has been observed in the measurements. The effect of springing on fatigue accumulation has been quantified using the strain measurements.

2.3.4. WAVE PRESSURE

In the side shell area, wave pressure acting on the hull plating will result in local deformation of the plates and stiffeners between web frames. Three zones in the vertical direction can be distinguished in the side shell. The top zone is not submerged and is therefore not experiencing any wave pressure induced loads. The bottom zone is fully submerged and experiences a static pressure and an exponential decay of the pressure fluctuations with water depth. The third zone in between the two others is the intermittent wetting area.

As a result of the passing waves, any part of the side shell plating in the area with intermittent wetting can be submerged or non-submerged. While submerged, the plating experiences a static and dynamic pressure in the same way as the submerged structure does. When not submerged, the plating does not experience any pressure. There is a discontinuity in the pressure and consequently in the structural response as a result of the intermittent wetting effect. Further details on the definition of wave pressure can be found in e.g. Cramer *et al.* [85].

The work conducted by van der Cammen [86] shows the importance of wave pressures on the side shell when considering fatigue accumulation. Van der Cammen conducted a systematic analysis of wave pressure induced loads using both model test and in-service measurement data. This work considers the wave pressure deterministically in time-domain including the full nonlinear intermittent wetting effect. Friis Hansen *et al.* [87] discusses the fatigue accumulation in the side shell of a container ship under joint wave pressure and hull girder loads. This analysis is also executed in time-domain. The results of this study were also used by Folsø [88] who showed a satisfactory comparison with a strip theory method, although the author indicates better results may be

achieved by using panel methods.

Diffraction methods assess the wave-induced pressure in frequency domain. However, linear diffraction calculations do not incorporate an intermittent wetting effect. Instead, only the part of the hull below the mean water line is modelled and experiences pressure fluctuations with exponential decay related to water depth. A more realistic description of the wave pressure over the side shell can be obtained using nonlinear pressure models, an example can be found in the work by Bigot *et al.* [89]. Their proposed pressure distribution is shown in Figure 2.5.

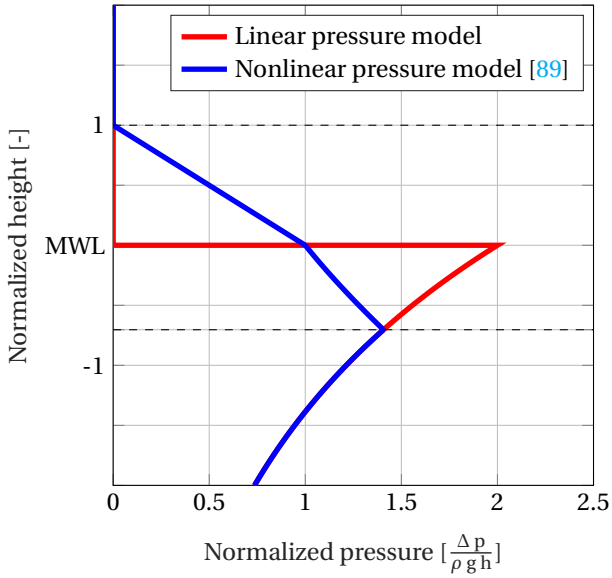

Figure 2.5: Linear and nonlinear pressure models used to describe wave pressure in the intermittent wetting area around the mean water line (MWL).

There is no clear definition of the boundaries of the intermittent wetting area in irregular sea states. Bigot *et al.* [89] evaluated the use of pressure linearisation in the side shell using a definition based on regular and irregular waves. Fatigue assessment of six container ships in irregular sea states were performed by comparing time-domain calculations and frequency-domain calculations. The authors conclude that an intermittent wetting area using a definition with irregular sea states results in a more realistic definition over a larger area compared to the regular wave definition.

For offshore production units, a further complication in the assessment of wave pressure is that the mean water line may continuously change. As a result, the linearisation procedure has to be executed multiple times for representative loading conditions and their associated hydrostatic conditions, see e.g. the method described by BV [90]. At the same time, the changing loading conditions also results in a different part of the side shell being loaded by wave pressures. Hence, the fatigue accumulation is spread over an area rather than a single part of the side shell structure.

2.3.5. LOADING-INDUCED LOADS

Loading and loading operations lead to a relatively small number of high-amplitude stress cycles on cargo supporting structures. These stress cycles can be considerable and even result in local plasticity of the structure. As mentioned by Wang *et al.* [91], loading-induced loads have received little attention from the research community. This is possibly the result of the reasonable predictability of such load cycles. However, Megharbi *et al.* [92] stresses the importance of selecting appropriate loading conditions to determine the large amplitude stress cycles.

As a result of the high stresses in loading cycles, the material behaviour cannot be considered linear anymore. Nonlinear stress-strain relations can be used to calculate the actual strain and associated apparent linear stress, see the procedure by DNV [38]. Under such elasto-plastic material behaviour, the crack growth behaviour is altered. An important overview of the state of the art in this field is provided by Megharbi [93]. This work also discusses a sequence of dedicated tests for longitudinal attachments subjected to loading-induced fatigue. An S-N curve for the assessment of this type of fatigue accumulation was proposed.

2.3.6. THERMAL LOADS

A structure which is exposed to temperature variations is subject to thermal expansion and contraction. When expansion occurs without constraints, it does not result in any stresses in the structure. However, thermal expansion on offshore structures does not occur equally over the entire unit. The submerged part of the structure will be in continuous contact with the sea and experience negligible temperature variations, whereas the upper part of the structure will experience thermal day-night cycles. Moreover, different parts of the structure can be subjected to different exposure to the sun and therefore experience different thermal expansion. The unequal temperature through the structure will induce global bending and lead to mechanical stresses in local areas of the structure. This effect can be identified from its clear dominant frequency content. For the ease of discussion it will be referred to as temperature-induced stress variations.

2.3.7. OMITTED LOADING EFFECTS

Additional loading effects on offshore structures exist. However, in this research the analysis is focused on loads originating from seakeeping or operational effects which exist throughout the hull. Accidental loads such green water loads, as described by e.g. He *et al.* [94] can result in high pressure loads on both deck and superstructure but are not considered here.

Dynamic pressure loading inside cargo and ballast tanks also lead to stresses in the hull structure. The instrumentation setup allowed for quantification of this effect on a very limited number of structural details only. Under this condition, no general statements on the contribution of this load effect on the total fatigue accumulation and the performance of design tools can be made. This load effect has not been examined in this work.

Another source of high-frequency excitation in the hull structure is the result of machinery. However, machinery is often mechanically isolated from the hull structure. Secondly, the resulting stresses will be very localized and not lead to large stress response in

the entire hull structure. Loads from machinery have therefore not been considered in this research.

2.4. SOURCES OF UNCERTAINTY

2.4.1. OUTLINE

In this section, the nature and quantification of uncertainties in fatigue assessments are discussed. The fatigue calculation method as summarized in section 2.2.2 is used as reference. The origin of the various uncertainties in the analysis are summarized in section 2.4.2. In this section, the nature of those sources are addressed. Section 2.4.3 discusses how these uncertainties can be incorporated in the calculations from section 2.2.2.

2.4.2. CLASSIFICATION OF UNCERTAINTIES

The uncertainties in the analysis of fatigue loads can be subdivided into aleatoric and epistemic uncertainties. Aleatoric uncertainties are the result of random variations in environmental and operational conditions. An example is the description of the sea state. This is described using statistical parameters, but the exact wave train at the location of the unit is undefined and subject to chance. A different random realization of the wave field with the same statistical properties may lead to a different fatigue accumulation in those conditions. This type of uncertainty cannot be avoided by improving analyses or models. On the other hand, there are uncertainties which are introduced through modelling choices. These epistemic uncertainties can be influenced by the researchers or engineers by adopting different models and can therefore, to some degree, be mitigated. An overview of the identified sources of uncertainty and their classification is provided in Table 2.2.

Origin	Abbreviation	Type
Long-term environmental conditions	LT	Aleatoric
Short-term environmental realization	ST	Aleatoric
Operating Conditions	OC	Aleatoric
Hydrodynamic model	Hyd	Epistemic
Intermittent Wetting effects	IW	Epistemic
Structural model	Struc	Epistemic
Spectral Fatigue Method	Meth	Epistemic
Strong nonlinear response	HF	Epistemic
Loading fluctuations	OL	Aleatoric
Loading stress variations	LS	Epistemic
Temperature-related loading	Temp	Epistemic

Table 2.2: Classification of uncertainties in a fatigue assessment

2.4.3. INCORPORATION OF UNCERTAINTIES IN FATIGUE ASSESSMENT

The loading components described in section 2.3 have been classified as either low-frequent, wave-frequent or high-frequent loading components. This distinction is important when addressing the uncertainty introduced by these different components. In this work, the wave-frequency loads are assessed using a spectral calculation method. The high-frequency loads, whipping and springing, also relate to environmental conditions. However, this dependency will be characterized by strong nonlinear relations. The low-frequency loads are generally very weakly correlated to the wave environment and therefore require an independent method.

Throughout this section, the uncertainties listed in Table 2.2 will be included as a factor α_i in the fatigue assessment. The subscript i denotes the origin of the uncertainty as listed in Table 2.2. α_i are stochastic parameters that will be determined for individual measurement details. However, these factors will be compared across units and loading effects to examine generalization of these findings.

WAVE-FREQUENCY LOADS

The wave-frequency fatigue accumulation in a sea state is evaluated through the spectral fatigue assessment. The structural response in each condition is obtained through a multiplication of wave spectrum and the square of the RAO of stress in frequency domain. The wave description itself features numerous sources of uncertainty and modelling choices as shown by Bitner-Gregersen *et al.* [95]. These depend on, among others, the presence of multiple wave systems, maturity of the sea state and bathymetry. Tuitman [70] noted the importance of modelling short-crested sea states in the assessment of the structural response. Bitner-Gregersen *et al.* concludes that the wave conditions are often the most significant uncertainty in the prediction of long-term behaviour of offshore units [96].

The stress RAO contains numerous sources of uncertainty. First of all, the hydrodynamic model used to calculate the pressure on the hull introduces some uncertainty due to the discretization of this model. The most common modern hydrodynamic calculation methods are diffraction models which are based on potential theory and therefore neglect viscous damping. To overcome this limitation, empirical parameters are introduced, e.g. to correctly model the roll behaviour. These calculations are repeated for a limited number of loading conditions. The structural model is another source of uncertainty due to numerical discretization and extrapolation to stresses at hot-spots. Typically, the Finite Element Method is applied, see e.g. Zienkiewicz *et al.* [137]. Corrosion is not explicitly accounted for in the structural model. This would require a time-dependent model which represent multiple stages of the corroded condition. Instead, common practice is to use a single condition with intermediate general corrosion in the calculation.

An underlying assumption of the spectral fatigue assessment is that all response is linear with the waves acting on the structure. Weak nonlinearities in the hydrodynamic response will be present. Moreover, the fatigue contribution of wave pressure in the intermittent wetting zone must be linearised, which is introduced in the stress RAOs. The combination of multiple loading mechanisms at a single location will also adversely affect the linearity of the response. Finally, the calculation provides an exact evaluation

of the fatigue accumulation for a time series of infinite duration. In reality, operating times in various conditions are limited and therefore statistical variation in the short term condition is present. The items above all introduce some uncertainty as a result of the assumptions underlying the spectral fatigue assessment. They are represented as different sources of uncertainty because the importance of each individual effect is different depending on the considered structural detail.

The various sources of uncertainty enter the calculation process at different stages. Based on the discussion above, the RAOs as used in equation 2.3, short-term fatigue evaluation in equation 2.10 and long-term fatigue evaluation in equation 2.14 should be modified to account for the various sources of uncertainty:

$$\begin{aligned} RAO^*(\omega|LC) &= \alpha_{Hyd}\alpha_{Struc}\alpha_{IW}RAO(\omega|LC) \\ D^*_{WF}(LC,\theta,H_S,T_P,RAO^*) &= \alpha_{Meth}D(T) \\ D^*_{WF} &= \alpha_{OC}\alpha_{LT}\alpha_{ST}\sum_{LC}\sum_{\theta}\sum_{H_S}\sum_{T_P}p(LC,\theta,H_S,T_P)D^*_{WF}(LC,\theta,H_S,T_P,RAO^*) \end{aligned} \tag{2.16}$$

The star symbol $*$ is used to denote that the contribution of uncertainty is included in the respective results.

HIGH-FREQUENCY LOADS

The springing and whipping responses are strongly nonlinear responses which are related to governing wave conditions. The frequencies of high-frequency responses are typically between 0.5 and 4 Hz. This frequency range is still comparable to the frequency range of the wave-frequency loads which varies from 0.05 to 0.5 Hz. As a result the high-frequency and wave-frequency stresses cannot be considered independent for a fatigue assessment. For offshore units, these responses are generally not explicitly calculated. Therefore, the uncertainty from the high-frequency response is defined directly on fatigue life as assessed using the wave-frequency response:

$$\begin{aligned} D^*_{HFWF}(LC,\theta,H_S,T_P,RAO^*) &= \alpha_{HF}D^*_{WF}(LC,\theta,H_S,T_P,RAO^*) \\ D^*_{HFWF} &= \alpha_{OC}\sum_{LC}\alpha_{LT}\sum_{\theta}\sum_{H_S}\sum_{T_P}p(LC,\theta,H_S,T_P)D^*_{HFWF}(LC,\theta,H_S,T_P,RAO^*) \end{aligned} \tag{2.17}$$

The parameter α_{HF} depends on the different environmental and operating conditions. It should be noted that springing occurs in wave conditions which feature wave components with periods that are an integer multiple of the period of the flexural vibration modes. These are generally benign wave conditions. On the other hand, whipping occurs when the ship is operating in high and steep waves at higher speed. As a result, the high-frequency contribution can be minor in a large number of operating conditions, but can become significant in both very mild conditions, due to springing, or harsh conditions, due to whipping. The remaining uncertainties related to the numerical models and environmental and operating conditions are introduced through the use of D^*_{WF}.

LOW-FREQUENCY LOADS

The low-frequency load components are independent of the wave induced loads. Moreover, the frequency range from the low-frequency is considered to vary between 10^{-7} to 10^{-5} Hz, which corresponds to time scales of days to months. This is very distinct from those of the wave- and high-frequency stress components. For these reasons, the fatigue resulting from low-frequency stresses should be considered independent of the other loading components [36].

Loading-induced fatigue accumulation is independent from the environmental conditions and the choice of hydrodynamic model. It is sensitive to changes in the structural model, e.g. corrosion. Temperature-induced stresses are not included in a fatigue assessment, but can be isolated from the measurements using filtering. They are independent of the other loading processes. The fatigue assessment for low-frequency effects using the design stress range, $\Delta\sigma_{LF'D}$, and the number of predicted offloading cycles, N_{OL}, becomes:

$$D^*_{LF} = \alpha_{OL} N_{OL} \frac{(\alpha_{LS}\Delta\sigma_{LF'D})^m}{a} + \alpha_{Temp} \tag{2.18}$$

TOTAL FATIGUE ACCUMULATION

The total fatigue accumulation is obtained by adding the low-frequency fatigue and the combined wave and high-frequency components in the following way:

$$D^* = D^*_{LF} + \alpha_{OC} \sum_{LC} \alpha_{LT} \sum_{\theta} \sum_{H_S} \sum_{T_P} p(LC,\theta,H_S,T_P) D^*_{HFWF}(LC,\theta,H_S,T_P,RAO^*) \tag{2.19}$$

In this total fatigue assessment formulation, all uncertainties indicated in Table 2.2 are included. The parameters which are not explicitly mentioned in this equation are included in the definitions of D^*_{LF} and D^*_{HFWF} as provided in equations 2.18 and 2.17 respectively.

2.5. UNCERTAINTY QUANTIFICATION

2.5.1. LONG TERM WAVE ENVIRONMENT

The long term wave environment has an important contribution towards the uncertainty on the prediction of fatigue accumulation. This is related to both the accuracy of the predicted environment and statistical uncertainty. These two aspects are independent and can therefore be studied separately. However, both aspects are captured in the parameter α_{LT} from equation 2.16. For turret moored unit, the orientation of the unit with respect to the waves needs to be assessed using a heading analysis.

WAVE STATISTICS

In order to assess the accuracy of the long term predictions, the wave-frequency fatigue accumulation, equation 2.14, will be evaluated using multiple data sets describing the wave environment. Each data set provides a different probability of the long term environmental conditions, $p(\theta, H_S, T_P)$. A cross comparison between the fatigue accumulation obtained with these different data sets is used to quantify the parameter α_{LT}. The

same analysis will be repeated for multiple structural details on multiple units to investigate if the uncertainty varies between these details and how the uncertainty between different units correlates.

During a finite period of time, only a subset of the conditions defined by the scatter diagram is encountered by an offshore unit. The effect of statistical variability of the data can be assessed through a Bootstrap analysis, as shown by Efron and Tibshirani [97]. The design scatter diagram and the operational profile consisting of different load cases and their occurrence are available for the individual units. Per unit, the design data often yields a number of conditions in excess of 10,000 with their associated probability of occurrence. To estimate the uncertainty due to statistical variability in the environmental conditions, the following procedure is applied:

1. Select a number of random environmental conditions. Conditions are assumed stationary during three hour periods. E.g. to assess variability for a ten year period 29,200 random conditions are selected. This resampling scheme is based on Bayesian statistics and is described in more detail by van der Meulen and Hageman [98].
2. Assess the fatigue accumulation in each separate condition at different details.
3. Obtain the overall fatigue accumulation.
4. Repeat steps 1 to 3, 10,000 times

The distribution provided by these simulations provides the part of α_{LT} that relates to the statistical uncertainty.

The procedure above inherently assumes that the individual three hour environmental conditions are independent. This is however not the case and is of special importance for areas that are dominated by storm conditions. Storms result in a number of subsequent bad weather conditions that are strongly correlated. This will increase the statistical uncertainty as the contribution of an individual storm becomes more significant. In order to account for this, the number of conditions can be reduced by assuming a longer stationarity period. Increased periods up to 2 days will be considered for an area that features storm conditions.

The majority of the fatigue accumulation occurs during the production phase in the field. Offshore units are often constructed in East Asia and then transported to their field of operation. The transport of these units from the construction yard to the area of operation is subject to special consideration, because the loads in that condition deviate from the normal operating loads and the resulting fatigue accumulation may be significant even though the duration of the transport is short. Fatigue accumulation is evaluated in the same way as fatigue accumulation during production using equation 2.14. However, a dedicated set of input data on environmental and operational conditions is used. The uncertainty arising from the long-term environmental conditions, α_{LT}, are therefore evaluated separately during the transport and operation.

The fatigue accumulation rate is not constant over the year as a result of changes in the seasons. When studying the long-term fatigue accumulation, this feature does not result in any added uncertainty. However, when interpreting the results of a fatigue calculation over a short duration period, it is important to relate the expected fatigue accu-

mulation in this period against the average yearly variations. The fatigue accumulation per month has been examined to establish the variation in fatigue rate over the year. In order to establish consistent and the most representative results, the average fatigue accumulation per month has been calculated from the locally measured stresses. For each unit, four representative details with different loading characteristics have been selected. The average fatigue rate per month has been normalized with the overall average rate over the entire year for each detail. Because the fatigue accumulation is normalized per structural detail, the results of these representative details can be compared against those of similar details on different units. These results will be influenced by some annual variation, especially for units which operate in highly variable environments and for which less years of data is available.

HEADING OF TURRET MOORED UNITS

The heading of a turret moored units with respect to the waves can be assessed in the design stage using a quasi-static assessment. In such an analysis, the equilibrium between forces from currents, wind and waves is determined. Current coefficients and the quadratic transfer function, to determine second order wave forces, are obtained from diffraction calculations. Wind coefficients are obtained from wind tunnel tests. The heading assessment does not incorporate stick-slip behaviour, if any exists, in the rotation of the turret. Due to the uncertainty in the different analyses and measurements, the true heading of a unit may deviate from that determined in the design stage.

In order to quantify this effect, spectral fatigue assessments will be conducted with different wave direction data as input.

In the first analysis, the wave data as measured in the field will be used. For a comparison with the design assumptions, the wave direction, as predicted during design, will be supplemented. The deviation between these two results can originate from either a difference in the weather conditions used in the design assessment, or from uncertainties in the heading calculation as was discussed above. In order to isolate these differences, a third calculation will be executed using the heading distribution observed in the field. By comparing the results of this calculation with those of the calculation using the design heading distribution, the uncertainty of the heading assessment on fatigue life can be quantified. The highest fatigue accumulation can be expected when the unit is operating in head waves. An additional case with only head sea conditions will also be analysed in the sensitivity study. The wave direction mentioned above refers to the wave system with the largest energy. If multiple wave systems coexist, the relative direction between these components will be maintained.

In summary, the following four sets of wave data are used as input to study the uncertainty arising from the unit heading in the fatigue assessment:

1. Wave data as measured in field,
2. Wave height and period as measured in field, wave direction distribution from measurements
3. Wave height and period as measured in field, wave direction distribution from design
4. Wave height and period as measured in field using only head sea conditions

2.5.2. SHORT TERM WAVE ENVIRONMENT

SPECTRAL SHAPE AND SPREADING

The short term wave environment is modelled using the wave spectrum $S_\zeta(\omega,\theta)$ in equation 2.4. Rather than using a non parametric description for the wave spectrum, a limited set of statistical properties and parametric formulas are often used to describe the wave spectrum. The relation between frequency and direction are considered independent so that $S_\zeta(\omega,\theta)$ can be rewritten as:

$$S_\zeta(\omega,\theta) = S_\zeta(\omega)D_\zeta(\theta) \tag{2.20}$$

In this research, four different spectral wave descriptions have been used. These are the JONSWAP (JW), Bretschneider (Bret), Ochi-Hubble (OH), also known as the Wallops spectrum, and Gaussian (Gaus) spectra, described by the following formulations:

$$S_{JW}(\omega) = \frac{5}{16}H_s^2\frac{\omega_p^4}{\omega^5}(1-0.287ln(\gamma))e^{-\frac{5}{4}\left(\frac{\omega_p}{\omega}\right)^4}\gamma^{e^{-\frac{1}{2}\left(\frac{\omega-\omega_p}{\sigma\omega_p}\right)^2}} \tag{2.21}$$

$$S_{Bret}(\omega) = \frac{5}{16}H_s^2\frac{\omega_p^4}{\omega^5}e^{-\frac{5}{4}\left(\frac{\omega_p}{\omega}\right)^4} \tag{2.22}$$

$$S_{OH}(\omega) = \frac{1}{4}H_s^2\frac{\left(\frac{4\lambda+1}{4}\omega_p^4\right)^\lambda}{\Gamma(\lambda)}\frac{1}{\omega^{4\lambda+1}}e^{-\frac{4\lambda+1}{4}\left(\frac{\omega_p}{\omega}\right)^4} \tag{2.23}$$

$$S_{Gaus}(\omega) = \frac{1}{4}H_s^2\frac{1}{\sigma_G\omega_p\sqrt{2\pi}}e^{-50\left(\frac{\omega}{\omega_p-2\pi}\right)^2} \tag{2.24}$$

The spectral shapes are shown in the left graph of Figure 2.6. All definitions include the significant wave height H_s and the peak angular frequency ω_p. Γ denotes the Gamma function. The remaining parameters are obtained from Hasselmann *et al.* [99], Ochi and Hubble [100] and Wichers [101] and are given by the following values:

$$\gamma = 3.3$$

$$\sigma = \begin{cases} 0.07 & \text{if } \omega \le \omega_p \\ 0.09 & \text{if } \omega > \omega_p \end{cases}$$

$$\lambda = 2.67$$

$$\sigma_G = 0.1$$

The different spreading formulas used in this research are the cos^2, cos^8 and wrapped-normal (WN) spreading formulations given by the following equations. In addition, longcrested (LCr) waves without any spreading are considered as well.

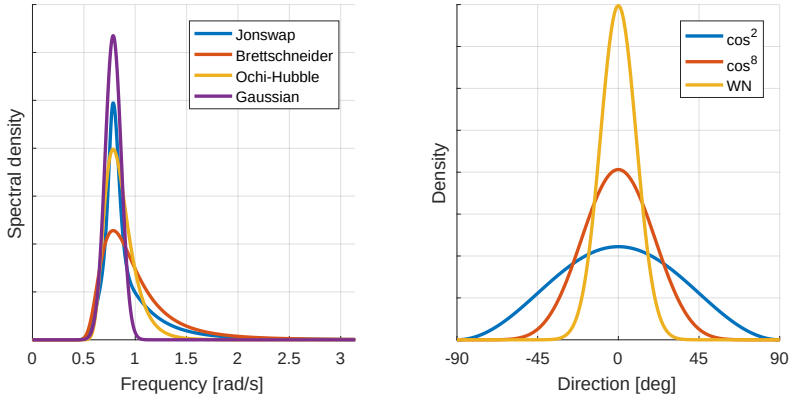

Figure 2.6: Selected wave spectrum and spreading functions. The wave spectra are shown with a peak period of 8 seconds.

$$D_{c2}(\theta_R) = \frac{2}{\pi} cos^2(\theta_R) \tag{2.25}$$

$$D_{c8}(\theta_R) = \frac{2^7}{35\pi} cos^8(\theta_R) \tag{2.26}$$

$$D_{WN}(\theta_R) = \frac{1}{\sigma\sqrt{2\pi}} \sum_{k=-\infty}^{\infty} e^{\frac{-(\theta_R+2\pi k)^2}{2\sigma^2}} \tag{2.27}$$

$$D_{LCr}(\theta_R) = \delta(\theta_R) \tag{2.28}$$

The parameter θ_R denotes the incoming wave angle with respect to the mean direction. All formulations are defined on the interval $\theta_R \in [-180, 180]$ deg and zero elsewhere. The integral of these functions over this interval equals unity for all spreading functions. The parameter σ in the Wrapped Normal distribution is set to 10. For practical purposes the summation over k in this distribution has been limited to $k \in [-6, 6]$, see also the discussion by Jona-Lasinio [102]. The different spreading functions are shown in the right graph of Figure 2.6.

A comparison of the fatigue calculations using the other spectral shapes and distribution functions mentioned above is provided in section 4.3. It should be noted that there are site-specific recommendations on the wave spectrum and spreading. The goal of this study is to examine sensitivity of the fatigue accumulation with respect to such definitions and the site-specific recommendations will be ignored. Some of the calculations will therefore not be representative of actual conditions in a specific area. Unless stated otherwise, longcrested waves with a JONSWAP spectral description are adopted in the other calculations.

MULTIMODAL SEAS

Ocean wave can consist of multiple wave systems that originate from multiple sources. In these conditions, also referred to as confused sea states, wave energy from multiple

directions and with different frequency content can appear. The importance of appropriately modelling these sea states to asses the ship response was already signalled in the early 1990s by, amongst others Kjeldsen [103]. A multimodal sea state can be modelled through the following definition of $S_\zeta(\omega,\theta)$:

$$S_\zeta(\omega,\theta) = \sum_{i=1}^{N} S_{\zeta' i}(\omega) D_{\zeta' i}(\theta) \tag{2.29}$$

The number of components N is area dependent, but is typically limited to 2 or 3. Often one component is used to model developing seas under the local wind field. This is referred to as windsea. The other wave systems propagate from different areas and are called swells. Swells are associated with longer periods and less wave spreading. The presence and characteristics of swell and windsea are site-specific.

In order to quantify the uncertainty associated with the presence of one or multiple wave systems, fatigue calculations will be executed using the unimodal and multimodal sea state descriptions from equations 2.20 and 2.29, respectively. This difference will be assessed for multiple details on various units.

CONVERGENCE OF SEA STATES

Operational and environmental conditions change gradually. In a calculation, conditions are assumed to be constant for a period with finite duration, typically 3 hours. When executing a spectral calculation, the fatigue accumulation is evaluated analytically. However, when executing this analysis in the time-domain, the finite duration of the period will affect the fatigue accumulation. In order to assess this uncertainty, Monte Carlo simulations have been executed in the following way:

- Different wave time series of a 1 metre, 8 second sea state have been generated using the procedure by Tuitman [70].
- Stress time series have been calculated for a structural detail subject to wave bending moment and wave pressure. The unit is assumed to be operating in aft incoming conditions using the stress RAO associated with intermediate draft.
- Fatigue accumulation resulting from the individual stress time series has been calculated using rainflow counting.
- Steps 1 to 3 have been repeated 10,000 times.
- The coefficient of variation of the fatigue accumulation at each detail has been calculated.

This analysis has been executed for time series of durations up to 24 hours in order to be able to address the convergence of this uncertainty with increasing duration.

CONCLUDING REMARKS

The uncertainty from the short term sea state definition, α_{ST}, has been defined in equation 2.16 as an uncertainty on accumulated fatigue life. In principle, this uncertainty is related to operating and environmental conditions and will vary between different sea

states. It could therefore also have been defined as part of the fatigue accumulation per sea state, $D^*_{WF}(T|LC,\theta,H_S,T_P,RAO^*)$. This definition would allow for defining the relation between the uncertainty and environmental and operational parameters. However, because uncertainties in individual conditions can be very large and there are a large number of parameters involved, this will result in complicated relationships which do not necessarily provide good insights and for which it is not straightforward to assess their relevance for other units. Therefore, the aggregated parameter, as defined in equation 2.16, will be studied for a number of different units and structural details in order to appreciate the effect on the total fatigue accumulation.

The epistemic uncertainties discussed in this section are captured by the parameter α_{ST}. However, it should be noted that the statistical convergence only relates to a time-domain assessment. Moreover, in physical sea states, spectral shapes, spreading and multimodality are not independent. In order to gain insight in the relative contributions, the uncertainties of these components are presented individually.

2.5.3. OPERATION EFFECTS

Some operator decisions can influence fatigue accumulation on a floating production unit. One of these is related to cargo handling, which tanks are used and how often offloading is executed. Another operator action which influences fatigue accumulation, is heading control. Both effects are independent and are therefore assessed separately, but can collectively be captured through the use of a single uncertainty parameter, α_{OC}.

LOADING

The loading conditions on an offshore production unit change continuously. These loading conditions influence the response of the unit with respect to the environmental loads. This effect is incorporated in the design calculation of equation 2.14 by using multiple loading conditions, each with a respective probability of occurrence.

Larger units operate according to a fixed load sequence in which trim variations are very small. The draft fluctuations are therefore representative of the changes in the loading conditions themselves. On the smaller units, *SA-AUS* and *NS*, trim fluctuations are more significant. Especially on unit *NS*, which is operating in a harsh environment, the loading conditions may also temporarily be changed to improve seakeeping performance and reduce loads on the hull.

The draft fluctuations for the different units will be quantified from the measurements. The fatigue contribution will be quantified for all structural details by calculating the wave-frequency fatigue accumulation in each of the considered loading conditions separately. By comparing these values, conditions that have a significant contribution to the fatigue accumulations for specific details can be identified.

The combination of the long-term draft information and the fatigue contribution per loading condition can be used to quantify the uncertainty represented by α_{OC}. For each monitored structural detail, the fatigue assessment using the assumed design load profile and the measured load profile will be assessed using equation 2.14. The ratio of these values indicates the typical uncertainty that can be expected from loading conditions during operation.

The direct stresses and associated fatigue accumulation as a result of loading and

offloading cycles is considered separately in section 2.5.6.

HEADING CONTROL

On turret-moored units, the passive heading of a unit is the result of an equilibrium between the yaw moments generated by the various wave systems, winds and currents as well as possible friction forces in the turret bearings of an FPSO. Operators may choose to actively deploy thrusters to orient the unit towards more favourable wave conditions. This procedure is generally applied to minimize motions and in particular roll, to allow maximum efficiency of the production facility. The drawback of this process is that it takes fuel and is therefore expensive. A minimization of the roll motion generally occurs when the unit is oriented with its bow into the dominant wave direction. In those conditions, the unit will be subjected to maximum vertical bending moments. Hence, when applying heading control to minimize roll motions, the fatigue accumulation on structural details subjected to vertical bending moments will increase.

None of the turret-moored units considered in this study is regularly using heading control for orientation. Therefore, this aspect cannot be evaluated for the units. However, section 2.5.1 has discussed a sensitivity study of the fatigue accumulation on turret-moored units with respect to wave direction. The final analysis in this study includes a condition with the dominant wave system from the bow. This condition can be considered a maximum heading control situation and is therefore representative for the maximum difference on fatigue accumulation that can be expected from heading control.

2.5.4. LOAD PROCESSES - WAVE-FREQUENT

The uncertainties related to the calculation of wave-frequency fatigue loads were summarized in equation 2.16. These uncertainties were categorized in two types. First of all, the uncertainties arising from the numerical hydrodynamic, structural analysis and intermittent wetting were denoted as α_{Hyd}, α_{Struc} and α_{IW}. These are defined as factors on the stress RAOs used in the calculation. Secondly, the uncertainties arising from weak nonlinear effects and the calculation method were defined as a factor on the fatigue accumulation, α_{Meth}.

HYDRODYNAMIC AND STRUCTURE UNCERTAINTIES

The uncertainties covered by α_{Hyd} are related to the calculation of hydrodynamic load effects acting on the hull, such as wave pressure and the global bending moments. The uncertainties from α_{Struc} are related to the calculation of local stresses resulting from these hydrodynamic load effects. It is not possible to measure directly the global bending moments on a structure in-service. While it is possible to measure pressures on the hull, this is rarely executed. One measurement campaign on an offshore unit including wave pressure is introduced by van der Boom *et al.* [104], although no pressure measurements were presented. The main drawbacks of pressure sensors is that these require a puncture of the hull and have limited life expectancy in an offshore environment. No pressure measurements are available for this study.

Because information on the hydrodynamic loads are missing, it is not possible to differentiate between the uncertainties arising from hydrodynamic and structural analysis. Therefore, only the product of these two parameters can be quantified using the

measurements. This parameter will be referred to as α_{HS}. In case of a structural detail which is located on the side shell, the intermittent wetting effect is included as well and the parameter will be referred to as α_{HSI}. It should be noted that intermittent wetting is a hydrodynamic effect, but will be treated separately from the global hydrodynamics which warrants the use of a dedicated notation. Whether to include intermittent wetting depends only on the selection of the structural detail to be examined. The mathematical treatment of these two parameters is identical and in the following derivation $\alpha_{HS(I)}$ will be used to represent both parameters.

Recall equation 2.4, which shows the relation between energy spectra and the numerically determined RAOs:

$$S_\sigma(\omega|LC) = \oint_0^{360} RAO_\sigma^2(\omega,\theta|LC) S_\zeta(\omega,\theta) d\theta$$

When both the stress and wave spectra are available, the uncertainty parameter $\alpha_{HS(I)}$ can be quantified using this equation. It should be noted that the RAO is loading condition dependent. It was chosen to determine $\alpha_{HS(I)}$ for each loading condition separately. This will allow the determination of loading condition dependent features, which are especially of importance when analysing intermittent wetting. Conversely, $\alpha_{HS(I)}$ could also be considered frequency and direction dependent. However, wave energy only occurs in a limited frequency range. In the high and low-frequency regions, the signal to noise ratio is very low and poor results will be obtained. Also, information on certain directions may be very sparse due to the preferred direction from the environment and unit orientation. While, in theory, the whole response operator can be estimated using stress and wave information, this was found to be an unproductive course of action by Bonaschi *et al.* [105]. By using a single factor per loading condition, these data limitations are overcome, see the procedure by Hageman *et al.* [17]. The parameter $\alpha_{HS(I)}$ can thus be introduced as follows:

$$S_\sigma(\omega|LC) = \oint_0^{360} (\alpha_{HS(I)}(LC) RAO_\sigma(\omega,\theta|LC))^2 S_\zeta(\omega,\theta) d\theta \tag{2.30}$$

and can be solved using:

$$\begin{aligned} S_\sigma(\omega|LC) &= \alpha_{HS(I)}^2(LC) \oint_0^{360} RAO_\sigma^2(\omega,\theta|LC) S_\zeta(\omega,\theta|LC) d\theta \\ \alpha_{HS(I)}(LC) &= \sqrt{\frac{S_\sigma(\omega|LC)}{\oint_0^{360} RAO_\sigma^2(\omega,\theta|LC) S_\zeta(\omega,\theta|LC) d\theta}} \end{aligned} \tag{2.31}$$

Only periods for which detailed wave and stress data and loading data are available can be used in the analysis of $\alpha_{HS(I)}(LC)$. The parameter can be estimated from a set of wave and stress spectra which is sufficiently representative of the loading conditions and the encountered wave directions and frequencies. An estimate of $\alpha_{HS(I)}(LC)$ from a single or small number of conditions has no practical value.

FATIGUE ASSESSMENT METHOD

The accuracy of the spectral fatigue assessment method in capturing the true fatigue accumulation is captured by the parameter α_{Meth}. The performance of the fatigue assessment method can be quantified by comparing the output of a spectral calculation with that of the measurements during the same time interval. The data from a dedicated wave measurement system will be used to achieve the best possible definition of the wave system. The results of all time windows will be presented in a scatter plot. From this scatter plot, the statistics and distribution of α_{Meth} can be derived.

The analysis of the instantaneous values of α_{Meth} can be used to understand the performance of the fatigue assessment method and its expected level of accuracy. However, fatigue accumulation is a cumulative process. Therefore, under- or overestimation of the fatigue accumulation in a single time interval is of limited importance to the overall analysis. For this reason, the total accumulated fatigue using the spectral assessment method will also be compared to the measured fatigue accumulation. This parameter is referred to as the Tool Accuracy Factor (TAF) and is defined as:

$$TAF = \frac{\sum_{T=T_0}^{T_{end}} D_{WF}^{Meas}(LC, \theta, H_S, T_P, RAO*)}{\sum_{T=T_0}^{T_{end}} D_{WF}^{*}(LC, \theta, H_S, T_P, RAO*)} \tag{2.32}$$

D_{WF}^{Meas} indicates the wave-frequency component of the fatigue accumulation determined from measurements of a strain gauge using rainflow counting, see also Section 2.2.2.

Three assumptions in the spectral fatigue assessment method require further attention. First assumption is that loads are distributed following a Rayleigh distribution. This assumption resulted in an elegant simplification of the fatigue evaluation formula, see equation 2.13. Secondly, the loads are assumed to be linear. However, weak nonlinear effects, such as Froude-Krylov forces, can exist. Strong nonlinear effects, i.e. whipping and springing, are associated with higher frequencies compared to the wave-frequency excitation and are addressed in the next section. Finally, another contribution to α_{Meth} arises from the numerical modelling where only a discrete number of loading conditions have been analysed and used in the long-term prediction.

The narrowbandedness and weak nonlinear effects are studied separately to improve understanding of the underlying assumptions. However, to avoid double counting of these contributions, only the total fatigue method uncertainty α_{Meth} is used in the final evaluation of all uncertainties.

Using a time series of measured stress, fatigue can be evaluated by performing a Rainflow count. This is considered the most accurate way of addressing fatigue accumulation and hence the reference value. In section 2.2.2, it was noted that the Rayleigh distribution of stress amplitudes is uniquely defined by the standard deviation of the stress signal. Hence, for the same time window, fatigue can be evaluated using equation 2.13 using the standard deviation of that signal as input to define the Rayleigh parameter B. A direct comparison between the two approaches can be used to quantify the effect of the assumed narrowbanded stress cycle distribution on the fatigue accumulation.

Some degree of the nonlinearity in the structural response can be quantified by comparing the distribution of positive and negative stress peaks. In a linear case, these two

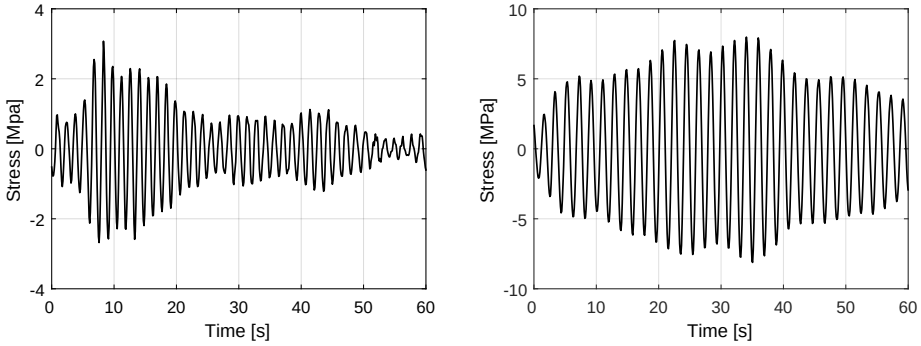

Figure 2.7: Example of a whipping (left) and springing (right) response obtained from unit *SA-AUS* and *WA2* respectively. The response has been derived from a strain gauge measurement after applying a high-pass filter.

distributions are equal. However, when a nonlinearity is introduced, either from Froude-Krylov forces or intermittent wetting, these distributions will diverge. An exceedance plot can be used to quantify this difference. A number of different details will be examined to study the nonlinearity in several representative structural details.

While the factor $\alpha_{HS(I)}$ is accounting for variations in the stress, the nonlinear relation between stress and fatigue accumulation results in a deviation between the fatigue assessment using the new RAO and the true fatigue accumulation. Intermittent wetting in the numerical calculation has been linearised, but the nonlinear nature of this effect will also result in a contribution towards α_{Meth}. So, while the mathematical formulation in equation 2.16 implies a clear distinction between the hydrodynamic and structural analyses on one hand and the fatigue method on the other hand, some overlap between the two uncertainties will exist.

2.5.5. LOAD PROCESSES - HIGH-FREQUENT

The uncertainties as a result of response of flexural modes are quantified using the parameter α_{HF}, as used in equation 2.17. This parameter allows for incorporating the trends between the flexural response and the environmental conditions. These effects include both whipping and springing, as shown in Figure 2.7. This figure shows the different characteristics of whipping, which is characterized by decaying amplitudes after an impact, and springing, which is characterized by a more constant amplitude as a result of resonance. Whipping and springing result in an increase in bending moment loads and are most pronounced in the midship area.

The distinction between whipping and springing can be made visually, but is not straightforward to automate. Also, the parameter α_{HF} does not require an explicit distinction. However, the relation between whipping and springing in relation to the environmental and operational parameters is different. The presence and severity of whipping will be dominated by the significant wave height and period and the related wave steepness. However, the presence of springing will be dominated by the exciting wave period and to some degree by the loading conditions, which influences the natural period of the hull.

To aid interpretation of the findings on α_{HF}, a distinction will be made between these two contributions through conjecture based on the descriptions of the environment and the units as presented in section 1.3. The spread-moored units are all large barge shaped units which have low natural frequencies. They are operated in a benign environment. Hence, these units experience little whipping, but can experience springing because of the low natural frequency of the structure and some wave systems with low periods. On the other hand, unit *NS* and *SA-AUS* are more stiff units with higher natural frequencies, which makes springing unlikely. They are operated in areas known for heavy environmental conditions, which can introduce whipping. Only unit *AUS* is expected to experience both effects, because this is a large unit operating in generally mild conditions, which makes it susceptible to springing, but can also experience whipping during storm conditions. In summary, any high-frequency response observed on the spread-moored units is assumed to be related to springing. The high-frequency response on unit *NS* and *SA-AUS* is assumed to be whipping. On unit *AUS*, the high-frequency response is assumed to be springing, unless the unit is operating in a storm, when it will be considered whipping.

The contribution of the high-frequency effects on fatigue is determined from strain gauge measurements using the filtering procedure described in section 2.3. For each short term condition, a realization of α_{HF} can be determined using the following relation:

$$\alpha_{HF'i}(LC,\theta,H_S,T_P) = \frac{D_{HF+WF'i}(LC,\theta,H_S,T_P) - D_{WF'i}(LC,\theta,H_S,T_P)}{D_{WF'i}(LC,\theta,H_S,T_P)} \tag{2.33}$$

The parameter $\alpha_{HF'i}$ indicates a realization of the stochastic variable α_{HF}. $D_{WF'i}$ and $D_{HF+WF'i}$ denote the fatigue accumulation including only the wave-frequency stress and including both the wave and high-frequency stress, respectively. These values were obtained from a time series using Rainflow counting. The relation between $\alpha_{HF'i}$ and the environmental and operational conditions is mentioned explicitly to indicate that these relationships will be studied. At the same time, the total contribution of the high-frequency effects over the measurement period will be quantified and presented.

As springing is a resonance phenomenon, the natural frequency of the hull and the excitation frequency are of importance. The contribution of springing in individual sea states will be examined in relation to the wave period.

2.5.6. LOAD PROCESSES - LOW-FREQUENT

The low-frequency stress signal, which is described in section 2.3, contains loading-induced stresses and temperature-related stresses. These components feature different frequency content. The global temperature-related effects occur around a frequency associated with a period of one day and the loading effects feature a period between 3 to 20 days. Therefore, the contribution of temperature-related effects can be removed using low pass filtering. A filtering frequency of $4.2 * 10^{-5} rad/s$, corresponding to a period of 1.75 days, is used. A rainflow count on the unfiltered and filtered signal provide the fatigue accumulation with and without the temperature-related effects.

LOADING-INDUCED LOADS

The uncertainty related to loading-induced loads as defined in section 2.4.3 and equation 2.18 contains two sources which are examined further. First is α_{LS}, the multiplicative factor on the observed stress ranges which is the result of the uncertainty in the structural model, corrosion allowance and loading sequences. Second is α_{Load}, a multiplicative factor on fatigue accumulation related to uncertainty in loading frequency.

The factor α_{Load} indicates how often offloadings take place compared to what was expected in the design phase. This parameter is therefore mainly related to productivity of the field and because loading sequences will vary somewhat with time, it is reasonable to assess this factor with a value for each structural detail. A general distribution on α_{Load} can be obtained by determining this parameter on multiple units and structural details.

The actual stress ranges experienced during operations will vary continuously. A full distribution of the loading-induced stress ranges, $p(\Delta\sigma)$, can be obtained from rainflow counting the loading-induced stresses. In order to obtain a distribution describing α_{LS}, these stresses should be normalized using the design stress range as follows:

$$\alpha_{LS} = p\left(\frac{\Delta\sigma}{\Delta\sigma_{LF'D}}\right) \tag{2.34}$$

α_{LS} results in uncertainty both as a result of the bias and of the distribution of this parameter. Four fatigue assessments have been conducted in the following manner to examine the influence of α_{Load} and α_{LS}:

1. Fatigue assessment using design parameters
2. Fatigue assessment using design stress ranges and observed number of stress cycles
3. Fatigue assessment using mean measured stress range and observed number of stress cycles
4. Fatigue assessment using all observed cycles

By comparing the result of the first two calculations, the contribution of α_{Load} is assessed. By comparing the results of the second and third calculation, the importance of the bias in α_{LS} is obtained. By comparing the last two results, the importance of the observed variations in the stress ranges, in other words the variation in α_{LS}, is assessed.

TEMPERATURE-INDUCED LOADS

The fatigue contribution of the temperature-induced effects can be evaluated by comparing the total low-frequent and the loading-induced fatigue component as follows:

$$\alpha_{Temp} = D_{LF} - \sum_{i=1}^{N} \frac{(\Delta\sigma^{m}_{LF'i})}{a} \tag{2.35}$$

In order to gain more understanding of this parameter, the temperature-induced stress cycles can be identified by removing the loading-induced cycles from the total number of low-frequent stress cycles. An example of the distribution and number of these cycles, $p(\Delta\sigma_{TI})$ and N_{TI} will be presented.

2.6. STATISTICAL MODELLING

2.6.1. DEFINITION OF UNCERTAINTY MEASURES

Uncertainties are characterised by bias and scatter. A systematic deviation or bias indicates the accuracy, i.e. a systematic deviation of the calculation method or modelling. The bias is the deviation of the mean value of a parameter from unity. It may indicate that the true fatigue accumulation is larger or lower than predicted using the models. In the latter case, the use of a model or method is effectively introducing an additional implicit safety margin in the fatigue design.

The scatter or precision are the point-to-point deviations of an individual measurement point from the mean value. This is represented using the standard deviation of the parameters. To facilitate comparisons, the coefficient of variation, i.e. the standard deviation normalized using the mean value, is sometimes shown. The coefficient of variation will be presented as a percentage.

Scatter in the data set can be random in which case the scatter indicates an inherent uncertainty in the applied method or model. In some cases, the scatter may also show dependency with certain parameters. If such a trend is observed, it's influence on a long-term load estimate will be discussed.

The bias and standard deviation of these factors will be presented as measures of uncertainty introduced by the individual loading effects. The different correction factors α_i will be determined for multiple structural details and units and, where possible, compared between them.

2.6.2. FITTING OF PROBABILITY DISTRIBUTIONS

For some parameters, the data may be skewed and feature outliers. For such cases, it is convenient to provide a fitted parametric distribution function. In order to estimate the parameters of each family of parametric distribution functions, use will be made of Maximum Likelihood Estimators (MLE), see e.g. Hill and Lewicki [106]. This procedure ensures that the selected parameters are chosen such that the probability of the data set being generated by that distribution function is maximum. In practice, rather than maximizing the likelihood functions, the log-likelihood function will be maximized. This is mathematically equivalent, but has improved numerical convergence.

Different parametric distribution functions will be compared to each other. The comparison can be made graphically and numerically. The graphical comparison will be performed using a quantile-quantile plot (Q-Q plot) as defined by Wilk and Gnanade-

	Skewness	Boundaries	No. of parameters
Normal	No	None	2
Lognormal	Yes	Lower bound	2 or 3
Weibull	Yes	Lower bound	2 or 3
Gumbel	Yes	None	2

Table 2.3: Some fundamental properties of selected families of parametric probability distributions that will be commonly used throughout this research. The use of 2 or 3 parameters in the Lognormal and Weibull distribution depends on whether one allows a shift of the lower bound of these distributions.

sikan [107]. Filliben [108] introduces statistical tests to judge the goodness-of-fit from such a probability plot numerically. The maximum likelihood value itself also provides a degree of the quality of the fit. Procedures with a larger number of parameters will generally result in better fits. At the same time, using a large number of parameters will reduce the general applicability of the model. Other model selection criteria, such as the Akaike Information Criterion (AIC) [109] or Bayesian Information Criterion (BIC) [110], introduce a penalty for using a large number of degrees of freedom in the fit. Both the AIC and BIC will be used to compare the performance of different parametric distributions numerically. For these criteria, a lower score indicates a better model.

Throughout this thesis, the normal, lognormal, Weibull and Gumbel distribution, as defined by Walck [111], will be used. An overview of some basic characteristics of these distributions is provided in Table 2.3.

3

DATA COLLECTION

Accurate and minute measurement seems to the non-scientific imagination, a less lofty and dignified work than looking for something new. But nearly all the grandest discoveries of science have been but the rewards of accurate measurement and patient long-continued labour in the minute sifting of numerical results.

William Thomson - Lord Kelvin

3.1. OUTLINE

This chapter discusses the different types of measurement devices and data sources used in this study. A subdivision is made for systems related to wave measurements, section 3.2, measurements of operating conditions, section 3.3, and measurements of both the global and local responses 3.4. Section 3.5 discusses how data is assimilated and combined.

3

3.2. WAVE ENVIRONMENT

The wave environment provides one of the major uncertainties when assessing the integrity of an offshore unit, both during design as well as during operations. There are various solutions available to obtain wave data. For this research extensive use has been made of wave buoy data, wave radar and hindcast data. Other solutions, such as the level gauge and motion-based wave measurement (MBWM), are also available and, while not used in this study, are briefly discussed. Prior to the availability of measurement systems, visual observations from the crew were used to gain some appreciation of the encountered weather conditions. Table 3.1 provides a summary of the results discussed in the subsequent sections relating to the considered methods and how they are used in this research.

	Buoy	Radar	Level Gauge	MBWM	Hindcast
Availability	60%	90%	95%	95%	100%
Bulk statistics	All	All	No direction	All	All
Spectrum description	Yes	Yes	No	Possible	ERA5
Swell separation	Yes	Yes	No	Possible	Yes
Bias of wave height	Reference value	-5%	+70%	0%	0%
Precision of wave height		10%	0.15m	10%	0.2m
Bias of wave period	Reference value	-1s	0s	0s	2s
Precision of wave period		0.5s	0.6s	12%	2s
Bias of wave direction	Reference value	0°	-	-	0°
Precision of wave direction		5°	-	-	10°
Application	All analysis	All analysis	No	No	Long term analysis

Table 3.1: Summary of properties of the different wave assessment methods with MBWM identifying motion-based wave measurement. The values of the wave radar are partially based on the work by Hanson *et al.* [112]. The assessment of availability is indicative only. An absolute reference on wave data is missing and the numbers related to bias and precision are using the wave buoy as a reference. These numbers are indicative only, additional discussion can be found in the related sections.

3.2.1. WAVE BUOY

Wave buoys, such as shown in Figure 3.1 are generally considered the most accurate way to capture the sea state. These buoys record their motion and infer the wave elevation from these measurements. By accounting for roll and pitch motions from the buoy, the wave directionality can also be determined. This allows the wave buoys to provide spectrum and directionality information. Some smoothing can be applied to obtain a realistic energy distribution. A notable example concerns the energy distribution over the directions which can be captured using a Fourier series expansion of limited order. In such a setup, the estimated Fourier coefficients are provided, rather than an energy estimate for the individual directions, see e.g. Forristall and Ewans [113]. This approach eliminates discontinuity in the measurements, but to accurately capture the directional spreading in nearly long-crested conditions, an extensive series expansion is required.

Wave buoys rely on accelerometer data to obtain wave characteristics. As a result, wave buoys can fail to provide reliable data when accelerations are small. This is the case for long shallow waves, see e.g. van Essen *et al.* [114]. Wave buoys are typically located several kilometres away from the unit and cannot be used to obtain the deterministic wave train at the unit location, but can provide meaningful statistical and spectral data.

To deploy a wave buoy or perform maintenance on it a separate vessel is required. As a result, the wave buoy is both an expensive piece of equipment and, due to the effort required in retrieving and redeployment for maintenance, may be unavailable for prolonged periods of time. When using a wave buoy as primary source of wave data, a second source of data as a backup is advisable. Moreover, in harsh weather environments, Aalberts *et al.* shows that one runs the risk of losing the buoy [18].

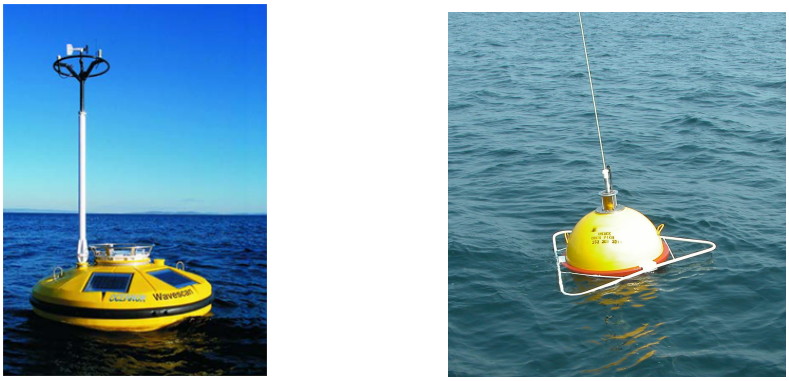

Figure 3.1: Examples of wave buoys

3.2.2. WAVE RADAR

The wave radar is a vessel mounted device which scans the waves of the surrounding area, an example is shown in Figure 3.2. The radar analyses backscatter from the waves which requires some perturbations of the waves through for example wind. A wave radar can therefore operate only with some wind present. The radar will normally issue a warning if insufficient backscatter has been obtained.

Similarly to a wave buoy, a wave radar provides statistical information and frequency and direction dependency of the wave energy, see Wyatt [115]. However, when the radar is mounted on a floating structure, the frame of reference of the radar is continuously changing. As a result, the wave direction and period can be assessed accurately, but due to the vertical motion, the wave height estimates may suffer. Therefore, the wave radar needs to be properly calibrated after installation. Another remedy is to compare the measured motions, notably pitch and heave, against the observed wave field. This procedure is known as wave data fusion and is demonstrated by Thornhill and Stredulinksy [116].

Wave buoys and radars are only rarely used in conjunction in one measurement system[1]. One such occasion is reported and discussed by Hanson *et al.* [112]. Their paper shows that the wave buoy and radar show good agreement in wave heights varying between 2 and 4 metre, but the radar shows a more irregular result than the buoy. The maximum significant wave height, reported by the buoy as 8 metre, shows an underestimation by the radar of over one metre.

Figure 3.2: Wave radar installed on FPSO

3.2.3. LEVEL GAUGE

A level gauge uses an acoustic signal to measure the wave profile underneath the sensor. Rather than using a level gauge to estimate the sea state, these sensors are commonly used to measure the wave profile along the hull of a vessel. Level gauges are mounted directly on the unit hull, as shown in Figure 3.3. As a result the wave measurements take place in the diffracted wave field around the units hull. This effect can be reduced if the sensor is mounted under an angle with respect to the horizontal plane. However, the measurement range of the sensor should allow for this tilted placement.

When mounted on the side of an FPSO, the average distance to the mean water level slowly, but continuously changes with draft variations. The measurement range of the level gauge should accommodate to capture the whole range of drafts. Since these draft variations occur very slowly, they are not a problem when determining the significant wave height. The wave-frequency motions like heave and pitch can have an effect on perception of the wave height from this sensor. Measurements from accelerometers can be used to improve the wave height estimates from level gauges.

[1] As a wave radar is vessel mounted, there is no risk of losing the device in bad weather. On top of that, maintenance on the wave radar is easier compared to a wave buoy as it does not require the assistance of a separate vessel for retrieval. However, a wave radar remains an expensive piece of equipment [117].

Figure 3.3: Level gauge, as mounted on the hull of an FPSO

The performance of a level gauge mounted on one of the offshore units is shown in Figure 3.4. The level gauge is able to provide relatively accurate results on the wave period. The wave height measurements are perturbed through the diffracted wave field and vessel motions. Because the level gauge provides a point measurement, no information on wave directionality can be extracted from a single sensor. Because of these reasons, the level gauge was dismissed as a measurement device in this work.

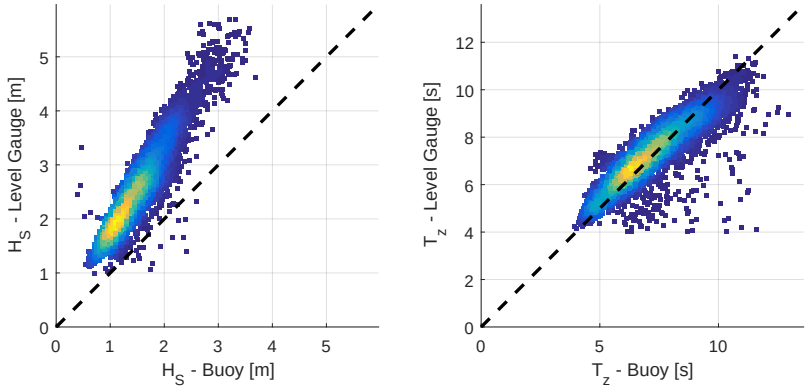

Figure 3.4: Statistical parameters obtained from a level gauge compared against those of a nearby wave buoy. The wave height obtained from the level gauge shows a systematic deviation from the wave buoy as a result of vessel motion and diffraction. The wave height from the level gauge shows a 70% higher wave. After removing this systematic deviation, the remaining scatter has a standard deviation of 0.15 metre. The scatter in the results of the period has a standard deviation of 0.6 seconds.

3.2.4. MOTION BASED WAVE MEASUREMENT

Because of the challenges involved in direct wave measurements a number of procedures using the response of the units have been devised. These methods are often based on motion measurements, but can also include other types of global responses such as bending moments, see for example Thompson *et al.* [118]. These methods require transfer functions between the units response and the wave field in all relevant operating conditions.

Methods based on response measurements can be used to estimate parametric or non-parametric sea states. Parametrization can also be executed in several ways. An overview of the most common procedures is provided by Nielsen [119]. Another example of this application for a ship during trial conditions is provided by Pascoal *et al.* [120]. Details of the accuracy of such an approach are provided by Nielsen [119]. This work shows an accuracy of around 10% on wave height in conditions ranging between 2 and 4 metre significant wave height and around 12% for zero-crossing periods ranging between 8 and 10 seconds.

Machine Learning methods have been deployed to obtain sea state description using response measurements. An inherent drawback of these methods is that they require data to develop the model before it can be used. A possible solution is the use of numerically generated data. An example of the integration of numerical and in-service data to strengthen the procedure is provided by Düz *et al.* [121]. Both parameter estimation and non-parametric sea state estimation can be executed using the same interpretation framework as shown by Scholcz and Mak [122].

Due to the specialized methods required and availability of other data sources, the use of response measurements to obtain wave statistics have not been used in this work.

3.2.5. HINDCAST

Wave models can be used to predict wave propagation under wind excitation. Using wind forecasts, the wave propagation models can be used to predict wave conditions in the near future, which is a wave forecast. Applying the models in hindsight by using the wind fields obtained from satellite measurements, hindcast wave data is obtained. Information from a number of hindcast wave models is made publicly available. These models operate on a global grid. Local details in specific areas are therefore not included. These local details can be relevant for areas which feature complex bathymetry, shallow water or areas with upwind islands. For such areas, local models can improve on the results obtained by global models. Because of their almost guaranteed availability, hindcast data were found to be an important additional data source to supplement the in-service measurements and will be discussed in detail. In this research, only results from the global models were used.

WAVEWATCH-III is a third generation wave model developed and used by the US government agency NOAA, see also Tolman [123]. Statistical wave data obtained from this model is made available by various institutions. Data of the model used in this study covers the world between 77° Northern and Southern latitude. The data points for the prediction are provided at every 1° latitude and 1.25° longitude at intervals of 3 hours. Comprised in this data set are significant wave height, period and direction. The data is available since 1999.

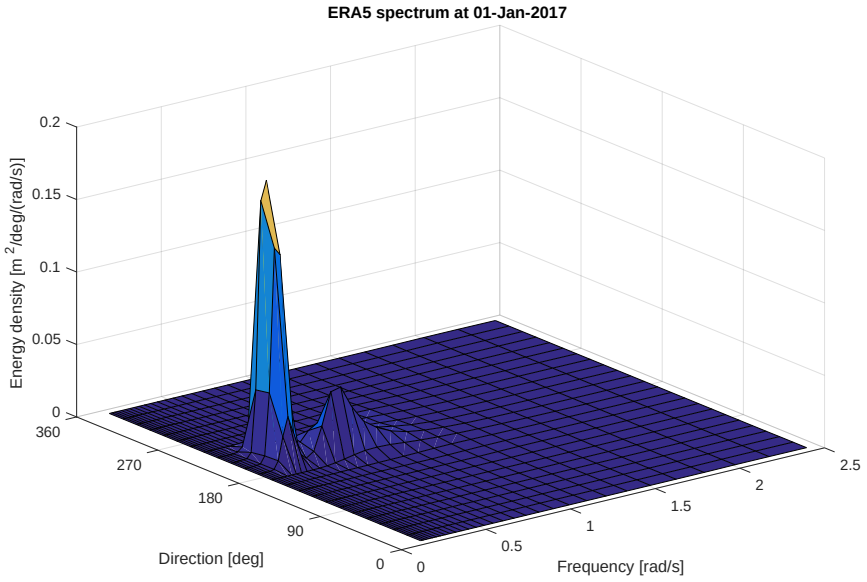

Figure 3.5: An example of a wave spectrum provided by ERA5. The spectrum shows a clear swell peak and a minor peak resulting from windsea from the south-southwest wave direction.

The wave propagation model underlying the Copernicus data is the third generation wave model from ECMWF. This model uses wind data as excitation in the wave propagation model, but also includes a correction based on a limited number of in-situ wave height observations. The model covers the world except the area south of the 80° Southern latitude and the time interval is 3 hours. The data is provided at a resolution of 0.083°, which is much more detailed than the WAVEWATCH-III model. Because of the finer grid and the wave height corrections, Copernicus can outperform WAVEWATCH-III, especially in local developing wind conditions. The data set contains bulk wave statistics, but also statistical data on three separate wave systems including windsea and two swell components. The data of Copernicus is however relatively new and only available since April 2016. See also the discussion by Janssen *et al.* [124].

ERA5 hindcast data is another implementation of the ECMWF wave model with a time interval of 1 hour and spatial resolution of 0.25°. The ERA5 data provides not only the statistical hindcast data, but also full spectral information, an example of which is shown in Figure 3.5. This data is an intermediate result of the wave model, but due to its size, many metocean providers do not store this data or make it publicly available. ERA5 covers the majority of the earth surface, but due to the large volume of data, public access is somewhat controlled. The data of ERA5 is available since 1950, although the specifications of the data changes over time. See also the information provided by Hersbach *et al.* [125].

A brief summary of the different hindcast models is provided in Table 3.2. A com-

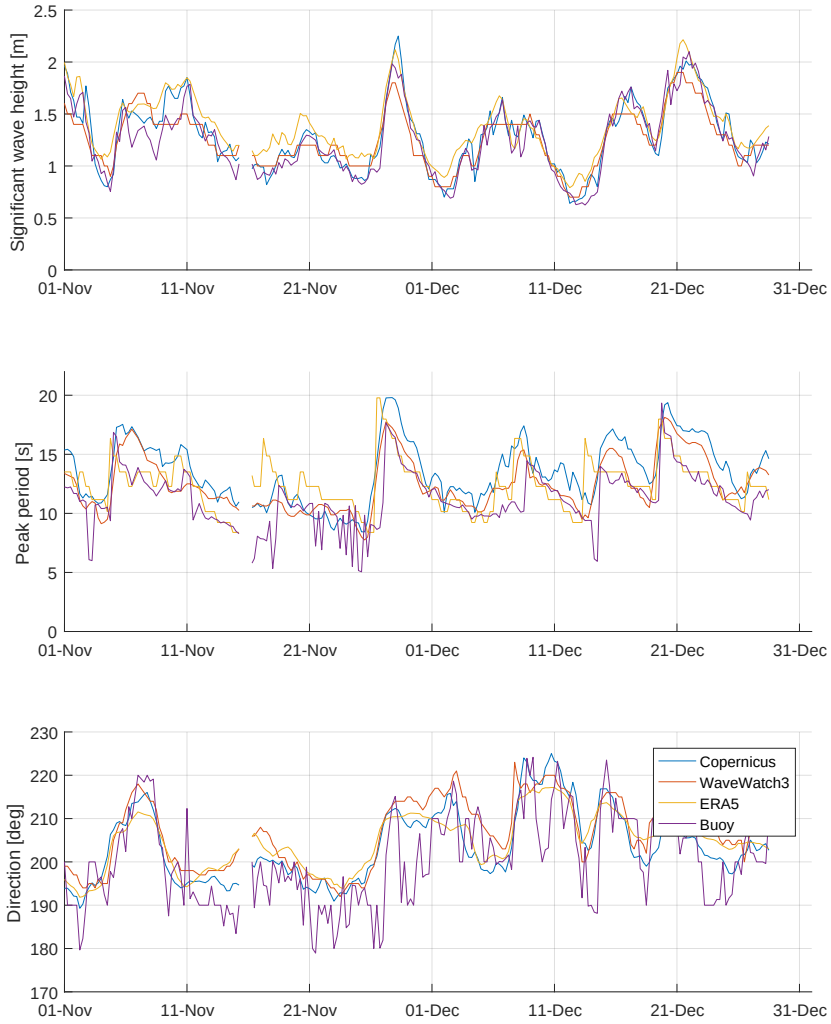

Figure 3.6: Time series of statistical data obtained from wave buoy and hindcast data at the location of *WA*3.

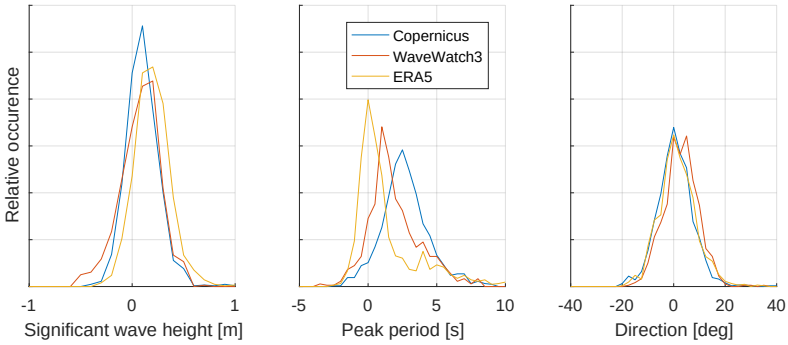

Figure 3.7: Deviation of the statistical parameters obtained from the hindcast model with respect to the wave buoy statistics at the location of units *WA*3 and *WA*4. Similar numbers have been found at the location of *WA*1 and *WA*2 and therefore these numbers are thought to be representative of the West-Africa region.

parison of statistical parameters obtained from the hindcast models over a two month period can be found in Figure 3.6. This figure presents one year of statistical properties near unit *WA*3 compared to the wave buoy. The hindcast data follows the trends shown by the wave buoy data accurately. The deviation of the statistical properties of the hindcast models with respect to the wave buoy have been calculated. The distributions of the deviations are shown in Figure 3.7 and the summary statistics are shown in Table 3.3. Note that, although many hindcast models provide multiple wave components, only data from Copernicus has been used in this way over the course of this research.

The hindcast models provide a significant wave height comparable to the wave height measured by the buoy. It should be noted however, that the West-Africa area has a very benign environment and more significant deviations have been observed in storm conditions, see e.g. Plouvier and Hageman [126]. The periods calculated by the hindcast models are mostly overestimated compared to the buoy measurements. Waves with a higher peak period are longer and propagate faster through the ocean. Apparently, the hindcast models overestimate the growth of the length and speed of the waves. The period obtained from ERA5 is on average closest to the buoy measurement. However, a number of outliers result in a larger standard deviation compared to the other models. The deviation of the wave direction is fairly symmetrical and limited to a range of 20 degrees in both directions.

	Copernicus	WaveWatchIII	ERA5
Available since	April 2016	1999	1950
Grid size [deg]	0.083	1(Lat)/1.25(Lon)	0.25
Multiple wave components	Yes	Yes	Yes
Provides spectrum	No	No	Yes
Wave height assimilation	Yes	No	No

Table 3.2: Summary of properties of the different hindcast models.

		Copernicus	WaveWatchIII	ERA5
H_S [m]	bias	+0.10	+0.08	+0.19
	std	0.16	0.20	0.17
T_P [s]	bias	+2.7	+1.9	+1.3
	std	1.7	1.9	2.3
θ [deg]	bias	+0.5	+2.7	+1.4
	std	7.4	7.1	7.7

Table 3.3: Summary of the deviation of wave statistics related to the measurements in the West-Africa region presented in Figure 3.6.

	Windsea	Primary swell	Secondary swell
Wave buoy			
Presence [%]	16	100	60
H_S - average [m]	0.55	1.18	0.58
T_P - average [s]	4.2	11.5	7.4
θ - average [deg]	196	203	200
Wave energy [%]	3	85	12
Copernicus			
Presence [%]	23	100	85
H_S - average [m]	0.32	1.18	0.60
T_P - average [s]	2.9	12.4	13.2
θ - average [deg]	185	203	208
Wave energy [%]	1	81	18

Table 3.4: Summary statistics of the individual wave components obtained from the wave buoy and Copernicus hindcast data of the year shown in Figure3.6. The wave energy contribution has been calculated using the significant wave height from each wave system.

The wave spectrum as obtained by the buoy has been subdivided into multiple swell components and windsea using the method presented by Hanson [127]. Each of these wave components can be described by another triplet of statistical parameters containing wave height, period and direction. In this study, the sea states are subdivided into at most three wave systems, one windsea and two swell components. The statistical parameters obtained after subdivision into multiple components are shown in Figure 3.8. This figure also shows the statistical data for multiple wave systems obtained from the Copernicus hindcast model. A summary of statistical data of an entire year is presented in Table 3.4.

It can be observed that there is a very good match between the primary swell components obtained from both data sources. However, there are some differences between the windsea and secondary swell components. The discrepancy on the period can partially be explained from the measurement method of the wave buoy. The provided frequency components have a limit at $0.35Hz$ or $2.9s$. As a result, the wave buoy cannot represent waves with a period below $2.9s$. Moreover, waves with high periods and low amplitude result in small accelerations which are harder to measure by the wave buoy.

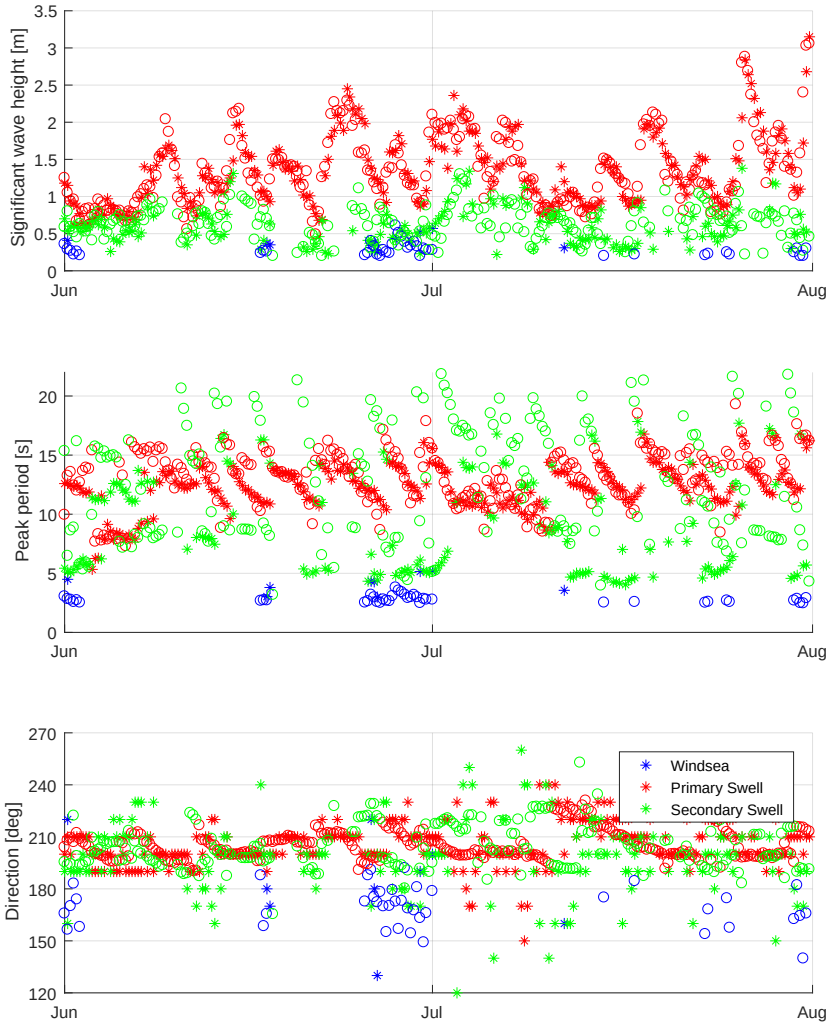

Figure 3.8: Time series of statistical data at the location of *WA*3 separated into 3 wave systems. The stars indicate results obtained from the wave buoy and the circles show data from Copernicus. A minimum wave height of 0.1 metre was used.

This contributes to the smaller periods which the wave buoy returns for both swell components. In both cases, the primarily swell component covers over 80% of the total wave energy.

The measurements in Table 3.4 confirm that the West-Africa region is strongly dominated by a south to south westerly swell. Additional data at the location of unit *NS* and *AUS* has been obtained from Copernicus and is presented in Table 3.5. In these areas, especially the Atlantic ocean area, the wave environment features a stronger multimodality. The windsea and secondary swell are present more frequently and also contribute significantly, especially the windsea, to the total wave energy with combined values around 40 to 50% while this was only 20% in the West-Africa region. Unsurprisingly, the wave height and period of the windsea component in the Atlantic Ocean are significantly higher indicating stronger and more frequent wind in this area.

Section 4.2 discusses the influence of the measurement accuracy and other characteristics of the hindcast models on the fatigue life in more detail.

	Windsea	Primary swell	Secondary swell
NS			
Presence [%]	85	99	93
H_S - average [m]	1.57	2.06	0.84
T_P - average [s]	5.5	11.3	10.1
θ - average [deg]	192	226	180
Wave energy [%]	37	54	9
AUS			
Presence [%]	46	99	84
H_S - average [m]	0.71	0.86	0.46
T_P - average [s]	3.9	11.0	12.0
θ - average [deg][2]	195	217	206
Wave energy [%]	28	58	14

Table 3.5: Summary statistics of the individual wave components of one year obtained from Copernicus hindcast data for two other operating areas.

3.3. OPERATING CONDITIONS

Loading computers are a vital part of the operation of an offshore production unit. These systems visualize measurements of the individual tank contents, including volume, level and density. There is a variety of tanks onboard, such as cargo, ballast, potable water and fuel tanks. Based on the current tank levels and the units hydrodynamic model and configuration, the loading computer will derive hydrostatic parameters and still water bending moments at a number of sections. Information from the loading computer is necessary to properly assess fatigue loads related to loading. This includes variations in stress levels of loading-induced fatigue as well as variations in the still water bending moment.

[2] The actual wave field consists at this location consists of a Easterly and Southwesterly component. The directions displayed here contain interference between these two components.

In one of the systems, a digital link between the monitoring system and the loading computer was not implemented[3]. Instead, use was made of the regular noon reports, provided once per day. Loading conditions change only gradually and noon reports are typically sufficient to address global loading effects. However, because changes in individual tanks can occur more rapidly, the noon reports will be insufficient to address specific tank supporting structures.

In order to assess the relative wave and wind direction, the heading of the unit must be monitored. This is especially important for the units equipped with a single point mooring system. These systems will be able to weathervane in accordance with the prevailing environment or be oriented for operational purposes. On spread-moored units the variation of heading is very small and the orientation of the unit is already known with reasonable accuracy. Still, also for these systems, heading information is included in the analysis. A normal GPS requires forward speed to estimate the direction and will therefore not provide reliable results in stationary conditions. A dual antenna GPS or Gyrocompass system can accurately provide such data. According to Minnebo *et al.*, the heading obtained from such systems has a measurement accuracy in the order of magnitude of 0.1 deg [128].

3.4. RESPONSE MEASUREMENTS

3.4.1. MOTIONS

The rigid body motions of an offshore unit can be registered. The centre of gravity of such a unit is normally in the production area with restricted access. Moreover, the centre of gravity is continuously shifting due to production and storage. Offshore units are generally considered rigid and any flexural deformations will be limited. In that case, motion measurements can be conducted anywhere on the unit and transformed to a reference location using translation formulas.

Motion reference units are normally composed of accelerometers and gyroscopes. The accelerometers are used to obtain linear translation and the gyroscopes are used to derive rotation motions using appropriate integration and filtering procedures. The RMS of the accuracy of the measured motions are in the order of 5 cm and of the measured rotations are around 0.03 deg [129]. For the purpose of this study, motion measurements are only used as a supporting source of information. No conclusions are solely based on motion measurements.

3.4.2. ACCELERATIONS

Accelerations on various locations of the hull can be monitored using accelerometers. Such sensors are rarely used for hulls which are considered rigid, but are used more frequently in hulls which have significant flexural deformation, see the example by Koning and Kapsenberg [130]. Drummen *et al.* uses an array of accelerometers to estimate the rigid body motions [69]. The RMS of the accuracy of high performance accelerometers is around 0.01 m/s^2 [129].

[3] Retrieving this data in an offshore environment for use in a structural monitoring system is subject to cybersecurity concerns.

Figure 3.9: An encapsulated strain gauge after installation.

3.4.3. STRAINS

Depending on the monitoring strategy, strain gauges can be installed at several locations in the hull structure. In order to monitor the fatigue accumulation as closely as possible, one would like to install strain gauges near the critical locations, the hot-spots. However, there are some challenges in doing so. First of all, the stress field near hot-spots is complicated resulting in high sensitivity due to sensor placement, both in orientation and location. Secondly, there are numerous hot-spots in the structure which means that one either has to select a limited number of locations to analyse or spend a large amount of time and budget on installation and analyses. This will generally also reduce the attention given to the individual measurement locations. Lastly, Phelps and Morris note that such sensors often have a limited life expectation [131].

Proposed initially by Kaminski [132], an alternative approach uses sensors on a number of non-critical locations, called cold-spots. These locations feature a simple stress field making them suitable for comparison with numerical tools, but less suited for assessment of the condition of structural details. The strain gauges used in this research are installed at cold-spots, which suits the goal of this research. Because of the uniform strains at the measurement locations, the local stresses can be determined by multiplication of the strains with Young's Modulus. The phrase 'structural detail' normally pertains to hot-spot locations. In the course of this research, structural detail or measurement detail will be used to refer to measurement locations at cold-spots as well.

Two different types of strain sensors will be used in this research. These are traditional strain gauges which have dimensions of a couple of centimetres. These sensors can be installed in virtually any location and orientation, provided that access is available. These sensors use the principle of a full Wheatstone bridge circuit, see e.g. Hoffman [133]. Through the combination of resistors in the sensor, the deformations resulting from temperature changes are not measured provided that the change in temperature in the sensor and underlying structure is the same [131]. This is called a temperature compensated sensor.

Another type of strain gauge is the Long Base Strain Gauge (LBSG). These are rods with lengths between 1 and 2 metre which are fixed to the structure at one end. The displacement at the other end is measured using a Linear Variable Displacement Trans-

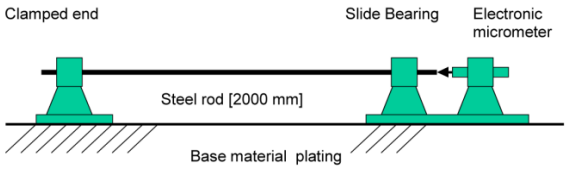

Figure 3.10: Schematic representation of a Long Base Strain Gauge by Koning [134].

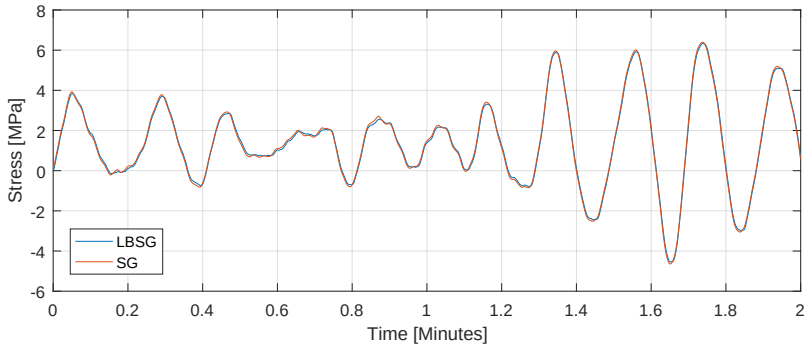

Figure 3.11: Comparison of measurement signals obtained from LBSG and SG installed at the same location.

ducer (LVDT), see also Figure 3.10. An LBSG effectively provides the average strain over the rod location and therefore provides a somewhat more smooth signal compared to the smaller sensor. LBSGs are also used to derive global bending moments. For this aim, they are frequently installed near longitudinal bulkheads.

An example of the measurement signals of the two types of sensors, installed at the same location, is given in Figure 3.11. The deviation in the latter figure has an RMS of 0.1 MPa. A cross-comparison of different types of strain sensors by Lydon *et al.* [135] showed an accuracy of these sensors of around 0.2 MPa in a different industrial application.

A typical installation of sensors as used in this research is shown in Figure 3.12. Three typical locations are instrumented. These are the main deck on top of a longitudinal bulkhead, side shell near the neutral axis and central stringer. At the deck location, deformations are governed by vertical and to a lesser degree horizontal bending of the hull. The installation of both types of sensors in this example is for redundancy only and is not present on all units. At the side shell, the deformation is governed by wave-pressure induced local bending and horizontal bending of the hull. The sensor mounted on the stringer registers cargo induced loads and some horizontal bending. These last two sensors are installed near the neutral axis. At this location, the stress originating from the vertical bending moments are the smallest which results in deformations dominated by either wave pressure or cargo loads. Furthermore, not all units feature sensors installed on the stringers.

The instrumentation as shown in Figure 3.12 is present on both starboard and port

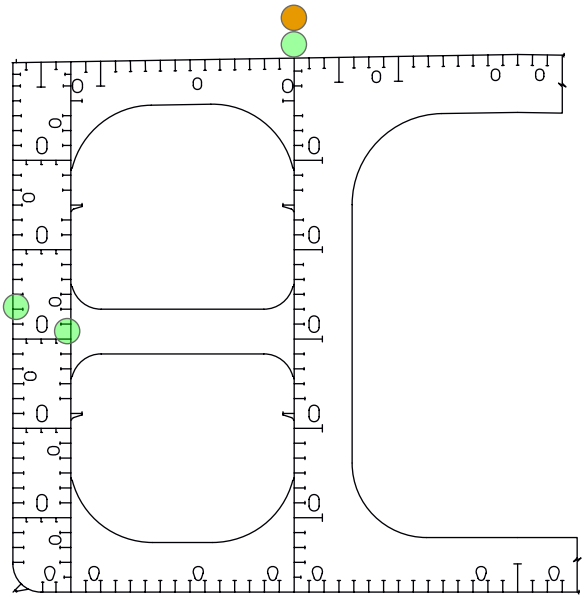

Figure 3.12: Configuration of Strain Gauges in a unit cross-section from Hageman *et al.* [17]. The green markers indicate small strain gauges, while the orange marker denotes an LBSG.

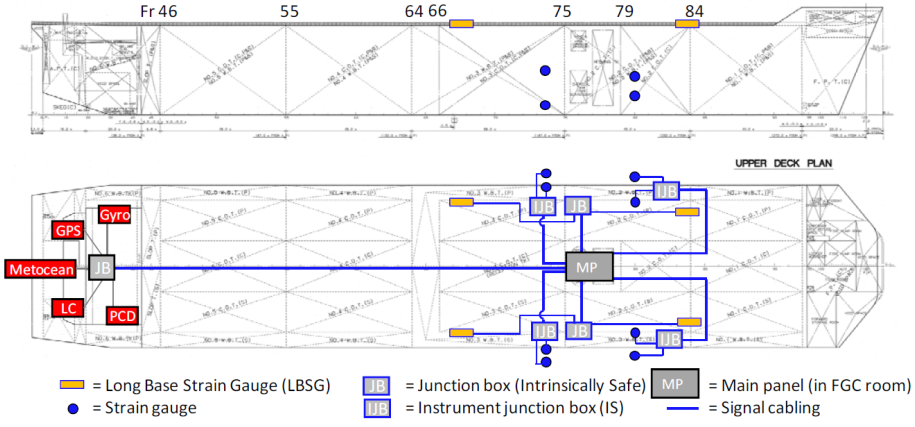

Figure 3.13: Example instrumentation plan as presented by Aalberts *et al.* [136].

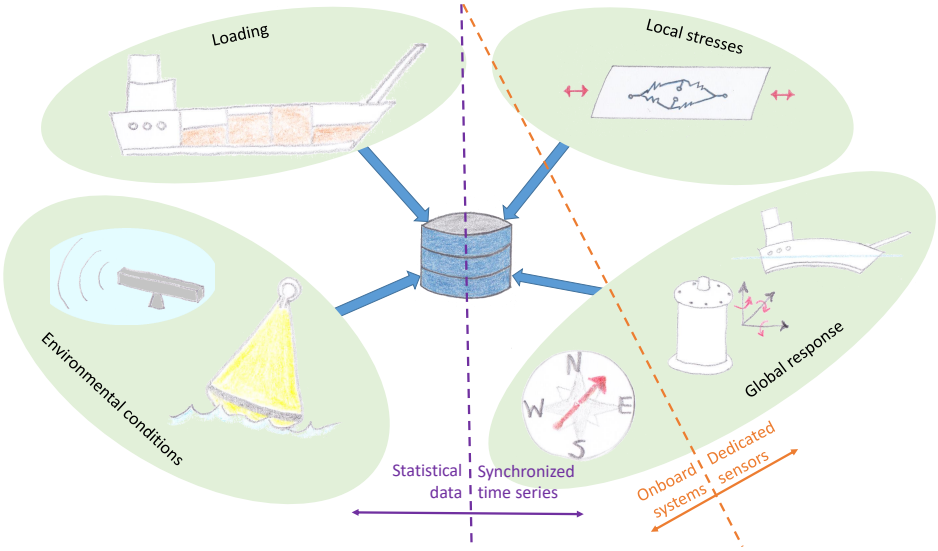

Figure 3.14: Configuration of an onboard measurement system.

side. Typically, two sections are instrumented in this way, one of which is close to midship. This is shown in the example instrumentation plan in Figure 3.13. Occasionally, data from additional sensors will be available. Examples of additional instrumented locations are bottom longitudinals, additional side shell stiffeners and webframes. However, to facilitate comparisons between different units, results from these sensors will not be presented in this thesis.

3.5. DATA ASSIMILATION

Various types of measurement data from multiple sensors are gathered and need to be stored in a consistent and meaningful manner. An overview of the sensors and systems which are connected to the monitoring system are shown in Figure 3.14. The central data collection system can be placed at any convenient location onboard. Some monitoring systems are used for multiple goals and data from such systems can be directly stored by the Hull Structure Monitoring system. Typically, an environmental system, loading computer and gyrocompass are systems which are readily available. These are connected through a communication link and the remaining dedicated sensors can be connected to data acquisition systems. Strain gauges will be located at some distance and require amplifiers in order to transmit the signal reliably over longer distances.

As was discussed in this chapter, the monitoring instrumentation varies slightly between the individual units. The most important differences are listed in Table3.6. This table shows whether two sensors have been used at each deck location for redundancy purposes, whether the stringers have been implemented and the type of wave monitoring system that has been used. It should be noted that for each unit, hindcast data has been retrieved to support the wave measurements. This table also provides an indication

	*WA*1	*WA*2	*WA*3	*WA*4	*NS*	*AUS*	*SA-AUS*
Available data [years]	2	7	4	5	2	3	3
Redundant sensor on deck	no	yes	no	yes	no	yes	yes
Stringers instrumented	yes	yes	yes	yes	no	yes	no
Wave buoy or radar	buoy	buoy	buoy	buoy	radar	buoy	both

Table 3.6: High-level summary of the data and instrumentation present of the various units considered in this study.

of the amount of data that is available from each unit at the execution of this research. It should be noted that only full years of data have been used to ensure that seasonal effects do not come into play.

Strain gauges are analogue sensors which respond electrically on the current applied to the sensor. Timing and synchronization can be controlled very accurately for analogue sensors. Sensors providing digital input to a central storage system may be subject to some latency. The processing executed by the motion sensor and gyrocompass are quick and little latency can be expected. The processing executed by the loading computer and environmental system is more significant and more latency will be present. Environmental systems often provide statistical properties or a frequency-domain representation of the wave conditions. These systems provide information on slowly varying characteristics and the statistical parameters, which are less time-critical. The provided information is therefore sufficient for the purpose of this study.

4

UNCERTAINTY QUANTIFICATION

All models are wrong, but some are useful

George Box

4.1. OUTLINE

This chapter presents the quantified uncertainties related to various sources as discussed in chapter 2. These uncertainties have been determined through in-service measurements or simulations using the procedures described in section 2.5. Section 4.2 discusses the uncertainties related to the definition of the long-term wave environment including the on-site and transport periods. The sensitivity with respect to the definition of the short-term wave environment is covered in section 4.3. Section 4.4 addresses the uncertainties arising from operation of the unit. Finally, the uncertainties of the individual load processes are discussed. These are separated into wave, high and low-frequent effects and are discussed in sections 4.5, 4.6 and 4.7 respectively. Section 4.8 provides a summary of the observed uncertainties.

4.2. LONG TERM WAVE ENVIRONMENT

4.2.1. OPERATION

WAVE DATA SOURCES

Fatigue assessments during on field operations have been executed using a one-year data set to address the uncertainty in long term wave statistics according to section 2.5.1. Measurements from a wave buoy and statistical data obtained from hindcast models, as described in section 3.2, were used. A comparison of the statistical data itself is shown in Figure 3.6 and 3.7. The fatigue accumulation for four selected structural details of unit *WA4* is shown in Figure 4.1. For each calculation, wave statistics have been retrieved from either the wave buoy or one of the hindcast models. Longcrested waves with a JONSWAP spectrum were assumed. The selected structural details are located symmetrically on port and starboard side. At each side two details have been selected which are located on the deck and in the side shell, see also Figure 3.12. At the deck sensor, the loading is dominated by global bending loads, while the sensor in the side shell has been located near the neutral axis and the stresses at this location are therefore dominated by wave pressures. The same analysis for similar details on unit *AUS* has been executed and its results are shown in Figure 4.2. The calculation only serves to compare the fatigue accumulation based on different sets of wave statistics. The calculation is performed to gain insight in the influence of variability in wave statistics and understand the applicability of each data set for a long-term fatigue assessment. No comparison between the different units is made at this stage.

The results on unit *WA4* show a very gradual fatigue accumulation on all details. The details with dominant wave bending loads show a difference in fatigue accumulation of up to a factor 2 between the different hindcast data sets. The fatigue accumulation calculated using the wave buoy measurements is considerably lower. Table 3.3 and Figure 3.7 showed that the hindcast models provide only a slightly higher estimation of the significant wave height and total wave energy. However, the buoy provides a significantly lower wave period than the hindcast data. Figure 4.3 shows that the peak of the stress RAO at these locations is associated with a frequency of $0.45 rad/s$ which is equivalent to a period of $14 s$. These structural details experience very little stress as a result of waves with frequencies above $0.65 rad/s$ or periods below $10 s$. Figure 3.6 shows that the peak periods of the buoy are somewhat smaller than those obtained from the hindcast mo-

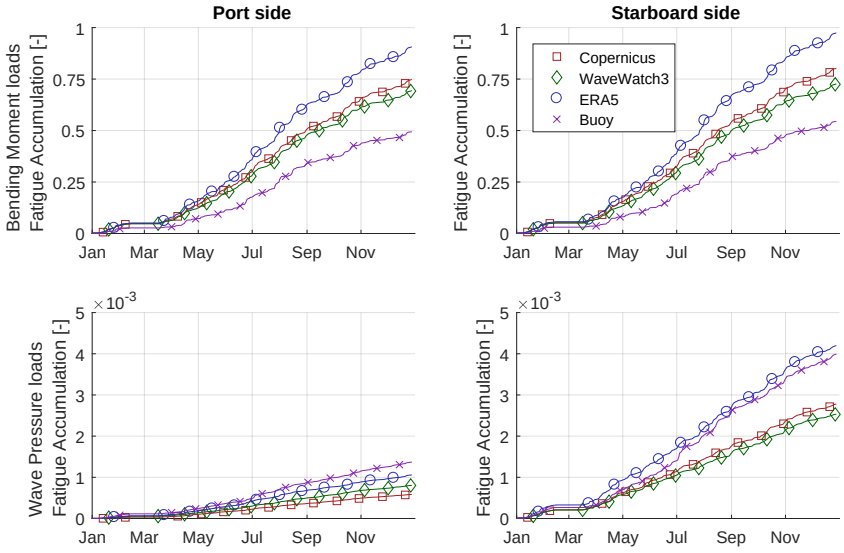

Figure 4.1: Fatigue accumulation on four typical details during one year on unit *WA4*. The fatigue accumulation has been normalized using the design yearly fatigue accumulation of the port side location subjected to bending moment loads.

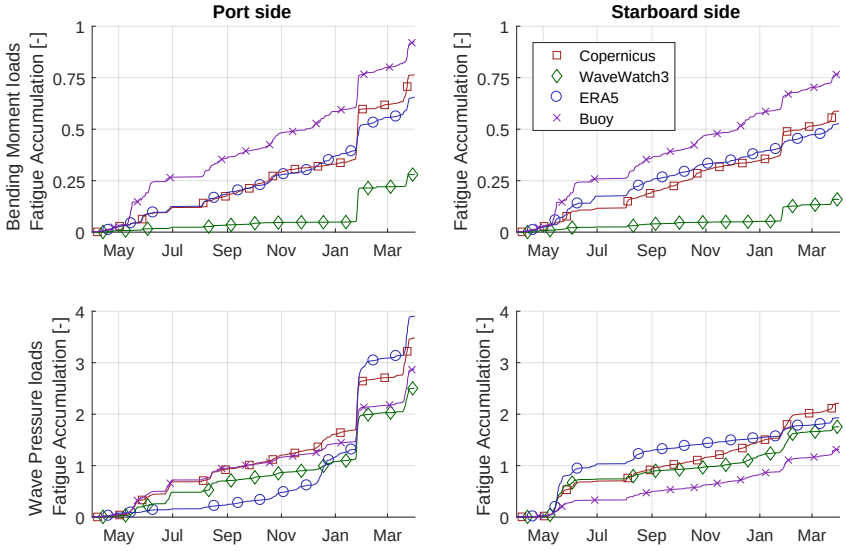

Figure 4.2: Fatigue accumulation on four typical details during one year on unit *AUS*. The fatigue accumulation has been normalized using the design yearly fatigue accumulation of the port side location subjected to bending moment loads.

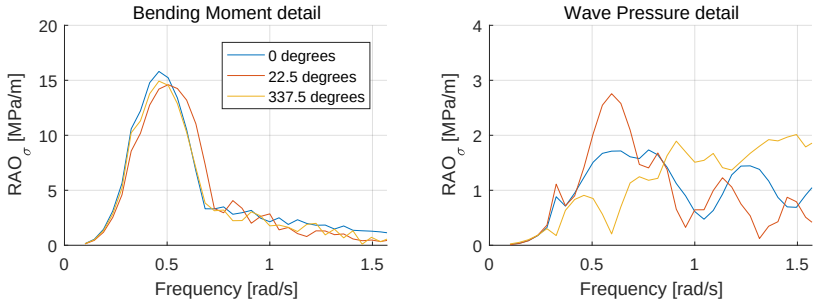

Figure 4.3: Stress RAO of unit *WA4* associated with aft incoming waves of the port side details shown in Figure 4.1. The RAOs with an offset of 22.5 degrees to both port (337.5 degrees) and starboard side (22.5 degrees) are also shown.

dels. This difference is more pronounced in the conditions with higher wave heights. This combined deviation in wave height and wave periods explains the smaller fatigue accumulation obtained from the calculations using buoy wave data.

The details dominated by wave pressure loads have a significant response in a wider range of frequencies, as can be seen through the RAOs from unit *WA4* in Figure 4.3. At these locations, the response declines for waves with a frequency lower than $0.50 rad/s$ or period above $12s$. At these frequencies, the associated wave length exceeds the unit length. In such cases, the heave motion becomes similar to the wave elevation and as a result the wave pressure on the hull, and consequently the stress, becomes negligible. The response at the side shell is more sensitive to directionality. This unit is oriented at a slight angle with respect to the dominant wave direction where the starboard side is more exposed to the environment.

The wave data associated with the location of unit *AUS* during the selected period is shown in Figure 4.4. The fatigue accumulation on unit *AUS* shows gradual fatigue accumulation over the majority of the year, but also shows a jump in the fatigue accumulation at the end of January which occurs during a 5-day period. Depending on location and wave data, this jump represents between 20% to 50% of the total fatigue accumulation in this year. This jump is similar for all wave models except the ERA5 results, which show a larger jump on the port side detail subject to wave pressure, but negligible jumps on the other locations. The detailed wave data encountered during this period is shown in Figure 4.5. There is a good match between all parameters except for the relative wave direction. The buoy, WAVEWATCH III and Copernicus show predominant bow quartering wave conditions, while the results from ERA5 show beam sea conditions. Under such conditions, there is little fatigue accumulation at locations which are subjected to vertical hull girder bending loads. At the same time, the starboard detail sustaining wave pressure loads, is sheltered by the unit. The port side location is exposed to the incoming waves and therefore a higher fatigue accumulation is calculated. The significant wave height in this period is around $3m$. This is high for this operating area, but are not yet full cyclone conditions which can occur as well. The relative fatigue contribution of a nearby cyclone is expected to be even more significant than the effect which was shown in Figure 4.2.

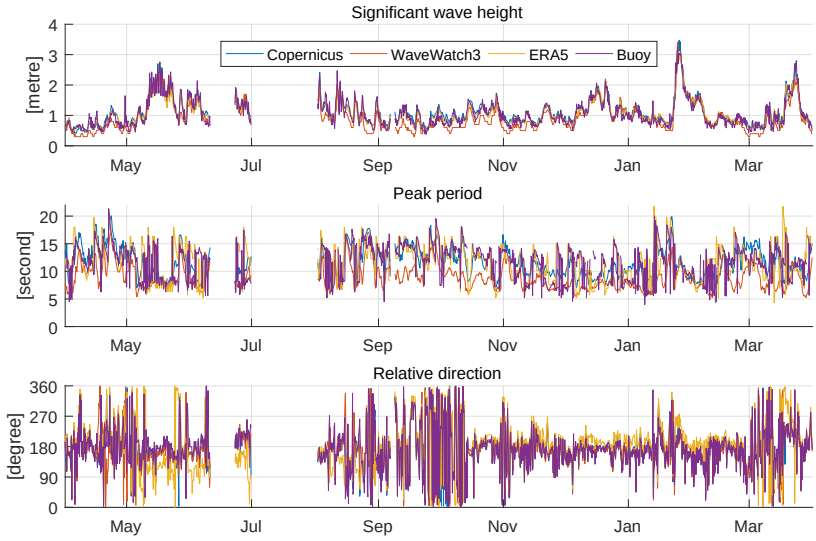

Figure 4.4: Statistical wave data obtained from the wave buoy and hindcast models at the location of unit *AUS* during the year considered in Figure 4.2

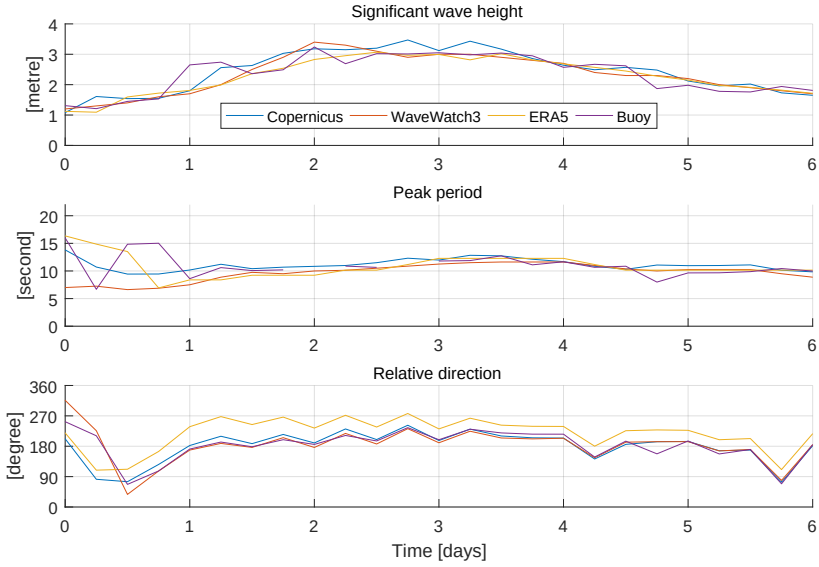

Figure 4.5: Statistical wave data obtained from the wave buoy and hindcast models at the location of unit *AUS* during the 5 day period of rapid fatigue accumulation at the end of January observed in Figure 4.2

The locations subjected to hull girder bending loads show the largest fatigue accumulation when using buoy statistics and the lowest when using WAVEWATCH III data. The difference between these two is a factor 5 on fatigue life as can be seen in Figure 4.2. Moreover, the fatigue assessment using WAVEWATCH III data shows a negligible fatigue accumulation in the period between September and January. This strong deviation is the result of a discrepancy of the wave statistics. Figure 4.4 shows that the significant wave height obtained from WAVEWATCH III is somewhat lower than that of the other data sets. However, the main deviation is the wave period which is around 10s in WAVEWATCH III in the period between September and January, but 15s for the other data sets. The relation between period and stress response observed earlier on unit *WA*4 also holds true for this unit. Hence, the deviation in wave period has a stronger effect on the fatigue accumulation than the deviation in wave height.

When comparing Figures 4.1 and 4.2, it can be observed that the difference in fatigue accumulation between port side and starboard side wave pressure-dominated details is smaller on unit *AUS* compared to unit *WA*4. The former unit can weathervane around its turret which results in a more uniform spreading of waves over port side and starboard side. The notable exception here is the result of the calculation using ERA5 statistics. Figure 4.4 shows that a deviating wave direction can be observed over the whole year. This deviation is not random. In the period from May until August, the deviation shows more Easterly waves, whereas in the period from November to March, the deviation shows more Westerly wave conditions.

STATISTICAL VARIATION

The statistical uncertainty has been assessed using the procedures described in section 2.5.1. Figure 4.6 shows the statistical variation of the fatigue accumulation for the four representative details on unit *WA*4 represented by their coefficients of variation. Only statistical data from the wave buoy was used in the analysis. In line with the theoretical argument of Central Limit Theorem, the coefficient of variation is inversely proportional with the square root of number of samples, or equivalently, the period for which the environmental variation is assessed. The coefficient of variation has been assessed for multiple details on the side shell and deck on the different units. This value for a 10-year prediction at each separate analysis location is shown in Figure 4.7.

On the spread-moored units, the scatter of a 10-year prediction is in the order of magnitude of 1%. At the details loaded by wave pressures mainly, the scatter is somewhat smaller. For these details, the repeating loading cycles have an important contribution to the overall uncertainty. The side shell plating is either submerged, non-submerged or in the intermittent wetting area as a result of these loading cycles. This effect has a large influence on the stresses observed at these details. The loading cycles occur very regularly and feature less statistical variation compared to wave loading. As a result, the loads at details subjected to wave pressure show less variation compared to the details subject to wave bending moments which only include statistical variation from wave loads.

On unit *AUS*, which operates in a cyclone dominated environment, the scatter is somewhat larger at 2 to 4% for details loaded by wave pressure and can be over 10% for details subjected to bending moment loads. However, the resampling scheme inherently

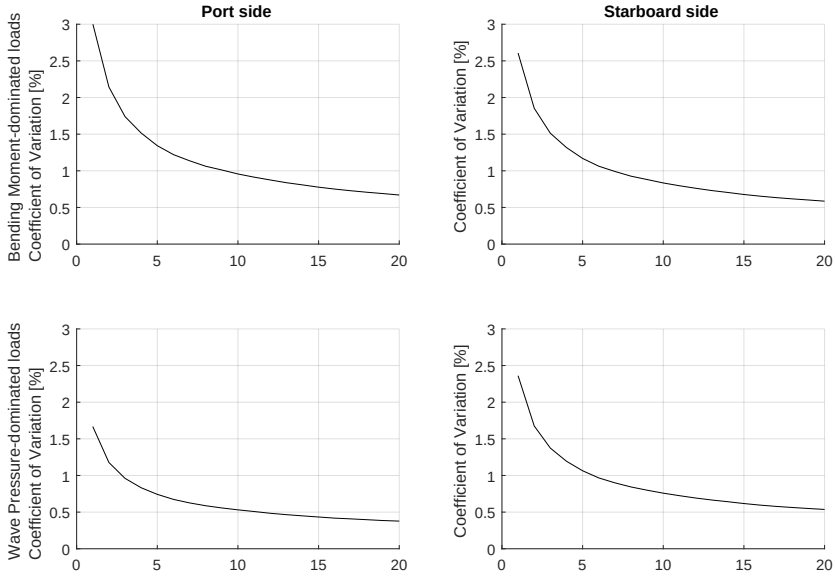

Figure 4.6: Uncertainty in fatigue accumulation in a 10-year prediction as a result of statistical variation of environmental and operating conditions as a function of time for various details on unit *WA*4.

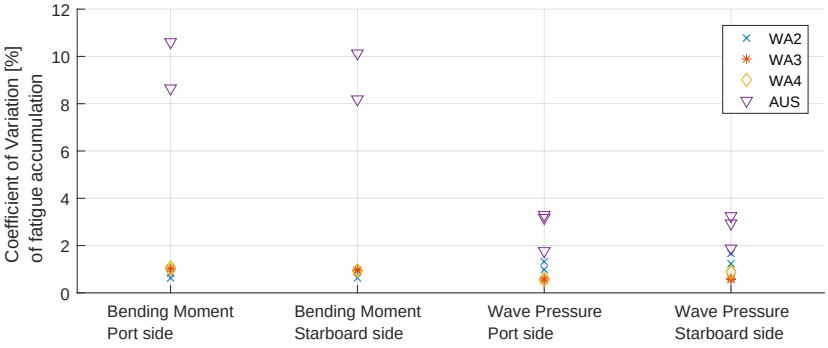

Figure 4.7: Uncertainty in fatigue accumulation as a result of statistical variation of environmental and operating conditions on multiple units.

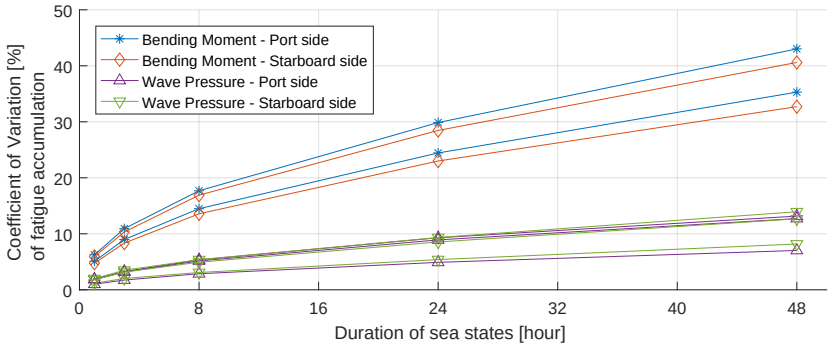

Figure 4.8: Uncertainty in fatigue accumulation as a result of statistical variation of environmental and operating conditions on multiple units as function of the duration of the sea states on unit *AUS*.

assumes that subsequent sea states are independent. This is not a realistic assumption as storm events exceed a 3-hour period. It was proposed in section 2.5.1 to quantify this effect by assuming longer stationary sea states which effectively reduces the number of conditions in a certain period. The result of that analysis is shown in Figure 4.8. The uncertainty becomes much more significant with values up to 40% when assuming storm conditions which last around 2 days. Recall that Figure 4.5 showed that this is a reasonable duration for a storm condition. This observation highlights the importance which individual storm have on the fatigue accumulation of units operating in otherwise moderate conditions. This was also supported by the single storm event shown Figure 4.2.

The units *WA*4 and *AUS* have been considered in this section in most detail. These units are both located in areas with mostly very benign environmental conditions. However, unit *AUS* can encounter cyclonic conditions on an irregular basis. With a limited number of moderate sea states, this leads to loads that are characterized by a binary behaviour and an associated large statistical uncertainty as a result of these storm conditions.

The uncertainty arising from long-term environmental conditions during operations consists of uncertainty introduced from wave parameters and statistical variability. The contribution of the wave parameters is quantified using results from unit *WA*4, which have been visualized in Figure 4.1. These indicate a typical uncertainty up to a factor of 2. When comparing the various hindcast models against the buoy data, there is not a single model that performs best for all structural details. It has also been noted that the wave buoy is unable to accurately represent wave energy with both high and low frequencies. Therefore, the calculations using buoy data also incorporate some inherent uncertainty. Unit *AUS* shows a larger uncertainty as a result of the use of hindcast models. However, the wave conditions at this location are characterized by confused sea states. For this unit in particular, the short-term sea state definition introduces an additional uncertainty which is addressed in section 4.3.

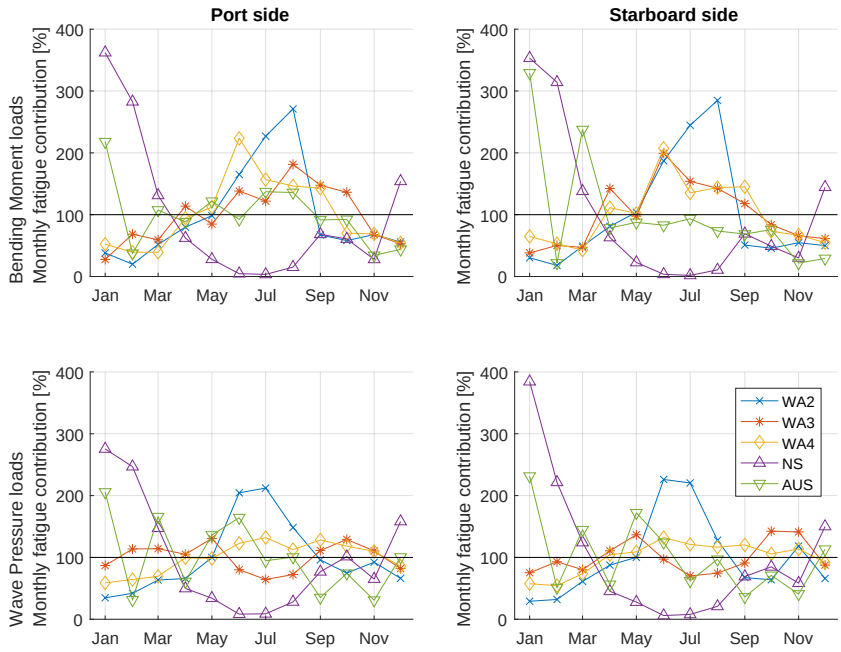

Figure 4.9: Fatigue accumulation rate per month compared to the average fatigue over the entire year for different structural details and multiple units.

SEASONALITY

The fatigue accumulation rate varies over the year. The procedure defined in section 2.5.1 was used to assess the month-to-month variation in the fatigue accumulation rate. For each unit, two analysis locations subjected to hull girder bending and two subjected to wave pressure loads were analysed. These details are located near the midship section and are symmetrical in port side and starboard side. The results of this analysis are shown in Figure 4.9.

It can be concluded that seasonality effects on the fatigue accumulation are more strongly present in the details dominated by hull girder bending. For the spread-moored units in West-Africa, the fatigue accumulation between June and August accounts for around half of the total yearly fatigue accumulation. The unit *WA*4, which is located more to the South, experiences the highest fatigue accumulation in June, whereas the unit *WA*2 in the North experience the highest accumulation in August. The unit *WA*3 shows a discrepancy between port and starboard side. The seasonality effect can also be observed in Figure 4.1 and Figure 4.2. These figures have indicated a more pronounced effect at the location of unit *AUS* as a result of the rare cyclonic conditions in this area. This observation can be found in Figure 4.9 as well.

At the structural details dominated by wave pressure loads, the seasonality trend is

similar, though less pronounced to the trends observed in the details subjected to bending moments. Unit *WA*3 shows an opposite trend with the fatigue rate decreasing in the heavy weather season. A summary of the wave statistics per month at the location of unit *WA*4 is displayed in Figure 4.10. This figure shows that the wave height is larger than average in the period between April and September. The fatigue accumulation in this period is also above average, except for the month of May which shows a lower wave period. The reduced period will also result in reduced pressure fluctuations in the side shell and a reduction in the fatigue accumulation. Conversely, the increased wave height will result in higher pressure fluctuations. A fatigue reduction has been observed in Figure 4.9, indicating that the influence of the wave period exceeds the change of the wave height. Finally, a discrepancy in fatigue accumulation between port and starboard side has been observed between July and August. In these two months, the average wave direction also changes with a couple of degrees.

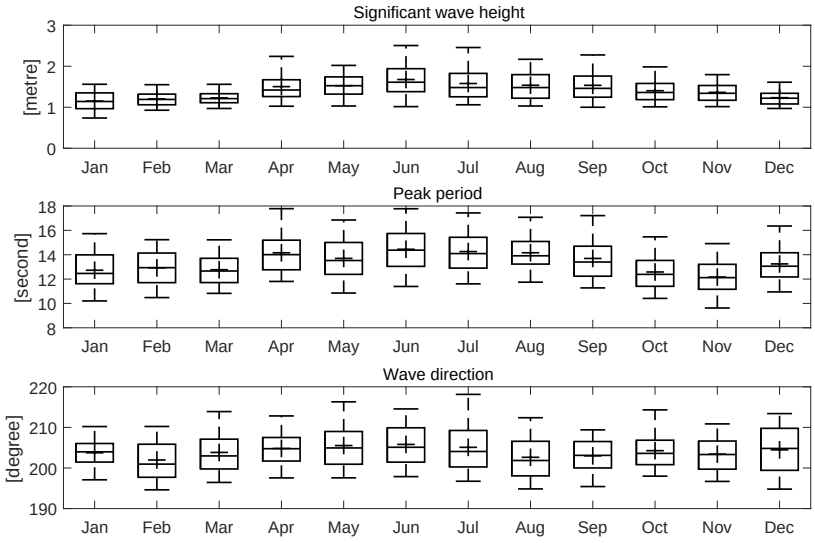

Figure 4.10: Variation of wave statistics over the months at the location of unit *WA*4 obtained using Copernicus hindcast.

ORIENTATION IN WAVES

On turret moored units, the orientation of the unit with respect to the environment is subject to some uncertainty. This arises from the procedure used to determine the equilibrium orientation and not from the wave environment itself. The sensitivity of the fatigue assessment with respect to the heading on turret moored units is examined. More details on this procedure were discussed in section 2.5.1. Data from unit *AUS* has been used to conduct this analysis.

A design assessment to determine the orientation of the unit with respect to the waves has been executed. The distribution of relative wave directions from this analysis

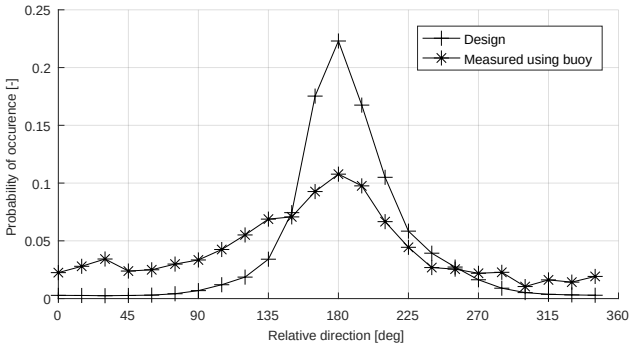

Figure 4.11: Distribution of the design and true orientation with respect to the primary wave system of unit *AUS*. 180 degrees specify head sea conditions.

is shown in Figure 4.11. This figure also shows the distribution which has been measured in the field. The true orientation shows a larger variety of relative wave directions. The design assessment showed that the incoming wave conditions were expected to be within 30 degrees off the bow in around 80% of the time. The measured wave conditions show a probability of 40% instead. The measured conditions show relatively frequent occurrence of waves coming from starboard side, and less conditions with waves coming from the port side. It should be noted that the wave conditions in this area are very mild for the majority of the time and the heading is therefore strongly influenced by wind and current. This results in weak correspondence between wave direction and heading of the unit.

Fatigue assessments have been conducted using the measured scatter diagram and several wave direction distributions. These fatigue assessments have been compared against the fatigue assessment using the actual measured wave conditions. The results for various locations are shown in Figure 4.12.

The first calculation involved a fatigue analysis using all measured sea states and using the measured distribution of the heading. This comparison can be used to quantify the correlation between the wave direction and other statistical parameters. On the locations dominated by bending moment loads, this results in an increase in fatigue accumulation compared to the true measured conditions. Higher fatigue accumulation is sustained when the unit is operating in bow to head sea conditions. Therefore, the figure suggests that in higher sea states, the unit is less aligned with the waves. In a heading analysis, especially the short, high-frequency waves exert a mean yaw moment through the second-order wave forces. In sea states with longer waves the unit can therefore be less well aligned. However, these are conditions resulting in larger fatigue accumulation from bending moments, which explains this observation. Structural details subjected to wave loads show quite different results though. These details experience larger fatigue accumulation in shorter waves and therefore fatigue accumulation at these details show a strong correlation with the orientation. By removing this correlation, the fatigue accumulation changes strongly up or down depending on the side of the detail.

When using the orientation of the unit as determined during design, the fatigue ac-

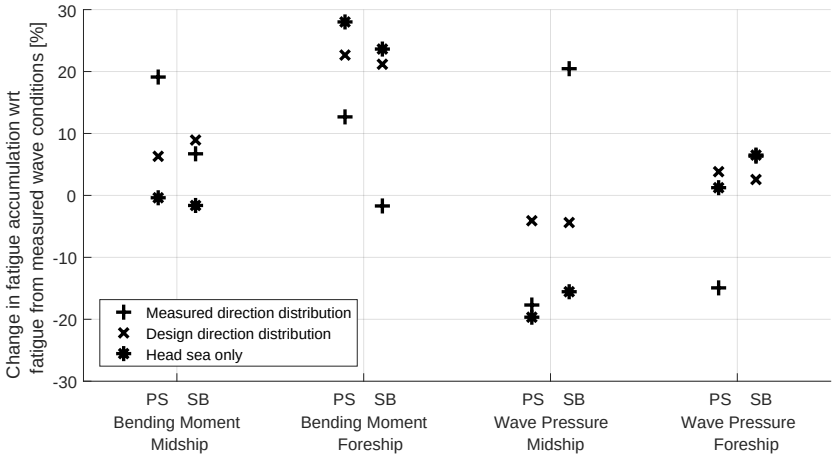

Figure 4.12: Changes in the fatigue accumulation using the measured scatter diagram and different heading definitions with respect to the fatigue assessment using the true measured wave conditions.

cumulation changes up to 25% on details subjected to global bending and up to 5% for details subjected to wave pressures. The differences between both sides of the unit are small. When using only head sea conditions, the fatigue accumulation changes little compared to the analysis using the design orientation, except for the details in the side shell located around midship. At these locations, the wave diffraction is the most strongly related to the local stresses. In head sea conditions, diffraction of the wave field is minimal resulting in a reduced pressure and hence stress.

The condition using only head seas in Figure 4.12 shows that the fatigue accumulation is nearly symmetrical between port side and starboard side structural details. The use of the direction distribution as predicted during the design also shows a very symmetrical change in fatigue accumulation. However, when the actual measured direction distribution is adopted, differences in fatigue accumulation become visible. On details subjected to bending moments, the difference is in the order of 15%. On details subject to wave pressures, the difference varies between 20% and 40% and is most strongly visible in the midship area. In this area of the hull, diffraction and shielding effects are the most prominent, resulting in the largest differences between both sides of the hull.

The bias that may be expected from the procedure to determine the orientation of the unit with respect to the waves is given by the x-marks in Figure 4.12. For details subjected to hull girder bending, the bias can be up to around 20%. For details subjected to wave pressure loading the bias is less pronounced at around 5%.

4.2.2. TRANSPORT TO FIELD

Units operating in benign environments may be subjected to significant loads during the transportation from yard to operating field. During this period, the unit is subjected to moderate sea states with conditions exceeding normal operating conditions in the field. Moreover, the directionality of the waves can result in significant horizontal bend-

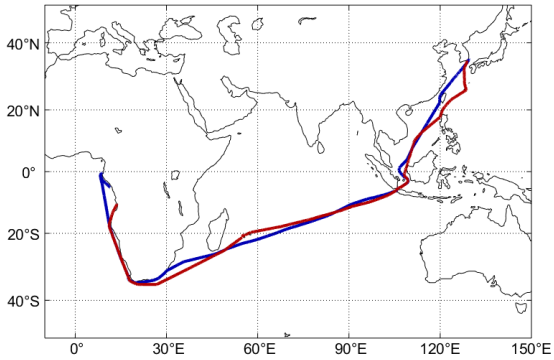

Figure 4.13: Tracks of the units *WA*3 (blue) and *WA*4 (red) during transport from Asia to West-Africa. The transports have been conducted between August and November of two different years.

ing moments. These are normally small during production, but may result in significant stresses in the side shell area. For the units considered in this research, the fatigue accumulation in the side shell details which is sustained during tow, is typically equivalent to around one year of operation in the field.

GPS data during the transport phase are used to retrieve wave conditions from hindcast models. GPS data is available for unit *WA*3, *WA*4 and *AUS*. The wave conditions have been retrieved from WAVEWATCH III only, because Copernicus was not available at the time of the earliest transport. Two examples of transport routes between Asia and West-Africa are shown in Figure 4.13. The global routes are the same, although some minor differences can be observed. For example, one unit traverses the Taiwan Strait, while the other travels over the Philippine Sea. One of the units travels past the islands of Reúnion and Mauritius, while the other does not.

The wave conditions experienced by unit *WA*4 during its transport are shown in Figure 4.14. A number of waypoints can be clearly identified in this figure:

- The heavy weather between day 7 and 10 is experienced on the Philippine Sea.
- On day 20, the convoy is in the centre of the South China Sea.
- On day 32, the Sunda Strait is traversed.
- Between day 48 and 53, the unit is near Reúnion and Mauritius and is sheltered from the dominant swell on the Indian Ocean resulting in lower waves and more scattered directionality.
- From day 60 to 67, the unit is approaching and sailing across South Africa

This unit is being towed using ocean going tugs. The speed of the convoy in open sea varies between 4 to 5 knots.

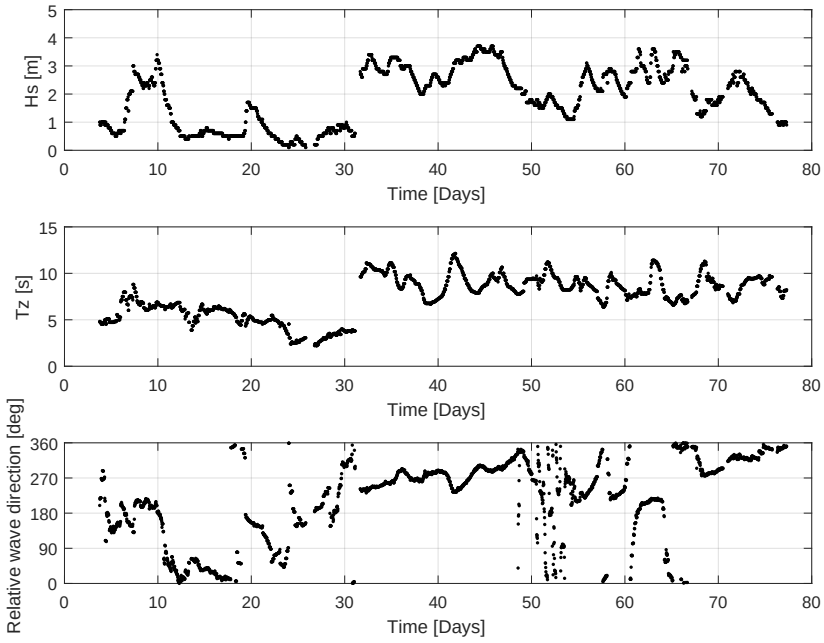

Figure 4.14: Wave statistics obtained during the tow of unit *WA4* from South Korea to West Africa.

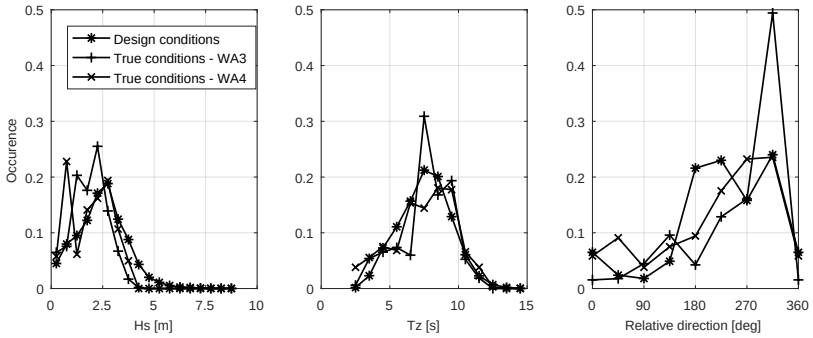

Figure 4.15: Histograms of wave statistics obtained during the transport of both units *WA*3 and *WA*4 in combination with the design assumptions used for both units.

The wave statistics obtained during the transportation of both unit *WA*3 and *WA*4 are summarized in histograms in Figure 4.15. For both units, the same conditions have been used during design. The maximum significant wave height during both trips is around 4 metre. However, in the design conditions, it was assumed that the significant wave height exceeds 4 metre in 9% of the conditions. For unit *WA*4, around 20% of the wave conditions have a significant wave height below 1 metre. Figure 4.14 shows that these conditions are experienced while traversing the South China Sea. For unit *WA*3, which traversed the South China Sea later in the season, the wave conditions are more evenly distributed between 1 to 3 metres.

The wave direction in the design conditions show dominant port side waves. This is the result of the dominant swell conditions on the Indian Ocean. The measurements show that the wave conditions are more strongly dominated by beam and aft quartering waves from port side than initially predicted. This is especially true for unit *WA*3 which traverses the Indian Ocean on a more direct route and is thereby subjected to a more constant swell condition. This also explains the more pronounced peak in the observed periods for this unit.

Unit *AUS* has been towed from South-Korea to its operating location near Australia. The wave conditions experienced during the tow are depicted in Figure 4.16. During the tow the unit has experienced the tail of a tropical storm resulting in a short exposure to waves of around 4 metre significant, see also Figure 4.16. This condition was not anticipated in the design, which used a probability of encountering sea states with significant wave heights exceeding 4 metres equal to 0.07%. This is equivalent to a period of 30 minutes during 30 days. To withstand these unfavourable weather conditions, the convoy turned to experience head on or slight starboard bow quartering seas.

Spectral fatigue assessments have been executed for units *WA*3, *WA*4 and *AUS* for several sensor locations using both design conditions and the measured conditions as input. The ratio of these two calculations is assessed for the measurement details and is displayed in Figure 4.17. Both measurement locations on the deck and on the side shell are analysed, see also Figure 3.12 for a typical sensor arrangement. During transportation the sensors in the side shell are located well above the mean water line and will

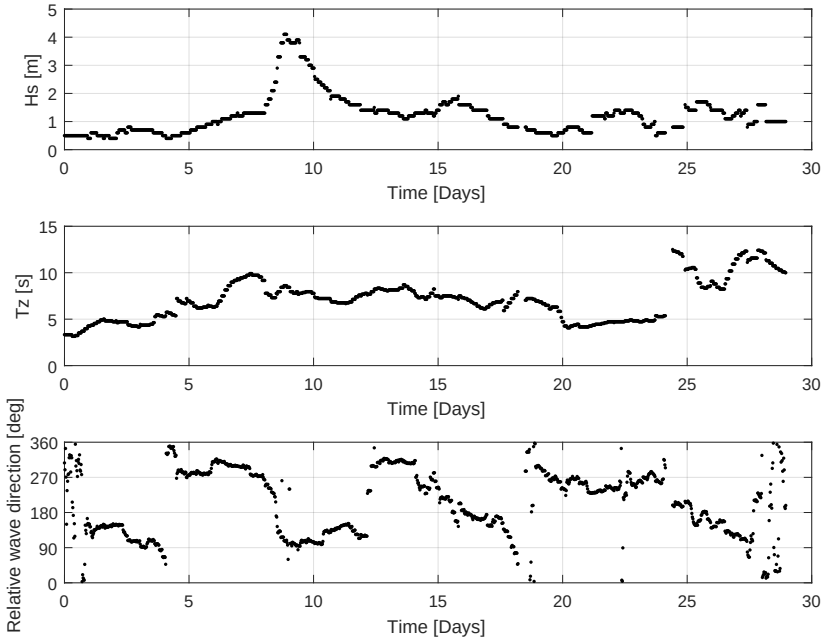

Figure 4.16: Wave conditions obtained during the tow of unit *AUS*. The figure shows a brief period with disadvantageous weather for which the convoy changed direction.

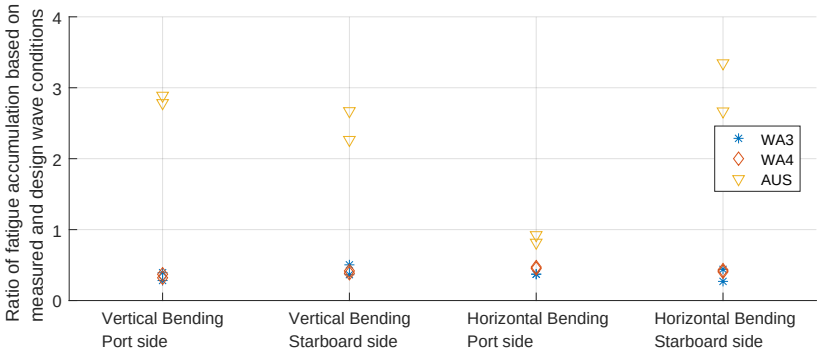

Figure 4.17: Observed ratio of fatigue accumulation calculated using design assumptions on weather and using actual weather conditions during tow. A ratio below one indicates an overestimation of the fatigue accumulation using design conditions.

experience little wave induced pressures, nor will they experience vertical hull girder bending due to their proximity to the Neutral Axis. They will however encounter significant horizontal hull girder bending due to the dominant beam and quartering seas. This loading mechanism normally has a small contribution during operation. The details on the deck are subjected to vertical and horizontal hull girder bending. Due to the placement of the sensor, the vertical component is dominant. In the calculation use has been made of the RAOs describing the ballast condition. This is the condition for which hydro-structural calculations have been executed that is most close to the loading condition of the unit during transport. However, the true loading conditions is different than the ballast condition used in the calculations.

Figure 4.17 show that the design conditions for the West-Africa units result in a conservative fatigue assessment. The fatigue accumulation from the encountered conditions is between a factor of 2 to 3 less than predicted. The port side locations subjected to vertical hull girder bending are even somewhat more conservative. For the locations subject to horizontal bending, no significant difference between both sides are observed. However, on unit *AUS*, the design conditions are not conservative. Here, the structural details subject to vertical hull girder bending show a factor 3 larger fatigue accumulation. A similar value can be found for the details subjected to horizontal bending on starboard side. However, on the port side details a slightly lower than predicted fatigue accumulation is observed. These observations are in line with the previous discussion of the wave heights observed during transport which were conservative for unit *WA*3 and *WA*4, but not for *AUS* due to the storm event. The directional presence of the waves during the storm resulted in the discrepancies between port and starboard side on unit *AUS*.

On unit *WA*4, the stress at the considered locations was measured during the tow. The standard deviation of the stress per half-hour window is shown in Figure 4.18. This figure indicates that there is little difference between the port and starboard side locations. However, there are noticeable differences between the locations subject to vertical and horizontal bending. The stresses that resulted from vertical bending are roughly five times higher compared to those of horizontal bending. Secondly, at the horizontal bend-

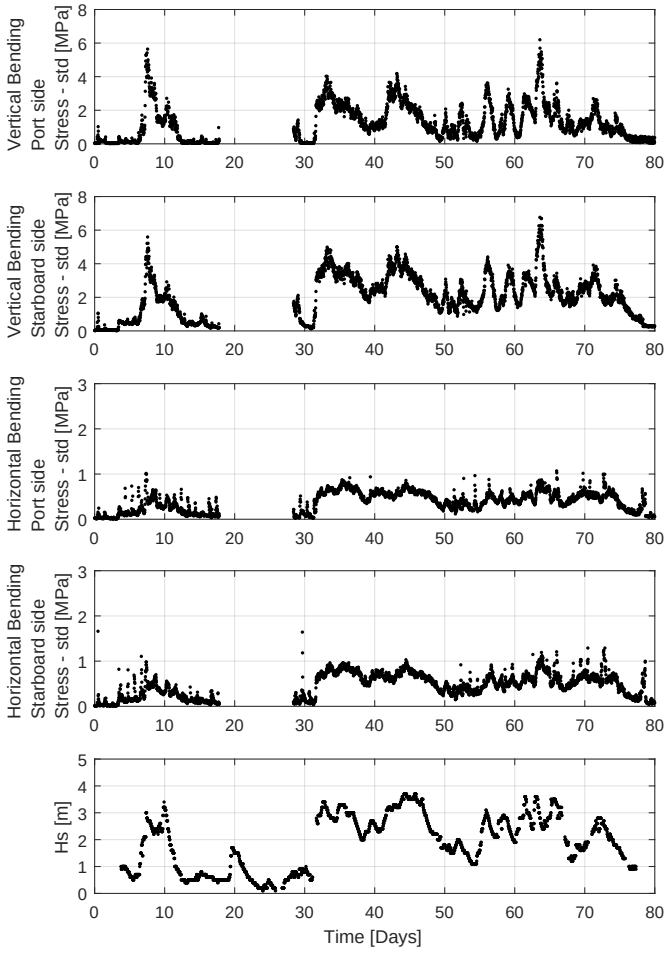

Figure 4.18: Standard deviation of stress at different measurement locations during the tow of unit *WA4*.

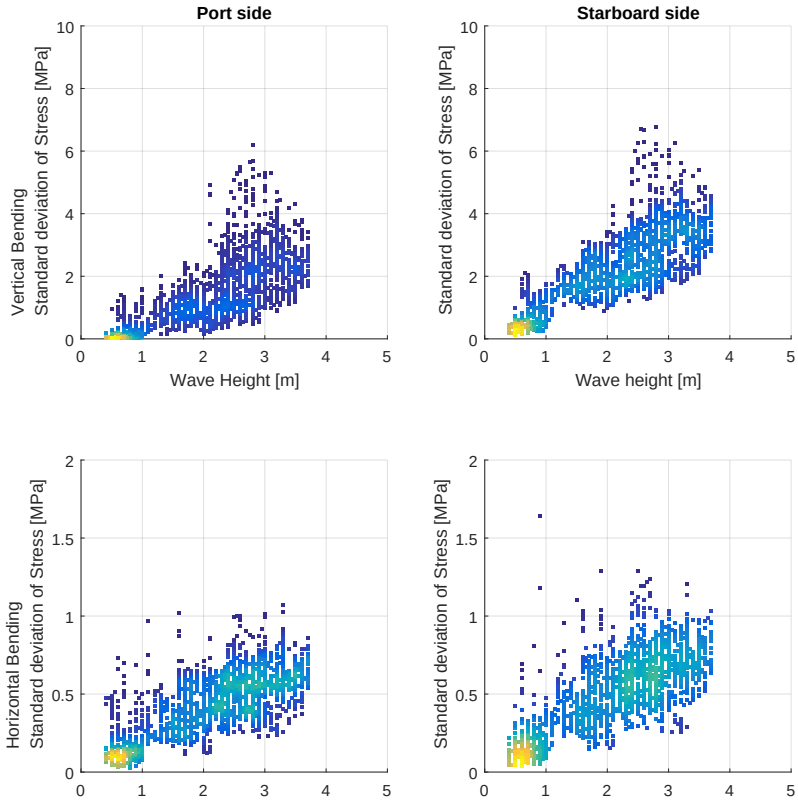

Figure 4.19: Scatter plot of stress at the different locations against the wave height during the tow of unit *WA4*.

ing locations a repetitive pattern with a period of around one day is visible. This effect is believed to be related to temperature fluctuations. Finally, the stresses at the deck show gradual developing peaks, for example around day 8 and 63, which do not appear at the horizontal bending dominated locations.

At first sight, the stresses appear to correlate well with the wave height. This relation is indicated in the scatter plots in Figure 4.19. The relation between stress and significant wave height is indeed very strong for the locations dominated by horizontal bending. However, the relation breaks down for locations subject to vertical bending where the highest stresses and the highest waves do not coincide. A clear example can be found by comparing the stresses observed on day 8 and day 10. On both days, the wave height is similar at around 3 metre significant. On the other hand, the stresses at the vertical bending dominated locations on day 8 are twice as large as those on day 10. Figure 4.14 indicates that this is related to a shift in wave direction and a large wave period, and

consequently longer waves, on day 8. This effect will be further explored in section 4.5.1 on account of the analysis of the spectral fatigue method itself.

4.2.3. SUMMARY

Wave loads are the main contributor to fatigue loads on floating offshore production units. There are various measurement devices, with their respective benefits and drawbacks, that can be used to assess wave conditions. On top of these, oceanographic wave models are able to provide hindcast wave statistics which can also be used in a fatigue assessment.

Fatigue accumulation is a long-term cumulative process. Therefore, any uncertainty in the individual estimates of the wave statistics, as reported in e.g. Table 3.3, has limited importance. A bias of these statistical parameters can have a large influence on the fatigue accumulation though. Typically, the bias in the fatigue assessment using different wave data sources can be up to a factor of 2. This stresses the importance of using appropriate wave statistics in the fatigue analysis. For unit *AUS*, a significant difference between fatigue assessment using WAVEWATCH III data and the other data sources was observed as a result of a deviating wave period. In storm conditions, minor differences in the statistical parameters can lead to a more significant deviations in the fatigue estimates.

The fatigue accumulation rate changes strongly over the year. This variation is more pronounced on structural details subject to bending moments. The reason is that these details only experience stresses due to wave loads from a narrow frequency range and are therefore very sensitive to changes in wave period. Details subjected to wave pressure experience stresses in a more broad frequency range and are therefore less sensitive to variations in wave period.

On turret moored units, the orientation of the unit with respect to the waves can be different than expected. This difference arises from uncertainties in wind and current coefficients and nonlinear wave forces. On unit *AUS*, the deviation between the true and predicted orientation resulted in a typical bias of around 20% on the total fatigue accumulation.

For units operating in a mild environment, the wave conditions experienced during the transportation from yard to production location can be significant. For such units, dedicated analysis of these conditions is executed. However, the actual transportation is conducted in a period in which the most favourable weather conditions can be expected. As a result, the true fatigue accumulation during the transportation phase is often likely to be much smaller than predicted. For the two units studied here, a factor of one third on fatigue life was observed.

4.3. SHORT TERM WAVE DEFINITION

4.3.1. SPECTRAL SHAPE AND SPREADING

Fatigue assessments have been executed using different spectral shapes and distribution functions as input for both unit *WA*4 and *AUS*. The spectral shapes and distribution functions were defined in section 2.5.2 and are visualized in Figure 2.6. Bulk statistics of the wave buoy have been used as input parameters and a calculation using a JONSWAP

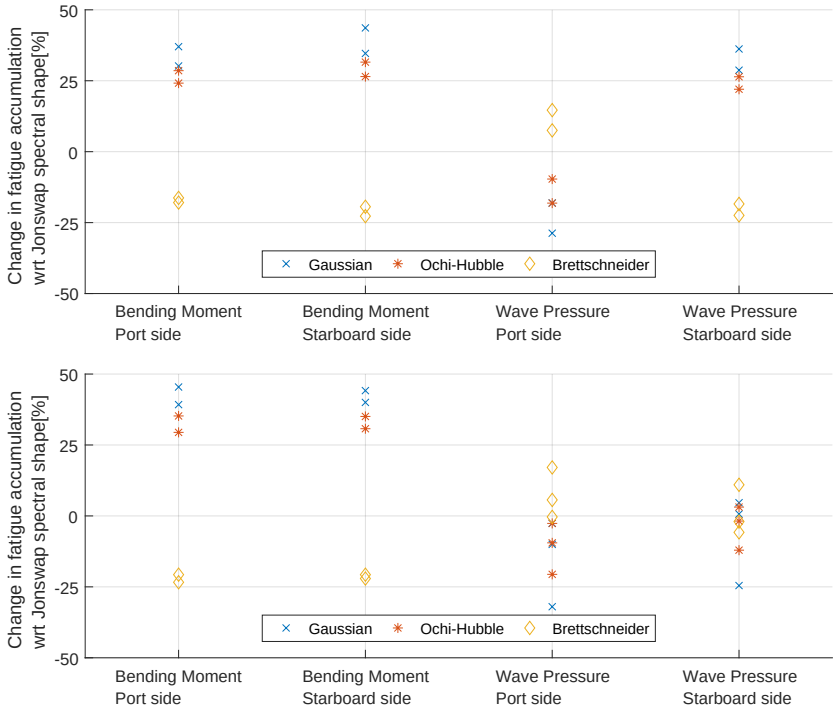

Figure 4.20: Change in fatigue accumulation when using different wave spectral shapes in the calculations. Depicted are the results for unit *WA*4 (top) and *AUS* (bottom). The calculations are executed using all available bulk wave statistics from the local wave buoy. The reference values for the fatigue accumulation are obtained using the JONSWAP wave spectrum. Multiple measurement locations are plotted jointly in these graphs.

spectrum and longcrested waves was executed to establish reference values. Fatigue assessments using different spectral shapes have been executed and the deviation from the reference case, using JONSWAP with γ of 3.3, is given in Figure 4.20. In this calculation, no wave spreading was applied. Spectral fatigue assessments have also been executed using various spreading functions. The deviation from the reference calculation is provided by Figure 4.21.

Figure 4.20 shows that there is little difference between the port side and starboard side details which are subjected to hull girder bending. A clear trend can be identified between the different spectra. The Brettschneider spectrum results in a lower fatigue accumulation, but the other spectra result in a higher fatigue accumulation compared to the case using the JONSWAP spectrum. The Brettschneider spectrum is in fact the most broad spectrum, that is, the wave energy is distributed more equally over the frequency range. The Gaussian and Ochi-Hubble spectrum are both quite narrow, i.e. the range of frequencies over which the wave energy is distributed is small. Note that the peak energy density of the JONSWAP spectrum is larger than that of the Ochi-Hubble spectrum. However, the Ochi-Hubble spectrum diminishes quicker with increasing frequency and is therefore still considered a more narrow spectrum. Note that the RAO presented in

Figure 4.3 shows that the structure also responds to a limited range of frequencies. The high-frequency energy present in the JONSWAP and Brettschneider spectra does therefore not result in notable structural response and results in a smaller fatigue accumulation when selecting these models compared to the Ochi-Hubble and Gaussian spectra.

On the details subjected to wave pressure, the trend is exactly opposite, except for the starboard side detail on unit *WA*4. The RAO of details subjected to wave pressure show that these details are equally sensitive to a wide range of frequencies. Under those conditions, the spectra which includes more high-frequency energy content will result in a larger number of load cycles and therefore a larger fatigue accumulation. The sensitivity to spectral shapes on the details loaded by wave pressure is somewhat smaller than was observed for the details subject to global hull bending.

Unit *WA*4 is spread moored and the largest waves are encountered at port side under a small angle from the aft incoming wave direction. As such the detail at starboard side is somewhat sheltered from direct wave pressures and the global bending becomes a more dominant feature of the stress response under these conditions. This can be seen in the similarity in the RAOs of this structural detail, which were shown in Figure 4.3, for this wave direction. Hence, the sensitivity to spectral shape is more in line with that of the bending moment dominated loads.

It can be concluded that the choice of the spectral shape used in the fatigue assessment has a significant contribution to a potential bias in the calculation. The observed deviation between the Brettschneider and Gaussian spectra is close to a factor of 2 for certain details. Furthermore, not one spectral shape can be used to obtain the most conservative estimate under all conditions. This is related to how the structure responds to certain load frequencies. For bending moment induced loads, the Gaussian spectrum results in the highest fatigue estimate. However, for details subjected to wave pressure loads, the Brettschneider spectrum may result in the highest fatigue accumulation.

Offshore production units are generally oriented towards the main wave direction. This orientation results in the smallest roll motions which is beneficial for the production plant. This orientation is either fixed for spread moored units or, in case of turret moored units, achieved passively through an equilibrium of environmental loads or active heading control. In aft or bow incoming waves the bending moments on the hull are quite significant. When introducing wave spreading, a part of the wave energy becomes associated with other directions which results in smaller bending moments and hence smaller loads. As expected, Figure 4.21 shows that the fatigue accumulation on details with dominant bending moments reduces when broader spreading functions are applied. The details on unit *WA*4 show a different trend. Here the fatigue accumulation increases slightly for narrow spreading functions. This is the result of interaction between horizontal and vertical hull girder bending. When combining these two load effects, a small discrepancy between the port and starboard side details occur, which results, on this unit, in an advantageous bias for the port side details, but disadvantageous bias for the starboard side details. This same effect is visible in the results of unit *AUS*, but to a smaller degree and longcrested waves remain conservative for both sides. This is because the unit weathervanes and experiences waves from both directions resulting in a less significant deviation.

On the locations loaded by wave pressure, mixed results can be seen. On unit *AUS*,

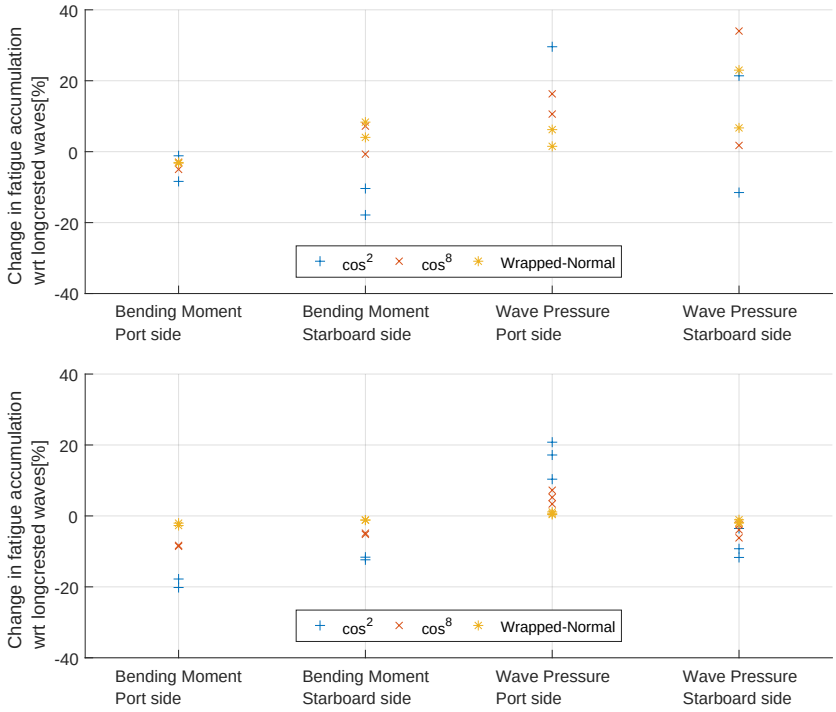

Figure 4.21: Change in fatigue accumulation when using different wave spreading functions in the calculations. Depicted are the results for unit *WA*4 (top) and *AUS* (bottom). The calculations are executed using all available bulk wave statistics from the local wave buoy. The reference values for the fatigue accumulation are obtained using the longcrested wave spectrum. Multiple measurement locations are plotted jointly in these graphs.

the starboard side is more exposed to the environment. Therefore, when wave spreading is introduced in the calculation, the fatigue accumulation reduces. The exact opposite trend can be observed on the port side. This effect becomes larger when wave spreading is increased. On unit *WA*4, the fatigue accumulation increases on both sides when wave spreading is adopted. This is the result of the small structural response in aft incoming wave conditions. When the wave direction changes, the structural response becomes larger, either, when becoming more exposed to the waves, as a result of increased pressure on the hull, or, in the other direction, as a result of the increased horizontal bending. See also the discussion earlier on in this section and Figure 4.3.

Overall, the effect of wave spreading shows smaller deviations than those of the spectral shape with changes up to a factor of 2. The assumption of longcrested waves most often results in the most conservative fatigue estimate for details subject to bending moment loads. However, this is not the case for details in the side shell. Here, the interaction between horizontal bending loads and wave pressure and preferred wave directionality will often result in a higher fatigue accumulation when introducing wave spreading. A typical bias for this effect here is 20%, but can be larger than that for specific details.

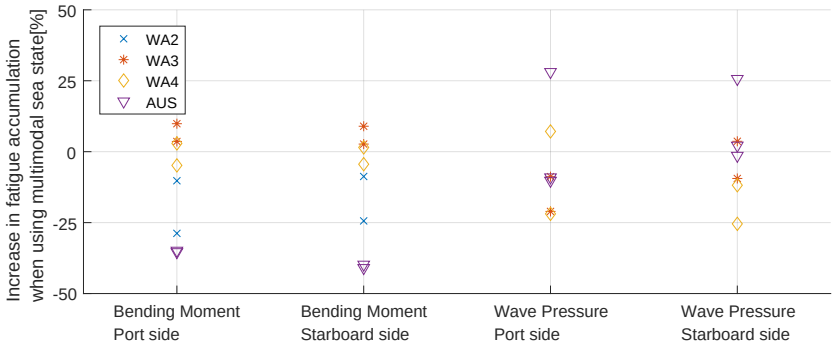

Figure 4.22: Change in calculated fatigue accumulation when adopting a multimodal sea state descriptions with respect to the corresponding unimodal description. The spectrum subdivision was created using data from the dedicated wave measurement of each individual unit. Multiple measurement locations are plotted jointly in this graph.

4.3.2. MULTIMODAL SEAS

A multimodal sea state description allows multiple wave systems to be incorporated in each short term sea state. In order to quantify the effect of a multimodal sea state description, the procedure from section 2.5.2 was adopted and the results are presented in Figure 4.22.

At the locations dominated by bending moments, there are little differences between the port side and starboard side locations. Unit *WA*3 and *WA*4 are operating in the same area and experience nearly identical environmental conditions. However, unit *WA*3 shows a slight increase in the fatigue accumulation of up to 10% as a result of multimodality, while unit *WA*4 shows a smaller increase or reduction of the fatigue accumulation. Unit *WA*3 is somewhat smaller than unit *WA*4. The peak frequency of the wave bending moment is therefore somewhat higher. When separating wave conditions into multiple components, part of the wave energy is projected on a windsea component, which has a lower period than the primary swell. Unit *WA*4 experiences less bending as a result of the windsea contribution. On the other hand, unit *WA*3 experiences a small increase in the wave bending moment as a result of the added windsea component. However, the differences between these units remain very small. At the location of unit *WA*2, the relative contribution of the windsea to the overall environmental conditions is much larger. Hence, the effect as described above on unit *WA*4 is more strongly present here.

The results of unit *AUS* show a much stronger reduction in fatigue accumulation as a result of a multimodal wave description. This can be related to the wave environment at these locations as was described in section 1.3. At this location the wave conditions show two components with two distinct directions, East and South-West. In the unimodal description all wave energy is projected onto a single direction. Because this is a turret moored unit, this is also, in most cases, the direction which the unit will be facing. Hence, in the unimodal calculation, the energy contained in the secondary wave system, which in reality is a beam to stern quartering condition, will be represented as additional energy in the head seas direction. This results in a larger bending moment response in

this calculation.

The results on the details dominated by wave pressure are mixed. On unit *WA*3 and *WA*4, the fatigue accumulation mostly reduces when using multimodal calculations. These units are oriented at a small angle with respect to the dominant wave environment. This orientation results in a small increase in wave pressure, but also introduces a small amount of bending at the measurement locations. When introducing multimodality, part of the wave energy from the dominant directions is transferred to other directions. This results in a reduction of the effects mentioned above. However, at other details, it can also result in a small increase in the fatigue accumulation as a result of the combination of load effects.

On unit *AUS*, the response generally increases more significantly. In the discussion above, it was indicated that in the multimodal representation, this unit experiences beam and stern quartering wave conditions. This introduces additional wave pressure and horizontal bending at these locations. Due to the combination of these load effects, a small reduction in fatigue accumulation at some details is also possible. Because unit *AUS* operates in both mild confused sea states as well as storm conditions, the difference in fatigue accumulation between the unimodal and multimodal descriptions is visualized in Figure 4.23 for the same period as was shown in Figure 4.2. It should be noted that this period is a part of the total data set considered, which is why the numbers from this graph do not coincide exactly with those presented in Figure 4.22.

Figure 4.23 shows that the details subject to wave pressure loads show consistent results over the entire period. During the storm event at the end of January, the uni- and bimodal calculations show nearly identical fatigue accumulation for the details subject to bending moments. During a storm event, the environmental conditions are dominated by a single large wave system and secondary wave systems have a minor contribution. Hence, the multimodal calculation results in a very similar fatigue assessment as the unimodal calculation. For details subjected to bending moments, large differences between both calculations occur. An example is found in the middle of May and early June. In this period, there is a bias of a factor of five between the two calculations. The bimodal wave statistics from this period are depicted in Figure 4.24. Both in the middle of May and early June, two wave systems with similar wave heights, but with different directions and periods, can be observed. The peak periods of the windsea component are between 3 and 5 seconds. The unit will experience little hull girder bending as a result of such short waves. In case of the unimodal analysis, all wave energy will be associated with the swell period and direction which therefore results in an overestimated global bending response. The direct wave pressure acting on the side shell is less sensitive to the excitation frequency, hence, the difference in those areas is negligible.

4.3.3. CONVERGENCE OF SEA STATES

The scatter in a time domain fatigue assessment as a result of time series truncation has been assessed using the procedures described in section 2.5.2. Figure 4.25 shows the coefficient of variation as function of the simulation duration for two different locations.

The coefficient of variation depends on the selected spectral shape. The ordering is similar to what was observed earlier, e.g. in Figure 4.20. Compared to this earlier figure, the order of the JONSWAP and Ochi-Hubble spectra has been switched. Regard-

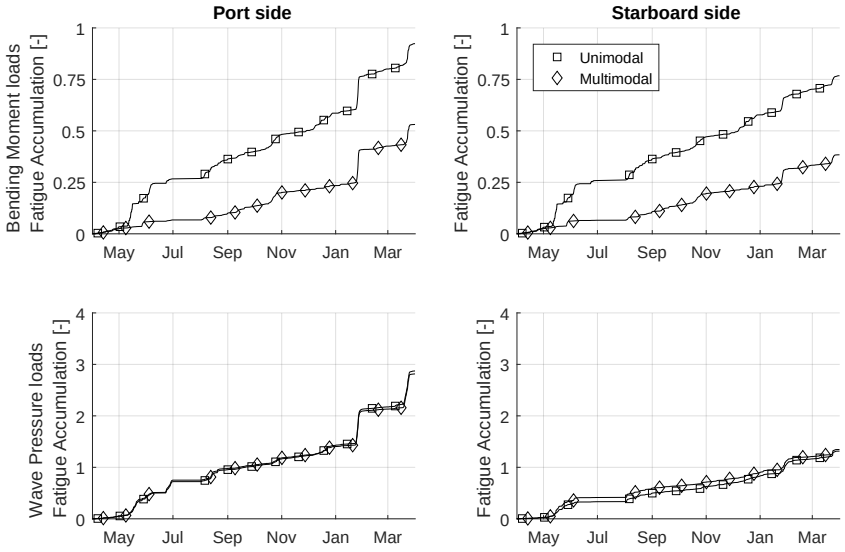

Figure 4.23: Fatigue accumulation on four typical details of unit *AUS*during one year using unimodal and bimodal description of the sea state using a spectral division obtained from wave buoy data.

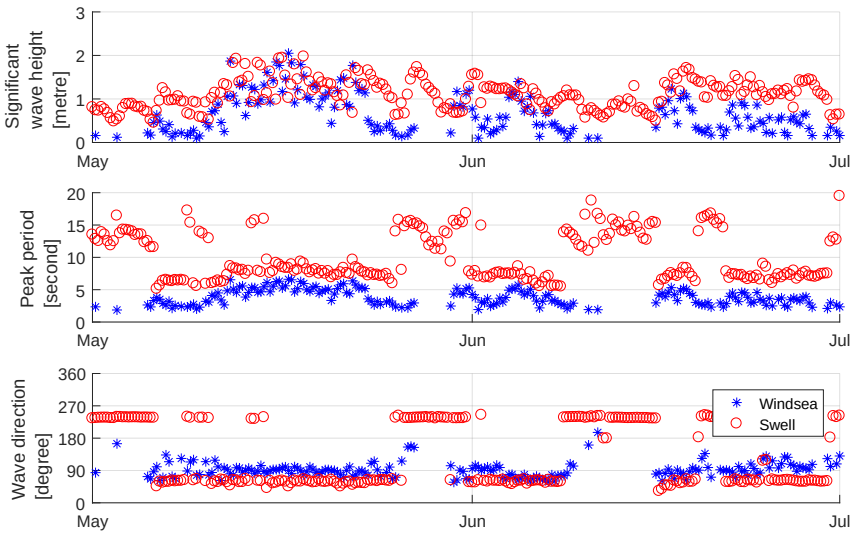

Figure 4.24: The bimodal wave statistics from May and June at the location of unit *AUS*. In this period, a large discrepancy between the fatigue calculations using unimodal and multimodal wave statistics was observed in Figure 4.23.

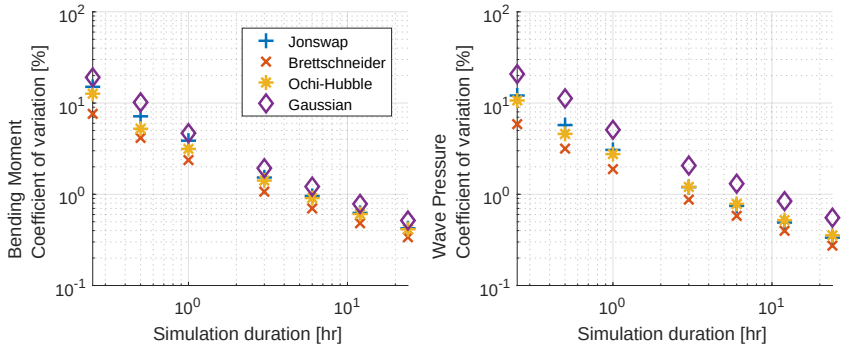

Figure 4.25: Variation of fatigue accumulation as a result of truncation of sea states. The data from two different locations on port side midship on unit *WA4* as calculated using different wave models is shown. The coefficient of variation is evaluated for sea states with a duration of 15 and 30 minutes and 1, 3, 6, 12 and 24 hours.

ing Figure 4.20, it was concluded that the spectral width of the selected spectra was the dominant feature which led to the observed relations. In this case, the peak value of the spectrum is more important, see also Figure 2.6. When the load spectrum is dominated by a few frequencies only, the phase shifts between these components will dominate the overall uncertainty. For such cases, a strong variation between individual simulations is seen, resulting in a larger scatter. However, the overall difference between these two spectral shapes is very small.

The sensitivity with respect to spectral shape is larger at details with dominant wave pressure loads than at details subject to bending moments. It should be remembered that the response operator at these details is more broadband, see also Figure 4.3. As a result, the differences in spectral shape are more pronounced, resulting in stronger deviations between the spectral shapes.

The graphs indicate a clear inverse linear trend with time on the log-log scale. For the examples using the JONSWAP spectrum, the coefficient of variation for both locations can be approximated by the following equations:

$$CoV_{BM}(t) = 4.5 * t^{-0.8} \tag{4.1}$$

$$CoV_{WP}(t) = 3.5 * t^{-0.8} \tag{4.2}$$

In which t is expressed in hours. It can be observed that the decay of the variation is equal for both locations. Typical industry practice is to consider simulations of 3 hours to assess the response. For such simulations, the coefficient of variation is in the order of magnitude between 1% and 2%. In that case, the scatter can be considered negligible. However, for shorter simulations, for example of 30 minutes duration, the typical variation is more significant with values between 5% and 10%.

4.3.4. SUMMARY OF SHORT TERM UNCERTAINTIES

The uncertainties related to the short term sea state definition as discussed in this section are summarized in Table 4.1. This table provides an indication of the scatter, ex-

pressed as the coefficients of variation, that can be expected from these different effects. The results in this table are based on findings from multiple units and can be considered baseline estimates. For specific units and units operating in specific environments, these values may be modified. Section 5.3 provides a further qualitative evaluation.

It is found that the most significant scatter is related to the definition of the spectral shape. However, these mathematical descriptions are always a simplification of the true conditions. Moreover, it should also be noted that one spectral shape, spreading function and multimodal description does not always provide the most conservative results for all different structural details. Hence, even though a significant part of the scatter can be eliminated through careful analysis, an inherent uncertainty as a result of these assumptions should always be considered.

In a time domain calculation, an additional uncertainty is introduced through truncation of the time signal. However, as discussed in section 4.3.3, this contribution only becomes significant when considering short simulations of up to 30 minutes.

The values from Table 4.1 can be used to quantify the uncertainty related to the short-term sea state definition, α_{ST}, as it was defined in section 2.4.3. The parameters related to the sea state description are significant and can result in both higher and lower fatigue estimates. The combined coefficient of variation has been calculated using equation 4.3 and the values from Table 4.1. The truncation effect should only be incorporated for time-domain methods, but the associated scatter is very small and therefore has a negligible influence. The combined coefficient of variation was found to be 53%.

$$CoV_{ST} = \sqrt{CoV^2_{spectrum} + CoV^2_{spreading} + CoV^2_{multimodal} + CoV^2_{truncation}} \tag{4.3}$$

Source	Fatigue assessment procedure	Coefficient of Variation [%]
Spectral shape	Time domain & Spectral	40
Spreading function	Time domain & Spectral	25
Multimodality	Time domain & Spectral	25
Time series truncation	Time domain	1-2
Combined	Time domain & Spectral	53

Table 4.1: Summary of the scatter in fatigue predictions introduced through various assumptions in the modelling of sea states. The additional scatter from truncation of time series was based on a 3-hour duration analysis.

The values derived here are based on a wide range of models to capture environmental descriptions. Careful examination of the typical conditions at the site of operation can significantly reduce, though not eliminate, this uncertainty. Therefore, the author proposes to model the uncertainty α_{ST} using a coefficient of variation of 0.25 on the condition that detailed analysis of the environmental conditions are conducted. This value is approximately one-half of the combined value of 0.53 from Table 4.1. Different short-term sea state representations may result in both under- and overestimates of the fatigue accumulation. A normal distribution is therefore a suitable choice:

$$\alpha_{ST} := N(1; 0.25) \tag{4.4}$$

4.4. LOADING AND OFFLOADING

The procedure to capture the uncertainty as a result of loading variations was discussed in section 2.5.3 and consisted of quantifying the variations in loading conditions from the onboard loading computer and an assessment of the differences in fatigue accumulation per condition.

The sensitivity of various details with respect to loading conditions was quantified by comparing the fatigue accumulation in the worst operating condition with the weighted average over all conditions. This ratio for various structural details and units is shown in Figure 4.26.

It can be seen that unit *WA2* is the most sensitive for changes in the loading condition and unit *AUS* is the least sensitive. Unit *WA2* has the largest cargo capacity with respect to it's lightweight at 150%. Conversely, unit *AUS* has the lowest ratio at around 60%. Hence, the difference in the external loading on the hull between the minimum and maximum loading condition is much larger on unit *WA2* compared to unit *AUS*. Deck locations, which experience mainly vertical bending, have a deviation limited to 50%. However, on the other locations the deviation is more significant. On the side shell locations, which are subject to wave pressures, the maximum response is found in a condition in which the sensor is located in the intermittent wetting area. For all other details, the maximum response is associated with the maximum draft condition.

The distribution of drafts of different units is reported in Figure 4.27. These curves show Bell-shaped curves for all units. This is the result of irregular offloading by tankers. When tankers do not arrive at regular intervals, the unit will sometimes be operating at higher drafts and not be fully offloaded by tankers. The intermediate drafts will therefore be more pronounced in the histogram than the extreme high and low drafts, as is indeed the case. In a design assessment, only a limited number of loading conditions, typically three or four, are considered.

The spread moored units operate along a wide range of drafts, even including drafts below the minimal design condition. It should be noted that the minimal design condition is not a condition without any cargo onboard but a ballast condition. Hence, drafts below the draft of the minimum condition are indeed possible during operations following an offloading operation. The distribution of the draft for unit *AUS* shows a generally higher loading and smaller variation. This will be partially related to the relative short measurement period available for this unit.

Fatigue assessments have been executed for the different units using the assumed loading profile from the design and the measured operational profile. These results are shown in Figure 4.28. This figure shows that in most cases the design operational profile results in a conservative fatigue assessment. This is especially true for the details in the side shell and stringer of unit *WA2*. Figure 4.26 showed that this unit is especially sensitive to changes in the loading conditions. On the other hand, unit *AUS* shows some non conservative results. On a number of side shell details, the fatigue accumulation has a bias up to 17% when using the measured loading profile compared to the design loading profile. Figure 4.27 showed that this unit has indeed been operating a significant amount of the time at larger drafts compared to the other units, resulting in a larger than expected fatigue accumulation.

It should be noted that the sensitivity study displayed in Figure 4.26 showed a clear

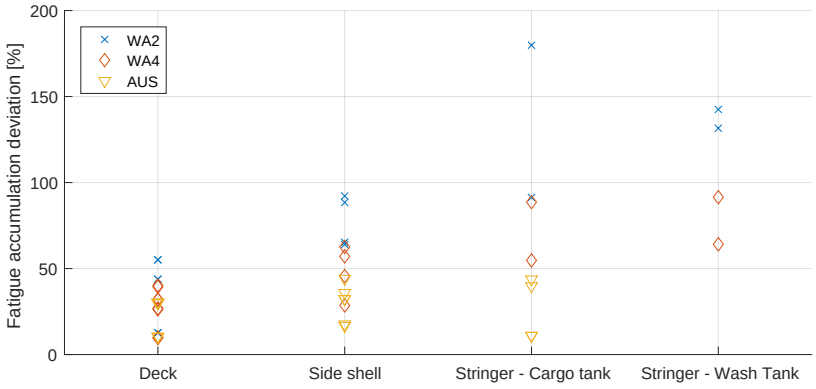

Figure 4.26: Increase of fatigue accumulation in the loading condition which results in the maximum fatigue accumulation with respect to the weighted average fatigue accumulation over all loading condition. Multiple measurement locations are plotted jointly in these graphs.

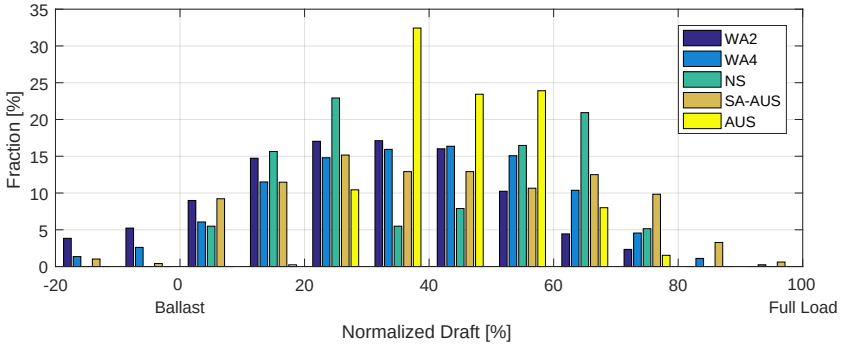

Figure 4.27: Distribution of draft on multiple units. The draft has been normalized using the minimal design draft as 0% and the maximum draft as 100%.

ordering between the different units, which is also visible on the side shell and stringer locations in Figure 4.28. However, the differences between the deck locations were relatively small and no clear ordering between the units is visible.

The observed bias in the fatigue accumulation on the side shell structural details is unit dependent. Figure 4.28 shows that the random scatter of the fatigue accumulation in the side shell between the individual units is quite consistent with a coefficient of variation of around 10%. Hence, it is concluded that the loading conditions should be monitored for an accurate assessment of the fatigue accumulation in side shell and stringer structural details and an additional coefficient of variation of 10% can be adopted to account for random scatter.

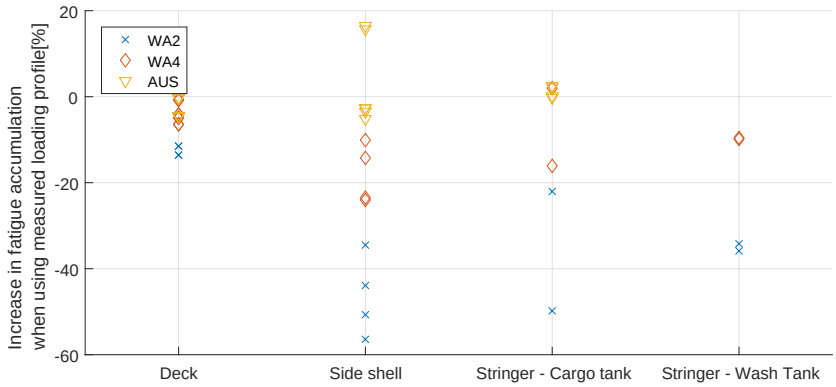

Figure 4.28: Change in fatigue accumulation between the true and assumed loading condition for various units and structural details. Multiple measurement locations are plotted jointly in these graphs.

4.5. LOAD PROCESSES - WAVE-FREQUENT

4.5.1. HULL GIRDER BENDING

In this section, the uncertainty in the prediction of stresses resulting from wave bending moments is examined. These uncertainties include an uncertainty in the prediction of stress from the numerical models, quantified by α_{HS}, and an uncertainty in the fatigue assessment method, α_{Meth}. A dedicated subsection is included which reviews the fatigue accumulation while en route from yard to production field. During this transportation, the unit can encounter significant horizontal bending of the hull, which is not normally encountered during production.

HYDRODYNAMIC AND STRUCTURAL UNCERTAINTIES

The procedure for calculation of the joint uncertainty arising from hydrodynamic and structural analysis was discussed in section 2.5.4. The spread-moored units in this study are barge shaped configurations, while the turret-moored units are more streamlined units. There are both purpose built FPSOs as well as converted tankers in this latter group. Weather conditions at the majority of the locations are mild and operations occur,

of course, at zero speed. The hydrodynamic analysis procedures for such cases are well established and were discussed in section 2.3.1. The calculation of structural response is executed using the Finite Element Method.

The input used in the structural analysis is not always representative of the actual new built structure. In order to account for general corrosion over the lifetime of the unit, additional material thickness is added to the structure beyond the minimal scantlings required from strength requirements. Regulations stipulate that numerical analyses for fatigue design are executed accounting only partially for this additional corrosion allowance, see e.g. the codes by ABS and DNV [20, 23]. Because of the added material, when measuring structural stresses at the beginning of the life of the unit, these are lower than predicted using the design model. As time progresses, corrosion may occur in the structure. However, general corrosion over an entire cross section is very rare and corrosion typically occurs on parts of the cross section only. Hence, the global strength characteristics change only a little over time. Stresses induced by global bending loads are governed by the global strength characteristics and these will therefore change by a small amount. In section 4.5.2, stresses resulting from local wave pressures are studied. In that case, the strength characteristics of the stiffened panel will govern the stresses. Local corrosion of an entire stiffened panel is more likely according to de Farias and Netto [138] and therefore, stresses induced by wave pressures can change over the lifetime of the unit. Local corrosion effects, such as pitting, can result in new fatigue hotspots, but will not be considered in this study and are not generally modelled in design assessments.

The requirements imposed by the calculation procedure as discussed in section 2.5.4 are quite strict. A sufficient amount of simultaneous wave, strain and draft information needs to be available. For this reason, only results from four units are provided. The parameters α_{HS} indicates the ratio of the true stresses and the calculated stresses based on a spectral calculation using the wave environment as registered by the wave buoy and RAOs obtained from the numerical model. This parameter is determined at each measurement detail for all individual loading conditions of each unit using all available data. The results are shown in Figure 4.29. The values have been subdivided into multiple groups. A distinction was made based on the loading condition, since the units rarely operate at maximum or minimum draft. The amount of data associated with these loading conditions is therefore relatively small. For some units, multiple intermediate conditions have been defined. Secondly, a subdivision was made based on the cross section which has been monitored. The points indicated in Figure 4.29 do not differentiate between structural details on port and starboard side. Since the points from each unit for a specific loading condition and cross section show small deviations, the findings on the port and starboard side structural details are quite consistent.

In the intermediate loading condition, α_{HS} varies between 0.65 and 1.15. This means that the RAOs determined from the numerical hydrodynamic and structural software result in a bias between -35% and +15%. The estimated values for the ballast and fully laden loading conditions, when available, show larger deviations. Table 4.2 shows the summary statistics of all data points of all units, both including and excluding the ballast and fully laden loading conditions. The table shows the mean value of the α_{HS} hardly changes, but the standard deviation increases from 0.12 to 0.16 when including these

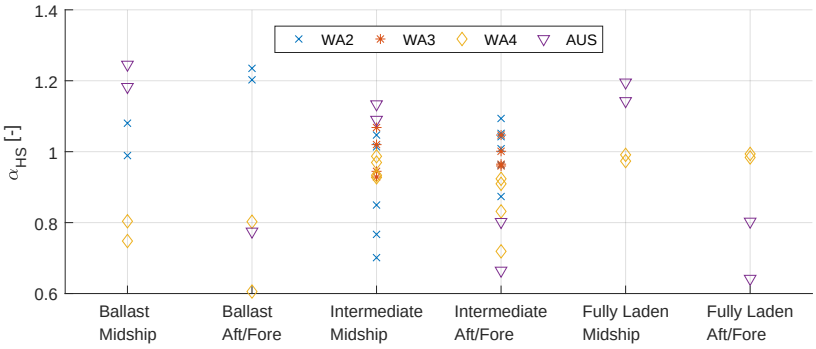

Figure 4.29: The scale factor α_{HS} as determined for multiple structural details subjected to hull girder bending.

	Bias	Standard deviation
All loading conditions	-0.05	0.16
Intermediate loading condition	-0.06	0.12

Table 4.2: Statistics of the joint hydrodynamic and structural analysis uncertainty parameter α_{HS} corresponding to the observed values from Figure 4.29.

two loading conditions with sparse data.

For unit *AUS*, the difference between the observed values at the midship and aft- or foreship sections is significant. The foreship measurement section is located in way of the turret area. The consistent result between both measurement locations and multiple loading conditions indicates that, at this section, a systematic difference in the hydrodynamic and/or structural model exists. This part of the structure will feature additional safety margins to accommodate mechanical loads from the turret and mooring system. For the other units, no significant difference between the measurement sections was observed.

Several distributions have been fitted to the data of α_{HS} using Maximum Likelihood Estimators. Only the data of the intermediate loading conditions has been used for this analysis. The data presented in Figure 4.29 show that α_{HS} has a tail towards lower values, i.e. a left-hand tail. The distributions which have been fitted are summarized in Table 2.3. These distribution families are either symmetrical or feature a right-hand tail.

	$\mathscr{L}$	AIC	BIC
Normal	24.5	-45.0	-42.1
Inverted Weibull	24.8	-45.7	-42.8
Inverted Lognormal	22.1	-40.2	-37.3
Inverted Gumbel	24.6	-45.1	-42.3

Table 4.3: Goodness of fit parameters for various families of distributions used to model α_{HS}. The shown parameters include the Loglikelihood function $\mathscr{L}$ and both the Akaike and Bayesian Information Criterion.

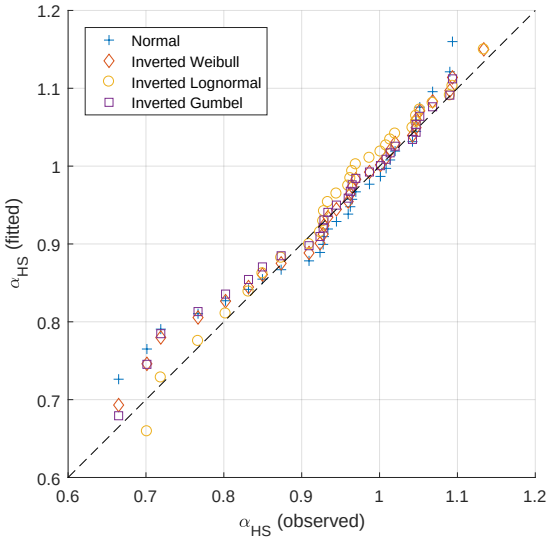

Figure 4.30: Q-Q plot of the observed α_{HS} and fits from a selected number of families of continuous distribution functions.

Therefore, the asymmetric distributions have been inverted and fitted to $1.15-\alpha_{HS}$ instead. The Q-Q plots of the fitted distributions are shown in Figure 4.30. The goodness-of-fit statistics, see also section 2.6, of these distributions are given in Table 4.3.

The Q-Q plot shows that the lognormal distribution is superior in modelling the tails of the observed α_{HS}. As a result, this distribution achieves the best score in the goodness-of-fit statistics. The distribution as plotted in Figure 4.30 is given by the following formulation:

$$1.15-\alpha_{HS} := L(-1.77, 0.70) \tag{4.5}$$

FATIGUE ASSESSMENT METHOD

The performance of the fatigue assessment method is quantified through the parameter α_{Meth}. For this aim, the same set of data to define α_{HS}, was used. Scatter plots of the fatigue assessment from the spectral method and as directly assessed using the strain gauge are shown in Figure 4.31. Only results of the midship area locations are discussed here. The spectral analyses are based on half-hour wave spectra obtained from the dedicated wave buoys. The direct assessments use strain data from the corresponding time interval.

The scatter plots show a good correspondence between the value determined using the spectral calculation and from the strain gauges. Overall, the spectral method provides a slightly higher fatigue accumulation rate. At higher fatigue accumulation rate, the scatter between the two methods becomes smaller. Other researchers have found similar results. Kyoung *et al.* [139] provide an example of a similar comparison for a complex

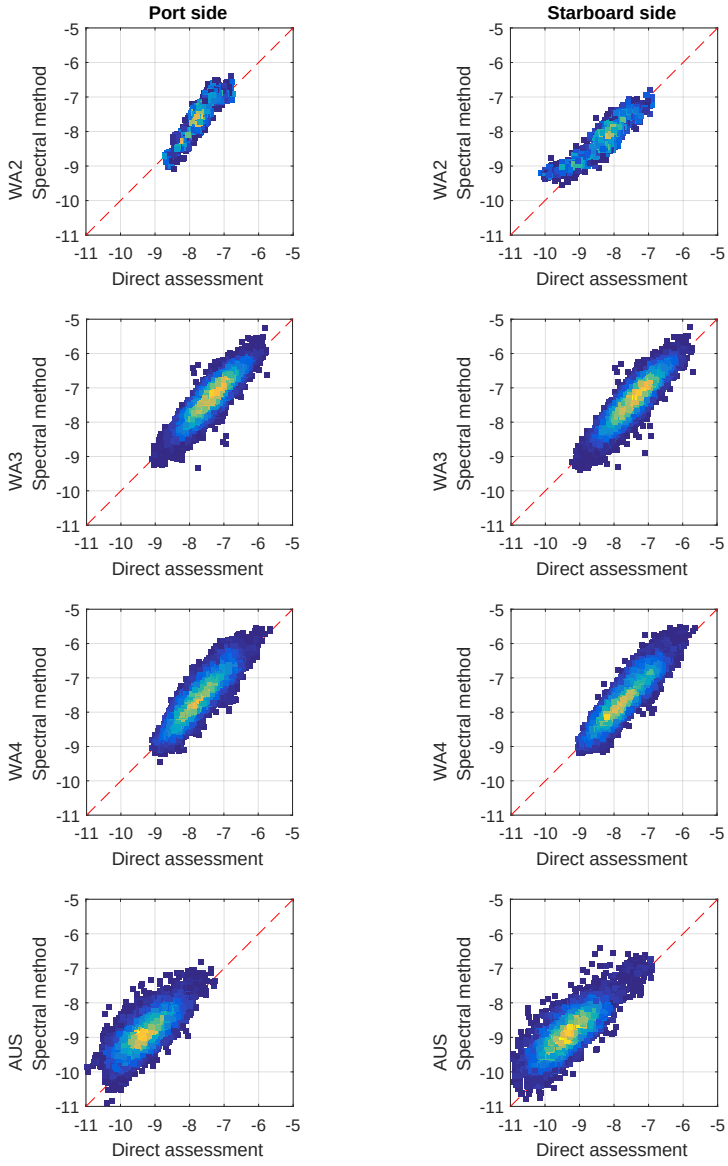

Figure 4.31: Scatter plot of the calculated and measured fatigue accumulation rate (logarithmic scale) of the midship deck locations for the selected units.

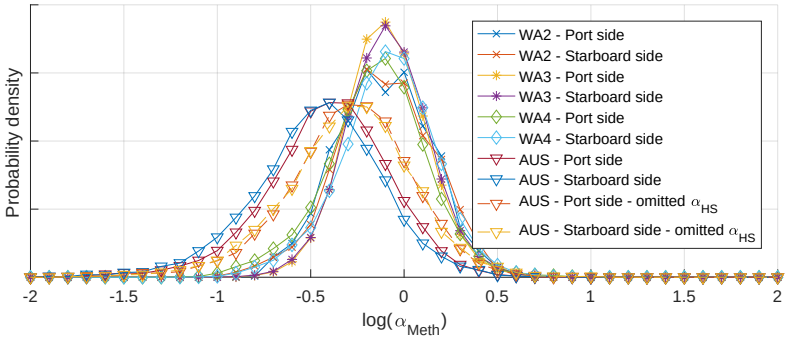

Figure 4.32: Probability density of α_{Meth} for the selected locations from Figure 4.31.

structure in a semi-submersible where multiple load phenomena interact. These authors show that the spectral method is most conservative in smaller sea states and both methods converge in higher sea states. This occurs because one of the involved loading mechanisms becomes more dominant over the other loading effects and the stress field becomes more uniform.

The results from unit *AUS* deviate more strongly. It should be noted though that this unit is operating in a more complicated sea state with windsea and swell components from distinct directions. Figure 4.22 has already shown that at this location, multimodality of the sea state has a significant effect on the fatigue accumulation. The decomposition of wave energy into a frequency-direction spectrum can be one of the limiting factors in the accuracy. Moreover, the spectral calculation shows a larger conservatism for this unit. Figure 4.29 has shown that the RAO at the midship location has been increased based on the comparison between strain and wave measurements. This correction contributes to the higher fatigue accumulation rate using the spectral method. For this unit only, the spectral assessment has been repeated omitting the numerical model correction factor α_{HS}.

The probability density of the correction factor α_{Meth} is shown in Figure 4.32. The associated bias and standard deviation are given in Table 4.4. On average, α_{Meth} indicates that the spectral fatigue assessment procedure returns a bias of around -10% compared to the true fatigue accumulation. This indicates that the method provides an overestimate of the true fatigue accumulation. However, there is a significant scatter between the individual observations. The conservatism on unit *AUS* is much higher at around a factor two on average. There is an interaction between the uncertainties introduced through α_{Meth} and α_{HS}, which was particularly high for this unit. When removing the additional conservatism introduced through α_{HS} on unit *AUS*, the characteristics of α_{Meth} resemble those of the other units better, but the calculation method still provides larger values compared to the other units on account of the more complicated sea states.

Figure 4.32 indicates that the distribution of α_{Meth} can be modelled using a Lognormal distribution. The associated distributions are described in Table 4.5. The estimated parameters relate well to a visual inspection of the distributions shown in Figure 4.32.

The Tool Accuracy Factor (TAF) was defined in Equation 2.32 as the ratio of the true

	Port side		Starboard side	
	bias	standard deviation	bias	standard deviation
*WA*2	-0.09	0.55	-0.07	0.57
*WA*3	-0.09	0.52	-0.07	0.55
*WA*4	-0.14	0.62	-0.04	0.61
AUS	-0.482	0.44	-0.53	0.45
AUS - omitted α_{HS}	-0.33	0.57	-0.32	0.65

Table 4.4: Statistics of α_{Meth} corresponding to the probability functions in Figure 4.32 as determined on the midship deck locations on several units.

	Port side	Starboard side
*WA*2	L(-0.11;0.25)	L(-0.11;0.26)
*WA*3	L(-0.10;0.22)	L(-0.090; 0.22)
*WA*4	L(-0.15;0.27)	L(-0.093;0.26)
AUS	L(-0.41;0.33)	L(-0.46;0.35)
AUS - omitted α_{HS}	L(-0.29;0.33)	L(-0.30;0.35)

Table 4.5: Definition of the best fitting Lognormal distribution on α_{NLin}.

fatigue accumulation and the fatigue accumulation calculated using the spectral method over the entire analysis period. While α_{meth} provides instantaneous values which help to understand the average performance of the design tool and its uncertainty, the TAF provides a more practical quantification of the same uncertainty over the entire lifetime of the unit. Table 4.6 shows the TAF of the selected details. This table implies that the calculation method results in larger fatigue accumulation compared to the measured values, i.e. is more conservative. The factors found in this procedure are smaller than the mean values of α_{Meth} as shown in Table 4.4. This is a result of the fact that the fatigue assessment method becomes more conservative when the fatigue accumulation rate is larger. This can be observed in Figure 4.31 by noting that the point clouds feature a slightly upward tilted angle compared to the reference line where computations and measurements are equal.

Two aspects of the fatigue assessment method are examined further. These are the assumed narrowbandness of the observed stress cycles and weak nonlinearities. The

	Port side	Starboard side
*WA*2	0.57	0.87
*WA*3	0.70	0.70
*WA*4	0.55	0.61
AUS	0.40	0.40
AUS - omitted α_{HS}	0.51	0.58

Table 4.6: Tool Accuracy Factor as determined on the midship locations subject to hull girder bending.

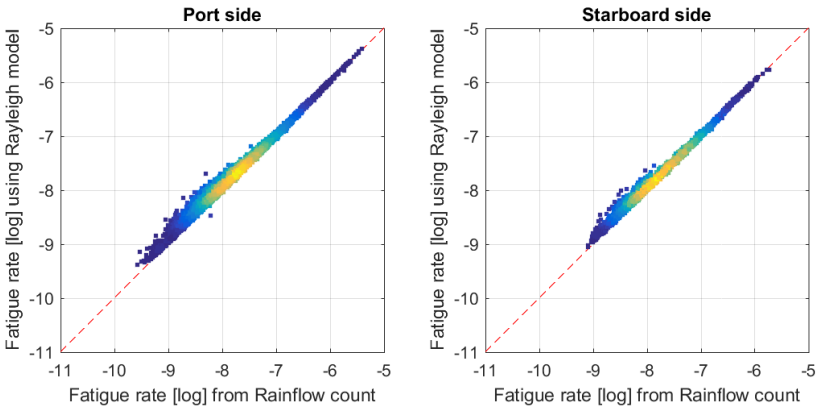

Figure 4.33: Fatigue accumulation rate calculated from Rainflow count and assuming Rayleigh distributed stress ranges on unit *WA*4.

procedures to do so were discussed in Section 2.5.4.

NARROWBANDED LOADS

By assuming narrowbanded load cycles, the short-term stress distribution can be modelled with a Rayleigh distribution. This assumption results in the analytical expression of the fatigue accumulation in Equation 2.13. Work by Friis Hansen [140] already indicated that the assumption on narrowbandedness of the response introduces some uncertainty and simulations should be executed to verify the validity of this assumption for specific cases. In this study, the true fatigue accumulation, based on rainflow counting, has been compared with the fatigue accumulation using the assumed Rayleigh distribution. In the latter case, the distribution was defined by deriving the standard deviation of each time series of measured stress. The actual zero-crossing period was also retrieved from the time series, such that the actual number of cycles is equal. Hence, the only difference between the two calculations originates from the assumption of the Rayleigh distribution to capture the short-term stress distribution. A representative example of a scatter plot comparing both fatigue assessments is shown in Figure 4.33. This figure shows two representative locations from unit *WA*4.

Figure 4.33 indicates a very strong relation between the fatigue evaluated using the Rainflow count method and spectral formula. The narrowbanded load distribution results in a slightly conservative result and a minor variation. Both are however much smaller than the overall calculation method uncertainty and bias as were shown in Figure 4.31. The statistics of the difference between both calculations are reported in Table 4.7 and can be compared to the statistics of the complete method in Table 4.4. The bias in the overall fatigue assessment is similar to the bias introduced by using the narrowbanded assumption. This means there is a similar degree of conservatism in both cases. However, Figure 4.31 showed a slightly progressive conservatism in the calulca-

	Port side		Starboard side	
	bias	standard deviation	bias	standard deviation
*WA*1	-0.10	0.084	-0.12	0.12
*WA*2	-0.09	0.056	-0.09	0.060
*WA*3	-0.05	0.055	-0.05	0.053
*WA*4	-0.08	0.080	-0.07	0.058
NS	-0.03	0.041	-0.04	0.045
AUS	-0.12	0.086	-0.14	0.082

Table 4.7: Statistics of the difference between the true fatigue accumulation and that obtained assuming Rayleigh distributed stress cycles as determined on the midship deck locations on several units.

tion, i.e. at a higher fatigue accumulation rate, the spectral method provides slightly larger fatigue accumulation rate. This is not the case when looking at the narrowbandedness alone. In fact, at higher fatigue accumulation rates, the scatter introduced by this assumption reduces. Overall, the scatter introduced through the narrowbanded assumption is an order of magnitude smaller than the scatter of the total fatigue assessment method.

WEAK NONLINEAR LOADS

The influence of weak nonlinearity of the stress cycle distribution has been examined. For this aim, exceedance plots of the tensile and compressive stress peaks of the seakeeping loads have been generated. Two examples of a spread moored and a turret moored unit are shown in Figure 4.34. These figures show that there is very little difference between the tensile and compressive stress and consequently between the hogging and sagging bending moments. These offshore units are strongly barge-shaped units without flare which results in the symmetrical behaviour as observed here.

In order to compare the difference between hogging and sagging induced stresses, the difference between these has been assessed for multiple midship sensors at several levels of the probability of exceedance curve. These results are shown in Figure 4.35. The tails of these distributions is heavily influenced by outliers and have therefore been removed.

Most units show a very consistent deviation between the compressive and tensile stress at the two opposing locations. For example, unit *WA*3 and *WA*4 show a good match between both locations and also a gradually increasing difference between the compressive and tensile stresses. At lower levels of probability of exceedance, the difference becomes larger but rarely exceeds 5%. The most pronounced difference between the compressive and tensile stress can be observed on unit *NS*. This unit is a tanker shaped unit, whereas the others are barge-shaped and a larger difference can be expected as a result of the bow flare shape. This unit also shows the largest difference between port and starboard side sensors. The measurements on this unit have started relatively recently and this distribution is governed by a few storm conditions only. When such storms have an incoming direction which is slightly off the bow, this will affect the relation between the stresses on both sides of the unit. It is therefore argued that the results for this unit are

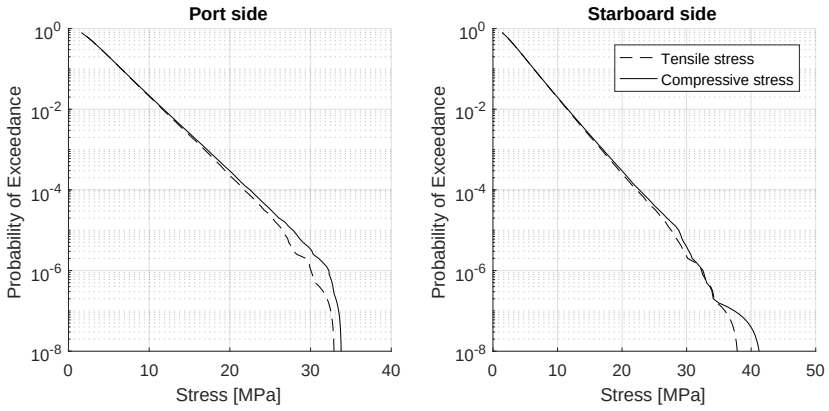

(a) Spread moored unit *WA3*

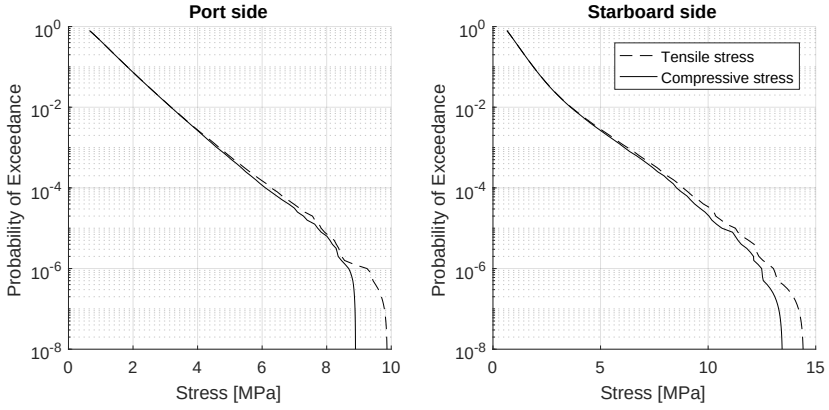

(b) Turret moored unit *AUS*

Figure 4.34: The probability of exceedance distributions of the stresses measured by deck sensors at the mid-ship section.

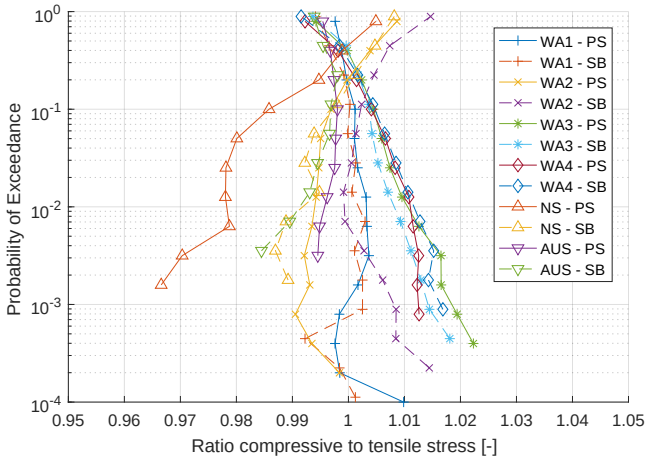

Figure 4.35: The difference between tensile and compressive stresses at several levels of the probability of exceedance for multiple units and port (continuous lines) and starboard side (dashed lines) mounted sensors.

likely not fully converged yet and should be used with caution. Still, the observed difference between the tensile and compressive stresses is very small for all cases and remains within 4% up to the 10^{-3} probability of exceedance level.

FATIGUE ACCUMULATION DURING TOWING

While only short in duration, the transportation phase of the unit can be of significant importance. During the tow, an FPSO may encounter beam sea conditions which result in significant horizontal bending, a loading mechanism that is not normally encountered during operation. For the units operating in West-Africa, the in-field conditions are mild, but during the transport, harsher environmental conditions can be encountered. As examples, design analyses have indicated that the fatigue contribution of the transportation phase is equivalent to 1 year of in-field operation for selected details on unit *WA4* and 3 years for selected details on unit *AUS*. The analysis of weather conditions, and the associated spectral fatigue assessments, from some of the units was provided in Section 4.2.2. In this section, a comparison between the spectral analysis and the direct assessment using strain gauge measurements for units *WA4* and *AUS* is given.

The fatigue accumulation during the tow on the two selected units is shown in Figure 4.36. This figure shows the port side locations on two different cross sections. In both cases, the fatigue accumulation on the midship section is lower than that on the other section. This can be observed for both the spectral assessment as well as the direct analysis using the strain gauge measurements and rainflow counting. In case of unit *WA4*, section 4.2.2 has shown that the unit experiences significant stern quartering sea states. These conditions result in larger fatigue accumulation in the aftship section than in the midship section. In case of unit *AUS*, a brief storm event with head sea conditions was encountered resulting in larger loads in the foreship area in a short period.

The fatigue accumulation obtained from the spectral method on the aftship section

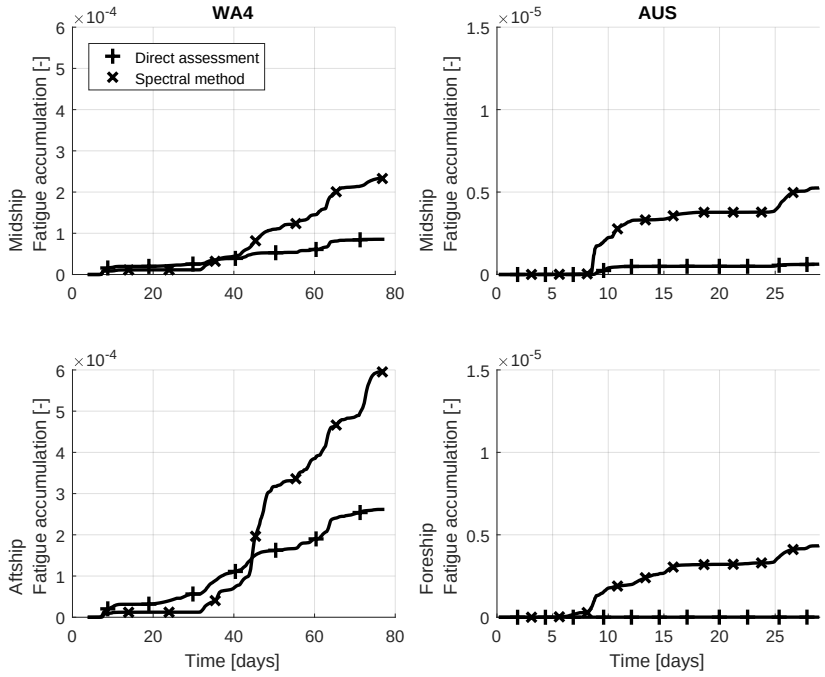

Figure 4.36: Fatigue accumulation during tow determined from the spectral assessment and obtained from strain gauges at two locations on both unit *WA4* and unit *AUS*.

of unit *WA4* is strongly dominated by a single event. The associated wave statistics, shown in Figure 4.14, show that this event is associated with head sea conditions and a large peak period of around 12 seconds. However, the fatigue accumulation determined from the strain gauge does not increase that strongly in this interval. It should be remembered that for this analysis only bulk statistics were available. The presence of confused sea states and wave spreading are therefore potential reasons for this deviation, see also sections 4.3.1 and 4.3.2. On unit *AUS*, the fatigue accumulation on both sections is dominated by the aforementioned storm event and a secondary event which was identified as the moment the unit leaves the Indonesian Archipelago and enters the swell dominated environment of the Indian Ocean.

Table 4.8 presents the Tool Accuracy Factor, i.e. the ratio between the true fatigue accumulation and that obtained from the spectral analysis. These factors are reasonably in line with those obtained during the in-field deployment as reported in Table 4.6. The observed difference at the midship section on unit *AUS* is particularly large. Unfortunately, with the opposing starboard side sensor being unavailable during the tow, there is no possibility of a comparison with that sensor. Other than that, the observed numbers are only slightly lower. The wave conditions during the tow are more severe than during the in-field deployment. Figure 4.31 has shown that the calculation method pro-

vides a larger overestimation of the fatigue accumulation when the fatigue accumulation rate increases. Since the transportation period features more severe weather condition, this explains the somewhat lower Tool Accuracy Factors observed during the tow than during the in-field deployment.

	Midship	Fore-/Aftship
WA4	0.37	0.44
AUS	0.12	0.37

Table 4.8: Tool Accuracy Factor as determined on the port side locations at multiple sections subject to hull girder bending during the transportation phase.

4.5.2. WAVE PRESSURE

In this section, the uncertainty in the prediction of stresses resulting from wave pressures is examined. These uncertainties have been defined in section 2.5.4 and include an uncertainty in the prediction of stress, quantified by α_{HSI}, and an uncertainty of the fatigue assessment method, α_{Meth}.

HYDRODYNAMIC AND STRUCTURAL UNCERTAINTIES

The procedure for calculation of the joint uncertainty arising from hydrodynamic and structural analysis was discussed in section 2.5.4. The uncertainties arising from the hydrodynamic and structural models were already discussed in section 4.5.1 for structural details subjected to global bending loads. The linearisation of wave pressures introduces an additional uncertainty to the structural details examined here. The linearisation procedure was described in Section 2.3.4.

In order to quantify the bias and scatter in the prediction of structural stress from the measurements, a couple of different data sources need to be combined. Simultaneous availability of strain measurements, wave buoy measurements and loading condition information needs to be achieved. A sufficient amount of data needs to be available as well in order to make a justified comparison. As in Section 4.5.1, this restricts the analysis to four units.

The importance of intermittent wetting on the fatigue accumulation of structural details in the side shell can be shown by comparing the measured structural response and the location of the sensor with respect to the mean water line. This relation is shown in Figure 4.37 for two units. This figure shows the fatigue accumulation rate determined from the strain sensor in all weather conditions. It is clear that the largest fatigue accumulation is sustained when the sensor is slightly below the water line. The fatigue accumulation reduces fast when the draft becomes smaller and the sensors rises higher above the mean water line. The fatigue rate slowly reduces when the draft increases. In that case, the panel on which the sensor is mounted becomes fully wetted. Wave pressure variations decrease exponentially with the water depth. This trend is visible in the graph. On unit *WA4*, it can be observed that the maximum fatigue accumulation occurs when the sensor is located around 1 metre below the mean water line instead of exactly at the water line crossing. The deformation of the panel on which the sensor is

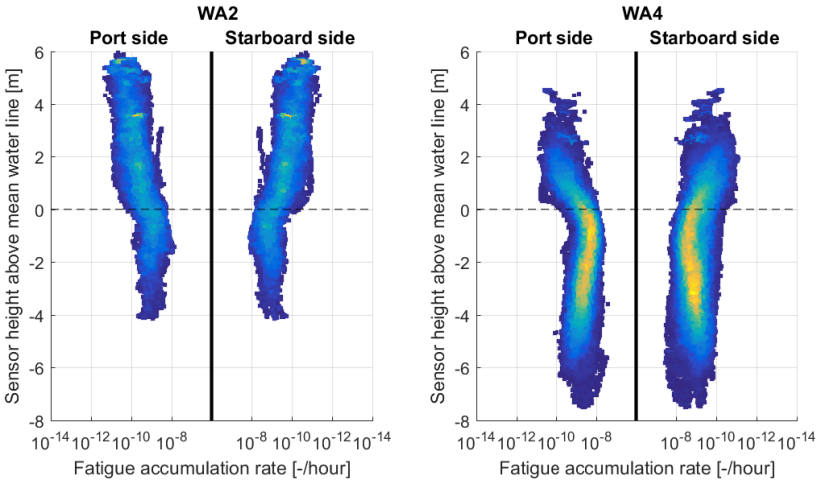

Figure 4.37: Fatigue accumulation rate observed at measurement locations in the side shell in relation to the location of the sensor with respect to the mean water line. The selected measurement locations are around the midship area and port side and starboard side sensor are mounted symmetrically.

mounted, is governed by wave pressure over the whole panel. The largest pressure variations on this panel, and consequently deformations at the measurement location, are observed when the mean water line is near the centre of the panel, not when it is at the height of the sensor itself.

Intermittent wetting is only incorporated for structural details in the side shell which are close to the mean water line. Other structural details are either fully submerged, in which case continuous pressure variations on the hull are incorporated, or not submerged at all. In this context 'being close' to the water line is a relative feature and depends on the governing environmental conditions. In areas with more violent sea states, a larger part of the side shell is subjected to intermittent wetting. The size of the affected area in various conditions can be examined by determining the Probability of Exceedance (PoE) curves of the instantaneous wave heights at each location. These have been obtained through summation of the individual sea states using equation 4.6. In this equation, $T_{z'i}$ and $\bar{T}_z$ indicate the zero-crossing period in the i'th sea state and the average period over all sea states. The cumulative distribution function of the wave height in each sea state, $CDF_i(h)$, complies with the Rayleigh distribution as defined in Equation 2.9.

$$PoE(h) = 1 - \sum_{i=1}^{N} \frac{\bar{T}_z}{T_{z'i}} CDF_i(h) \tag{4.6}$$

A 5-year period of wave data has been retrieved from hindcast models for this analysis. The curves obtained for the various units are shown in Figure 4.38. In West-Africa the typical wave amplitudes are very small and increase only a little for lower PoE levels. Unit *AUS*, which is operating in Australia, also experiences a large amount of very small waves. However, this unit is operating in a cyclone prone area and, as a result, the

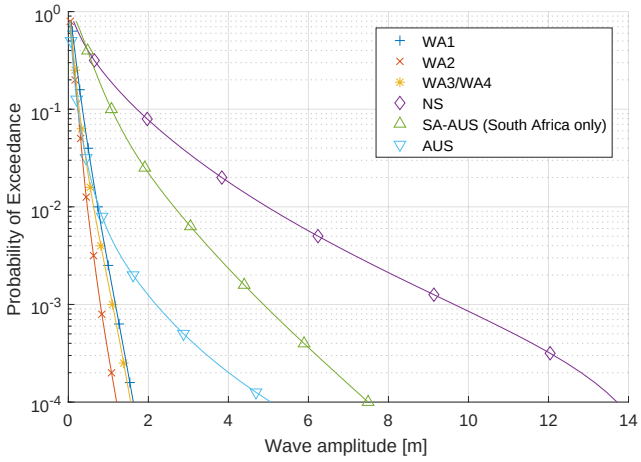

Figure 4.38: The probability of exceedance of wave amplitudes at various locations.

wave amplitude increases rapidly for lower PoE levels. Unit *SA-AUS* is operating in an environment dominated by strong swells from two oceans which results in even higher wave amplitudes compared to unit *AUS*, but with a more gradual increase. The West of Shetland area is an area dominated by Atlantic swells and frequent storms. As a result, much larger waves are observed here.

The linearisation procedure is applied to a discrete number of load cases. For each load case, a different part of the side shell hull will be affected by intermittent wetting. The linearisation procedure will perform best for structural details which are located at the same height as the mean water line of a loading condition. This procedure works well for trading vessels which operate at a discrete number of loading conditions. Offshore production units work at continuously changing drafts and this leads to a larger uncertainty in the overall method. Figure 4.38 shows that on the West-Africa units, an area of 1 metre above and below the mean water line will encounter frequent intermittent wetting. This also means that for structural details in the side shell which are not within 1 metre of a predefined load case, no intermittent wetting is incorporated in the assessment. For the other units, a larger area will be affected by intermittent wetting and structural details may include intermittent wetting effects in multiple load cases.

The stress scaling factors α_{HSI} have been determined according to the procedures from section 2.5.4. These results are shown in Figure 4.39. As with the global hull girder loads, the figure shows results from the ballast and fully laden loading conditions separately, because a smaller amount of data was available to analyse these conditions.

The observed correction factors are relatively constant per unit. On unit *WA*2 and *WA*4, α_{HSI} varies between 0.7 and 1.1, although on unit *WA*2 both ballast aftship sensors show and outlier. On the other two units, α_{HSI} is much lower. On unit *WA*3, the correction factor varies between 0.15 and 0.65 and unit *AUS*, it varies between 0.2 and 0.5. In most cases, a systematic difference between the midship and aft or foreship section can be observed. For each loading condition, the results of opposing port and starboard side

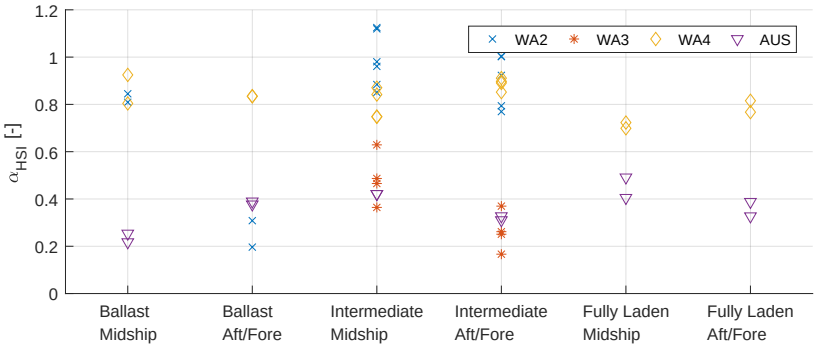

Figure 4.39: The scale factor α_{HSI} as determined for the various structural details subjected to wave pressure induced stresses.

details are displayed. The difference between the parameters α_{HSI} on the two sides of the unit is often negligible.

In order to better understand these scaling factors, a comparison of the RAOs before and after application of α_{HSI} is provided in Figure 4.40. Two load features can be distinguished in these graphs. First of all, at low frequencies there is a peak resulting from global deformation modes. The frequency and magnitude of this peak varies per unit, depending on unit size, but also on the location of the sensor with respect to the neutral axis of the cross-section. Secondly, the response to wave pressure can be identified. This response is a quasi-static response to the relative wave elevation. It is therefore characterized by a near-constant value at higher frequencies. In long waves at low frequencies, the unit is moving with the waves resulting in no relative wave elevation, while in short, high-frequency waves, the units remains stationary, resulting in a near constant stress response. Given that all units are of similar dimensions, a comparable level would be expected. The design RAOs from unit *WA*3 and *AUS* show a relative high quasi-static response level. After application of α_{HSI}, the response level becomes more comparable between the different units. It is therefore argued that the original design methods from these units provide overestimates of the stress response.

Having established that the mean of α_{HSI} varies strongly per unit, an overall model to capture the scatter can be derived by removing the unit-specific bias. In this analysis, the ballast condition of unit *WA*2 has been ignored due to the low number of data points used when obtaining these values. The mean values of α_{HSI} for each unit are reported in Table 4.9

*WA*2	*WA*3	*WA*4	*AUS*
0.94	0.37	0.82	0.36

Table 4.9: Mean value of α_{HSI} for the different units corresponding to the observed values from Figure 4.39.

The parameter $\Delta\alpha_{HSI}$ is defined as α_{HSI} after removing the unit specific bias. The data from $\Delta\alpha_{HSI}$ from all units has been analysed jointly. This parameter was found to

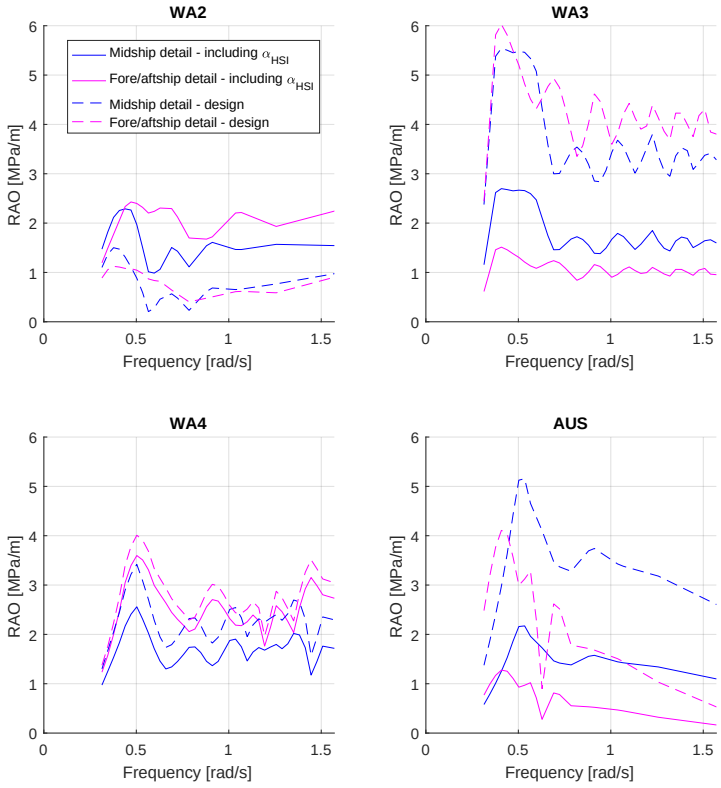

Figure 4.40: RAOs of the stress in head sea conditions at the midship measurement locations, both including and excluding the scale factor α_{HSI}.

have a standard deviation of 0.10. To examine the probability distribution of $\Delta\alpha_{HSI}$, several parametric distributions from section 2.6 have been fitted to the observed values. These include the Normal, Weibull, Lognormal and Gumbel distributions. To accommodate the possibility of a tail on either end of the distribution, these last three models have also been inverted before fitting to the data set. Because the parameter $\Delta\alpha_{HSI}$ has a mean of zero by definition, an offset must be applied to the bounded distributions. A value of 0.3, i.e. three times the standard deviation, has been used as offset. The Q-Q plots of the fitted distributions are shown in Figure 4.41. This figure shows that both the Normal distribution as well as the Weibull distribution with the tail on either end, fits the data well. The other distributions show an overestimation of the left tail of the data. Since the data does not suggest a strong tail, it is proposed to adopt a normal distribution to model $\Delta\alpha_{HSI}$. Hence, the definition in equation 4.7 is proposed to capture the stochastic properties of α_{HSI}. $\overline{\alpha_{HS'unit}}$ indicates the mean value of α_{HSI} for a specific unit.

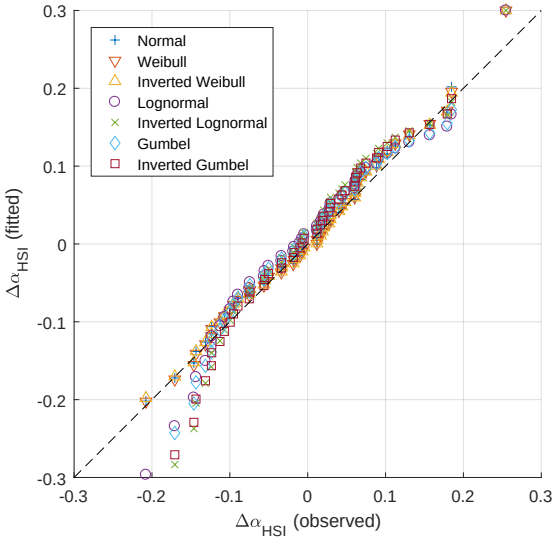

Figure 4.41: Q-Q plot of the observed α_{HSI} and fits from a selected number of families of continuous distribution functions.

$$\alpha_{HS} := N(\overline{\alpha_{HS'unit}}, 0.10) \tag{4.7}$$

FATIGUE ASSESSMENT METHOD

The performance of the fatigue assessment method is quantified through the parameter α_{Meth}. For this aim, the same set of data to define α_{HSI}, was used. Scatter plots of the fatigue assessment from the spectral method and as directly assessed using the strain gauge are shown in Figure 4.42. Only results of the midship area locations are discussed here. The spectral analyses are based on half-hour wave spectra obtained from the dedicated wave buoys. The direct assessments use strain data from the corresponding time interval.

The scatter plots show a reasonable correspondence between the value determined using the spectral calculation and from the strain gauges. Depending on the unit and the structural detail which is being analysed, the spectral method can provide both a slightly higher or lower fatigue accumulation rate. The variation on unit *AUS* is larger than on the other units. However, this observation primarily pertains to conditions in which there is low fatigue accumulation and therefore, the total fatigue accumulation is expected to match well.

The bias and standard deviation of the correction factor α_{Meth} are given in Table 4.10. Similar numbers for structural details subjected to global loads were provided in Table 4.4. In that case, the observed statistics were consistent between analysed structural details. For the structural details subjected to wave pressure, no consistency between the

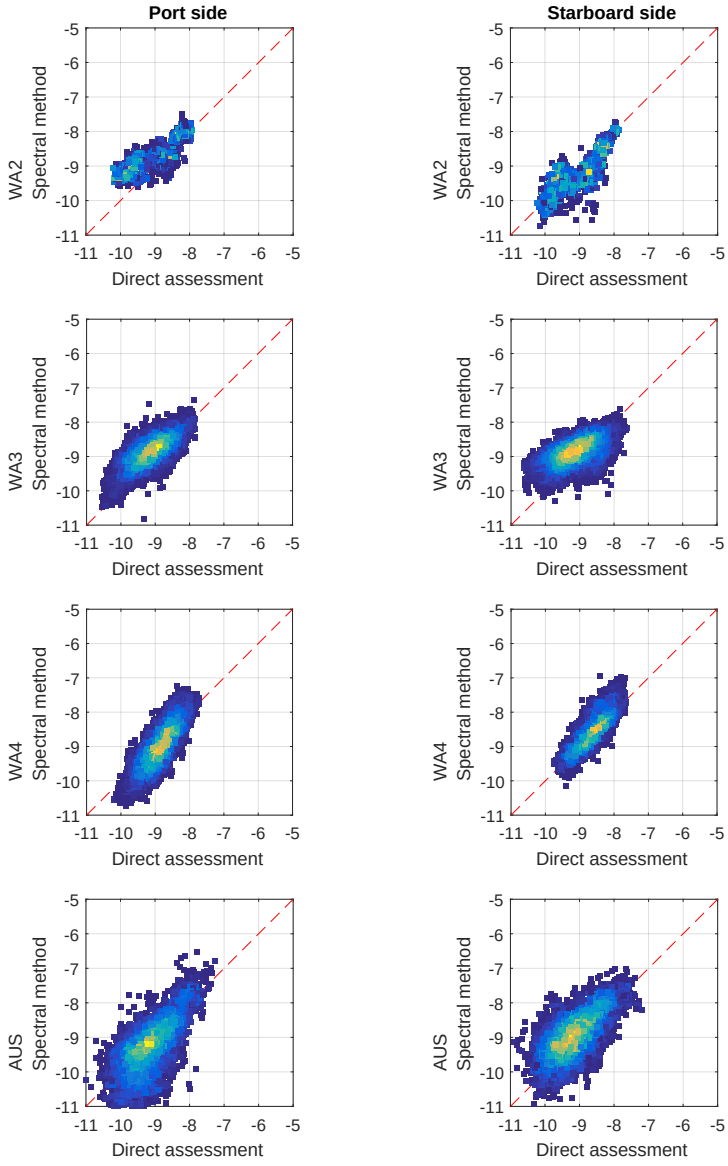

Figure 4.42: Scatter plot of the calculated and measured fatigue accumulation rate (logarithmic scale) of the midship side shell locations for the selected units.

	Port side		Starboard side	
	bias	standard deviation	bias	standard deviation
WA2	-0.33	0.77	+0.87	1.66
WA3	-0.32	0.54	-0.15	1.08
WA4	+0.69	1.36	-0.04	0.50
AUS	+0.72	1.82	-0.03	1.17

Table 4.10: Statistics of α_{Meth} corresponding to the probability functions in Figure 4.43 as determined on the midship deck locations on several units.

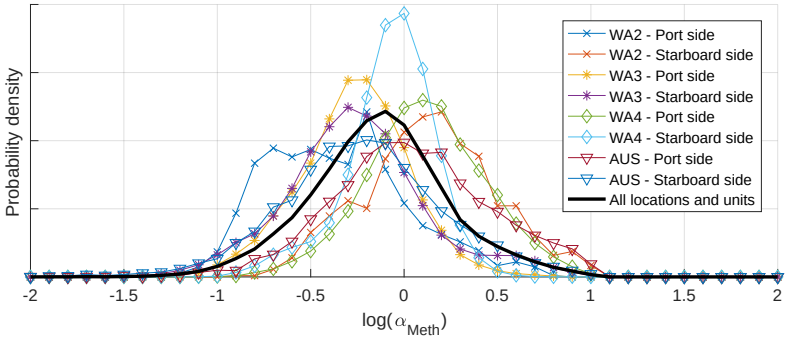

Figure 4.43: Probability density of α_{Meth} for the selected locations from Figure 4.31.

individual locations can be observed. The data from all details discussed in this section has been examined jointly. The associated probability distribution has a mean value of 1.06 and a standard deviation of 1.13. Hence, the uncertainty associated with the calculation method for structural details subjected to wave pressure is about twice as large as the same parameter for details subjected to hull girder loads.

The distribution functions of the individual details as well as the joint distribution are shown in Figure 4.43. For most cases, a Lognormal distribution appears as a natural choice to model α_{Meth}. The most notable exception is unit *WA2*. Figure 4.42 shows that this distribution is based on a limited number of data points and it is considered that too little data is available for a reliable estimate for this unit. As with the results of the bending moment dominated loads, see Figure 4.32, Lognormal distributions are fitted to all example details. The joint distribution of all data is considered a representative distribution.

The Tool Accuracy Factor (TAF) was defined in Equation 2.32 as the ratio of the true fatigue accumulation and the fatigue accumulation calculated using the spectral method over the entire analysis period. The TAF of the selected locations is shown in Table 4.12. This table shows that for all locations, except one, the total accumulated fatigue is lower than predicted using the spectral calculation and encountered weather conditions. The average over all details shows a total fatigue accumulation which is around 30% lower than obtained using the spectral analysis. This observation deviates from the observa-

	Port side	Starboard side
WA2	L(-0.35;0.38)	L(0.13;0.35)
WA3	L(-0.27;0.30)	L(-0.26;0.38)
WA4	L(0.11;0.32)	L(-0.078;0.24)
AUS	L(0.039;0.42)	L(-0.23;0.43)
All data	L(-0.14;0.37)	

Table 4.11: Definition of the best fitting Lognormal distribution on α_{Meth}.

	Port side	Starboard side
WA2	0.67	1.37
WA3	0.62	0.77
WA4	0.85	0.65
AUS	0.71	0.57

Table 4.12: Tool Accuracy Factor as determined on the midship locations subject to wave pressure loads.

tion in Table 4.10 which shows that the average prediction accuracy factor for various details is around 1 or higher which indicates that the spectral calculation provides a higher fatigue accumulation. This is related to the large scatter in the calculation observed at lower fatigue accumulation rates. At higher fatigue accumulation rates, the spectral calculation generally provides a higher fatigue estimate compared to the fatigue assessment using the strain gauges. This effect is most strongly visible on unit *WA4* and *AUS* and as a result, the deviation between the mean values in Table 4.10 and the Tool Accuracy Factor in Table 4.12 deviate the most. The increasing conservatism of the spectral method at higher fatigue accumulation was also observed for the structural details subjected to hull girder bending loads, but is more pronounced at the wave pressure-dominated details.

Two aspects of the fatigue assessment method are examined further. These are the assumed narrowbandness of the observed stress cycles and weak nonlinearities. The procedures to do so were discussed in Section 2.5.4.

NARROWBANDED LOADS

The effect of narrowbanded load cycles was tested by comparing the fatigue accumulation from rainflow counting and the fatigue accumulation using the assumed Rayleigh distribution. In the latter case, the distribution was defined by deriving the standard deviation of each time series. The actual zero-crossing period was also retrieved from the time series, such that the actual number of cycles is equal. Hence, the only difference between the two calculations originates from the assumption of the Rayleigh distribution to capture the short-term stress distribution. A scatter plot comparing both fatigue assessments is shown in Figure 4.44. This figure shows two midship details in the side shell from unit *WA4*.

Figure 4.44 indicates a strong relation between the fatigue evaluated using the Rainflow count method and spectral formula. The relation is not as strong as observed for the details subjected to wave bending moments which was shown in Figure 4.33. However, this is to be expected as the nonlinear intermittent wetting effect at the side shell details

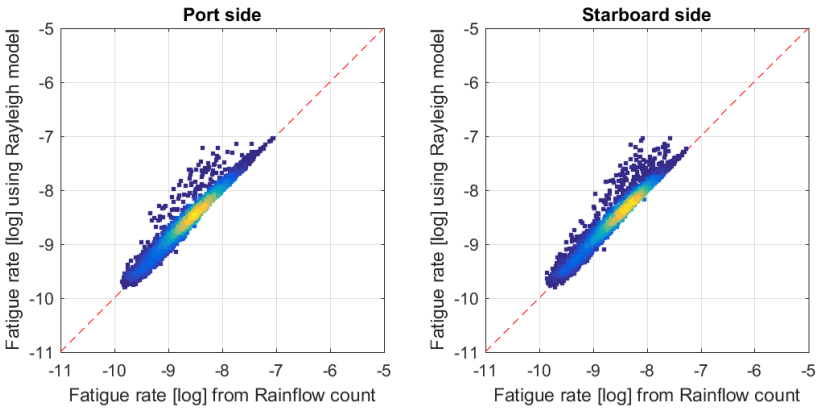

Figure 4.44: Fatigue accumulation rate calculated from Rainflow count and assuming Rayleigh distributed stress ranges on structural details in the side shell of the midship section of unit *WA*4.

	Port side		Starboard side	
	bias	standard deviation	bias	standard deviation
*WA*1	-0.15	0.17	-0.13	0.081
*WA*2	-0.13	0.098	-0.16	0.099
*WA*3	-0.11	0.10	-0.05	0.12
*WA*4	-0.11	0.093	-0.11	0.097
NS	-0.04	0.033	-0.04	0.033
AUS	-0.16	0.11	-0.16	0.11

Table 4.13: Statistics of the difference between the true fatigue accumulation and that obtained assuming Rayleigh distributed stress cycles as determined on the midship deck locations on several units.

does not comply with the assumptions underlying the narrowbanded load process. Table 4.13 presents the statistical data of the difference between the two calculations. This table indicates that the assumption of narrowbanded loads results in a bias on the fatigue accumulation of around -10%. This is a slightly larger bias than observed in the details subjected to hull girder bending, the statistics of which are shown in Table 4.7. The scatter in the results, given by the standard deviation, is around a factor two larger. However, the overall scatter from the calculation method for these details is also a factor two larger than that of the details subjected to hull girder bending loads. This indicates that the linearisation process used to incorporate wave pressures works quite well and does not introduce a significant amount of additional uncertainty in the calculation process. The assumption of narrowbanded loads remains a small contribution to the overall uncertainty of the calculation method.

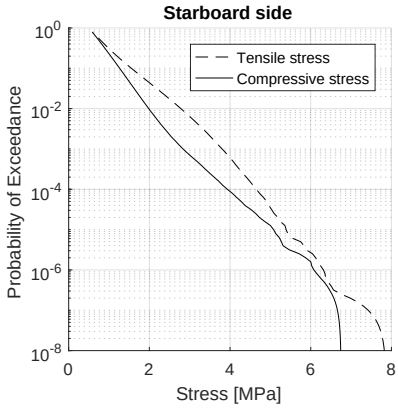

(a) Spread moored unit *WA*3

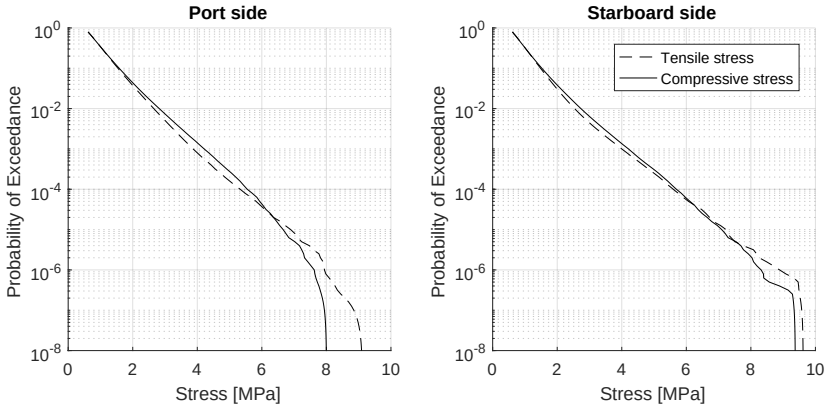

(b) Turret moored unit *AUS*

Figure 4.45: The probability of exceedance distributions of the stresses measured by sensors in the side shell at the midship section close to the neutral axis of the cross section. On unit *WA*3 only a sensor at the starboard side location was available.

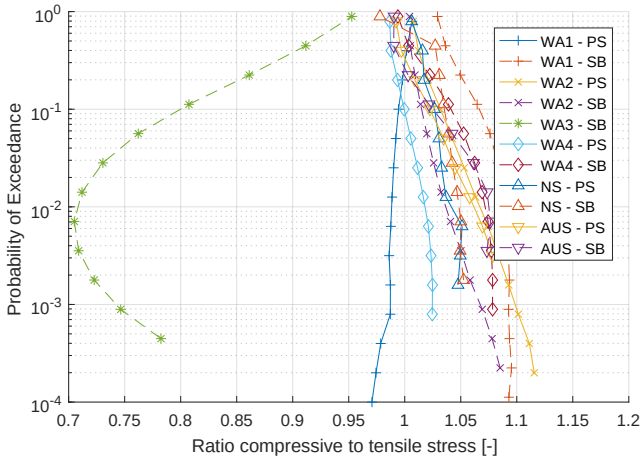

Figure 4.46: The difference between tensile and compressive stresses at several levels of the probability of exceedance for multiple units and port (continuous lines) and starboard side (dashed lines) mounted sensors.

WEAK NONLINEAR LOADS

The influence of weak nonlinearity of the stress cycle distribution has been examined. For this aim, exceedance plots have been generated. Two examples of a spread moored and a turret moored unit are shown in Figure 4.45. On unit *AUS* a strong resemblance between the tensile and compressive stresses can be seen. However, unit *WA*3 shows quite a remarkable difference between the tensile and compressive stresses. It should be noted that this unit is operating at a near constant draft and this sensor is installed just below the water line. Furthermore, these stresses are defined with respect to a mean stress level. Tensile stresses are registered by the sensor when wave pressure is applied to the side shell plating. Compressive stresses are associated with the wave throughs. As the sensor is mounted slightly below the mean water line, the majority of the wave throughs will result in low compressive stress values, while the tensile stress will be larger. This explains the observed discrepancy for this particular measurement location.

The difference between the tensile and compressive stresses has been examined for multiple details on different units. The difference between the probability of exceedance curves of the tensile and compressive stresses has been assessed and is shown in Figure 4.46. Only unit *WA*3 operates at a near-constant draft. All other units have a continuously changing draft and show a difference between the tensile and compressive stresses which is similar to the results of unit *AUS* from Figure 4.45. The observed difference between the tensile and compressive cycles is partially the result of asymmetry of the wave profile. Higher order wave components result in more pronounced peaks and more shallow troughs. This effect is described by e.g. Forristall [141]. The difference between the tensile and compressive stresses increases to 10% at the 10^{-3} probability of exceedance level. This is significantly larger than the asymmetry observed in details subjected to hull girder bending. This difference will contribute to the larger uncertainty of the calculation method for structural details subjected to wave pressure loads.

4.5.3. SUMMARY

The performance of design tools was evaluated by comparing calculated stress spectra using wave data and the RAOs and the measured stress spectra. For structural details subjected to hull girder bending, this procedure found biases in the stress of up to 20%. On unit *AUS*, a notable deviation between the results in the midship section and forward section was found. In the midship section, the design tools overestimated the stresses at the measurement location.

Structural details in the side shell are subject to intermittent wetting. This is a non-linear process which is linearised to facilitate the calculation procedure. This introduces some additional uncertainties. Figure 4.40 shows that the RAOs calculated for the different units vary strongly. After applying the updating procedure more comparable RAOs are found. This shows that the accuracy of the incorporation of the intermittent wetting effect varies between different designs. In principle, the linearisation procedure can work well, but the obtained RAO should be critically evaluated.

The performance of the spectral calculation procedure has been addressed by comparing its results with a direct fatigue assessment using strain gauge measurements. On average, the spectral calculation provides larger fatigue estimates compared to the direct assessment. The uncertainty in individual estimates is larger for side shell details than for details subjected to global bending loads. With increasing loads, the spectral procedure tends to provide larger values. As a result, when evaluating the total fatigue accumulation the spectral fatigue method provides a larger difference compared to the bias of the calculation from individual point estimates. The overall difference can be up to a factor of 2 for details with hull girder bending loads. On details with wave pressure loading, the difference is around a factor 1.5. On one location, out of the eight considered, the spectral calculation resulted in a fatigue assessment which was lower than the true fatigue accumulation. However, it was noted that for this location, relatively little data was available.

The uncertainty introduced in the spectral analysis can be partially attributed to the assumption that the stress distributions follow a Rayleigh distribution. This assumption resulted in a bias between 5 to 15% which is around half the total bias found in the fatigue assessment procedure. The scatter in the individual point estimates is an order of magnitude smaller compared to the overall scatter of the total calculation uncertainty.

The nonlinearity in the stress cycles has been quantified. The difference between hogging and sagging moments are quite small at around 2% at the 10^{-3} probability of exceedance level. This is expected given the barge shape structure of most units. In details in the side shell the difference is larger at 10%, partially due to nonlinear wave kinematics. Especially large deviations of up to 30% were found near the water line of a unit operating at constant draft.

4.6. LOAD PROCESSES - HIGH-FREQUENT

4.6.1. CONTRIBUTION TO FATIGUE ACCUMULATION

The total contribution of the high-frequency stress as a result of whipping and springing has been quantified through filtering of strain measurements according to the procedure described in section 2.5.5. The results of this analysis for all units and relevant measure-

ment locations is shown in Figure 4.47. This graph shows that the overall contribution of whipping and springing to most structural details is between 0 and 5%, but with some larger deviations on unit *WA*2, *NS* and *AUS*. The contribution of high-frequency effects is slightly larger in the midship area. At port and starboard side measurement details, which are always located symmetrically or nearly symmetrically with respect to the units centreline, the findings are very similar.

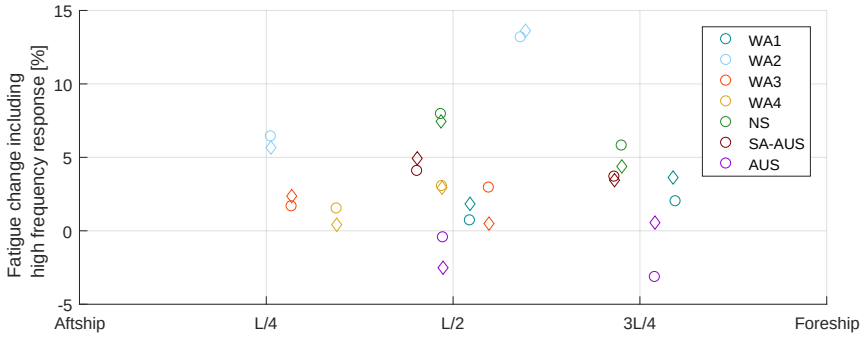

Figure 4.47: Contribution of the high-frequency stress to the fatigue accumulation for all units with respect to the measurement location. The circle and diamond symbols indicate port and starboard side locations respectively.

The increase in fatigue accumulation on unit *WA*2 is large compared to the other units. In section 1.3, it was noted that this is a large unit in excess of 300 metre resulting in a low natural period. At the same time, the unit is operating in mild weather conditions with low and short waves. This combination of environmental conditions and global dimensions makes the unit susceptible to springing. This is addressed in more detail in section 4.6.3. In that section, unit *WA*4, which is of similar dimension, but operating in a slightly different environment, will be considered as well.

On unit *AUS*, the removal of high-frequency stress components results in an increased fatigue accumulation. This counter-intuitive effect is the result of interaction between multiple load phenomena, including both horizontal and vertical bending components. As a result, there is a difference between the port and starboard side results as well. Because the effect is limited to 3% on fatigue accumulation at most, it is not investigated in more detail. Unit *NS* is operating in a heavy weather environment and can therefore experience some whipping. Both unit *NS* and *AUS* are considered for further analysis on whipping in section 4.6.2.

4.6.2. WHIPPING

The contribution of whipping has been determined from the strain gauges for individual sea states. For each sea state, the significant wave height, peak period and draft was determined. The sea states have been subdivided according to these properties and for each parameter a boxplot to visualize the uncertainty bounds has been generated. These results are shown for unit *NS* and *AUS* in Figure 4.48 and 4.49 respectively.

Whipping generally occurs in more violent wave conditions. Figure 4.48 and 4.49

shows that the whipping contribution increases in larger significant wave heights. In the area of unit *AUS*, waves up to 4 metre significant have been encountered. However, these conditions are very rare and wave heights exceeding 3 metre occur less than 1% of the time, see also Figure 4.51. Therefore, the observed uncertainty bound associated with the 4 metre conditions is very large and shouldn't be considered. However, the trend for unit *NS* is quite clear. This unit experiences heavy weather conditions for a prolonged period. Figure 4.51 shows that this unit experiences wave heights exceeding 5 metre for 20% of the time.

At the same time, these figures indicate that at higher wave periods, and consequently larger waves, whipping diminishes. Therefore, it is logical to compare the whipping contribution to wave steepness, defined as the ratio between wave height and peak period squared, which incorporates both the wave height and wave period. It can be seen that on unit *NS*, the whipping contribution increases with wave steepness. On unit *AUS*, the uncertainty bounds become much wider at larger wave steepness, but a trend is harder to identify. However, it should be noted that events with large wave steepness are rare for this unit. At the same time, this units is considerably longer at 330 metres than unit *NS* at around 250 metres.

When a unit is operating at higher draft, the area subject to wave slamming impacts is smaller. The results on unit *NS* show that the average whipping contribution is similar over all drafts. However, the uncertainty bound on the higher drafts show less large variations, indicating that the whipping response is somewhat less when operating with a large draft. On unit *AUS*, no such relation was found, but it should be noted that this unit experiences only a small amount of whipping and this unit has less bow flare.

The definition of α_{HF} as provided in equation 2.17 allows for an explicit relation between this parameter and dominant environmental conditions. Based on the findings in this section, it was found that this relation is unit dependent. For unit *AUS* this relation can be modelled using a variable average. Both wave height and wave steepness are viable options to model this dependency. For simplification, the wave height was used. For each individual bin, the uncertainty bounds at two standard deviations are of a similar size at 10%. This equals a standard deviation of 0.025. Based on Figure 4.48, the following approximation model for α_{HF} in equation 4.8 is proposed. On unit *AUS* too little whipping events have been registered to develop a similar model. This also indicates that the overall practical importance of whipping is small for this unit. Hence, apart from unit *NS*, for which the model from equation 4.8 has been based, the influence of whipping is considered negligible.

$$\begin{aligned} \alpha_{HF}(H_S) &:= N(1.03; 0.025) \qquad if\ H_s \leq 3m \\ \alpha_{HF}(H_S) &:= N(1 + 0.01 H_s; 0.025)\ if\ H_s > 3m \end{aligned} \tag{4.8}$$

4.6.3. SPRINGING

Based on the discussion regarding Figure 4.47, it was concluded that especially unit *WA2* is sensitive to springing. A further detailed analysis of this unit is presented in this section. For reference, these results are compared with similar analysis conducted for unit *WA4*, which is of similar size, but operating in a different environment. In section 2.5.5, it was discussed that springing is a resonance phenomenon and therefore sensitive to the

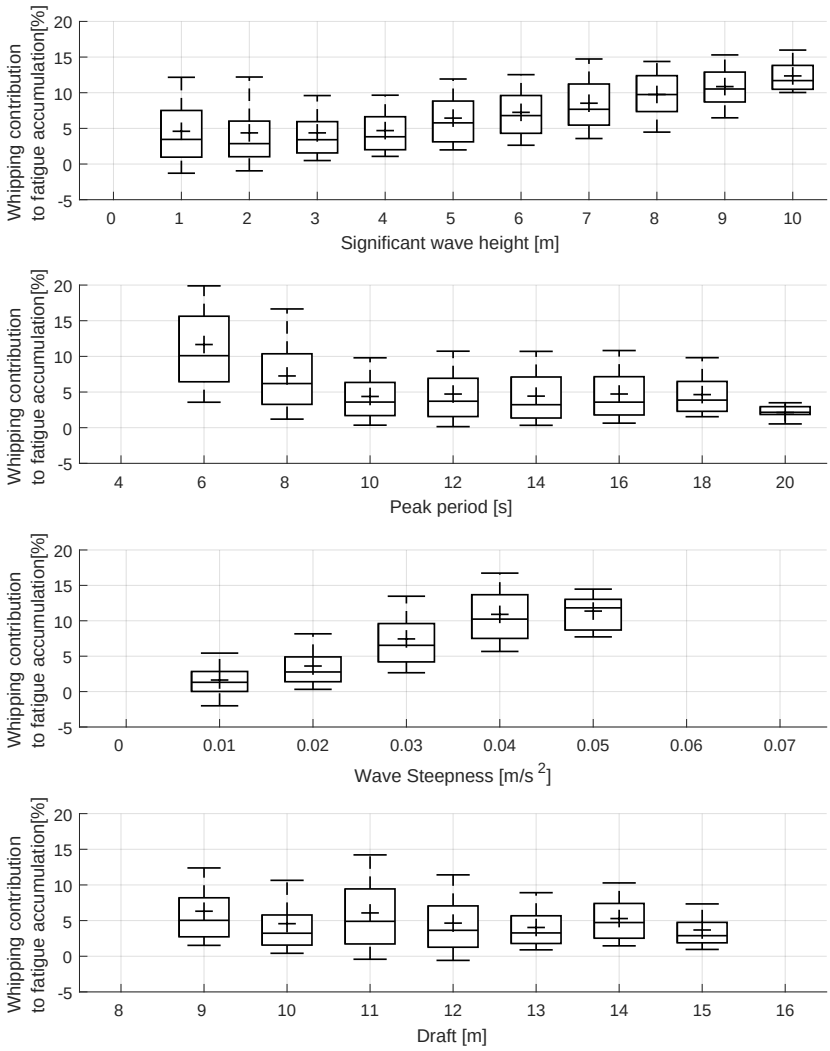

Figure 4.48: The relative contribution of whipping to the overall fatigue accumulation during the individual sea states in relation to several environmental and operating conditions on unit *NS*.

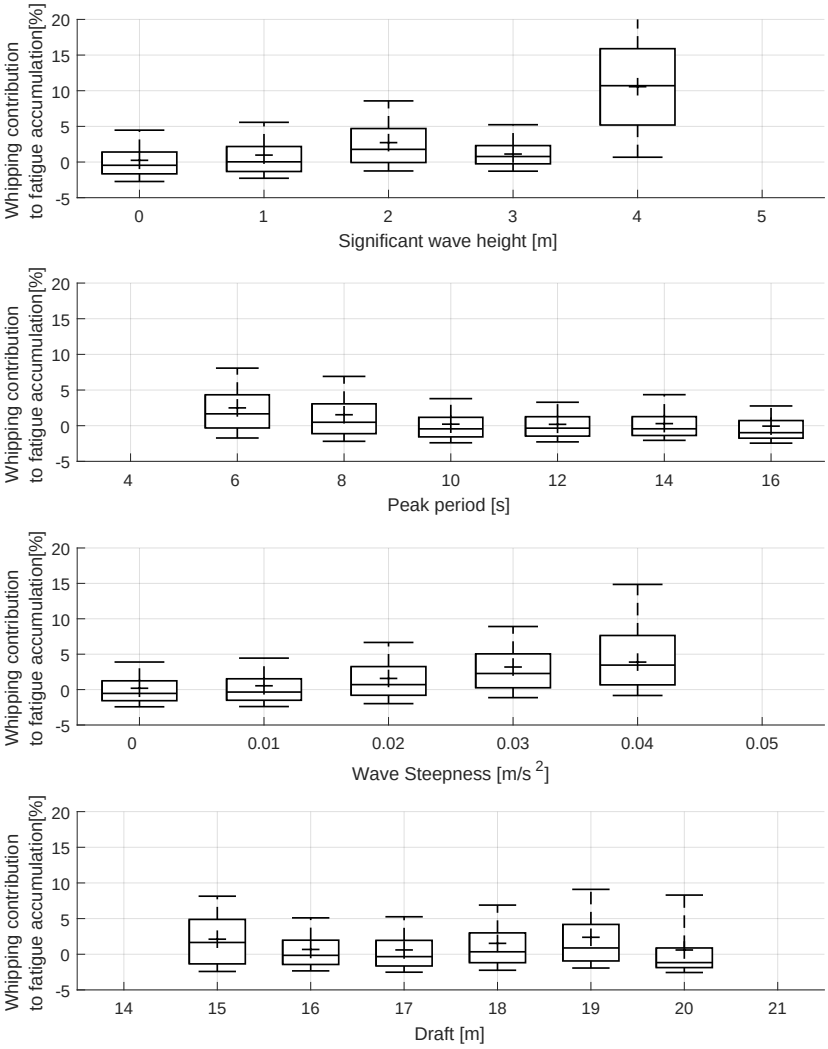

Figure 4.49: The relative contribution of whipping to the overall fatigue accumulation during the individual sea states in relation to several environmental and operating conditions on unit *AUS*.

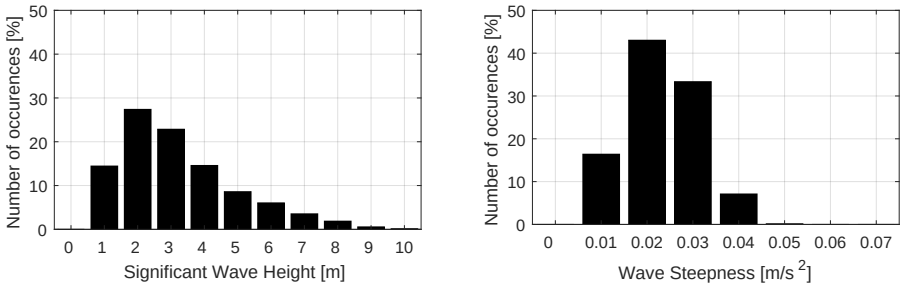

Figure 4.50: The relative occurrence of significant wave heights and wave steepness at the location of unit *NS*, as used in Figure 4.48.

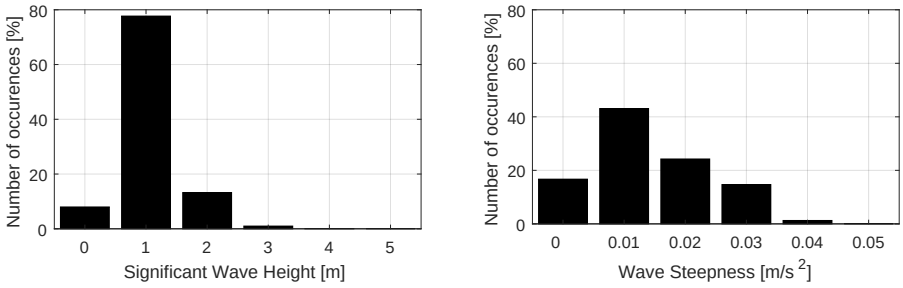

Figure 4.51: The relative occurrence of significant wave heights and wave steepness at the location of unit *AUS*, as used in Figure 4.49.

excitation frequency and mass of the unit.

For unit *WA*2 and *WA*4, the contribution of springing during each 30-minute measurement interval has been determined. The peak period of the waves in each interval has been obtained from the WAVEWATCH III hindcast data to ensure the most complete coverage. The results from each interval have been sorted according to the associated peak period and are visualized in a box plot in Figure 4.52 and 4.53 for unit *WA*2 and *WA*4 respectively. These figures indicate a clear trend with an increasing contribution of springing for smaller wave periods. In the midship area of unit *WA*2, the springing stress can result in a 100% or even higher increase in the fatigue accumulation. However, it should be noted that these conditions are rare. Histograms of the relative occurrence of the wave peak periods at both unit locations is given in Figure 4.54.

On unit *WA*4, the contribution of springing to the overall fatigue accumulation is much smaller at 3% instead of 13% on unit *WA*2. Compared to this unit, it can be seen that *WA*4 experiences fewer short period wave conditions. However, when comparing Figure 4.52 and 4.53, it can also be seen that the springing contribution at the same peak period is smaller for unit *WA*4. For example, at a peak period of 9 seconds, unit *WA*2 shows a contribution of around 35% at the midship area, which is only 20% for unit *WA*4. The reason for this difference is twofold; first, unit *WA*4 is slightly smaller and therefore has a somewhat smaller natural period compared to unit *WA*2. Secondly, section 1.3

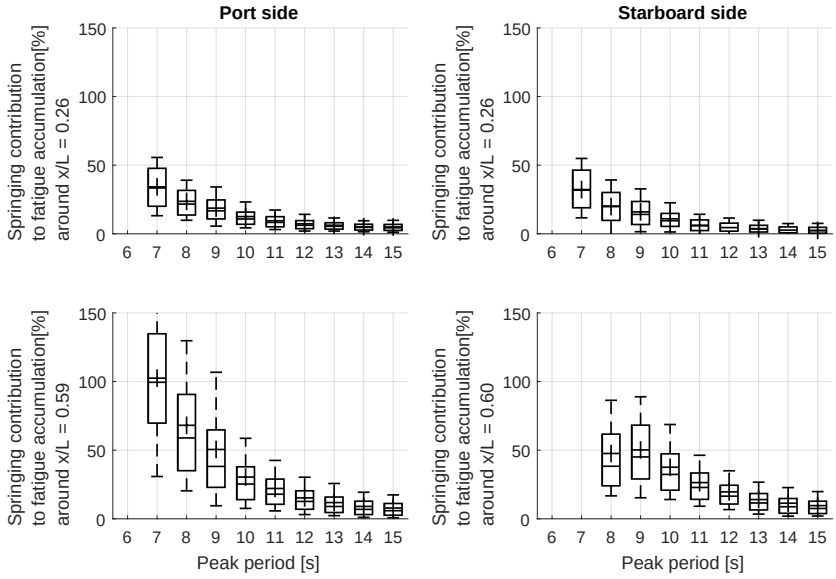

Figure 4.52: The relative contribution of springing to the overall fatigue accumulation during the individual sea states in relation to the peak period on unit *WA2*.

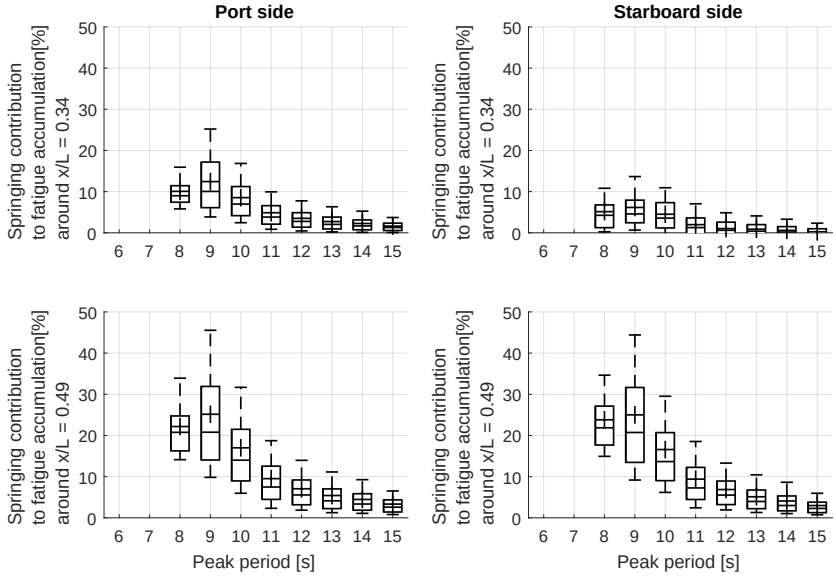

Figure 4.53: The relative contribution of springing to the overall fatigue accumulation during the individual sea states in relation to the peak period on unit *WA4*. Note that a different scale on the vertical axis compared to Figure 4.52 has been used to clearly visualize the findings.

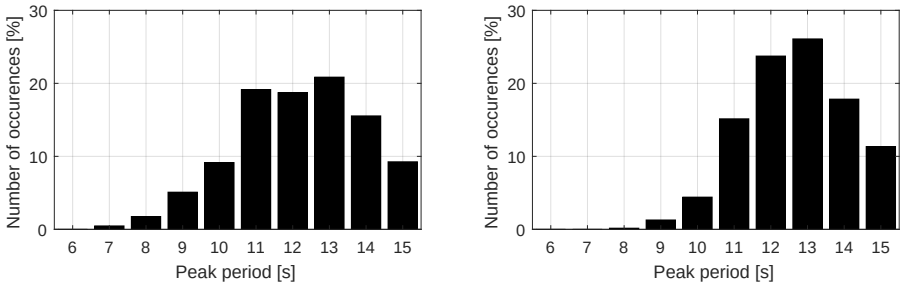

(a) Unit *WA2* (b) Unit *WA4*

Figure 4.54: The relative occurrence of the peak period subdivision, as used in Figure 4.52 and 4.53, in the area of unit *WA2* and *WA4*.

discussed that unit *WA2* is operating in a more wind-driven environment. Therefore, at the same peak period, the wave environment features a broader range of frequencies, especially the higher frequencies, which leads to increased dynamic response. See also the spectral definitions in Figure 2.6.

4.6.4. SUMMARY

The contribution of whipping and springing to the total fatigue accumulation on the monitored units is relatively small and 15% at most. However, the contribution of whipping and springing varies from sea state to sea state.

Whipping responses occur in higher sea states due to slamming impacts. Two units operate in areas where they may encounter sea states with significant wave heights of $10m$ and higher. On unit *NS*, operating West of Shetland, the whipping contribution to fatigue accumulation increases approximately linearly with wave height. Unit *AUS*, operating in a cyclone environment in Australia, has not yet seen very harsh weather conditions. Initial results suggest though that this unit is more susceptible to whipping. This could be related to the size of the unit as it is considerably larger than unit *NS*.

Springing of a unit occurs in lower sea states. The contribution of springing to fatigue accumulation can be significant. On a large unit operating in a benign environment, the contribution of springing resulted in a multiplication of the fatigue accumulation with a factor of 2. These conditions were quite rare for the monitored units resulting in a small contribution to the overall fatigue accumulation. However, this observation may be of importance for large units permanently operating in a benign environment with shorter waves.

4.7. LOAD PROCESSES - LOW-FREQUENT

4.7.1. CONTRIBUTION TO FATIGUE ACCUMULATION

This section discusses the importance of low-frequency load components to the overall fatigue accumulation. An example of stress time series showing the low-frequency load components at various measurement locations is given in Figure 4.55. This figure shows the mean stress level of 30-minute intervals. Clear loading and temperature-induced

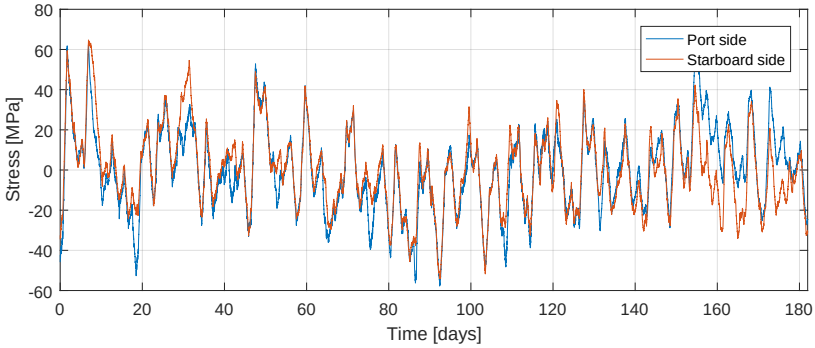

(a) Deck measurement location

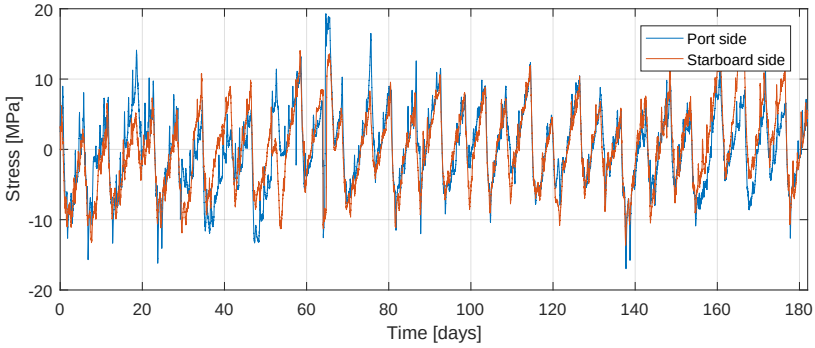

(b) Side shell measurement location

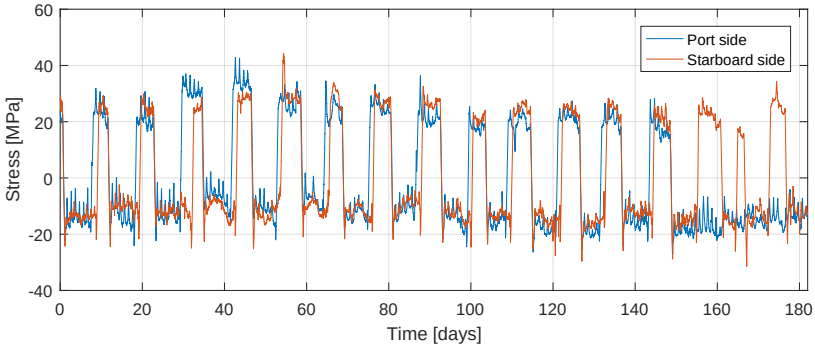

(c) Stringer measurement location

Figure 4.55: Example of measured stress time series over several months at various measurement locations in the same cross section on unit *WA4*. The signals have been filtered using a low-pass filter at 0.1 rad/s to remove wave-frequency load components.

stress variations in the side shell and stringers can be seen. Stress range histograms have been derived from these six measurement signals and are plotted in Figure 4.56. These graphs show that the loading and temperature-induced effects at the stringer have a clear difference in magnitude. However, for the other locations, the difference between those load effects is less clear.

The relative importance of the low-frequency contribution with respect to the total fatigue accumulation has been determined for the measurement locations using the procedure described in section 2.3. The stringers have been subdivided into two types. The first type is supporting cargo tanks which experience frequently a large variation in tank filling and therefore large stress variations. Stringers supporting wash tanks will experience only minor variations in the level inside the tank and therefore loading-induced stresses are smaller.

Figure 4.57 shows the relative contribution for each individual measurement location. The figure indicates that for most type of details, the fatigue contribution of the loading-induced stresses is small. At the deck locations, the low-frequency stresses show an irregular pattern as shown in Figure 4.55. The contribution of these stress variations to the overall fatigue accumulation is typically around 10%. Two structural details on two different units show a somewhat higher fatigue accumulation with contributions of 20 and 25% respectively. The contribution of low-frequency stresses to the overall fatigue on side shell locations is generally limited to 3%. A few outliers with larger contributions can be seen on unit *WA*1 and *AUS*.

The cargo supporting stringer locations show larger contributions from the low-frequency effects, up to 90%. It should be observed that the ratio is very consistent per unit, but differs between the individual units. Especially for unit *WA*2, the contribution is very high. This is also the result of the very mild environment in which this unit is operating, see also section 4.2 and 4.5. The structural details located on stringers adjacent to wash tanks show a smaller low-frequency contribution between 10% and 40%.

The low-frequency component contains both loading-induced and temperature-induced loads. The effect of these components can be separated using filtering as described in section 2.5.6. The contribution of the loading related effects is displayed in Figure 4.58 and can be compared with the total contribution as shown in Figure 4.57. From these figures, it can be concluded that the contribution of loading cycles, apart from the outliers, on deck and side shell areas is limited to 10% and 3% respectively. The temperature-related effects are small. On the stringer locations, a notable difference between the total and loading-induced low-frequent effects exist. This difference is typically 20 percentage point. Hence, both temperature- and loading-induced stresses have a considerable contribution to the fatigue accumulation.

A more detailed examination of the loads that resulted in the effects which can be observed in Figure 4.57 and 4.58 will be conducted in the following sections. In section 4.7.2, the effects related to loading and offloading of the cargo supporting structure are addressed in more detail. Section 4.7.3 discusses the thermal effects observed on all locations.

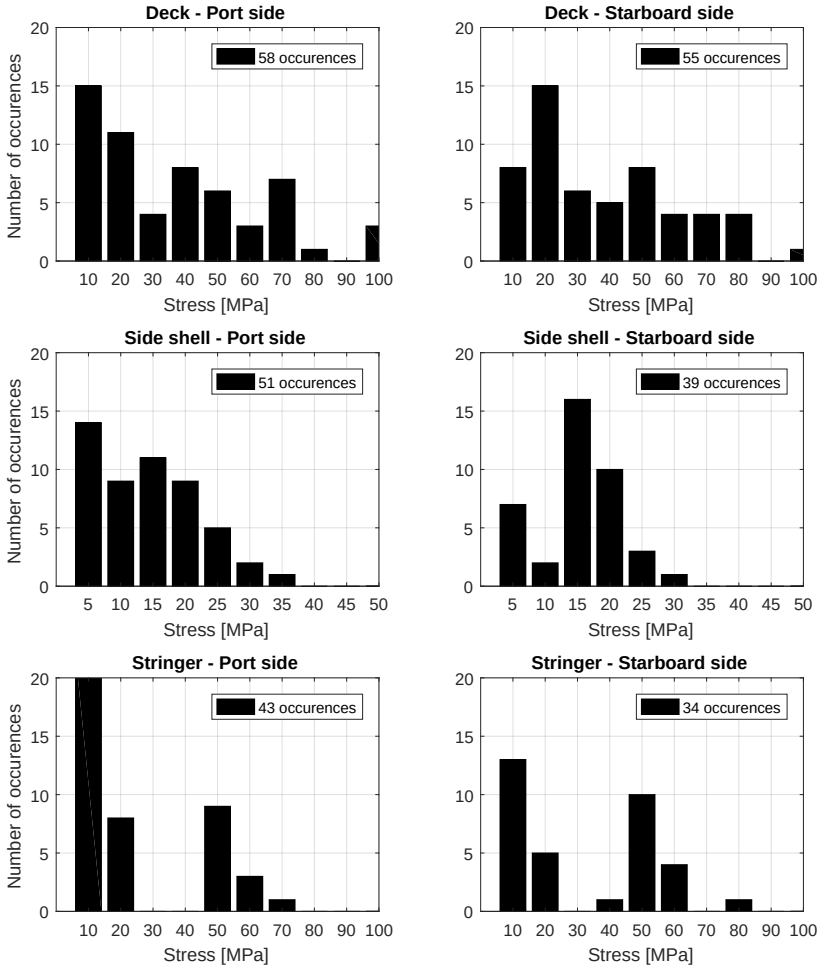

Figure 4.56: Histogram of the stress ranges based on time traces shown in Figure 4.55.

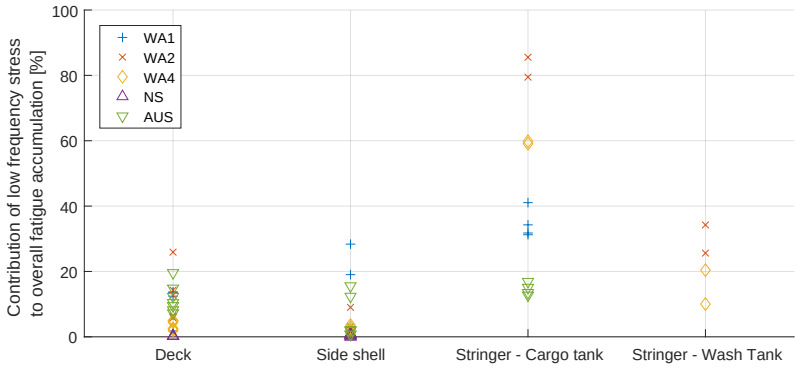

Figure 4.57: The relative importance of the low-frequency components in the total fatigue accumulation showing the results monitored onboard five units.

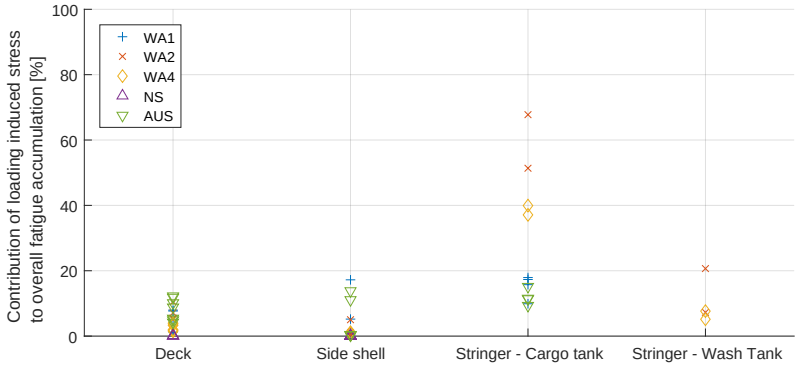

Figure 4.58: The relative importance of the loading-induced stress in the total fatigue accumulation showing the results monitored onboard five units.

4.7.2. LOADING-INDUCED LOADS

The distribution of loading-induced stress range variations for two stringer details on opposing sides of unit *WA4* over a period of 4.5 years is given in Figure 4.59. Both distributions have the same mean value with some small scatter. It should be noted that the starboard side cargo tanks are more frequently used and have therefore experienced 15% more load cycles than the opposing port side location.

Figure 4.60 presents the observed loading stress cycles in a box-plot for all cargo supporting locations on the various units. Due to differences in topology, tank dimensions, sensor placement etc., the absolute stress ranges cannot be compared between different units. However, some useful observations can still be made.

Unit *WA1* features two locations with lower and two locations with higher loading-induced stresses. The sensors with higher stress are located near the neutral axis, while the others are sensors placed at a higher stringer which therefore experience less loading-

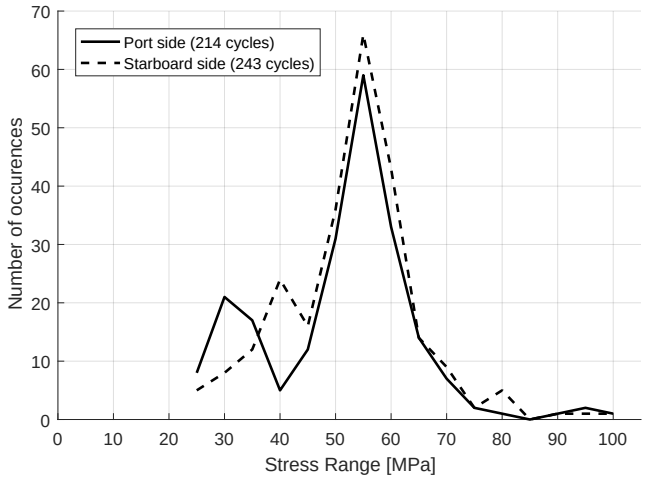

Figure 4.59: Distribution of loading-induced stress ranges for two symmetrical locations.

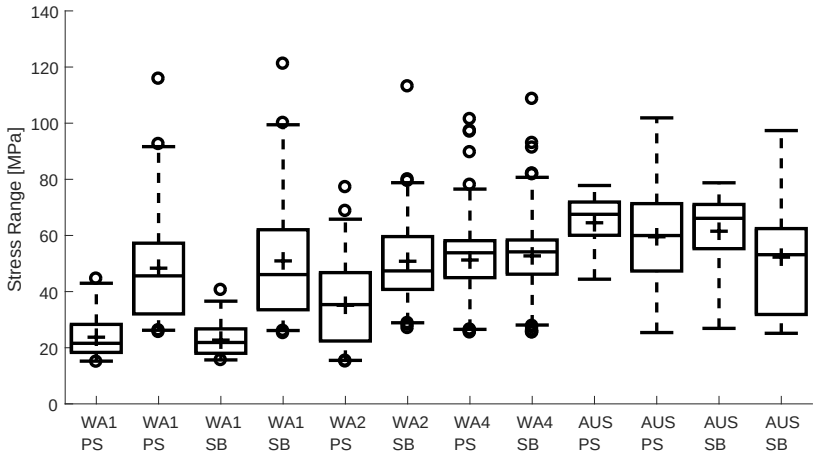

Figure 4.60: Boxplots indicating the loading-induced stress ranges for all stringers located near cargo tanks. The box indicates the first and third quartiles, while whiskers indicate the 2.5% probability of exceedance limits. Outliers are indicated using circles.

induced stress. The results between opposing port side and starboard side measurement locations are very comparable, except for the *WA2* unit. For most locations, there are a few stress cycles which exceed the average stress range with a factor two or higher. In the design procedure, only a single value for loading-induced stress cycles is calculated for the loading-induced stress variations. Deviations of such large magnitudes can result in significantly different fatigue accumulation rates and it is therefore important to understand where such deviations originate from.

To illustrate the stress variations, the data of the six month period in the top graph of Figure 4.61 is examined in more detail. This figure shows frequent stress variations of around 40 MPa which are directly linked to the variations in level of the adjacent cargo tank depicted in the centre graph. However, at the beginning of September, early October and the beginning of November, the mean stress level is changing as well. These changes lead to an additional stress variation of around 20 MPa which is added to one of the stress cycles obtained after rainflow counting. The variation of stress level is linked to the variation of the level in the adjacent water ballast tank, depicted in the bottom graph. These variation of the level in ballast tanks are not part of the design operating manual and are therefore not included in design assessments. However, such variations will result in an increased fatigue accumulation. On top of the stresses originating from loading variations, temperature-induced stresses can be seen in Figure 4.61. These variations result in a further increase of the effective low-frequency stress cycle. Similarly, the wave induced stresses, which have been removed in Figure 4.61, also result in an increase of the effective stress cycle.

QUANTIFICATION OF STRESS CONTRIBUTIONS

The effective loading-induced stress cycles comprise multiple components contributing to the overall stress range. The following components were identified:

1. Adjacent cargo tank level variations
2. Ballast tank level variations
3. Temperature-induced stress
4. Wave-induced stress

The variation of the levels in the adjacent cargo tanks dominates the overall stress at the stringer locations. The stress variations as a result of the temperature-induced stresses can be observed in Figure 4.55. These typical variations are in the order of 5 to 10 MPa. The wave-induced stress variations have been discussed in Section 4.5, these are typically around 1 to 2 MPa. These two effects combined result in the majority of the variation of the stress ranges which can be seen in Figure 4.56. However, the outliers observed in this graph are the result of additional loading operations. Besides the ballast tank variations, other tank load variations may also contribute to the stress cycles. These effects will collectively be referred to as secondary loading-induced effects. To assess the importance of individual loading parameters, a linear regression model was defined as follows:

$$\sigma(t) = \mathbf{A}\vec{L}(t) \tag{4.9}$$

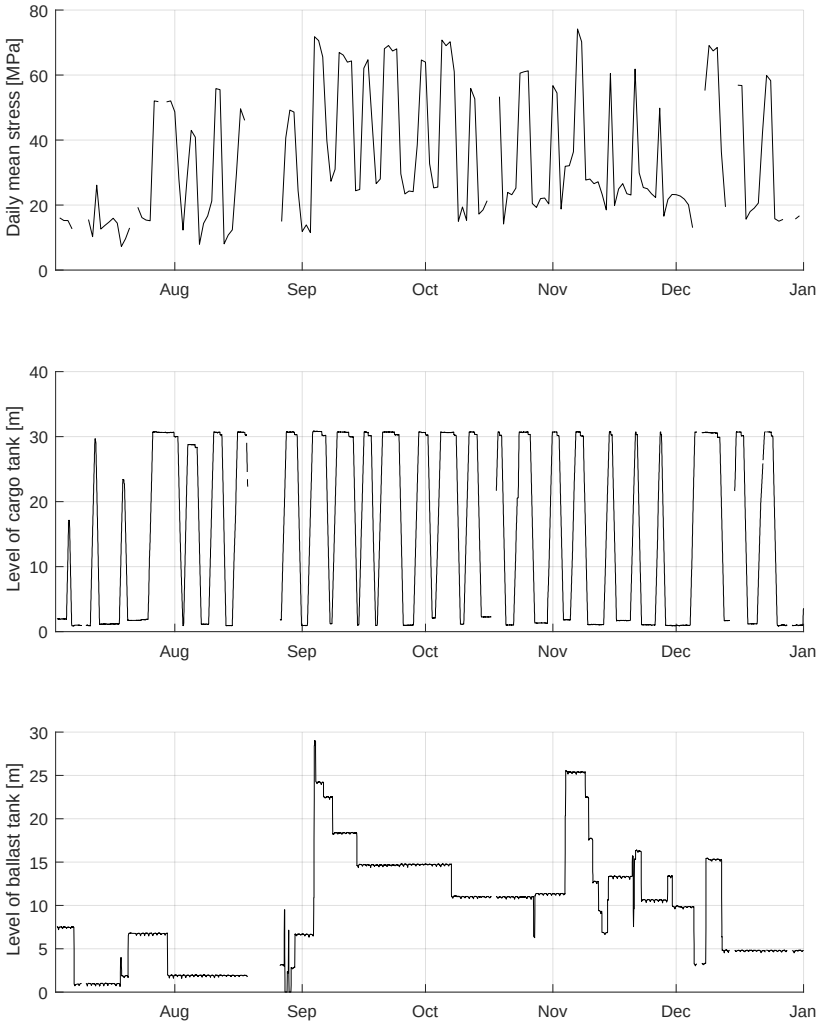

Figure 4.61: 6 months stress variations and tank level variations of the associated cargo and ballast tanks.

The matrix **A** denotes the regression matrix. The vector $\vec{L}(t)$ contains a number of loading parameters, defined as follows:

$$\vec{L}(t) = \begin{bmatrix} 1 \\ TL_{CT1} \\ \hline TL_{BT1} \\ \hline Draft \\ Trim \\ List \\ \hline TL_{CT2} \\ TL_{CT3} \end{bmatrix} \tag{4.10}$$

The load vector uses different sets of input data with an increasing number of variables. The horizontal lines indicate truncation points for models with increasing complexity. Because the variables have not been modified to have a zero average, this vector contains a one to account for a constant offset. The regression analysis has been applied to the daily average parameters, since the daily stress variations as shown in Figure 4.61 cannot be captured by this model.

Table 4.14 provides a description of the parameters included in each model as well as the total number of parameters. These models include the tank levels (TL) from adjacent cargo tanks (CT) and ballast tanks (BT). The global hydrostatics, i.e. draft, trim and list of the unit are included in the next level of complexity. Finally, another cargo and ballast tank which are close to, but not directly adjacent to the stringer, have been added.

Regression model	Number of variables	Bias in fatigue accumulation [%]
Cargo tank	1	-34
Cargo and ballast tank	2	-30
Adjacent tanks and hydrostatics	5	-26
Nearby tanks and hydrostatics	7	-27

Table 4.14: Description and results of various regression models tested to capture the loading-induced stress. The time series of the different models are shown in Figure 4.62.

The stress approximation obtained using these regression models are visualized in Figure 4.62. Table 4.14 also provides the fatigue accumulation of these signals, relative to the stress signal obtained from the daily average values. The model incorporating global hydrostatics shows a further improvement of the fatigue assessment, but inclusion of additional parameters does not result in a reduction of the bias of the fatigue estimate. It can therefore be concluded that level changes in adjacent ballast tanks and changes in global hydrostatics are responsible for the outliers in Figure 4.56.

EFFECT OF STRESS VARIATIONS ON FATIGUE ACCUMULATION

In the previous section, the physical phenomena that contribute to the low-frequency stress cycle have been identified. A simplified calculation is executed to assess the contribution of the small stress contributions from wave- and temperature-induced effects.

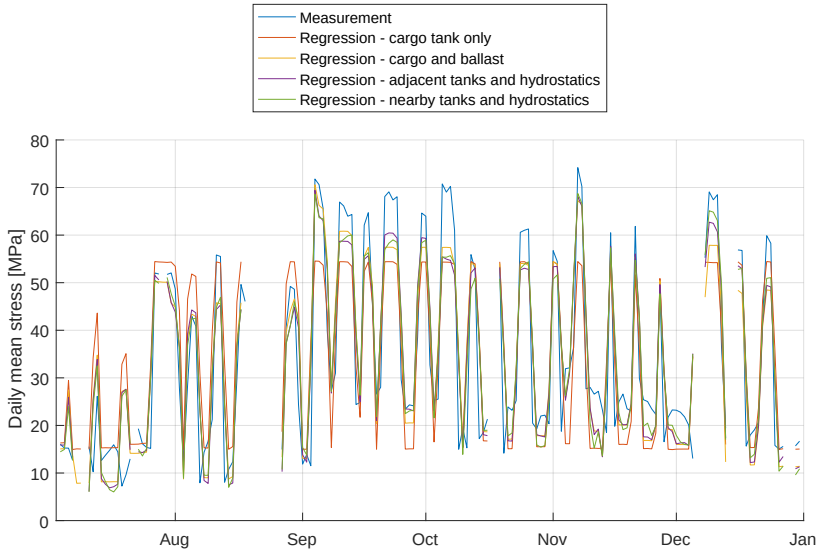

Figure 4.62: Stress signals obtained from regression models incorporating multiple sets of loading parameters.

Figure 4.61 shows that the stress variation as a result of loading and offloading is around 40 MPa, while the temperature-induced contribution varies between 5 and 10 MPa. The wave-induced component was valued at 2 MPa. When adding these components together the fatigue accumulation increases non proportionally. This is shown in Table 4.15. In the design calculations, the cargo- and wave-induced stresses are considered. However, the temperature-induced stresses are not. These additional stresses can result in a fatigue accumulation which is twice as high compared to the case where these stresses have not been considered.

Summary data regarding the number of observed stress cycles and their amplitude is given in Tables 4.16 and 4.17. These tables also indicate the corresponding values

Stress cycle contributions	Stress range [MPa]	Fatigue [%]
Cargo tank only	40	100
Cargo and wave-induced	42	116
Cargo and temperature-induced (Small)	45	142
Cargo and temperature-induced (Large)	50	195
Cargo, waves and temperature (Large)	52	220

Table 4.15: Effect of inclusion of wave- and temperature-induced stresses on the effective low-frequent stress range on fatigue accumulation. The temperature-induced stress cycle was found to vary between 5 and 10 MPa and calculations have been repeated using both values which is indicated by the notation Small and Large, respectively. The fatigue contribution is expressed as percentage of the fatigue contribution when only considering cargo tank loads.

		*WA*1	*WA*1	*WA*2	*WA*4	*AUS*	*AUS*
PS	Design	39	39	133	156	33	33
	Observed	46	58	84	214	10	17
SB	Design	39	39	133	156	33	33
	Observed	60	67	111	243	11	19

Table 4.16: Number of loading-induced stress cycles. The design parameter has been determined for the duration of available measurements.

		*WA*1	*WA*1	*WA*2	*WA*4	*AUS*	*AUS*
PS	Design	-	-	25.0	50.0	93.0	57.4
	Observed - mean [MPa]	23.8	48.3	35.1	51.3	64.5	59.5
	Observed - std [MPa]	7.6	18.3	14.0	13.4	10.5	20.9
SB	Design	-	-	26.0	50.0	91.0	57.8
	Observed - mean [MPa]	22.7	50.9	50.8	52.8	61.5	52.3
	Observed - std [MPa]	5.9	20.7	14.8	12.0	15.0	20.4

Table 4.17: Characteristics of design and observed stress ranges at the different measurement locations

used in the design assessment. The data from these tables can be used to quantify the uncertainty parameters α_{Load} and α_{LS} as discussed in section 2.5.6. Before doing so, the importance of these individual contributions is illustrated using the procedure from section 2.5.6. The results for the individual locations are shown in Figure 4.63. The contribution of the operating conditions is simply the results of the difference between the observed and measured stress cycles which can result in either an increase or decrease of fatigue rate with a typical contribution of up to 70%.

In the beginning of this section, it was shown that the omission of temperature-induced load cycles would result in a significant increase of up to a factor of 2 due to a bias in the stress range. Figure 4.63 shows that this is not the case. This is the result of partial omission of corrosion allowance in the design model, which results in a conservative estimate compared to the measured stress range. Even so, one can observe a couple of locations where the average stress range is underestimated as a result of the simplified representation of the actual stress variations. Finally, the variations in the stress ranges due to secondary loading components and wave and temperature-related effects results in a bias between 10% and 50%. The result is always a higher fatigue accumulation because of the nonlinear fatigue rate with respect to stress level. These results indicate that all three effects have a considerable contribution to the uncertainty in the fatigue assessment and should be analysed.

The factor related to operating conditions, α_{LS}, is relatively constant per unit. It is reasonable to assess this using a deterministic bias based on the units production rate. This value can change over time, for example, unit *AUS* has seen only a few offloadings and the parameter is not considered to be converged at this stage.

α_{LS} defines the distribution of stress ranges. The statistical parameters describing this distribution are shown in Table 4.17. The shape of the distribution has not been discussed yet. Figure 4.64 presents examples of this distribution for two typical details.

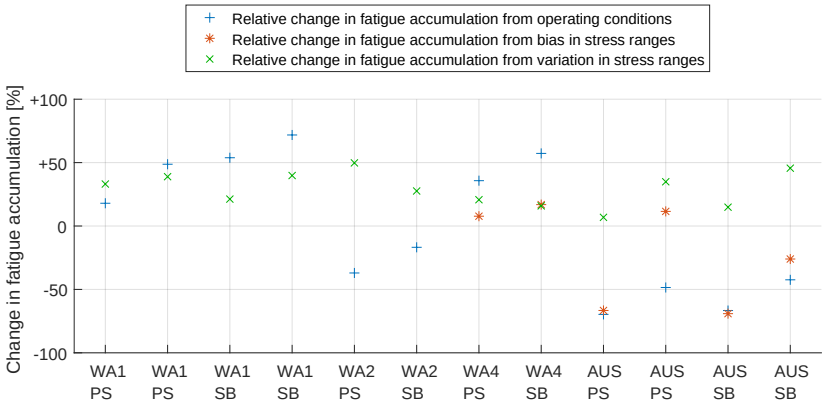

Figure 4.63: Contribution of various sources of uncertainty in the loading-induced fatigue assessment for all measured stringer locations.

These two examples are quite distinct; the first example resembles a uniform distribution with a number of outliers, while the second one strongly resembles a bell curve. By the definition of equation 2.34, the parameter is strictly positive. If one wants to use a parametric model to define this parameter, a distribution with the same restriction, such as a Weibull or lognormal distribution, would be a natural choice. These models have been fitted to the data and are also shown in Figure 4.64. It can be observed that in both cases, the lognormal distribution would be a natural choice to model α_{LS}.

Based on the numbers observed in this section, a simple model for α_{LS} is proposed. For all but one unit, the average stress range is estimated quite accurately or a too high value is obtained. Therefore, the joint model has a bias of 0. The standard deviation was set to 0.3 based on the findings from Table 4.17. Based on these values, the parameters of the lognormal distribution were determined and α_{LS} is defined as:

$$\alpha_{LS} \coloneqq L(-0.043, 0.29) \tag{4.11}$$

4.7.3. TEMPERATURE-INDUCED LOADS

An example of the observed temperature-induced stress cycles on a single cross section of a hull is shown in Figure 4.65. This figure shows a measurement location on deck, in the side shell and on a stringer at both port side and starboard side locations.

The first observation that can be made using this figure is that the stress cycles at different locations are of similar order of magnitude. This is in line with the reasoning that these stress cycles are the result of global deformations of the hull associated with day and night cycles as outlined in section 2.3.6. If the temperature effects were more localized, larger variations could have been expected.

A second observation is that the number of observed cycles is larger than the actual number of days in operation. This ratio varies between 1.2 and 2.1 and is likely the result of operations on the unit which give rise to small stress fluctuations as well. However, the

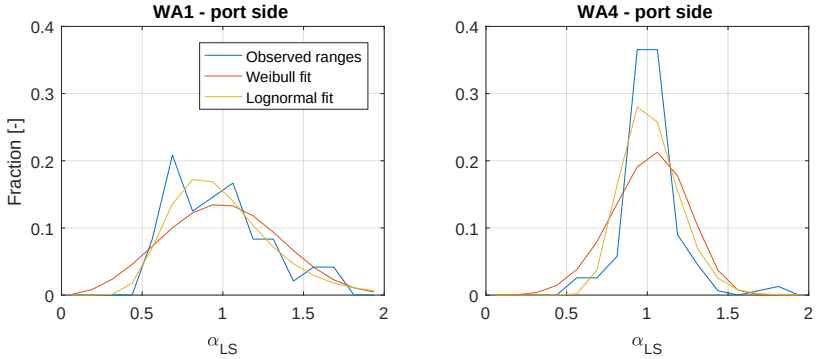

Figure 4.64: Distributions of α_{LS} at two example locations including fitted Weibull and lognormal distributions. A design value for unit *WA*1 was not available, instead, the stress ranges have been normalized using a reference value of 50 MPa.

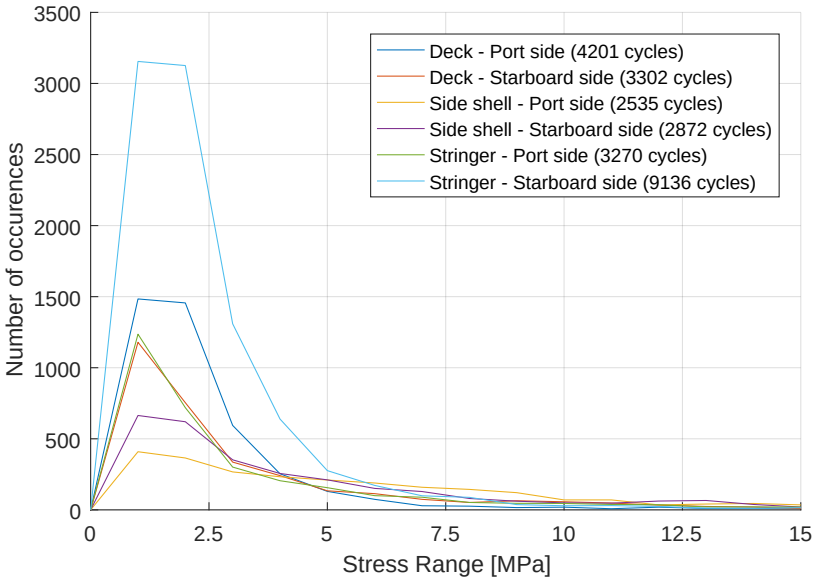

Figure 4.65: Distribution of stress ranges for multiple locations over a period of 1977 days.

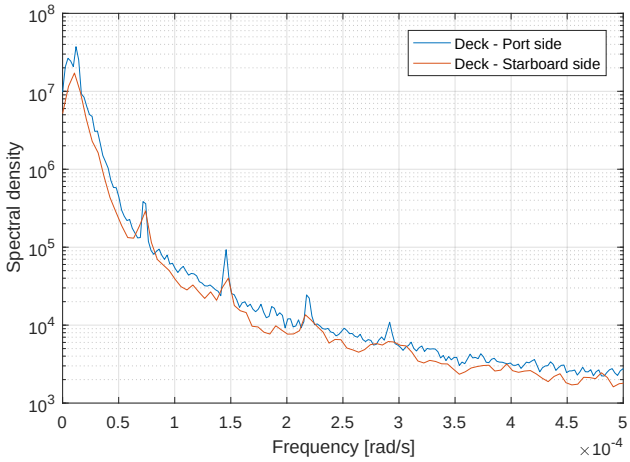

Figure 4.66: Energy spectra of opposing deck locations. The frequency associated with a one day period equals $0.7 * 10^{-4} rad/s$ and some response at this frequency can be found at both locations, while responses at integer multiples of this base frequency are only found at the port side location.

starboard side deck location is a considerable outlier with 5 times as many stress cycles as days in operation. This location is instrumented with both a Wheatstone bridge strain gauge and Long Base Strain Gauge, see section 3.4.3. The same result was found in both sensors and is therefore believed to be physical. The frequency spectra of the signals at both deck locations has been obtained and is shown in Figure 4.66. At both port side and starboard side, a peak is found in the signal at a frequency corresponding to a one day period. However, the port side spectrum are sharper and also shows more pronounced peaks at integer multiples of this base frequency which results in an additional number of load cycles.

Figure 4.67 presents an overview of the key statistical parameters which describe the temperature-induced stresses. Overall, the mean stress range and its variation are of the same order of magnitude between the different units and measurement locations. However, the side shell and deck area of unit *NS* and, to a lesser extent, the deck area of unit *WA4* show a larger number of stress cycles compared to the number of days in operation as a result of the higher harmonics in the stress spectrum. For the other locations, the number of observed cycles corresponds well with the number of days in operations.

The parameter α_{Temp} has been determined using the procedure from section 2.5.6. The results are shown in Figure 4.68. It should be remembered that the relative contribution of these cycles by themselves is very small, as was observed in Figure 4.57 and 4.58. Although these temperature-induced cycles by themselves do not introduce a significant fatigue accumulation, the interaction between the temperature cycles and loading cycles, as discussed in section 4.7.2, does result in a significant contribution that warrants further considerations.

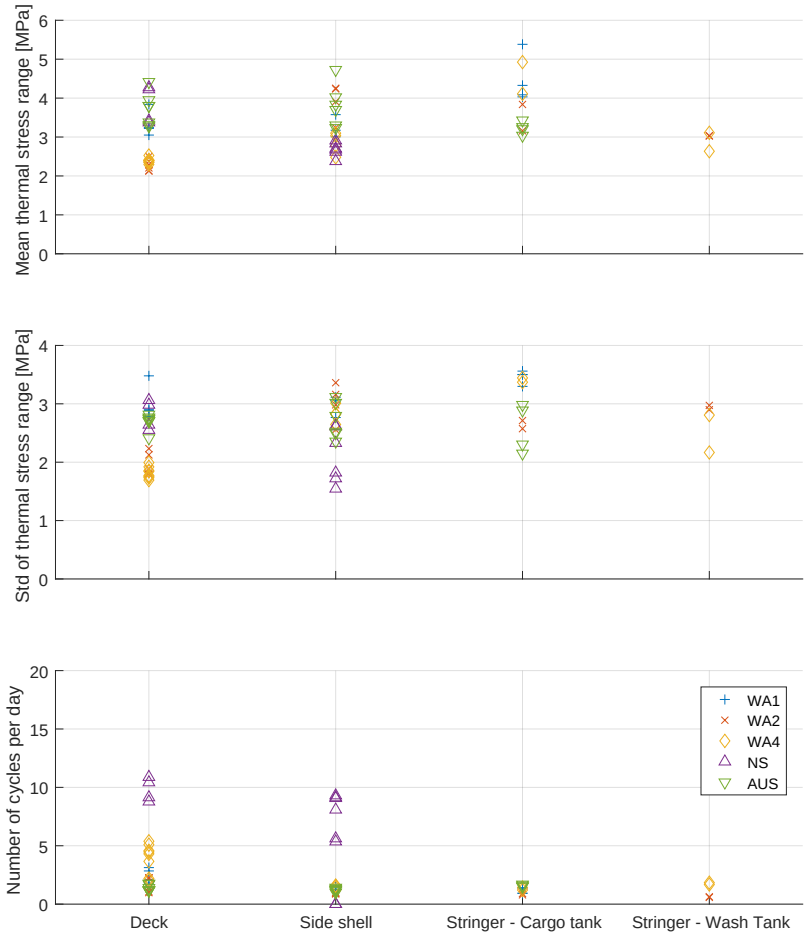

Figure 4.67: Descriptive statistical data of the observed thermal cycles on multiple units. The top graph shows the average thermal stress cycle, the middle graph shows the standard deviation of these cycles and the bottom graph shows the number of observed cycles relative to the number of days in operation.

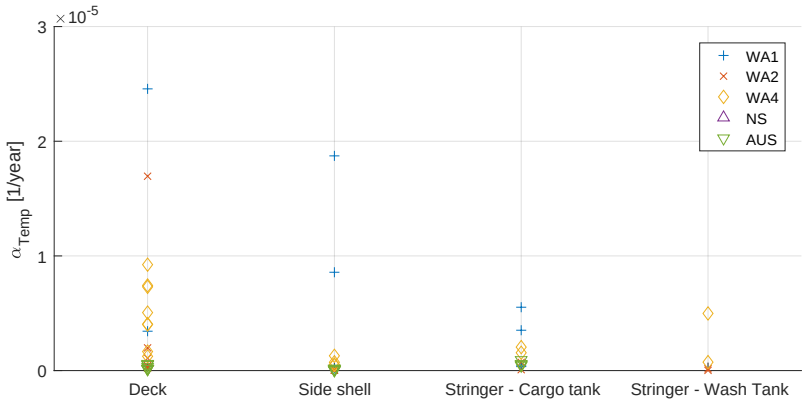

Figure 4.68: Contribution of the temperature-induced uncertainty in the loading-induced fatigue assessment for all measured locations.

4.7.4. SUMMARY

On cargo supporting structures such as stringers, an important contribution to the total fatigue accumulation arises from loading and offloading cycles. At the selected measurement locations up to 90% of the total fatigue accumulation was attributed to loading-induced fatigue.

The typical stress ranges at the measurement locations are around $50MPa$. Outliers have been observed which are stress cycles of around $120MPa$. These stress cycles are the result of joint cargo and ballast fluctuations, changes in global hydrostatics, temperature-induced deformations and wave-induced stresses. The stress variations from adjacent cargo tanks are by far the largest contribution to the stress cycles. However, the secondary stress component still result in a significant contribution to the overall fatigue accumulation, due to the nonlinear relation between stress and fatigue accumulation. Observations have shown that the secondary stress components can result in a fatigue accumulation which is more than double the fatigue accumulation derived from cargo loading only.

Design procedures introduce an additional stress range to account for wave loading effects. However, the additional stress variations resulting from more subtle changes in loading conditions resulting in changes to the global hydrostatics and temperature-induced effects are not accounted for. The effects result in an additional stress range of around $10MPa$.

The stress cycles introduced from the daily temperature fluctuations themselves result in a negligible fatigue accumulation and do not need to be considered in the design stage.

4.8. OVERVIEW OF OBSERVED UNCERTAINTIES

Table 2.2 provides an overview of various sources of uncertainties. This table has been expanded to provide an analysis of the importance of the individual uncertainty on the

overall fatigue accumulation and is shown in Table 4.18. A number of the parameters in this table were associated with different sources of uncertainties. These individual sources have been added to the table. Moreover, the results between locations also vary depending on the loading mechanism. The table shows a separate entries for the three main loading mechanisms.

The goal of Table 4.18 is to provide a general guideline for determination of the importance of several sources of uncertainty in fatigue design of floating offshore units. Therefore, the exact numbers of the individual units reviewed in this research are not presented here. For additional details on the units considered in this research, the relevant sections of this chapter can be consulted. A more detailed table with discussion and interpretation for specific types of offshore units in different environments will be provided in section 5.3.

	Loading Mechanism		
Source of uncertainty	Bending Moment	Wave Pressure	Loading-induced
Long-term environmental conditions	Large	Large	N/A
Short-term environmental description	Medium	Medium	N/A
Operating Conditions	Very Small	Small	N/A
Hydrodynamic and structural model	Medium	Large	N/A
Intermittent Wetting effects	N/A	Small	N/A
Fatigue calculation method	Medium	Large	N/A
Strong nonlinear response	Small	Very Small	N/A
Loading fluctuations	Very Small	Very Small	Medium
Loading-induced stress variations	Very Small	Very Small	Large
Temperature-induced loading	Very small	Very small	Very small

Table 4.18: Qualitative assessment of the importance of various uncertainties in the fatigue assessment.

5

Discussion

Keep your eyes on the stars and your feet on the ground

Theodore Roosevelt

5.1. OUTLINE

This chapter provides some reflection of the results which have been obtained in Chapter 4. The importance of different loading phenomena and the associated parameters varies between different units. Section 5.2 provides a reflection on the observed loading phenomena and potential effects on the global structure. Section 5.3 provides a discussion of how the loading phenomena should be weighed according to the characteristics of the unit and its operating environment. For future applications, the results of this work can be integrated with monitoring results of other units. Section 5.4 provides an overview of different in-service monitoring solutions which may be applied and how integration with the results presented herein, can be achieved. Finally, Section 5.5 presents a discussion on how monitoring, numerical models and uncertainty quantification can be combined in a structural digital twin to yield meaningful results.

5.2. LOAD EFFECTS

In this section, a general discussion on the different load effects will be provided. First, a discussion on the quality of wave and hindcast data will be provided in section 5.2.1. In the subsequent sections 5.2.2, 5.2.3 and 5.2.4, a discussion of the wave-frequent, high- and low-frequent load effects will be provided.

5.2.1. WAVE DATA

Detailed information on wave conditions is of the utmost importance for a fatigue assessment. The results in section 4.2 have shown that global hindcast models can provide suitable wave characteristics for a long-term fatigue assessment in the considered cases. To do so, one should take care that a representative short-term sea state description is adopted though. Dedicated local models, such as the work by Prevosto *et al.*[142] and Hoque *et al.*[143], can further improve the accuracy of this type of data.

While the hindcast models are a suitable data source for the assessment of the long-term wave statistics, the analysis of uncertainty factors in fatigue loads benefits greatly from having high quality wave data available for at least a limited amount of time. Such data can be provided by a wave buoy or radar. The required amount of data depends on variability of the environment, but as a guideline, around two years of data would be recommended to capture a representative set of conditions. The wave data can be used to examine wave characteristics and define the most appropriate way of using the hindcast data. It can also be used to verify the selected spectral and spreading models which were adopted during design. Some hindcast models are also able to provide spectral description, but it should be remembered that these are obtained from oceanographic models using wind measurements as input and will therefore introduce addictional scatter when compared to directly measured wave conditions.

Offshore units are designed for 20 years of operation or longer. Over such a period, the environmental conditions can gradually change as a results of climate effects. The work by Zou [144] addresses the effect of climate change in relation to fatigue accumulation of floating structures. In such analysis, it is important that not only the average conditions are examined, but also the presence and severity of storms at the specific location is addressed.

Turret moored units normally weathervane around their turret under the influence of environmental loads, including current, wind and multiple wave systems. The unit will find a heading under which an equilibrium of these forces is achieved. However, from an operational perspective, this heading may not be the optimal condition and operators can use thrusters to actively control the heading of the unit. The performance of the production facility can be improved by reducing roll motions by moving the unit with its bow into the dominating wave environment. Under these conditions, wave bending moments will be large though. Heading control may therefore negatively affect the fatigue life of details subjected to global hull girder bending. None of the units studied in this research apply active heading control continuously. However, Figure 4.12 has shown the effect on fatigue accumulation from various heading variations and a bias of up to 30% was found. The effect on fatigue accumulation caused by the orientation of the unit with respect to the waves is therefore significant.

5.2.2. WAVE-FREQUENT

The short-term sea state definition proofed to be quite important for evaluating the wave-frequent fatigue accumulation, see also section 4.3. The total fatigue accumulation could differ up to a factor two when adopting different spectral definitions. This observation stresses the importance of obtaining some high-quality wave data for at least some time during operations. This data can be used for a comparison with the wave definition which was used during design to gain insight in the accuracy of this model. The wave spectra, as adopted in this study, can be sorted according to their spectral width with the Bretschneider spectrum being the widest and the Gaussian spectrum the most narrow. Depending on the load effect and orientation with respect to the dominant environment, the adoption of either the Bretschneider or Gaussian spectrum resulted in the highest fatigue accumulation. For structural details subjected to hull girder bending, the Gaussian spectrum resulted in the largest fatigue accumulation on all units. However, in a similar study for a 120 metre naval vessel, Plouvier and Hageman [126] found the exact opposite trend, i.e. the Gaussian spectrum was the least conservative spectrum for details subjected to hull girder bending. The reason is that on a smaller vessel such as this, the peak of the vertical bending moment is found at a higher frequency. Overall, for larger vessels, a more narrow spectrum results in a larger fatigue accumulation, but also the bias in fatigue accumulation between different spectral shapes becomes larger.

Intermittent wetting affects the fatigue accumulation in the side shell. Intermittent wetting is a nonlinear loading which, for the sake of a spectral calculation, is often linearised. The linearisation procedure is well established for estimation of equivalent stress ranges. However, the area which is affected by intermittent wetting also depends on the wave height. On offshore structures, the area which is subject to intermittent wetting continuously changes. This results in a more uniform distribution of the intermittent wetting loads over the entire side shell. However, it also means that for all elements in the side shell intermittent wetting is to be accounted for. When the area selected for intermittent wetting is small compared to the changes in draft of the selected loading conditions, intermittent wetting effects will be underestimated for certain structural details. Care should be taken to ensure that for each structural detail analysed, intermittent wetting is incorporated by selecting appropriate loading conditions.

The analysis in Section 4.5 have shown that the fatigue assessment method provides a fairly accurate, or slightly overestimated, fatigue accumulation rate on average. There is significant scatter in the results between different time instants, which has resulted in the definition of a stochastic model for α_{Meth} to cover this variation. However, it was also shown that the conservatism in the calculation is progressive. That is, at higher fatigue accumulation rates, the procedure results in a slightly higher bias of the fatigue accumulation. Hence, even when adopting the stochastic model of α_{Meth} in the analysis as derived in this study, a part of the inherent safety margin from the fatigue assessment procedure remains in place.

The analysis of the uncertainty of wave-frequency load effects in section 4.5 used data obtained from a dedicated wave buoy. This has restricted the amount of data available for this study. An alternative is to use hindcast data for the evaluation of the performance of design procedures. While this increases the amount of available data, the scatter in the analysis is increased as a result of the modelling of the wave field. A related study using a part of the data set analysed in this study is shown by Andoniu *et al.* [145]. This study presents analysis from a wave buoy and hindcast data side by side. It shows that the scatter in the individual data points increases when using hindcast data in lieu of data from the wave buoy. In the analysis of the total accumulated fatigue consumption, the spectral calculations using the wave buoy perform better for four out of six structural details which have been addressed.

Numerical analysis and model tests of offshore structures are typically executed for periods of 3 hour to gather representative data. These analyses are executed to examine seakeeping behaviour of these structures or mooring analysis and may also be used to look at offloading events. The results in Figure 4.25 have indicated that for such analysis periods, the scatter in the fatigue estimate is of the order of 1%. Since this truncation effect is small, it is worthwhile to consider execution of a limited number of numerical time-domain simulations or model tests including structural response. The results obtained from these methods can be used to get an understanding of the accuracy of the long-term prediction obtained using spectral methods. The results from Figure 4.31 and 4.42 have indicated that the spectral calculations will generally introduce a small safety margin and the proposed analyses allow for a quantification of these safety margins for a given unit.

5.2.3. HIGH-FREQUENT

In the shipping industry much attention has been given to the assessment of flexural vibrations in container ships using in-service measurements. Container ships feature an open cross section and are therefore susceptible to significant flexural bending deformations. A survey by Storhaug *et al.* [146] on several ships shows the contribution of flexural vibrations to fatigue accumulation can exceed 50% for 8,600 TEU container ships over their entire lifetime.

Military vessels are also considered prone to whipping because these vessels are more commonly operated at high speed and in heavier environmental conditions than commercial ships. Analysis by Drummen *et al.* [69] and Thompson [147] provide two examples of vessels equipped with hull monitoring systems for which the contribution of whipping to fatigue accumulation is between 7% and 10%. This is of a similar magnitude

as the contribution observed on some of the offshore units considered in this research as is shown in Figure 4.47. It should be noted that the military vessels feature lengths between 120 and 130 metre and the relative contribution is expected to be more significant on larger vessels.

In this research only fatigue loads have been considered. However, whipping will also result in a significant increase in the maximum bending moment experienced by the hull. The results in section 4.6.2 have shown that whipping does occur and is significant in certain sea states. For units operating in these areas, however, the contribution of whipping to the extreme bending moments can be more important than the contribution of whipping to fatigue accumulation.

Flexural vibrations of the hull can also result in damage as a result of interaction with other parts of the structure. Benhamou *et al.* [148] describe the failure of a flare tower due to resonance between the hull and tower vibrations. This indicates the importance of structural analysis using a fully integrated numerical model of the entire structure.

Because springing is a resonance effect, it is also sensitive to the natural frequency of the hull. On an offshore production unit, this varies continuously as a result of the changing loading conditions. A small set of data of unit *WA*4 was used to examine the variation in the natural frequency. The natural frequency of the two-node vertical vibration mode was derived from the four strain gauges using Stochastic Subspace Identification from Overschee and De Moor [149] which simultaneously provides damping estimates as well. The derived frequency is shown in Figure 5.1. This figure shows that the variation of the natural frequency under different loading conditions is quite small and therefore has limited effect on the springing excitation. The natural frequency can be related directly to the loading condition. Displacement data is not available for this unit, but Figure 5.2 shows a strong correlation between the derived natural frequency and draft and trim.

5.2.4. LOW-FREQUENT

Two low-frequency load effects, loading-induced stresses and daily temperature-fluctuation related stresses, have been analysed. On most structural details, the contribution of these load effects was below 20% of the total fatigue accumulation. However, on stringers, the contribution can be up to 90%.

The majority of the low-frequent fatigue accumulation is the result of loading effects. In design stage, this effect is evaluated by calculating a stress range from two different loading conditions and the expected number of cycles. This calculated stress range is quite representative or conservative of the average encountered stress cycles onboard.

However, the onboard stress cycles vary in magnitude. The maximum stress range can be 2 to 2.5 times larger than the average stress cycle. The variation of these stress cycles is the result of variation in loading conditions and small perturbations resulting from wave action and daily temperature cycles. The variation in stress cycles can result in a bias on fatigue accumulation of 50% and should therefore be considered during this analysis. The proposed stochastic model of α_{LS} can easily be adopted in the design stage and should lead to a better representation of the low-frequent stresses.

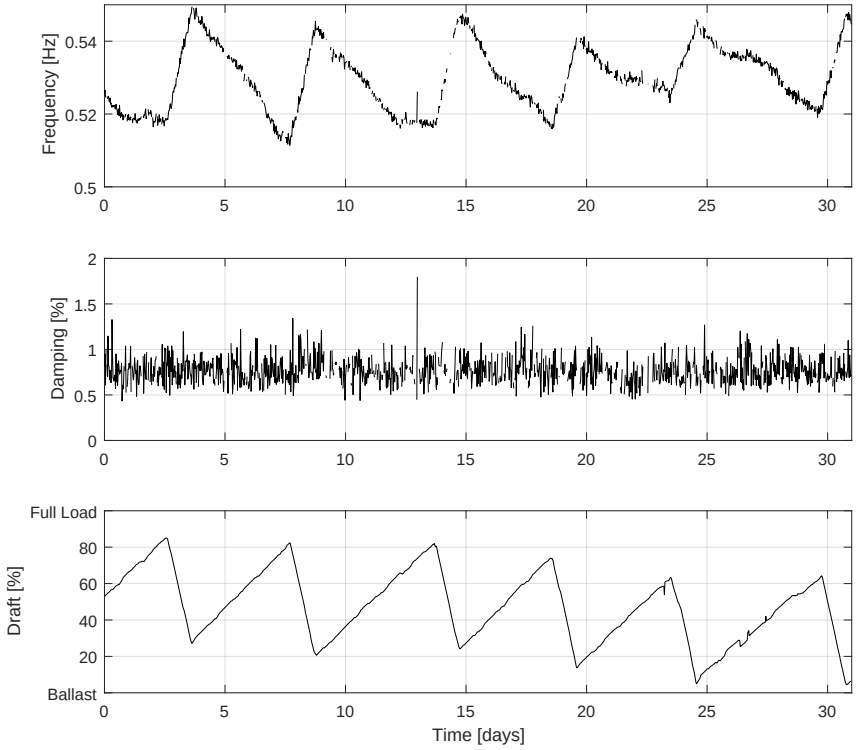

Figure 5.1: The observed natural frequency and associated damping (structural and hydrodynamic) on unit *WA4* during a one month period.

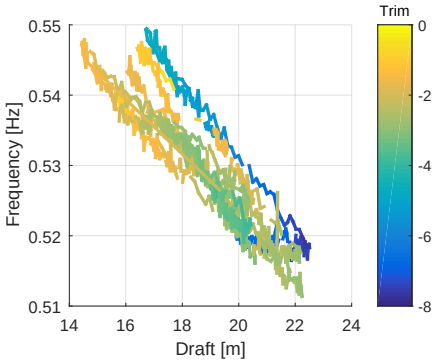

Figure 5.2: The relation between natural frequency and draft and trim on unit *WA4* during the one month period considered in Figure 5.1.

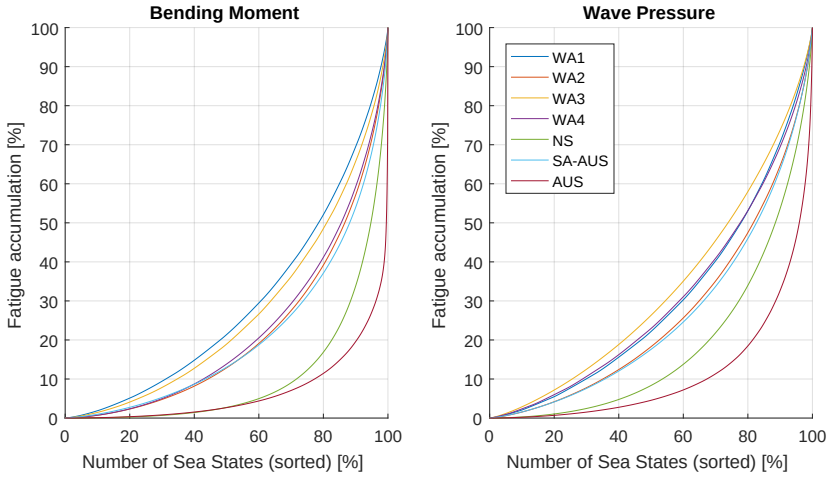

Figure 5.3: Fatigue accumulation during sea states in sorted order on two representative details of each floater in their respective environment.

5.3. UNCERTAINTY QUANTIFICATION IN CHARACTERISTIC ENVIRONMENTS

5.3.1. SUBDIVISION OF ENVIRONMENTS

In this study, a number of different units of various size and operating in different environments have been studied. Loading effects that are important on some units may be less so on different units and the associated uncertainties should be weighed accordingly. In this section, three types of environmental conditions are examined. These are mild environments, such as the conditions found in West-Africa, harsh environments, such as the conditions in the North Sea and tropical storm environments, such as Australia. In this last type of environment, weather conditions are generally mild, but rare storm events may occur.

The majority of the fatigue accumulation is often considered to be the result of intermediate range load cycles. The contribution of frequent, but mild sea states to the overall fatigue accumulation is considered to be small due to the low amplitudes encountered. On the other hand, the contribution of rare, but extreme sea state is also considered small due to their limited occurrence. The importance of low and high sea states has been quantified for the units in their environments. For a consistent comparison, 10 years of hindcast data at all locations has been retrieved and a spectral fatigue assessment, assuming head sea conditions, was executed.

Figure 5.3 shows the contribution to the total fatigue accumulation as function of the number of sea states when sorted in ascending order of fatigue contribution. For each unit, the calculations have been executed using two representative midship details, one subject to hull girder bending and one subject to wave pressure loading. The structural details subjected to bending moments show a stronger dependency than those subjected to wave pressure. The fatigue accumulation on the former details increases

	WA1	*WA2*	*WA3*	*WA4*	*NS*	*SA-AUS*	*AUS*
Bending Moment	0.3	0.7	0.5	0.7	1.4	0.8	19.9
Wave Pressure	0.3	0.5	0.3	0.4	0.7	0.4	3.2

Table 5.1: Contribution [%] of fatigue accumulation of conditions which occur less than once a year

strongly with increasing wave height. However, on the details subjected to wave pressure loading an interplay between wave height and period exists. The fatigue accumulation increases in higher waves, but reduces in longer periods due to the motion of the unit and the reduced number of cycles. Hence, for these details, the increase in fatigue accumulation in rare sea states is less strong compared to the details subjected to bending moments.

All units located in the West-Africa region show comparable results. For the details subjected to bending moments, one-third of the fatigue damage is accumulated during the lowest 70% of the sea states and one-third in consumed during the 10% worst sea states. However, the result is quite different for unit *NS*, operating West of Shetland, and unit *AUS*. Unit *NS* is operating in a generally harsh environment, but unit *AUS* is operating in a mild environment, but prone to cyclones. On both units, the lowest 70% of the sea states account for only 10% of the total fatigue accumulation. On the importance of the extreme conditions, the strongest effect can be seen on unit *AUS*. On this unit, 50% of the fatigue accumulation is generated during 1% of the sea states. This means that in a life of 20 years, half of the fatigue accumulation takes place in only 10 weeks. Table 5.1 presents the fatigue contribution of conditions with a return period of 1 year or less. This table shows that for most units the yearly extreme condition results in a relatively small contribution to the overall fatigue accumulation. However, on unit *AUS* the contribution is much more significant due to skewed nature of the environmental conditions at this location. In line with earlier findings, the extreme condition has a larger influence on structural details subjected to hull girder loads than those subjected to wave pressure loading.

These findings are in line with the observation in Figure 4.38 which shows that the wave amplitude increases the fastest at this location at lower probability of exceedance. For such a case, knowing the actual number of storm events which the unit has encountered is important for an accurate lifetime assessment. For the details subjected to wave pressure loads, the respective numbers are slightly different, but the main trends also hold for these details.

5.3.2. MILD ENVIRONMENT

The environment of West-Africa is considered to be very mild. The units designed for operation in this environment feature a relatively light structure. For such structures, the following observations on the loading phenomena have been made and should be considered in the design and reliability assessment of such a unit. A summary of the importance of different sources of uncertainty for this type of unit is given in Table 5.2.

- The long-term wave environment is very predictable and can be predicted with high confidence. Scatter in fatigue accumulation prediction from statistical varia-

Origin of uncertainty	Loading Mechanism		
	Bending Moment	Wave Pressure	Loading-induced
Long-term environmental conditions			
Wave statistics during operation	Medium	Medium	N/A
Statistical variability	Small	Small	N/A
Wave statistics during towing	Large	Large	N/A
Orientation in waves	Small	Small	N/A
Short-term environmental description			
Spectral shape	Large	Medium	N/A
Wave spreading	Small	Medium	N/A
Multimodal sea states	Small	Small	N/A
Convergence of sea states	Very Small	Very Small	N/A
Operating Conditions			
Loading profile	Small	Medium	N/A
Hydrodynamic and structural model	Medium	Large	N/A
Fatigue calculation method	Medium	Large	N/A
Strong nonlinear response			
Springing	Small	N/A	N/A
Loading fluctuations	N/A	N/A	Medium
Loading-induced stress variations	N/A	N/A	Large
Temperature-induced loading	Very small	Very small	N/A

Table 5.2: Qualitative assessment of the importance of various uncertainties in the fatigue assessment of offshore units operating in a mild environment.

tion of the wave environment is small.

- During transportation from yard to operating site, a unit may encounter relatively large waves and experience significant horizontal bending. Towing conditions may give rise to considerable fatigue accumulation in certain parts of the structures. A design assessment of towing conditions is recommended, but will generally use conservative wave conditions and thus introduce an implicit safety margin.
- An appropriate short term sea state definition of the wave conditions needs to be selected. A significant bias in the fatigue prediction from the spectrum definition may remain as a result of the high sensitivity of the structural response with respect to the spectral description.
- The hydromechanic, structural and fatigue calculation methods introduce some bias and scatter. The combined scatter is quite significant, but also a prediction bias is introduced. As a typical value, the bias is estimated at 50% on the fatigue lifetime.
- Flexural responses of the hulls have been identified. Large units in this environment are quite flexible and are more susceptible to springing than whipping. For

the considered cases, the increase in fatigue accumulation was 15% at most. However, a clear link with the governing wave period was found and in unfavourable conditions, the fatigue accumulation from springing could result in an increase of 100% in fatigue accumulation during that condition. A basic check to verify the susceptibility to springing is therefore recommended.

- Loading-induced loads are an important driver for the fatigue accumulation in cargo supporting structures, as wave loading on this type of unit is limited. These stress cycles are predicted well on average, but are also subject to significant bias and scatter due to secondary loading effects as well as global deformations introduced by wave action and day-night temperature cycles.

5.3.3. HARSH ENVIRONMENT

The environment of e.g. the North Sea is considered to be very harsh. The units designed for operation in this environment feature a sturdy structure and are turret-moored which allows them to orient in a favourable way. The monitoring data presented in this study yielded only a single unit in this type of environment with a limited monitoring duration yet. Therefore, the observations that can be made at present are limited. A summary of the importance of different sources of uncertainty for this type of unit is given in Table 5.3.

- The long-term wave environment at such a location, which will feature frequent storm events, remains quite predictable and scatter from statistical variation of the wave environment are small. To facilitate the design process for units operating in heavy weather conditions, screening procedures can be used to identify the most severe conditions. An example of such a procedure is presented by Fukusawa and Kadota [150]. These authors present a screening procedure using equivalent design waves to determine the sea states with a significant contribution towards fatigue accumulation. The selected conditions can be subjected to a more thorough analysis by means of model tests or numerical simulations.
- The wave conditions experienced during transportation from yard to site are not explicitly considered given that the conditions in the field are significant.
- An appropriate short term sea state definition of the wave conditions needs to be selected. In such an environment, local storms giving rise to significant windsea and large swells will coexist and appropriate modelling choices for both types of wave loading should be selected.
- The currently available results do not allow to judge the performance of hydromechanic, structural and fatigue calculation methods for this unit. However, given the strong consistency observed on the other units, there is no reason to suspect significant deviations. A notable exception could be the incorporation of intermittent wetting which was found a reason for concern on similar units in the past according to van der Cammen [86].
- Flexural responses of the hulls have been identified. Due to the harsh environment, whipping can occur at regular intervals. The whipping response resulted in

Origin of uncertainty	Loading Mechanism		
	Bending Moment	Wave Pressure	Loading-induced
Long-term environmental conditions			
Wave statistics during operation	Medium	Medium	N/A
Statistical variability	Small	Small	N/A
Wave statistics during towing	N/A	N/A	N/A
Orientation in waves	Medium	Medium	N/A
Short-term environmental description			
Spectral shape	Large	Medium	N/A
Wave spreading	Small	Medium	N/A
Multimodal sea states	Medium	Medium	N/A
Convergence of sea states	Very Small	Very Small	N/A
Operating Conditions			
Loading profile	Small	Medium	N/A
Hydrodynamic and structural model	Medium	Large	N/A
Fatigue calculation method	Medium	Large	N/A
Strong nonlinear response			
Whipping	Very small	N/A	N/A
Loading fluctuations	N/A	N/A	N/A
Loading-induced stress variations	N/A	N/A	N/A
Temperature-induced loading	Very small	Very small	N/A

Table 5.3: Qualitative assessment of the importance of various uncertainties in the fatigue assessment of offshore units operating in a harsh environment.

an increased fatigue accumulation of around 10% overall. The whipping response was found to increase in higher sea states, but also showed more scatter in these events.

- The relative contribution of loading-induced fatigue effects was found to be negligible compared to the high wave loads at the instrumented structural details.

5.3.4. TROPICAL STORM ENVIRONMENT

The environment of the area around Australia is generally very mild. However, tropical storm events may occur at irregular intervals. This introduces some unique characteristics when studying structural response on units operating in such environments. A summary of the importance of different sources of uncertainty for this type of unit is given in Table 5.4.

- The long-term wave environment is quite unpredictable and is subject to significant aleatoric uncertainty from statistical variation of those conditions. The total fatigue accumulation is governed by the fatigue rate in rare storm events.
- The wave conditions experienced during transportation from yard to site will not exceed the extreme conditions in the field and should not give rise for particular

Origin of uncertainty	Loading Mechanism		
	Bending Moment	Wave Pressure	Loading-induced
Long-term environmental conditions			
Wave statistics during operation	Medium	Medium	N/A
Statistical variability	Medium	Small	N/A
Wave statistics during towing	Medium	Medium	N/A
Orientation in waves	Medium	Medium	N/A
Short-term environmental description			
Spectral shape	Large	Medium	N/A
Wave spreading	Small	Medium	N/A
Multimodal sea states	Medium	Medium	N/A
Convergence of sea states	Very Small	Very Small	N/A
Operating Conditions			
Loading profile	Small	Medium	N/A
Hydrodynamic and structural model	Medium	Large	N/A
Fatigue calculation method	Medium	Large	N/A
Strong nonlinear response			
Springing	Very small	N/A	N/A
Loading fluctuations	N/A	N/A	Medium
Loading-induced stress variations	N/A	N/A	Large
Temperature-induced loading	Very small	Very small	N/A

Table 5.4: Qualitative assessment of the importance of various uncertainties in the fatigue assessment for units operating in an environment featuring tropical storms.

concerns.

- An appropriate short term sea state definition of the wave conditions needs to be selected. The conditions in Australia can be characterised by a strongly confused sea states and an appropriate sea state representation should be selected.

- The hydromechanic, structural and fatigue calculation methods for this unit were found to result in significant safety margins. The combined safety margin was higher than that obtained from the units in West-Africa. In the side shell structure, the safety margin was significantly higher than that of most units in West-Africa. This was related to the incorporation of intermittent wetting. After removing the observed bias in the stress response operator, the intermittent wetting effect on all units was found to give rise to similar stresses.

- The flexural response of this particular unit were found to be minimal. On the units in mild environments, significant flexural response could be observed, but their absence on this unit can be contributed to the larger stiffness of this unit.

- The loading-induced fatigue effects resulted in a relatively small contribution of up to 20% of the total fatigue accumulation. Variations in loading-induced stresses

could still be observed and the procedures applied for the mild environment units can still be applied here.

5.4. MONITORING STRATEGIES

5.4.1. GENERAL

Requirements for a hull monitoring systems are defined by classification, but remain a voluntary notation. These design codes define minimal requirements and can therefore be considered a good starting point for developing a minimal hull monitoring system. The regulations as provided by BV [153] show a focus on wave-induced response. ABS [154], CCS [155] and LR [156] have additional notations to specify monitoring of specific properties, such as loading computer and motions. Rules provided by ClassNK [157] and DNV [158] specifically mention the recording measurements using a sampling frequency on strain gauges which will include flexural effects of the hull.

In this section, different monitoring solutions will be discussed and evaluated. In his research, Stambaugh identifies two basic monitoring schemes, prognostic and reactive, and provides a framework of evaluating the added value of each approach [151]. The monitoring procedures used in support of this research are of the prognostic type and will be discussed first.

5.4.2. PROGNOSTIC MONITORING

Prognostic monitoring systems are used to validate and develop design models for predicting long-term loads on the structure and obtain a long-term track record. In combination with proper analysis procedures, the systems can be used to identify critical load aspects. Such systems can be used from the beginning of the operating life and can be maintained to the end of the unit's lifetime.

EXTENSIVE HULL MONITORING SYSTEM

An extensive hull monitoring system includes a wide variety and large number of sensors installed at various locations in the hull. The types of sensors vary between local strain gauges, accelerometers, pressure sensors and global sensors such as GPS, motions sensors, registrations from loading and control systems, and wave radar or buoys. This setup provides the most complete possible data set which can be used for cross-referencing. However, the effort of setting up such a system is significant.

The results of an extensive system can be used in academia for gaining understanding of load processes taking place inside the structure. However, these systems are expensive to maintain and detailed analysis takes a considerable amount of resources. When using such a system for long-term monitoring, the majority of the sensors will not be used effectively and analysis will generally converge on a number of key performance indicators which provide insight in the overall condition of the unit.

MINIMAL HULL MONITORING SYSTEM

After gaining understanding of the important physical aspects of the structure, a monitoring system with reduced instrumentation setups for similar structures can be developed. Such an approach helps defining cost-effective prognostic monitoring procedures

for future assets which can more easily be deployed on a larger number of units. The work conducted by van den Boom *et al.* on FPSOs [104] and van der Cammen [152] has initiated the development of the minimal hull monitoring system used in this research. A functional definition of the system was first given by Kaminski [132].

Minimal hull monitoring systems consist of a smaller amount of sensors. Both the variety of sensors as well as the number of sensors installed will be smaller compared to the extensive hull monitoring system. The reduced number of sensors will require more careful sensor placement, but will generally be more convenient for analysis by focussing efforts where they are needed. Wave data can be retrieved from (dedicated) wave buoys or vessel-mounted wave monitoring systems, but these systems are expensive and challenging to maintain and hindcast data may be a suitable alternative.

A minimal hull monitoring system is considered a cost-effective monitoring strategy. This allows enrolment of such a system on multiple assets. The strength of these systems for research or academic purposes is thus not so much the detailed knowledge from one structure, but the knowledge of scale gained by studying multiple assets in similar or different operational conditions.

VIRTUAL HULL MONITORING SYSTEM

It is not always necessary to define a dedicated monitoring campaign in order to gain insight in the assets performance during operations. A virtual hull monitoring system is based on a procedure which relies on non-dedicated data sources to make statements on the structural integrity of an asset. These data sources can range from a captain's log to publicly available data such as AIS or hindcast data. The structural response is assessed by using numerical models developed in the design stage.

The obvious benefit of such an approach is that it is easy to initiate and requires little investment costs. The method allows for quantification of some uncertainties resulting from operational decisions and environmental conditions. The drawback of such a method is that by relying on design tools, the accuracy of the calculation of structural response cannot be assessed. Additional analyses to address off-design conditions may be necessary. Also, the amount of work required to setup and check the analyses should not be underestimated as the types of data used are generally more complicated to interpret and call for additional quality assurance.

5.4.3. REACTIVE MONITORING

Reactive monitoring can be used to monitor the development of cracks in the structure. These approaches provide information on the integrity of individual welded details. Such approaches can be adopted if minor cracks have been identified or are expected to occur. As such, reactive monitoring schemes are typically applied in the later stages of the lifetime of a unit.

One technique for the assessment of the condition of structures is by using acoustic emission. In this monitoring technique, sensors register the growth rate of micro-cracks through the emitted sound waves. By using multiple sensors and triangulation, an area of a structure can be monitored. This technique has been applied successfully in civil engineering applications, see e.g. Pahlavan *et al.* [159]. Prolonged in-service monitoring campaigns to assess crack growth in ship structures are rare though. One example is the

work on a naval vessel published by Rogers and Stambaugh [160].

Guided wave monitoring uses the same type of sensing principle as acoustic emission monitoring. However, a guided wave system uses an array of active sensors to transmit sound waves through the structure. This type of assessment allows for quantification of crack size even if the crack is not actively propagating. An example application can be found in the work by Pahlavan and Blacquière [161].

An alternative procedure is the novel concept by van der Horst [162], which uses magnetic flux leakage to identify cracks. A device based on this technique must be deployed directly over the crack itself in order to register it. On the other hand, it can determine the actual crack size when active and does not need to be operational at all times.

5.5. INTELLIGENT STRUCTURAL DIGITAL TWIN

5.5.1. DIGITAL TWIN CONCEPT

Digital twins are a relatively new and developing concept which aim to provide a digital model of a physical structure. The digital twin is a container which can include various types of information ranging from design documents, numerical models, inspection reports and in-service measurements. The digital twin ensures that analysts can store and access the information that is needed. A visual representation of a digital twin representative of an application as examined in this study can be found in Figure 5.4.

A digital twin by itself does not feature data analysis procedures. It may feature interfaces with services that provide analysis capabilities such as numerical models or the data collection system as presented in Chapter 3. A digital twin generates more value as additional tools and analysis procedures become available and accessible to analysts.

Parts of the data set presented in this research have been used to study potential application of novel analysis techniques. In the following section, a number of these technologies are described. The developments are still considered to be at a research level, but may one day be applied in a digital twin.

5.5.2. FULL HULL ANALYSIS

Due to the vast amount of structural components on an offshore platform, it is unrealistic to inspect every joint [163]. Based on a an analysis of similarities in loading and scantlings between multiple structural analysis, van den Berg *et al.* show a procedure to reduce the amount of required inspections [164]. However, these methodologies require further validation before they can be applied to an actual floater.

In order to use measurement data to cover a wider range of structural details, Inverse FEM or IFEM, can be applied to the global or local structure. When using a limited set of measurements to estimate hull girder bending moments or local stresses at a large number of structural details, a rational basis of decomposition for these measurements needs to be found. Efforts in the shipping industry have started out by using wet flexural modes, see the work by Malenica and Derbanne [165]. However, in more recent years, practical evidence has shown that representative wave modes offer a better accuracy as decomposition basis. Applications of this technique occur on an ever growing range of container ships [146, 166, 167]. Another example is the work by Schiere *et al.* on a fast displacement ship [168]. Storhaug *et al.* [169] propose a calibration procedure to account

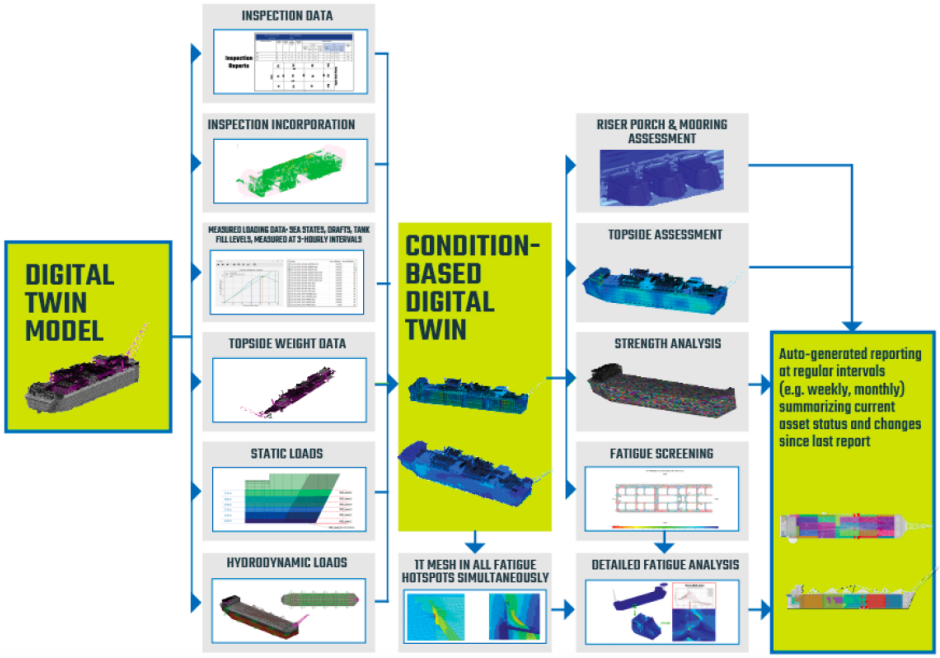

Figure 5.4: Representation of a digital twin for a typical offshore unit as considered in this study from Bhat *et al.* [16].

for the static deflection and axial compression introduced by pressure on the ship's front and stern. The applicability of such a procedure to offshore units is being investigated. Initial evidence by de Lauzon *et al.* has shown that the estimation of stresses at locations subject to hull girder bending loads work well [170]. However, the application to parts of the structure with more local loading effects, such as side shells, remain unclear at this stage.

5.5.3. CORROSION

The influence of corrosion allowances on fatigue life is not straightforward to assess. Design criteria define minimum scantlings and on top of these requirements, plate thicknesses are increased to account for corrosion. The amount of added material is related to the planned lifetime of the unit. In the design model used to assess fatigue accumulation, the plate thickness used are the minimum scantlings including some of the corrosion allowance. As such the interaction between fatigue and corrosion assumes general corrosion over the entire cross section. This situation is not very realistic as corrosion tends to occur locally in corners or small areas, but not equally over the entire cross section. As a result of this modelling choice, stresses which have been observed on the units are generally lower than predicted. A systematic analysis of changes in the failure modes of an FPSO subjected to corrosion can be found in the study by Petillo [171].

When corrosion occurs locally on a plated area, the stresses resulting from global

load effects would barely change. Under local corrosion, the overall cross section modulus would not change significantly. Local stress redistribution may occur, but the changes in the far-field stress would be small. However, when a structure is subject to local load effects, such as wave pressure loading, the stresses will be affected. Moreover, a more violent type of corrosion such as pitting could lead to strong stress redistribution and could create a fatigue sensitive location in a formerly moderately stressed area. Fatigue failure at such a location can however not be considered a fatigue problem, but should be considered a corrosion problem.

The work by de Farias and Netto [138] shows the challenges involved when dealing with handling and processing corrosion data obtained from an inspection. Challenges include dealing with partial data, erroneous measurements and proper referencing. A digital twin is a powerful tool to help with corrosion data analysis for both inspectors and analysts alike. Not only can it be used to track corrosion progression itself, it can also be used as data source for updating structural strength and fatigue analyses.

5.5.4. HYBRID MONITORING

In order to make optimal usage of information obtained from minimal or extensive monitoring systems, information can be shared for similar units. A digital twin can be used as framework to obtain key performance indicators which can be compared across platforms. The work presented in this study has shown a number of these indicators and how they can compared over multiple units.

These approaches are especially useful in shipping industry since series production is more common. However, event though a smaller number of units is in operation, the offshore industry can also benefit from hybrid analysis through sharing of information on similar units between different operators. The use of hybrid monitoring for the renewable energy sector is again clear as this sector will rely on a larger number of units in operation in a similar environment, although also in this sector, information may be shared across fields.

The concept of fleet monitoring is discussed by Groden *et al.* [172]. This paper presents the potential of reliability methods for integrated fleet monitoring. Such an approach can be strongly improved by using operational and environmental data retrieved from a virtual monitoring procedure as well as insight in design procedure uncertainties from a physical monitoring system.

5.5.5. MACHINE LEARNING

Over the last years, Machine Learning technologies have been developing rapidly. A number of initial studies have shown that the response of ship and offshore structures can be captured well using such approaches.

The estimation of ship motions is a useful application of such technologies. The work by Schirmann [173] considered the assessment of ship motions using a Neural Network using a public data set from a research vessel. The authors concluded that the Neural Network can help to improve the motion estimates. The Machine Learning model was developed as a full black box model, but also as a physics-informed model. The physics-informed model uses, in addition to environmental and operational parameters, a motion estimate for each condition obtained from physical reasoning. The authors con-

cluded that the physics informed model outperforms the black-box model, except for the roll motion. This was attributed to challenges in estimating roll motions in physical analysis due to roll damping and nonlinear behaviour.

The work by Düz *et al.* [121] considers the inverse motion problem. The authors aim to predict sea state characteristics using onboard measured motions using a convolutional neural network. The application has shown some promising initial results and can be used for direct onboard advice. Challenges in dealing with confused sea states and estimation of multiple wave systems remain to be addressed.

Hageman *et al.* present the estimation of structural loads on a naval vessels using a physics-informed model which has shown promising initial results [174]. The prediction of the structural loads by the physcial model was very good on average already. The machine learning model was able to reduce the uncertainty in the point estimates with a factor two.

Estimation of the fatigue accumulation on an offshore structure using machine learning approaches was addressed by Theodoridis [175]. The model developed by this author was able to predict the fatigue accumulation with promising accuracy using wave characteristics as input. Using stress concentration factors obtained from a numerical model, the stresses at measurement details were extrapolated to hot-spot areas and a fatigue reliability analysis was executed. Using IFEM models, the application of the model can potentially be extended beyond the instrumented area.

In a physcis-informed model, the machine learning model essentially acts as a correction model. This will greatly expand the operational relevance of such a model as they may be much more generally applicable. A physics-informed model will be able to capture basic differences in the load levels between different details, while the machine learning model can account for calculation errors. Still, care must be taken when applying such a correction model. The selection requirements for these models are yet to be defined, but will include correspondence of load effects and the application of correction models may be restricted of selected areas of the structure.

5.5.6. INTEGRITY MANAGEMENT

A digital twin supported by a measurement system and analysis tools can be used to aid integrity management in several ways. Examples that have been proposed over the years include damage identification, inspection planning and lifetime extension.

The identification of physical damage, being cracks and corrosion, using a measurement setup as used in this study has been studied by Tatsis [176]. Although some damages were identified in the numerical study as considered, the practical application of such a model remains challenging. The results have shown that, due to external perturbations, only large damages in local parts of the structure could be identified. On top of that, high requirements, in terms of accuracy and data volume, would be imposed on the measurement system and data processing methods.

The planning of frequency and scope of inspections is a subject under debate by the increased usage of Risk-Based Inspection procedures. A case study for a typical unit as considered in this research is presented by Hageman *et al.* [177]. The study presented in that article focussed on the updating of inspection planning based on fatigue criteria alone. In practice, inspection planning will be based on multiple criteria and appro-

priate weighing of this information should be applied. A digital twin can facilitate by providing access to such data. Rather than determining the frequency of inspections, an appropriate use of a load monitoring system will be to define the areas which have been most heavily loaded during operations.

A final application is the use of monitoring data to warrant lifetime extensions of units operating in the field. The results from this research have shown that fatigue assessment procedures typically introduce significant safety margins. On the other hands, assumption regarding the environmental conditions may result in both over- or underestimations of the fatigue accumulation during operation. These two effects need to be investigated and compared before a rational decision regarding lifetime extension can be made. Multiple studies aimed at using monitoring data for this purpose are currently being conducted.

6

CONCLUSIONS AND RECOMMENDATIONS

If you thought that science was certain - well, that is just an error on your part

Richard P. Feynman

6.1. CONCLUSIONS

Fatigue life assessment is associated with a high level of uncertainty due to the strong nonlinear relation between stresses and fatigue accumulation. Safety factors between 2 and 10 on fatigue life are applied to ensure sufficient margins on lifetime are available. As such, any biases in the fatigue loads that result in a deviation up to around 25% on fatigue life are considered minor uncertainties. Parameters leading to an biases of 50% and higher on fatigue life are considered of importance and warrant additional attention in fatigue designs. The objective of this study is to provide a qualitative comparison of the performance of different units in various operating environments. This information can subsequently be used as a reference for analysts when addressing the relative importance of individual aspects of fatigue assessments of hull structures.

Statistical wave parameters can be obtained from multiple sources, such as a wave buoy, radar or hindcast models. Provided that an appropriate representation of the sea state has been used, the bias between the fatigue accumulation using the different input data is typically between 25% and 50%, but can be as large as 100%. This bias is mainly the result of deviations in the wave statistics between the data sources and less related to scatter in the individual point estimates. Depending on the area and the structural detail which is examined, the hindcast models can give both an underestimate or overestimate of the fatigue accumulation with respect to the wave buoy. Hindcast data can be a good alternative data source for the analysis of long-term fatigue accumulation. However, when doing so, one needs to keep in mind potential bias and scatter arising from coarseness of calculation grid, wave spectrum and spreading definition and potential underestimation in storm events.

The orientation of the unit with respect to the waves has an effect on fatigue accumulation. On turret moored units, a difference between the expected and true orientation was observed. This deviation resulted in a bias in fatigue accumulation of 30% on one of the studied units.

The number of wave components that should be included in a fatigue assessment varies depending on the location. In the West-Africa region, a region dominated by Atlantic swells, a sea state described by bulk parameters will produce a reasonably accurate fatigue estimate. In other regions, where in addition to swells, large wind-driven seas may exist, multiple wave components need to be included to obtain an accurate assessment.

The fatigue accumulation was found to be quite sensitive to the sea state wave definition. The joint bias of spectral shape, spreading and multimodal wave components was estimated at around 50%. However, it was also noted that careful metocean analysis will significantly reduce the total bias, but not eliminate the full scatter in the predictions.

Wave conditions used to assess the transportation phase of an offshore unit are based on a year-round scatter diagram. In reality, these transports aim for a period with benign weather conditions, and hence, the actual wave conditions during the transportation phase are less severe. On two units operating in West-Africa the fatigue accumulation resulting from the experienced wave conditions were a factor of three smaller than as predicted.

Offshore production units operate at various drafts. In practice, the maximum draft condition is attained less than assumed in the design stage. As a result, fatigue accumu-

lation from bending moment loads is somewhat lower, in the order of 10%. However, it also means that parts of the side shell will be around the mean water line more often than predicted and sustain higher fatigue accumulation. This is a local effect that should be incorporated in case of a fatigue re-evaluation using information of the true loading history.

The numerical tools to calculate stresses from global bending loads are quite accurate with measurements showing a bias of up to 20% on stress. Varying results have been obtained for details in the side shell which are subject to wave pressure. For some units a large overestimation of the stress was observed. The linearised intermittent wetting results were found to deviate strongly between the different units and differences between the implementation of this procedure are deemed responsible for these deviations.

The spectral fatigue assessment procedure provides overestimates of the fatigue accumulation rate, but features significant uncertainty in the individual estimates. The procedure provides larger overestimates when the stress magnitude increases. As a result, the accumulated fatigue determined using the spectral method is between a factor of 1.5 and 2 larger than determined directly from the strain gauges.

The assumption of narrowbanded stress cycles results in a small bias in the fatigue assessment procedure leading the slight overestimation of the fatigue accumulation. It introduces only a small scatter in the individual fatigue rate estimates.

Nonlinearities between sagging and hogging loads were very small on the monitored units. Differences between compressive and tensile stresses in the side shell were larger, up to 10% at the probability of exceedance level of 10^{-3}, which is partially attributed to nonlinear wave kinematics.

Structural details in the side shell subjected to wave pressure experience the largest fatigue accumulation when they are operating near the mean water line.

The contribution of whipping and springing to the total fatigue accumulation on the observed units was small and did not exceed 15%. The contribution of whipping and springing depend strongly on the environmental conditions in which the unit is operating. In unfavourable, harsh weather conditions, whipping can lead to an increase in the fatigue accumulation between 10 to 15%. In environmental conditions with small periods, the contribution of springing to fatigue accumulation can result in an increase of 100% compared to the wave-frequency induced fatigue accumulation. The natural frequency of the hull also depends on the total mass of the units and therefore the loading condition. However, changes in the natural frequency as a result of loading variation are very small and do not significantly influence the springing response.

In the majority of the structural details, loading-induced fatigue accumulation is at most 20% of the total fatigue accumulation. However, in cargo supporting structures of units operating in mild environmental conditions, the loading-induced fatigue contribution can be up to 90% of the total fatigue accumulation. The loading-induced stresses are mainly the result of loading variations of adjacent cargo tanks. However, small additional stresses, resulting from wave loading, temperature variation and ballast and cargo variation in different parts of the unit, lead to a bias on fatigue accumulation which can be 100% resulting in larger fatigue accumulation compared to the case in which only cargo loads are considered.

6.2. RECOMMENDATIONS

Prognostic hull structure monitoring is an important tool that allows for analysing the in-service performance of floating structures. This will allow for determining biases and scatter in the design assessment and thereby quantification of the effective safety margins existing in the structure. Support for inspection planning and scope determination as well as lifetime extensions can be provided.

On permanently moored offshore units, a minimum amount of monitoring should be performed using a high performance system including detailed wave and stress data to capture a variety of environmental conditions. A single year of monitoring might not cover a full range of environmental and operational conditions and therefore a minimum period of two years is recommended. After that, it should be confirmed if convergence over these two years can be observed. If so, these measurements should suffice to obtain insight in a number of uncertainties related to performance of the hydrodynamic model, whipping and springing effects and loading-induced fatigue accumulation. Units operating in environments with a large variation in weather conditions, notably tropical storm areas, may require longer monitoring before the entire range of conditions will be encountered.

The long-term environmental and operational loads will have an important effect on the total fatigue accumulation and its uncertainty. It is recommended to perform a sort of monitoring and analysis of these loads over the entire lifetime. A compact measurement system should suffice to capture these long-term loads. This includes monitoring and analysis of cargo loading through the loading computer, heading and wave conditions. Hindcast data has shown to be a viable source of replacing a dedicated wave monitoring system for this aim. However, it should be remembered that an appropriate short-term sea state representation must be selected.

In this thesis, a framework was presented that allows for analysis of uncertainties in the design process. The individual sources of uncertainty were identified and as much as possible biases and scatter were quantified from in-service measurements or simulations. The values presented herein can be considered indicative of general industry practice. Performing monitoring on individual units can quantify (several of) these sources of uncertainty for that specific unit. Taking into account the characteristics of the unit, results from this work can be used for comparison and supplement missing data.

Hindcast data was identified as a suitable source of wave data for the long-term fatigue assessment. Special care should be taken when analysing storm events though. Small deviations in wave statistics during these events can lead to a large bias in the fatigue accumulation. In regions prone to local storm events, it is recommended to consult with metocean experts and perform some sensitivity analysis before adopting a hindcast model for fatigue assessment.

The fatigue accumulation rate changes strongly over the year. The difference between seasons varies depending on the structural detail under consideration. For some structural details, fatigue accumulation is lower than the yearly average during the harsh weather season. A carefully composed wave data set should be used to conduct a fatigue assessment. This data set should reflect the expected field conditions over the lifetime of the unit. It should be noted that higher sea states do not result in higher fatigue accumulation in all parts of the structure.

Due to careful planning, the actual weather conditions during the transportation are milder than those used in this design assessment which results in an overestimation of the fatigue accumulation during the transportation. It is recommended to repeat the fatigue evaluation directly after the transportation using GPS and hindcast data and update the records of the unit accordingly.

The result of a fatigue assessment are sensitive to spectral shape and spreading. A factor two difference has been observed between fatigue assessments using different spectral shapes. This sensitivity was found to be related to both frequency content as well as directionality and there is not one spectral shape that will result in the most conservative calculation under all conditions. Therefore, it is recommended to perform fatigue assessments using multiple spectral shapes and spreading functions when performing calculations. Potential spectra can be selected from a metocean analysis. Such calculations can be conducted at small computational expense and provide insight in the potential bias from short-term wave definitions in the calculation process.

Varying results have been obtained on the performance of linearisation methods to include intermittent wetting. Both the affected area as well as the load magnitude is governed by relative wave elevation. It is recommended that for units operating in a varying range of weather conditions, a set of RAOs are developed that incorporated intermittent wetting in these conditions to represent the load process more accurately.

Minor nonlinearities in the stress cycle distributions were found in this research. One exception is the stress cycle distribution in the side shell for a unit operating at constant draft. For units operating at a single draft, this may become an important design feature. It is recommended to perform analysis using nonlinear wave kinematics to quantify this aspect in a design stage.

The contribution of springing and whipping on fatigue accumulation is limited. However, in unfavourable conditions, whipping and springing could lead to a significant increase in the fatigue accumulation rate. Initial evidence suggests that large units operating in harsh conditions may experience significantly increased fatigue accumulation. Data pertaining to these cases is currently not available, but may become available in the near future for further analysis. Whipping will have a significant effect on the extreme loads experienced by such a unit and this contribution should be evaluated.

It is recommended that procedures are develop to assess the sensitivity of an offshore unit to whipping and springing. This can be achieved through model tests or numerical analyses. Time-domain analysis which incorporate these flexural response can be executed for a selected number of sea states. The analysis can be conducted using a hydrodynamic model to derive a bending moment multiplication factor. Verified numerical tools available for the analysis of ships should suffice for this assessment of whipping response. The analysis of springing response requires additional attention, due to its nonlinear excitation mechanism.

Loading-induced fatigue accumulation originates from cargo variations. In addition to these primary stresses, a number of minor stress contributions from wave loads, temperature variations and cargo and ballast variations in different parts of the unit, were identified. Although small, these additive stress effect results in a significant increase of the fatigue accumulation. The design codes provide procedures to account for the wave loads. For units which experience significant loading-induced fatigue, it is suggested to

include an additional factor to account for variation in loading conditions throughout the structure and temperature effects. Based on the data presented in this research an additional stress range of 10 MPa seems sufficient. An additional observation is that the loading-induced stress ranges vary in magnitude from changes in loading conditions and wave action. A stochastic model is suggested to capture these variations more accurately.

7

REFERENCES

[1] P. C. Paris, M. Gomez, and A. W.E, *A rational analytic theory of fatigue,* The trend in Engineering **13**, 9 (1961).

[2] M. Francois, O. Mo, W. Fricke, K. Mitchell, and B. Healy, *Fpso integrity: Comparative study of fatigue analysis methods,* in *Proceedings of the Offshore Technology Conference* (2000).

[3] I. Lotsberg, *Fatigue Design of Marine Structures* (Cambridge University Press, 2016).

[4] M. Tammer and M. Kaminski, *Fatigue oriented risk based inspection and structural health monitoring of FPSOs,* in *Proceedings of the Twenty-third International Ocean and Polar Engineering Conference* (2013) pp. 438–449.

[5] A. Mansour, *An introduction to structural reliability theory*, Tech. Rep. (Ship Structure Committee, 1990).

[6] O. Ditlevsen and H. Madsen, *Structural Reliability Methods* (1996).

[7] G. White and B. Ayyub, *Reliability methods for ship structures,* Naval Engineers Journal **97**, 86 (1985).

[8] L. Krishnasamy, F. Khan, and M. Haddara, *Development of a risk-based maintenance strategy for a power generation plant,* Journal of loss prevention in the process industry **78**, 69 (2005).

[9] A. Lee, C. Serratella, G. Wang, R. Basu, and R. Spong, *Flexible approaches to risk-based inspection of fpsos,* in *Proceedings of the Offshore Technology Conference* (2006).

[10] N. Shabakhty, P. van Gelder, and H. Boonstra, *Reliability analysis of jack-up platforms based on fatigue degradation,* in *Proceedings of the OMAE* (2002).

[11] ABS, *Survey using risk-based inspection for the offshore industry,* (2003).

[12] BV, *Guidance note, NI 567 DT R00 E, risk based verification of floating offshore units,* (2010).

[13] DNVGL, *DNVGL-RP-C210 - probabilistic methods for planning of inspection for fatigue cracks in offshore structures,* (2015).

[14] P. H. Wirsching, *Fatigue reliability for offshore structures,* Journal of Structural Engineering **110**, 2340 (1984).

[15] J. Rörup, Y. Garbatov, Y. Dong, E. Uzunoglu, G. Parmentier, A. Andoniu, Y. Quéméner, K.-C. Chen, S. Vhanmane, A. Negi, Y. PariharIndian, R. Villavicencio, V. Parsoya, L. Peng, and J. Yue, *Round robin study on spectral fatigue assessment of butt-welded joints,* in *Proceedings of the International Congress of the International Maritime Association of the Mediterranean* (2017).

[16] S. Bhat, V. Nadathur, D. Knezevic, P. Aalberts, H. Kolsters, D. Amude, O. Atebe, D. Pasalaand, T. Hoang, T. Luong, R. Righetti, R. Hageman, and J. Yu, *Structural digital twin of fpso for monitoring the hull and topsides based on inspection data and load measurement,* in *Proceedings of the Offshore Technology Conference*.

[17] R. Hageman, P. Aalberts, M. Shaik, and H. van den Boom, *Development of an advisory hull fatigue monitoring system,* SNAME Transactions (2014).

[18] P. Aalberts, J. van der Cammen, and M. Kaminski, *The monitas system for the glas dowr fpso,* in *Proceedings of the Offshore Technology Conference* (2010).

[19] M. Miner, *Cumulative damage in fatigue,* Journal of Applied Mechanics **3**, 159 (1945).

[20] DNV-GL, *Rp-c203: Fatigue design of offshore steel structures,* (2016).

[21] ABS, *Fatigue assessment of offshore structures,* (2018).

[22] M. Kerdabadi, A. Sakaki, and A. Izadi, *Evaluation of ship structure reliability during design, maintenance, and repair phases,* Journal of the Maritime University of Szczecin **53**, 19 (2018).

[23] ABS, *Spectral-based fatigue analysis for floating production, storage and offloading (fpso) installations,* (2018).

[24] X. Zhang, J. Paik, and N. Jones, *A new method for assessing the shakedown limit state associated with thebreakage of a ship's hull girder,* Ships and Offshore Structures **11**, 92 (2016).

[25] H. den Besten, *Fatigue resistance of welded joints in aluminium high-speed craft: A TOTAL STRESS CONCEPT*, Ph.D. thesis, Delft University of Technology (2015).

[26] A. Mansour, P. Wirsching, M. Luckett, and A. Plumpton, *Assessment of reliability of existing ship structures,* (1997).

[27] D. Leonetti, J. Maljaars, and H. Snijder, *Probabilistic fatigue resistance model for steel welded details under variable amplitude loading - inference and uncertainty estimation,* International Journal of Fatigue **135** (2020).

[28] M. Deul, *Fatigue damage accumulation in steel welded joints, subject to (random) variable amplitude loading conditions,* (2021).

[29] P. van Lieshout, *On the assessment of multiaxial fatigue resistance of welded steel joints in marine structures when exposed to non-proportional constant amplitude loading,* .

[30] I. Rychlik, *A new definition of the rainflow cycle counting method,* International Journal of Fatigue **9**, 119 (1987).

[31] P. Brodtkorb, P. Johannesson, G. Lindgren, I. Rychlik, J. Rydén, and E. Sjö, *Wafo - a matlab toolbox for analysis of random waves and loads,* in *Proceedings of the International Offshore and Polar Engineering Conference* (2000).

[32] ASTM, *Astm e1049 - 85 - standard practices for cycle counting in fatigue analysis,* (2017).

[33] K. Nolte and J. Hansford, *Closed-form expression for determining the fatigue damage of structures due to ocean waves,* in *Proceedings of the OTC* (1976).

[34] J. Journée and W. Massie, *Offshore Hydromechanics* (2001).

[35] Y.-L. Lee and H.-T. Kang, *Chapter 9 - vibration fatigue testing and analysis,* in *Metal Fatigue Analysis Handbook*, edited by Y.-L. Lee, M. E. Barkey, and H.-T. Kang (Butterworth-Heinemann, Boston, 2012) pp. 333 – 382.

[36] BV, *Ni 611 dt r00 e,* (2016).

[37] LR, *Rules and regulations for offshore units,* (2018).

[38] DNV-GL, *Classification notes 30.7: Fatigue assessment of ship structures,* (2014).

[39] J. P. SIKORA, A. DINSENBACHER, and J. E. BEACH, *A method for estimating lifetime loads and fatigue lives for swath and conventional monohull ships,* Naval Engineers Journal **95**, 63 (1983), https://onlinelibrary.wiley.com/doi/pdf/10.1111/j.1559-3584.1983.tb01627.x .

[40] G. Hautecloque, C. Monroy, F. Bigot, and Q. Derbanne, *New rules for container ships formulae for wave loads,* in *Proceedings of the 6th International Conference on Marine Structures* (2016).

[41] BV, *Structural rules for container ships - nr625 dtr03e,* (2020).

[42] Q. Derbanne, G. Storhaug, V. Shigunov, G. Xie, and G. Zheng, *Rule formulation of vertical hull girder wave loads based on direct computation,* in *Proceedings of the Conference on Practical Design of Ships* (2016).

[43] A. Ergin, E. Alley, A. Brandt, I. Drummen, O. Hermunstad, Y. Huh, A. Ivaldi, J. Liu, S. Malenica, O. el Moctar, R. Shyu, G. Storhaug, N. Valdimir, Y. Yamada, D. Zhan, and G. Zhang, *Committee ii.2: Dynamic response,* in *Proceedings of the 20th International Ship and Offshore Structures Congress*, edited by M. Kaminski and P. Rigo (2018).

[44] P.-K. Liao, Y. Quéméner, C.-F. Lee, and K.-C. Chen, *Load uncertainties effet on the fatigue life evaluation by the common structural rules,* in *Proceedings of the Internationational Conference on Ocean, Offshore and Arctic Engineering* (2015).

[45] G. Vasque, N. Fonseca, and C. G. Soares, *Experimental and numerical vertical bending moments of a bulk carrier and a roll-on/roll-off ship in extreme waves,* Ocean Engineering **124**, 404 (2016).

[46] S. Rajendran, N. Fonseca, and C. G. Soares, *Simplified body nonlinear time-domain calculation of vertical ship motions and wave loads in large amplitude waves,* Ocean Engineering **96**, 125 (2015).

[47] T. Kukkanen, *Wave load predictions for marine structures,* Journal of Structural Mechanics **43**, 150 (2010).

[48] D. Sengupta, R. Datta, and D. Sen, *A simplified approach for computation of nonlinear ship loads and motions using a 3d time-domain panel method,* Ocean Engineering , 99 (2016).

[49] T. Kukkanen and J. Matusiak, *Nonlinear hull girder loads of a ropax ship,* Ocean Engineering **75**, 1 (2014).

[50] F. van Walree and G. Struijk, *Validation of a time domain seakeeping code by model and full scale experiments for a rhib,* in *PRADS 2019* (2019).

[51] G. Shivaji and D. Sen, *Time domain simulation of side-by-side floating bodies using a 3d numerical wave tank approach,* Applied Ocean Research **58** (2015).

[52] J. Oberhagemann, V. Shigunov, and O. el Moctar, *Application of cfd in long-term extreme value analyses of wave loads,* Ship Technology Research **59**, 4 (2012).

[53] J. Oberhagemann, *On prediction of Wave-Induced Loads and Vibration of ship Structures with Finite Volume Fluid Dynamic Methods*, Ph.D. thesis, University of Duisburg-Essen (2016).

[54] L. Adegeest, *Nonlinear Hull Girder Loads in Ships*, Ph.D. thesis, TU Delft (1995).

[55] R. Hageman, I. Drummen, K. Stambaugh, T. Dupeau, N. Herel, Q. Derbanne, M. Schiere, Y. Shin, and P. Kim, *Structural fatigue loading predictions and comparisons with test data for a new class of us coast guard cutters,* in *Ship Structure Committee* (2014).

[56] J. P. Sikora, R. W. Michaelson, and B. M. Ayyub, *Assessment of cumulative lifetime seaway loads for ships,* Naval Engineers Journal **114**, 167 (2002), https://onlinelibrary.wiley.com/doi/pdf/10.1111/j.1559-3584.2002.tb00129.x .

[57] G. Clauss, C. Schmittner, J. Hennig, C. G. Soares, N. Fonseca, and R. Pascoal, *Bending moments of an fpso in rogue waves,* in *Proceedings of the international conference on Offshore Mechanics and Arctic Engineering* (2004).

[58] S. Mohammadi, M. Khedmati, and K. Vakilabadi, *Effect of hull damage on global loads acting on a trimaran ship,* Ship and Offshore Structures **10** (2015).

[59] A. von Graefe, O. el Moctar, J. Oberhagemann, and V. Shigunov, *Linear and nonlinear sectional loads with potential and field methods,* Journal of offshore mechanics and arctic engineering **136** (2014).

[60] G. Kapsenberg, A. van 't Veer, J. Hackett, and M. Levadou, *Whipping loads due to aft body slamming,* in *Proceedings of the Symposium on Naval Hydrodynamics* (2002).

[61] I. Senjanović, Š. Malenica, and S. Tomašević, *Hydroelasticity of large container ships,* Marine Structures **22**, 287 (2009).

[62] G. Storhaug, *Experimental investigation of wave induced vibrations and their effect on the fatigue loading of ships*, Ph.D. thesis, Norwegian University of Science and Technology (2007).

[63] M. Ochi, *Prediction of the occurrence and severity of ship slamming at sea,* in *Proceedings of the 5th Symposium on Naval Hydrodynamics.*

[64] A. Bereznitski, *Local hydroelastic response of ship structures under impact loads from water (slamming)*, Ph.D. thesis (2003).

[65] C. G. Soares, R. Pascoal, E. Antão, A. Voogt, and B. Buchner, *An approach to calculate probability of wave impact on an fpso bow,* in *Proceedings of the conference on Offshore Mechanics and Arctic Engineering* (2004).

[66] J. de Lauzon, Q. Derbanne, and S. Malenica, *Slamming induced whipping computations on a large database of container ships,* in *Proceedings of the Conference on Practical Design of Ships* (2019).

[67] H. Wagner, *Über stoß- und gleitvorgänge and der oberfläche von flüssigkeiten,* Zeitschrift für Angewandte Mathematik and Mechanik **12**, 193 (1932).

[68] G. Kapsenberg, *On the Slamming of ships*, Ph.D. thesis, TU Delft (2018).

[69] I. Drummen, M. Schiere, R. Dallinga, and K. Stambaugh, *Full scale trials, monitoring and model testing conducted to assess the structural fatigue life of a new us coast guard cutter,* in *Proceedings of the Ship Structure Committee* (2014).

[70] J. Tuitman, *Hydro-elastic response of ship structures to slamming induced whipping*, Ph.D. thesis, TU Delft (2010).

[71] S. Zhu and T. Moan, *Effect of heading angle on wave-induced vibrations and extreme vertical bending moments in a ultra large container ship model,* in *Proceedings of the 7th international conference on Hydroelasticity in Marine Technology* (2015).

[72] I. Drummen, *Experimental and Numerical Investigation of Nonlinear Wave-Induced Load Effects in Containerships considering Hydroelasticity,* Ph.D. thesis (2008).

[73] J. de Lauzon, A. Benhamou, and S. Malenica, *Numerical simulations of wils experiments,* in *Proceedings of the International Ocean and Polar Engineering Conference* (2015).

[74] Y. Kim, J. Kim, and Y. Kim, *Development of a high-fidelity procedure for the numerical analysis of ship structural hydroelasticity,* in *Proceedings of the 7th international conference on Hydroelasticity in Marine Technology* (2015).

[75] J. Kim and Y. Kim, *Parametric study of numerical prediction of slamming and whipping and an experimental validation for a 10,000 teu containership,* in *Proceedings of the International Ocean and Polar Engineering Conference*.

[76] O. el Moctar, J. Ley, and J. Oberhagemann, *Nonlinear computational methods for hydroelasticity effects of ships in extreme seas,* Ocean Engineering (2017).

[77] G. Kapsenberg, *Slamming of ships: Where are we now? a review,* Philisophical Transaction Royal Society A **369**, 2892 (2011).

[78] H. Ki, S. Park, and I. Jang, *Full scale measurements of 14k teu containership,* in *Proceedings of the 7th Internatinational Conference on Hydroelasticity in Marine Technology* (2015).

[79] G. Storhaug and A. Kahl, *Full scale measurements of torsional vibrations on post-panamax container ships,* in *Proceedings of the 7th Internatinational Conference on Hydroelasticity in Marine Technology* (2015) pp. 293–311.

[80] R. Hageman, A. Andoniu, and A. Benhamou, *Damping estimation methods applied to in service measurements of a 350 metre container ship,* in *Proceedings of the OMAE*.

[81] F. van Gunsteren, *Springing of ships in waves,* Ph.D. thesis (1987).

[82] K. Heo, W. Koo, and I. Park, *Quadratic strip theory for high-order dynamic behaviour of a large container ship with 3d flow effects,* International Journal of Naval Architecture and Ocean Engineering **8**, 127 (2016).

[83] Y. Lin, N. Ma, and D. Wang, *Hydroelastic analysis and experimental validation of a 350,000 dwt very large crude carrier,* in *Proceedings of the International Conference on Ocean, Offshore and Arctic Engineering* (2017).

[84] S. Hänninen, T. Mikkola, and J. Matusiak, *Development of vertical second harmonic wave loads of a large cruise ship in short and steep head waves,* Ocean Engineering **118**, 17 (2016).

[85] E. Cramer, R. Loseth, and E. Bitner-Gregersen, *Fatigue in side shell longitudinals due to external pressure,* in *Proceedings of the OMAE* (1993).

[86] J. van der Cammen, *Fatigue prediction and response monitoring of a FPSO*, Ph.D. thesis (2008).

[87] P. F. Hansen and S. Winterstein, *Fatigue damage in the side shells of ships,* Marine Structures **8**, 631 (1995).

[88] R. Folsø, *Spectral fatigue damage calculation in the side shell of ships, with due account taken of the effect of alternating wet and dry areas,* Marine Structures **11**, 319 (1998).

[89] F. Bigot, S. Mahérault-Mougin, and Q. Derbanne, *Comparison of different models for the fatigue analysis of details subject to side shell intermittent wetting effect,* in *Proceedings of the Conference on Practical Design of Ships* (2016).

[90] BV, *Guidance for long-term hydro-structure calculations, ni 638 dt r00 e,* (2019).

[91] X. Wang, J.-K. Kang, Y. Kim, and P. Wirsching, *Low cycle fatigue analysis of marine structures,* in *Proceedings of the conference on Offshore Mechanical and Arctic Engineering* (2006).

[92] A. Megharbi, H. Polezhayeva, M. Sarumi, and M. Kumar, *Representative operational loading conditions for low cycle fatigue assessment of fpso,* in *Proceedings of the International Ocean and Polar Engineering Conference* (2014).

[93] A. Megharbi, *Low Cycle Fatigue of FPSO ship structures*, Ph.D. thesis (2015).

[94] G. He, Z. Zhang, N. Tian, and Z. Wang, *Nonlinear analysis of green water impact on forward speed wigley hull,* in *Proceedings of the International Offshore and Polar Engineering Conference* (2017).

[95] E. Bitner-Gregersen, S. Dong, T. Fu, N. Ma, C. Maisondieu, R. Miyake, and I. Rychlik, *Sea sate conditions for marine structures'analysis and model tests,* Ocean Engineering **119**, 309 (2016).

[96] E. Bitner-Gregersen, K. Ewans, and M. Johnson, *Some uncertainties associated with wind and wave desciption and their importance for engineering applications,* Ocean Engineering (2014).

[97] B. Efron and R. Tibshirani, *An Introduction to the Bootstrap* (1993).

[98] F. H. van der Meulen and R. Hageman, *Fatigue predictions using statistical inference within the Monitas II project,* in *Proceedings of the Twenty-third International Offshore and Polar Engineering Conference* (2013).

[99] K. Hasselmann and D. Olbers, *Measurements of wind-wave growth and swell decay during the joint north sea wave project (jonswap),* Ergänzung zur Deut. Hydrogr. Z., Reihe A (8) **12**, 1 (1973).

[100] M. K. Ochi and E. N. Hubble, *Six-parameter wave spectra,* in *Coastal Engineering 1976*, pp. 301–328, https://ascelibrary.org/doi/pdf/10.1061/9780872620834.018 .

[101] J. Wichers, *Guide to Single Point Moorings* (2013).

[102] G. Jona-Lasinio, A. Gelfand, and M. Jona-Lasinio, *Spatial analysis of wave direction data using wrapped gaussian processes,* The Annals of Applied Statistics **6**, 1478 (2012).

[103] S. Kjeldsen, *The practical value of directional ocean wave spectra,* Johns Hopkins APL Technical Digest **11**, 381.

[104] H. van den Boom, M. Krekel, and P. Aalberts, *Fpso integrity; structural monitoring of glas dowr,* in *Proceedings of the OTC* (2000).

[105] G. Bonaschi, O. Filatova, C. Mercuri, A. Muntaen, M. Peletier, V. Shchetnikava, E. Siero, and I. Zisis, *Identification of a response amplitude operator for ships,* **5**, 1 (2013).

[106] T. Hill and P. Lewicki, *Statistics: Methods and Applications* (2005).

[107] M. B. Wilk and R. Gnanadesikan, *Probability plotting methods for the analysis of data,* Biometrika **55**, 1 (1968).

[108] J. Filliben, *The probability plot correlation coefficient test for normality,* **17**, 111 (1975).

[109] H. Akaike, *A new look at the statistical model identification,* **19**, 716 (1974).

[110] G. Schwarz, *Estimating the dimension of a model,* The Annals of Statistics **6**, 461 (1978).

[111] C. Walck, *Hand-book on Statistical Distributions for experimentalists* (1996).

[112] J. Hanson, A. Lubben, P. Aalberts, and M. Kaminski, *Wave measurements for the monitas system,* in *Proceedings of the Offshore Technology Conference* (2010).

[113] G. Forristall and K. Ewans, *Worldwide measurements of directional wave spreading,* **15**, 440.

[114] S. van Essen, K. Ewans, and J. McConochie, *Wave buoy performance in short and long wave, evaluated using tests on a hexapod,* in *OMAE 2018* (2018).

[115] L. Wyatt, *Measuring the ocean wave directional spectrum 'first five' with hf radar,* Ocean Dynamics **69**, 123 (2019).

[116] E. Thornhill and D. Stredulinsky, *Real time local sea state measurement using wave radar and ship motions,* SNAME Transactions **118**, 248 (2010).

[117] K. Stambaugh, I. Drummen, R. Hageman, and I. Thompson, *Hull structural monitoring of uscg cutters to support long term maintenance decisions,* in *Proceedings of the ASNE-TSS* (2019).

[118] I. Thompson, E. Huiskamp, N. Grasso, I. Drummen, and K. Stambaugh, *Virtual hull structural monitoring of a uscg cutter,* in *Proceedings of the ASNE-TSS* (2019).

[119] U. Nielsen, *Sea state estimation based on measurements of wave-induced ship responses,* (2019).

[120] R. Pascoal, L. Perera, and C. G. Soares, *Estimation of directional sea spectra from ship motions in sea trials,* Ocean Engineering (2017).

[121] B. Duz, B. Mak, R. Hageman, and N. Grasso, *Real time estimation of local wave characteristics from ship motions using artificial neural networks,* in *PRADS 2019* (2019).

[122] T. Scholcz and B. Mak, *Ship as a wave buoy - estimating full directional wave spectra from in-service ship motion measurements using deep learning,* in *Proceedings of the International Conference on Ocean, Offshore and Arctic Engineering* (2020).

[123] H. Tolman, *User Manual and system documentation of WAVEWATCH-III version 2.22* (2002).

[124] P. Janssen, L. Aouf, A. Behrens, G. Korres, L. Cavalieri, K. Christiensen, and O. Breivik, *Final report of workpackage i in my wave project,* (2019).

[125] H. Hersbach, B. Bell, P. Berrisford, A. Horanyi, J. Sabater, J. Nicolas, R. Radu, D. Schepers, A. Simmons, C. Soci, and D. Dee, *Global reanalysis: goodbye era-interim, hello era5,* (2019).

[126] M. Plouvier and R. Hageman, *Virtual hull monitoring systems for assessment of structural integrity of ships,* in *Proceedings of the International Naval Engineering Conference* (2020).

[127] J. Hanson and O. Phillips, *Wind sea growth and dissipation in the open ocean,* Journal of Physical Oceanography **29**, 1633 (199).

[128] J. Minnebo, P. Aalberts, and A. Duggal, *Mooring systems monitoring using dgps,* in *Proceedings of the Offshore Technology Conference* (2014).

[129] SMC, *SMC IMU - Motion Sensors* (2009).

[130] J. Koning and G. Kapsenberg, *Full scale container ship cross section loads - first results,* in *Proceedings of the Conference on Hydroelasticity in Marine Structures* (2012).

[131] B. Phelps and B. Morris, *Review of Hull Structural Monitoring Systems for Navy Ships*, Tech. Rep. (Defence Science and Technology Organization, 2013).

[132] M. Kaminski, *Sensing and understanding fatigue lifetime of new and converted fpsos,* in *Proceedings of the OTC* (2007).

[133] K. Hoffman, *Applying the wheatstone bridge circuit,* (1986).

[134] J. Koning, *Installation Report for the Lashing@Sea Project*, Tech. Rep. (MARIN, 2007).

[135] M. Lydon, S. Taylor, D. Robinson, P. Callendar, C. Doherty, S. Grattan, and E. OBrien, *Development of a bridge weigh-in-motion sensor: Performance comparison using fiber optic and electric resistance strain sensor systems,* Sensors Journal **14**, 4284 (2014).

[136] P. Aalberts, A. Ibekwe, R. Hageman, G. Oguntola, J. Izuchukwu, K. Sorensen, V. Nadathur, and R. van Vliet, *Advisory hull monitoring system for the bonga fpso,* in *Proceedings of the Offshore Technology Conference* (2019).

[137] O. Zienkiewicz, R. Taylor, and J. Zhu, *The Finite Element Method - Its basis and Fundamentals* (2005).

[138] B. V. de Farias and T. A. Netto, *Fpso hull structural integrity evaluation via bayesian updating of inspection data,* Ocean Engineering **56**, 10 (2012).

[139] J. Kyoung, S. Samaria, and J. Kim, *Projection and detection procedures for long-term wave climate change impact on fatigue damage of offshore floating structures,* in *Proceedings of the OMAE* (2020).

[140] P. F. Hansen, *Reliability Analysis of a midship section*, Ph.D. thesis (1994).

[141] G. Forristall, *Wave crest distributions: Observations and second-order theory,* .

[142] M. Prevosto, K. Ewans, G. Forristall, and M. Olagnon, *Swell genesis, modelling and measurements in west africa,* (2013).

[143] M. A. Hoque, W. Perrie, and S. M. Solomon, *Application of swan model for storm generated wave simulation in the canadian beaufort sea,* Journal of Ocean Engineering and Science **5**, 19 (2020).

[144] T. Zou, *Effect of global climate change projections on fatigue lifetime of permanently moored floating offshore structures*, Ph.D. thesis (2018).

[145] A. Andoniu, J. de Lauzon, R. Hageman, P. Aalberts, D. L'Hostis, and A. Ledoux, *Validation of spectral fatigue assessment of a west-africa fpso using full-scale measurements,* in *Proceedings of the Offshore Technology Conference*.

[146] G. Storhaug, *The measured contribution of whipping and springing on the fatigue and extreme loading of container vessels,* International Journal of Naval Architecture and Ocean Engineering **6**, 1096 (2014).

[147] I. Thompson, *Fatigue damage variation within a class of naval ships,* Ocean Engineering **165**, 123 (2018).

[148] A. Benhamou, J. Shimazaki, and F. Bontemps, *Influence of whipping on the structural response of the flare tower foundations of a typical spread-moored fpso,* in *Proceedings of the Offshore Technology Conference Brazil* (2019).

[149] P. van Overschee and B. D. Moor, *Subspace Indentification for linear systems* (KLUWER ACADEMIC PUBLISHERS, 1996).

[150] T. Fukusawa and K. Kadota, *Research on the method for determining significant short-term sea states for fatigue strength of a ship,* in *Proceedings of TEAM* (2015).

[151] K. Stambaugh, *On ship structural risk and toc management,* .

[152] J. van der Cammen, M. Francois, and M. Kaminski, *Is uncertainty of wave induced fatiguing loading of fpsos uncertain?* in *Proceedings of the conference on Offshore Mechanical and Arctic Engineering* (2004).

[153] BV, *Rules for the classification of steel ships, nr 467,* (2017).

[154] ABS, *Guide for hull condition monitoring system,* (2016).

[155] CCS, *Rules for classification of seagoing steel ships,* (2015).

[156] LR, *Rules and regulations for the classification of ships,* (2017).

[157] ClassNK, *Rules for hull monitoring systems,* (2017).

[158] DNV-GL, *Rules for classification of ships, part. 6,* (2017).

[159] P. Pahlavan, J. Paulissen, R. Pijpers, H. Hakkesteegt, and T. Jansen, *Acoustic emission health monitoring of steel bridges,* in *7th European Workshop on Structural Health Monitoring*.

[160] L. Rogers and K. Stambaugh, *Application of acoustic emission technology for health monitoring of ship structures,* in *Proceedings of the Ship Structure Committee* (2014).

[161] L. Pahlavan and G. Blacquière, *Fatigue crack sizing in steel bridge decks using ultrasonic guided waves,* **77**, 49.

[162] M. van der Horst, *On self magnetic flux leakage in support of fatigue crack monitoring in ship and offshore structures: A numerical, experimental, and full-scale application study*, Ph.D. thesis, Delft University of Technology (2018).

[163] M. Baker and B. Descamps, *Reliability-based methods in the inspection planning of fixed offshore steel structures,* Journal of Constructional Steel Research **52**, 117 (1999).

[164] D. van den Berg, M. Tammer, and M. Kaminski, *Updating fatigue reliability of uninspectable joints using structurally correlated inspection data,* in *Proceedings of the Twenty-fourth International Ocean and Polar Engineering Conference* (2014) pp. 423–432.

[165] S. Malenica and Q. Derbanne, *Hydro-elastic issues in the design of ultra large container ships - tulcs project,* in *Hydro-elasticity in marine technology* (2012).

[166] A. Andoniu, J. de Lauzon, and V. Lamaison, *Full scale measurements of the hydro-elastic behavior of a 13000 teus container ship,* in *Proceedings of the 7th International Conference on Marine Structures* (2019).

[167] F. Bigot, Q. Derbanne, and E. Baudin, *A review of strains to internal loads conversion methods in full scale measurements,* in *Proceedings of the Conference on Practical Design of Ships* (2013).

[168] M. Schiere, T. Bosman, Q. Derbanne, K. Stambaugh, and I. Drummen, *Sectional load effects derived from strain measurements using the modal approach,* in [168], pp. 188 – 209.

[169] G. Storhaug, O. Asgaard, and O. Frederiksen, *Calibration of hull monitoring strain sensors in deck including the effect of hydroelasticity,* in *Proceedings of the International Conference on Ocean, Offshore and Arctic Engineering* (2016) pp. 487–494.

[170] J. de Lauzon, A. Benhamou, and A. Andoniu, *A novel approach to expand the reach of classic structural health monitoring systems,* in *Proceedings of the ATMA conference.*

[171] F. Petillo, *Probability-based strength reassessment of corroded fpsos using measured loads,* (2015).

[172] M. Groden, Y.Liu, and M. Collette, *Fatigue life updating for vessel fleets,* in *Proceedings of IALCCE* (2016).

[173] M. Schirmann, M. Collette, and J. Gose, *Improved vessel motion predictions using full-scale measurements and data-driven models,* in *Proceedings of the 33rd Symposium on Naval Hydrodynamics.*

[174] R. Hageman, M. Schirmann, I. Drummen, M. Collette, and K. Stambaugh, *Structural reliability assessment for monitored uscg ship,* in *Proceedings of the ASNE-TSS* (2019).

[175] I. Theodoridis, *Feasibility study of the development of a digital twin for the structural health monitoring of marine structures using big data,* (2021).

[176] K. Tatsis, *Structural health assessment through vibration monitoring on fpsos,* (2016).

[177] R. Hageman, F. van der Meulen, A. Rouhan, and M. Kaminski, *Quantifying uncertainties for risk-based inspection planning using in-service hull structure monitoring of fpso hulls,* Marine Structures (in preparation) (2021).

ACKNOWLEDGEMENTS

Over the course of almost 10 years, I have worked on research which has eventually resulted in this thesis. Over that period, I have had the pleasure of working with a large variety of people from both academia and the industry on several projects related to load prediction and fatigue assessment.

First of all, I would like to thank my promotor, Mirek Kaminski. As one of the founding fathers of the Monitas Project, he has been instrumental in defining the concept of the measurement system and data analysis methods on which this research is based. I would also like to thank my co-promotor Pooria Pahlavan. Both were instrumental in the development and final design of this thesis.

Secondly, I would like to thank Hannes Bogaert, former team leader Hydro-Structural Services, and Henk van den Boom, former business unit manager Trials & Monitoring, for giving me the opportunity to work at MARIN. Not only was I able to work on motivating projects, but I was also able to enjoy a pleasant working environment.

During my time at MARIN, I have enjoyed working with many professional colleagues and hope to continue to do so for many years to come. I owe special thanks to two of my close colleagues. First of all, Pieter Aalberts, who has been able to supply me with an ever increasing number of offshore monitoring projects and was therefore instrumental in the development of this thesis. Secondly, I would also like to thank Ingo Drummen, who has acted as my primary research coach at MARIN and also provided me with new interesting research opportunities outside the scope of this work. Both gentlemen have also kindly revisited the draft of this thesis and made valuable suggestions.

I owe many thanks to the participants of the Monitas project for the support of this research. Their commitment to the project and input on many aspects of this research is much appreciated. An additional word of thanks goes out to Jeroen van der Cammen who has reviewed the draft thesis and provided valuable feedback.

A word of thanks to my readers who have picked up this booklet with the aim of learning and understanding. I hope you have been able to take some insights and ideas with you for the future.

A last word of thanks goes out to my family and friends who have supported me along the way. My parents Bert and Corry for their support during all the important steps in life. Mother-in-law Marina who has taken up the challenge of the cover design. Binky and Dotty have broken through many writer's block by simply being themselves. Finally, my dearest Sabrina, I cannot thank you enough for all the small things that keep me going every day.

Renco

CURRICULUM VITÆ

Remco Bastiaan HAGEMAN

Remco Hageman was born of May 28^{th}, 1987 in Terneuzen, The Netherlands and was raised in the village of Koewacht on the border of The Netherlands and Belgium. He attended the Reynaert college secondary school in Hulst. He graduated the Gymnasium with the joint profiles of Nature & Technology and Nature & Health. In his final year he was admitted to the national finals of 'De nationale Olympiade' in both Chemistry and Physics.

In 2005, Remco started his University career in Delft as a student Naval Architecture. During his Bachelor, he has been working part-time on the research project 'MEMSPACK' as FEM analyst. The final MSc. research project was conducted at TNO under the guidance of Johan Tuitman and considered a coupled hydro-structural analysis of a sloshing impact. He graduated in 2011 with Honours and was awarded a graduation award by the KNVTS (Koninklijke Nederlandse Vereniging van Technici op Scheepvaartgebied).

Since 2011, Remco has been employed at MARIN. Initial projects include developing, maintaining and using analysis software for fatigue monitoring projects. He has been involved in various long running Joint Industry Projects (JIPs) which address fatigue load monitoring on both offshore units and ships.

His current responsibilities at MARIN include research coordination in the field of Hydro-Structural interaction. He is involved in initiating new research projects on response monitoring and data analysis including data science. Since several years he has become an active member of the CRS community (Cooperative Research Ships). Within this community he has worked alongside peers to initiate new working groups and is currently serving as secretary on the working group Convirt and as chairman on the working group EVaP (Extreme Value Prediction).

List of Publications

.1. Journal Publications

4. **R.B. Hageman**, I. Thompson *Virtual hull monitoring using hindcast and motion data to assess frigate-size vessel stress response*, Ocean Engineering **245**, (2022).

3. **R.B. Hageman**, F. van der Meulen, A. Rouhan, M.L. Kaminski *Quantifying uncertainties for Risk-Based Inspection planning using in-service Hull Structure Monitoring of FPSO hulls*, Marine Structures **81**, (2022).

2. **R.B. Hageman**, I. Drummen *Modal Analysis for the global flexural response of ships*, Marine Structures **63**, 318-332 (2018).

1. **R.B. Hageman**, P.J. Aalberts, M. Shaik, H.J.J. van den Boom *Development of an Advisory Hull Fatigue Monitoring System*, SNAME Transactions 2014.

.2. Conference Proceedings

19. A. Andoniu, J. de Lauzon, **R.B. Hageman**, P.J. Aalberts, D. L'Hostis, A. Ledoux, *Validation of Spectral Fatigue Assessment of a West-Africa FPSO using Full-Scale Measurements*, OTC, August 2021.

18. S. Bhat, V. Nadathur, D. Knezevic, P.J. Aalberts, H. Kolsters, D. Amude, O. Atebe, D. Pasala, T. Hoang, T. Luong, R. Righetti, **R.B. Hageman**, J. Yu, *Structural Digital Twin of FPSO for Monitoring the Hull and Topsides Based on Inspection Data and Load Measurement*, OTC, August 2021.

17. **R.B. Hageman**, A. Andoniu, A. Benhamou, *Damping Estimation Methods applied to in service Measurements of a 350 Metre Container Ship*, OMAE, June 2021.

16. W. Pauw, **R.B. Hageman**, J. van den Berg, P.J. Aalberts, *Validation of Mooring Simulations with In-service Tension Measurements*, OMAE, June 2021.

15. M. Plouvier, **R.B. Hageman**, *Virtual hull monitoring systems for assessment of structural integrity of ships*, INEC, October 2020.

14. **R.B. Hageman**, P.J. Aalberts, D. L'Hostis, A. Ledoux, *Feasibility of using Hindcast data for Fatigue Assessment of Permanently Moored Offshore Units in West-Africa*, OMAE, August 2020.

13. R. Righetti, N. Troost, **R.B. Hageman**, P.J. Aalberts, *Integrity Assessment Of Mooring Lines By Position Measurements*, OTC, May 2020.

12. **R.B. Hageman**, I. Drummen, *Calculation of structural damping of the global hull structure from in-service measurements*, PRADS, September 2019.

11. B. Duz, B. Mak, **R.B. Hageman**, N. Grasso, *Real Time Estimation of Local Wave Characteristics From Ship Motions Using Artificial Neural Networks*, PRADS, September 2019.

10. **R.B. Hageman**, M. Schirmann, I. Drummen, M.D. Collette, K.A. Stambaugh *Structural Reliability Assessment for Monitored USCG ship*, ASNE-TSS, June 2019.

9. I. Drummen, L. Rogers, A. Benhamou, **R.B. Hageman**, K.A. Stambaugh *Hull Structure Monitoring of a new class of US Coast Guard Cutters*, ASNE-TSS, June 2019.

8. K.A. Stambaugh, I. Drummen, **R.B. Hageman**, I. Thompson *Hull Structural Monitoring of USCG Cutters to support Long Term Maintenance Decisions*, ASNE-TSS, June 2019.

7. **R.B. Hageman**, P.J. Aalberts, R. Leeuwenburgh, N. Grasso, *Integrity Management of Mooring Systems, OTC2019-29560*, OTC, May 2019.

6. P.J. Aalberts, A. Ibekwe, **R.B. Hageman**, G. Oguntola, J. Izuchukwu, K. Sorensen, V. Nadathur, R. van Vliet, *Advisory Hull Monitoring System for the Bonga FPSO, OTC2019-29250*, OTC, May 2019.

5. I. Drummen, **R.B. Hageman**, K.A. Stambaugh *Structural fatigue life assessment and maintenance needs for a new class of US Coast Guard Cutters*, IALCCE, October 2016.

4. **R.B. Hageman**, B. Vasconcelos de Farias *Identifying System Properties through Structural Inference using In-Service Measurements*, ISOPE, June 2014.

3. **R.B. Hageman**, I. Drummen, K.A. Stambaugh, T. Dupeau, N. Herel, Q. Derbanne, M. Schiere, Y. Shin, P. Kim *Structural Fatigue Loading Predictions and Comparisons with Test Data for a New Class of US Coast Guard Cutters*, SSC, May 2014.

2. F. van der Meulen, **R.B. Hageman** *Fatigue Predictions using Statistical Inference within the Monitas II Project*, ISOPE, July 2013.

1. D. L'Hostis, J.J. van der Cammen, **R.B. Hageman**, P.J. Aalberts *Overview of the Monitas II JIP*, ISOPE, July 2013.